# THERMAL ASPECTS OF METAL CUTTING

by

ERWIN GUSTAV LOEWEN

B.M.E., New York University
(1941)

S.M., M.E., Massachusetts Institute of Technology
(1949)(1950)

SUBMITTED IN PARTIAL FULFILLMENT OF THE

REQUIREMENTS FOR THE DEGREE OF

DOCTOR OF SCIENCE

at the

MASSACHUSETTS INSTITUTE OF TECHNOLOGY

(1952)

Signature Redacted

Signature of Author _____
Department of Mechanical Engineering, May 9, 1952

Certified by Signature Redacted
Thesis Supervisor

Signature Redacted

Chairman, Departmental Committee on Graduate Students

THERMAL ASPECTS OF METAL CUTTING by Erwin G. Loewen

Submitted to the Department of Mechanical Engineering on May 9, 1952 in partial fulfillment of the requirements for the degree of Doctor of Science.

Thermal effects in metal cutting, as evidenced by the breakdown of tools operated at excessive speeds, have been plaguing machinists since the earliest days of the art of machining. It is only very recently that the scientific approach to metal cutting has made possible an analytic study of the temperatures developed at the cutting edge of a tool.

This thesis presents a method by which the thermal aspects of the simple two-dimensional cutting process can be derived from the geometrical and force pictures, if the thermal properties of work and tool materials are known. In particular, the temperature on the cutting face of the tool will be calculated, since it is the quantity with the greatest practical significance.

Theppurpose of the analysis is to provide a quantitative procedure by which one can calculate the influence of speed, feed, and physical properties of tool and work materials on the cutting temperatures. Wherever possible, the analysis was checked by experimental data.

As a practical application, the analysis was used to explain the unusual temperature phenomena noted in the machining of Titanium.

Thesis Supervisor: M. C. Shaw

Title: Associate Professor of Mechanical Engineering

INDEX

## INTRODUCTION

That the production of heat always accompanies the metal cutting process must have been evident to the earliest workers in the field. This point appears to have been appreciated first by Count Rumford (23), whose report to the Royal Society in 1798 on the heat produced in the boring of cannon proved an important contribution to the theory of heat. The great practical importance of the heat thus generated was brought out much later by F. W. Taylor, whose monumental paper "On the Art of Cutting Metal" (39) in 1907 was a milestone in the field. Taylor's interest in mass production led him to study the factors which limit useful cutting speeds in machine tools, and he noted that as speeds increased, the tools became hotter and as a result broke down faster. He proposed that tool and materials be rated by the cutting speed at which a tool lasted just 20 minutes before breaking down completely.

Even today the empirical life tests on which such a rating depends are still the accepted method for classifying both tool and work materials for their machining characteristics. However, there are available now, through a development stretching over the last 25 years, a number of more scientific tools for studying the metal cutting process.

From a thermal viewpoint the most significant of these are the methods devised for measuring the temperatures at the tool tip, the simplest and most effective of which depends on measurement of the thermo-electric emf existing between tools and workpiece. This made possible not only quantitative measurements of temperatures that various tool materials can withstand for finite periods when cutting, but also an evaluation of work materials with respect to the temperatures they generate in cutting. In

Europe this method is being used to control the uniformity of some steels. Such measurements also make it possible to convert Taylor's approximate formula for tool life

$$\text{Life} = (\text{constant})\ (\text{cutting speed})^{1/m}$$

into the much more significant and more generally useful form of

$$\text{Life} = (\text{constant})\ (\text{tool temperature})^{1/n}$$

where the exponents m and n are large numbers (10 to 20).

Other developments in the field have brought the design of machine tool dynamometers to the point where measuring the forces on tools is no longer a difficult or mysterious process. Through the work of Ernst and Merchant (9) and others, fairly simple means have been devised for obtaining a detailed force picture in simple two-dimensional (orthogonal) cutting, if the geometry and tool and chip are known as well as two perpendicular force components. From this data the shear stress and strain, shear energy, coefficient of friction, etc. can be readily calculated.

The purpose of this thesis is to present a method by which the thermal aspects of the orthogonal cutting process can be derived from the geometrical and force pictures, and in particular, how the temperature at the cutting face of the tool can be calculated. To do this, it is necessary to know also the thermal properties of tool and work materials.

Such calculations are too involved to warrant their use in everyday shop practice, but they are very useful to the engineer in helping to predict the effects that speed and feed, geometry, and the physical properties of the Tool and Work materials are likely to have on cutting temperatures. As a practical example, the analysis was used successfully to explain the rather unusual temperature phenomena observed in the cutting of Titanium.

## FORCE MEASUREMENTS AND THEIR EVALUATION

The best machine tool for continuous orthogonal cuts is a lathe. The most important requirements for a lathe dynamometer with which to measure force components in two directions are a stiffness as high as the required sensitivity will allow, simplicity, and ability to measure each component without appreciable interference from the other (16) (25).

A unit that meets these requirements to a high degree was designed and is shown assembled in Fig. 1. Consisting of just two parts, except for screws, its simplicity can hardly be improved upon. The two members are a body that can be mounted directly on the cross-slide of a lathe and this body holds a cantilevered measuring bar, a picture of which is shown in Fig. 2. The measuring bar has a square section between the part clamped in the body and the part holding the tool, and the sides of this square are held accurately parallel with the square hole in which the tool is clamped. A total of 8 type A-8 SR-4 resistance strain gages are mounted symmetrically on this square section, two on each face. The gages are hooked up in two complete Wheatstone bridges, each of which is sensitive only to forces in one direction, interference being less than 1%. Torsion on the bar, which occurs when the cutting edge of the tool is not on the centerline, has no influence on the output of the bridges. With a Sanborn type amplifier, which is sensitive to strains down to $1 \times 10^{-6}$, sensitivity is about 5 pounds. The maximum safe load is over 10,000 pounds, which makes the unit almost indestructable. Stiffness is about 300,000 lb/in, which is much higher than that encountered in the usual type of lathe set-up.

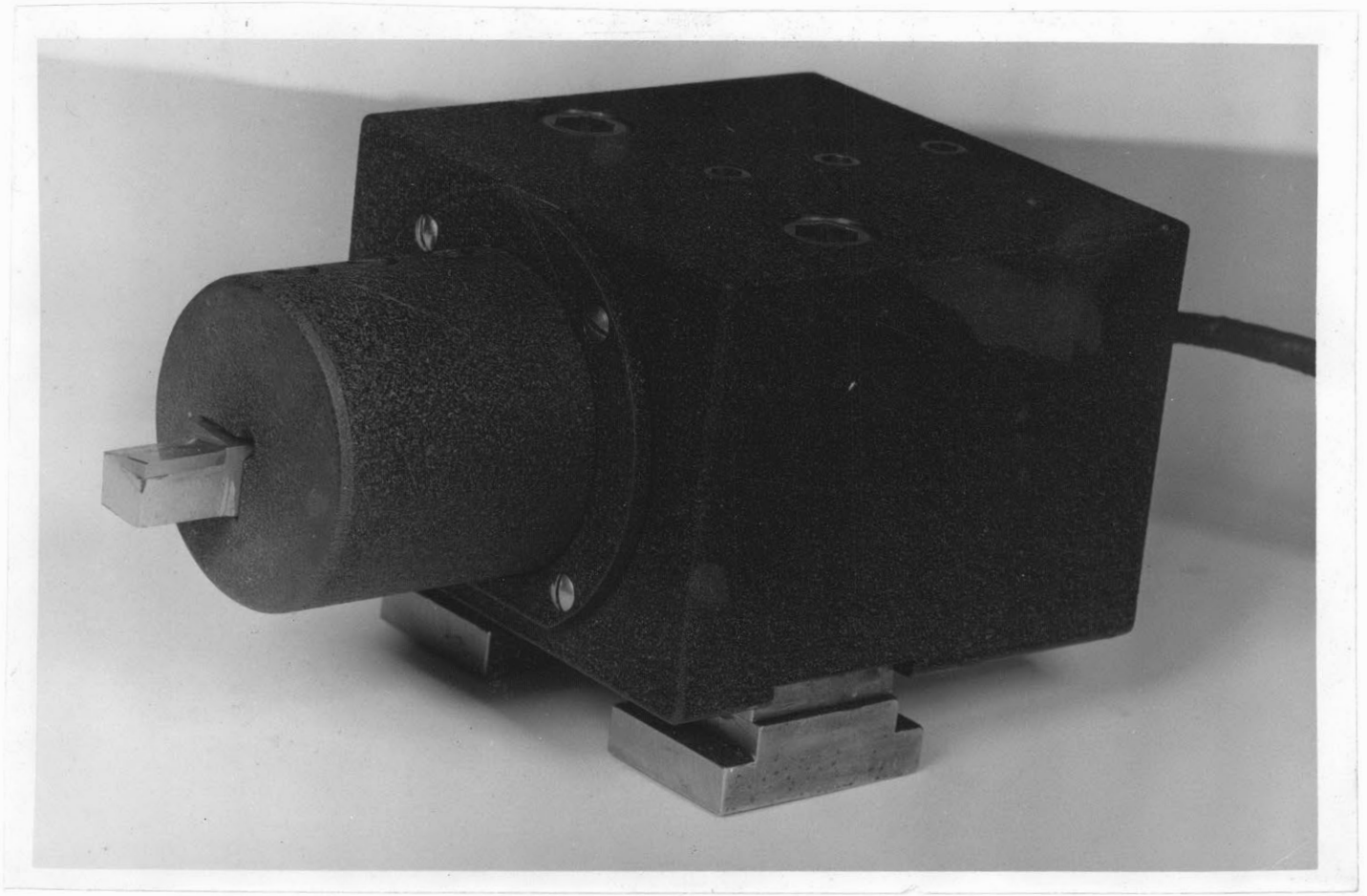

Figure 1

Model L-4 Two-dimensional Lathe Dynamometer
Note the T-Nuts which fit the compound slide of a Lathe.

Figure 2

Measuring Bar of Model L-4 Lathe Dynamometer

Strain gages on measuring section have been covered with a protective coating of wax.

The methods by which the interesting stresses and forces in the cutting process are derived from simple force and geometrical measurements were stated by Merchant (loc.cit.) and are listed below for reference purposes. To visualize the process Fig. 3 shows a diagram of the two-dimensional cut and Fig. 4 the corresponding free-body diagram of the chip alone.

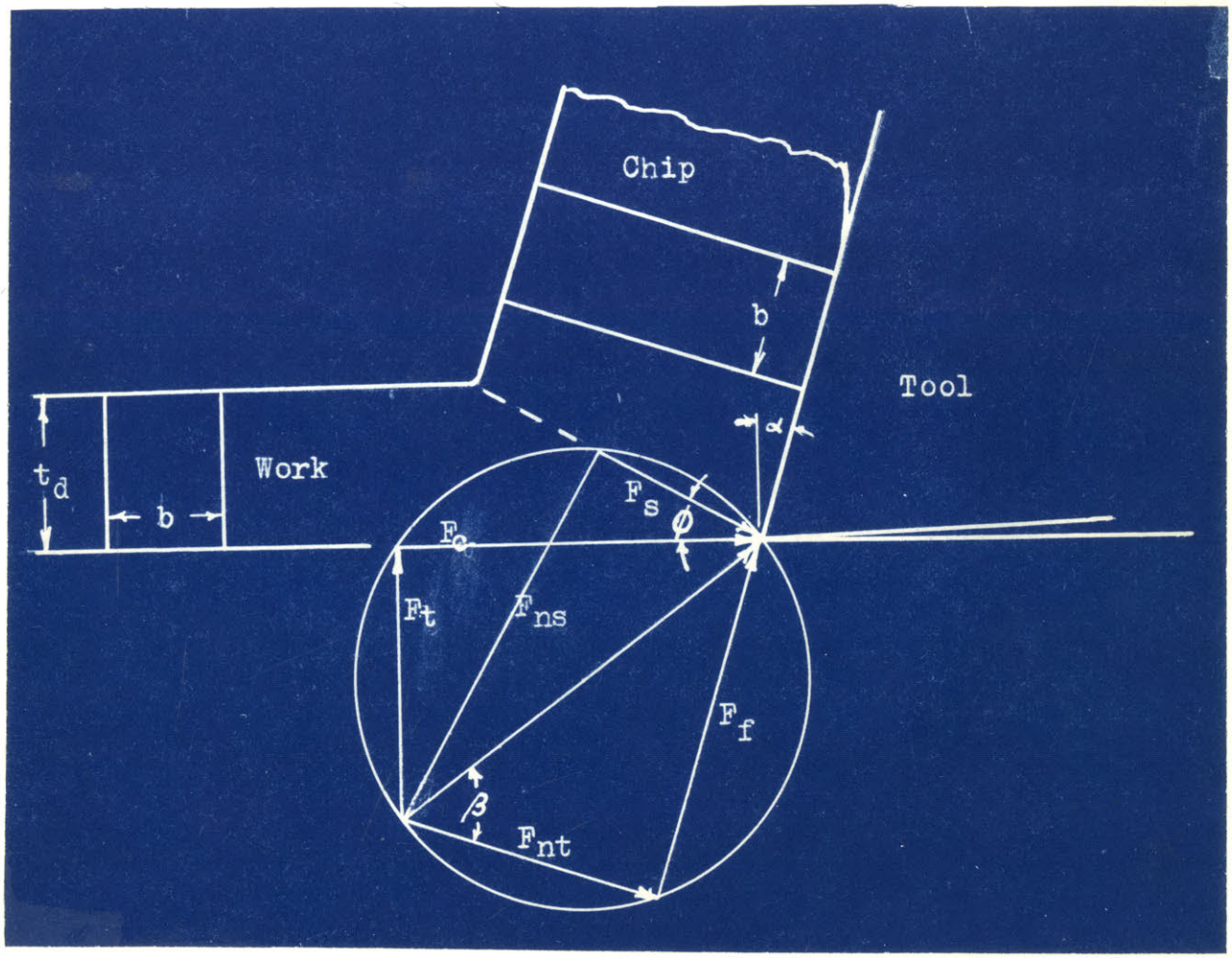


Figure 3.

Two-dimensional (orthogonal) cut, showing forces and geometry

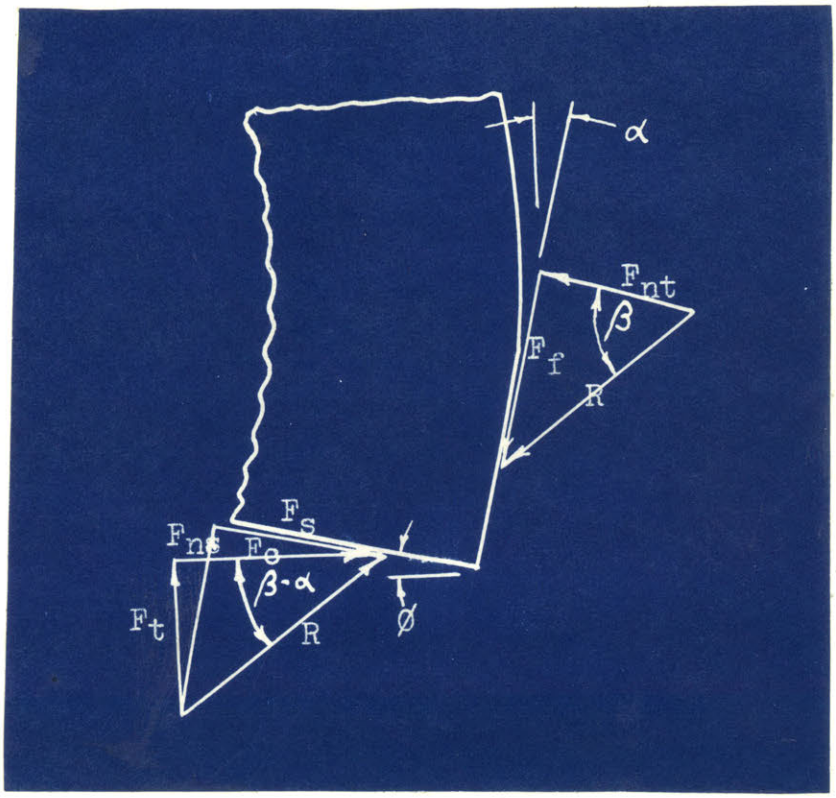


Figure 4.

Free body diagram of forces acting on the chip

The coefficient of friction along the tool face is then

$$\mu = \tan\beta = \frac{F_f}{F_{nt}} = \frac{F_c \tan\alpha + F_t}{F_c - F_t \tan\alpha} \qquad (a)$$

If the cross-sectional area of the chip is $A_o$ then the area along the shear plane is

$$A_s = \frac{A_o}{\sin\phi} \qquad (b)$$

When the forces along the perpendicular to the shear plane are divided by the area $A_s$ we have expressions for the average shear stress ($\tau$) and average normal stress ($S_n$) on the shear plane.

$$\tau = \frac{F_s}{A_s} = \frac{(F_c \cos\phi - F_t \sin\phi)\ \sin\phi}{A_o} \qquad (c)$$

$$S_n = \frac{F_{ns}}{A_s} = \frac{(F_c \sin\phi + F_t \cos\phi)\ \sin\phi}{A_o} \qquad (d)$$

The chip length ratio ($r_c$) by continuity is equal to the chip thickness ratio

$$r_c = \frac{t_d}{t_c} = \frac{\sin\phi}{\cos(\phi - \alpha)} \qquad (e)$$

so that $\phi$ is given by

$$\phi = \tan^{-1} \frac{r_c \cos\alpha}{1 - r_c \sin\alpha} \qquad (f)$$

The friction $F_f$ is given by

$$F_f = F_t \cos\alpha + F_c \sin\alpha \qquad (g)$$

The shear strain ($\gamma$) that the chip undergoes can be expressed in several different forms, all of which are equivalent:

$$\gamma = \tan(\phi - \alpha) + \cos\phi \qquad (h)$$

$$\gamma = \cot\phi + \tan(\phi - \alpha) \qquad (h')$$

$$\gamma = \frac{\cos}{\sin\phi \cos(\phi - \alpha)} \qquad (h'')$$

The chip velocity $V_c$ is a simple function if the cutting velocity $V_t$

$$V_c = r_c V_t \qquad (j)$$

The total energy consumed in the cutting process is given by

$$u = \frac{V_t F_c}{b t_d V_t} = \frac{F_c}{b t_d} \qquad (k)$$

The part of the energy consumed in the shear process alone ($u_s$) is the product of shear stress and strain:

$$u_s = \tau\gamma \qquad (m)$$

## EXPERIMENTAL METHODS OF MEASURING TOOL TIP TEMPERATURES

Up to the present time only three experimental methods have been proposed for tool tip temperature measurements that do not depend on thermoelectric measurements.

Schwerd (37) tackled the difficult problem of measuring the radiation from different points of the tool and chip, but had to construct an elaborate rocksalt optical system to do so. The experimental technique was a difficult one, especially the calibration. Since this is the only method capable of measuring temperature gradients in the work as well as the tool, it is unfortunate that the bulk of Schwerd's data has never been published. Obviously the most important part of the tool, the cutting face, is not subject to such radiation measurements, since it will always be obscured by the chip being produced. As a tool for extensive measurements, this technique is not suitable.

Another method was proposed by Schallbroch and Lang (26) who used a series of temperature sensitive paints on the clearance face of their tool and then measured the position of the various isothermal lines so indicated. Plotting these they could extrapolate to obtain the temperature of the cutting edge. A practical limitation lies in the fact that these paints are also time sensitive, so that cutting time must be standardized (5 min.), and at least 6 different paints must be used, to obtain 6 different isotherms. This means 30 minutes of cutting for each test, which can use up large quantities of test material. The authors noted that the tool tip temperature so determined was about 100°F higher than that measured by the two-tool thermocouple method (see following page). Later work of Lang (14)

recognized the fallacy behind the latter method, in fact he used the thermocolor technique to show that two geometrically similar tools made of different materials could have widely differing tool tip temperatures, thus disproving the basic assumption of which this method rested. Unfortunately Lang did not give any figures comparing the thermo-color method with the single tool thermocouple method.

This gap in information has recently been filled by Bickel (1) (2) who determined tool tip temperatures not by simple extrapolation of the isotherms but by building an electrolytic analog model of the steady state (after 18 min.) temperatures in the tool. Through a trial and error method voltages of 10 equivalent heat sources along the cutting face were varied until the constant voltage lines in the model corresponded to the known positions of the isotherms. This rather laborious procedure made it possible to obtain actural temperature distributions and to compare them with the single tool thermocouple method. The case reported, for a high speed steel tool having a slight wear crater behind the cutting edge, and cutting at about 120 ft/min, indicated a thermocouple temperature of 1040°F, while the thermocolor technique gave a variation of 1340 to 1020°F for the temperature along the cutting face. Perhaps an unworn tool would have given different results, in fact the authors infer that agreement would be better in such a case, but give no figures. A severe limitation of the thermocolor method lies in the length of the runs required (5 to 18 min). Not only does this use up large amounts of material, but, more important, limits measurements to those temperatures at which a tool may be expected to remain substantially unchanged during a test. This is in sharp contrast to high speed thermocouple measurements where readings can readily be obtained within 2 seconds or less. Nevertheless Lang (14) claims that by

improving and standardizing his equipment he can speed up thermocolor measurements to the point where they become practical for general use.

Pahlitzsch and Helmerdig (19) have elaborated on the technique for evaluating thermocolor isotherm measurements by performing a non-steady state analysis of heat flow in a tool, making use of Schmidt's (35) (36) finite difference method for solving the Fourier Heat Transfer equation in Linear, cylindrical and spherical coordinates. The finite chip contact area over which a tool receives its heat prevents exact application of any one of these coordinate systems, but by making suitable approximations a solution can be obtained from which rather complex corrections can be calculated. It is also possible to calculate the amount of heat energy passing into the tool, and a sample calculation showed that about 1% of the total energy in cutting steel at 60 ft/min passed into the tool. The authors also point out that thermal gradients in the tool are such that any cooling applied other than right at the cutting point can have but little effect on the tool tip temperature.

A third method is to perform calorimetric measurements on the whole cutting process, or more usually just the chips. While this does not lead to tool tip temperatures it gives the average chip temperature and it is a useful comparative method according to Schmidt (33), and of course is the only way in which the energy distribution in cutting can be measured directly. It is unfortunate that cutting conditions make it so difficult to perform calorimetric work with the high precision necessary to make useful energy studies.

The most popular technique now in use for tool tip temperature measurements is the tool-work thermocouple method, first proposed by Shore (M.I.T, 1924)

and independently by Gottwein in 1925 (10) and Herbert in 1926 (12). The idea is to make use of the different thermo-electric properties of tool and work materials and measure the thermal emf that is produced as a result at the hot junction between the tool and work, or more particularly between the cutting face of the tool and the chip. If suitable precautions are observed, and if a calibration is available, then this emf can be interpreted directly in terms of temperature.

Perhaps the first thing evident in an inspection of the usual tool-work thermo-electric circuit, shown below, is the vagueness of the cold junction conditions of the system. If the usual rules for accurate thermocouple measurements were to be followed, then the cold junction temperatures should be definitely established by keeping point (a) on the tool and the mercury connection at (c) at a fixed temperature, such as the ice point, 32°F. Furthermore, the connecting rod (r) and the disk at the end should both be made from the work material to keep from introducing extraneous emf's at (b). These are conditions very difficult to fulfill in practice. For instance, it is hard to visualize keeping the back end of the tool at 32°F, especially when it has to be clamped in a dynamometer.

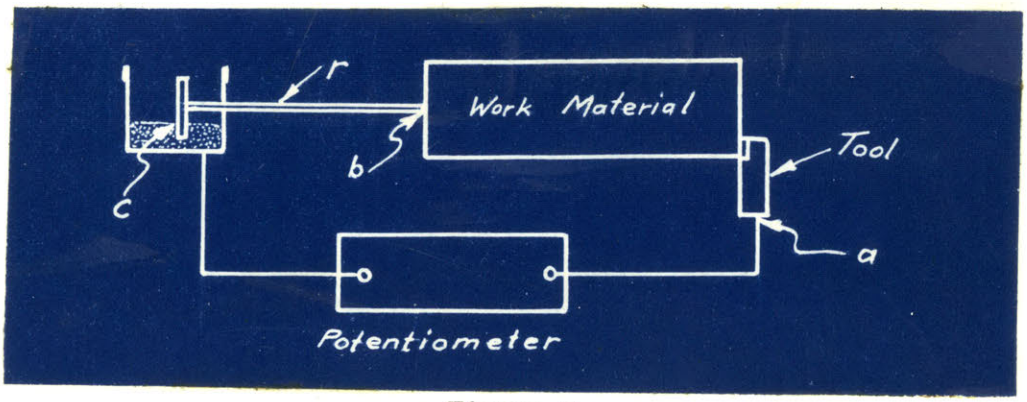


Figure 5.

Simple Thermoelectric circuit on Lathe.

Professor Bickel (1) has proposed some ingenious methods to get around these difficulties. For the tool he provided an artificial cold junction at the ice point by using a chromel-alumel couple attached to the free side of the tool and noting that the two wires are positive and negative

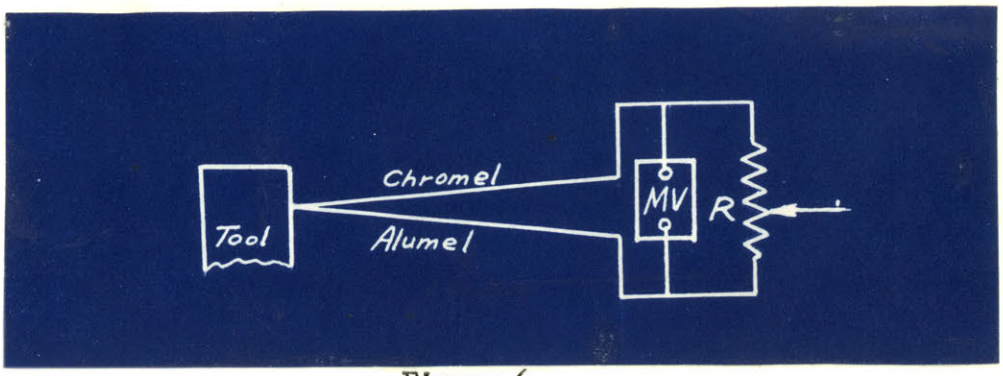


Figure 6.

Artificial Cold Junction for Tool.

respectively with respect to the ice-point emf of a high speed steel tool. Thus there must exist along the potentiometer wire R a position for which the potential is that of the tool at 32°F. This position is found by suitable calibration, although sometimes non-linearities make slight adjustments necessary as the tool heats up. Making the connecting rod (r) in Fig. 5 of the work material is most inconvenient, impossible when only a limited amount of material is available. Bickel's solution was to make a small arm of the work material, fastened to project from the rear of the workpiece, the tip (t) of which effectively remained at room temperature even when the main body of the work became hot and is shown in Fig. 7 below.

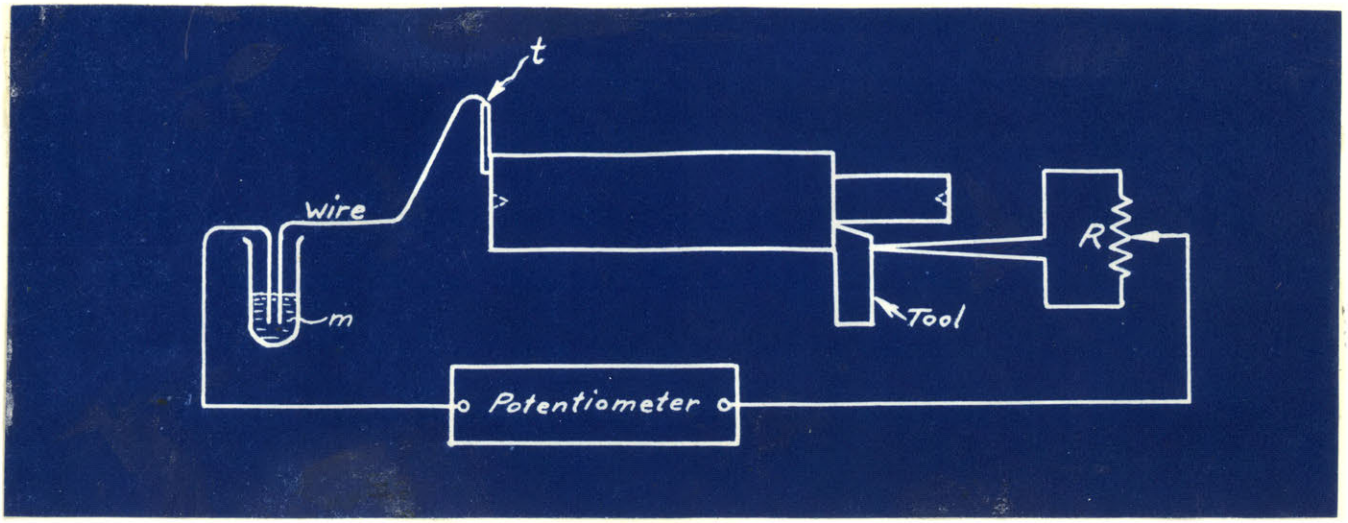


Figure 7.

Compensated Thermo-electric circuit for Lathe.

A flexible wire connected point (t) through the headstock of the lathe with the mercury bath (m), which was kept at 32°F. This had the same effect as keeping the end of the workpiece itself at 32°F.

While Bickel's method is the most accurate published so far, there is a question as to whether so many precautions are always warranted, in view of other uncertainties. For instance, the arrangement shown in Figure 5 may be entirely adequate when cutting with carbide tools whose high thermal emf's make results quite insensitive to small parasitic emfs at (b), and also when tests are of such short duration that both points (a) and (c) can be expected to remain at room temperature, which is then taken as the reference temperature. In this work 75°F was taken as the standard reference temperature during calibration. If ambient temperature rises above this, tool temperatures will appear too low and vice versa. However, for practical purposes such variations are less than the precision of measurement, so that the simplification is justifiable. To avoid the effect of circuit

resistances it is highly desirable that potentiometers rather than millivoltmeters are used for measurements. The G.E. Photoelectric recording potentiometer proved an ideal instrument for this job.

To realize the limitations of the thermo-electric temperature, measurement, it is necessary to consider just what takes place at the point of contact between the work (chip) and the tool. Figure 8 gives

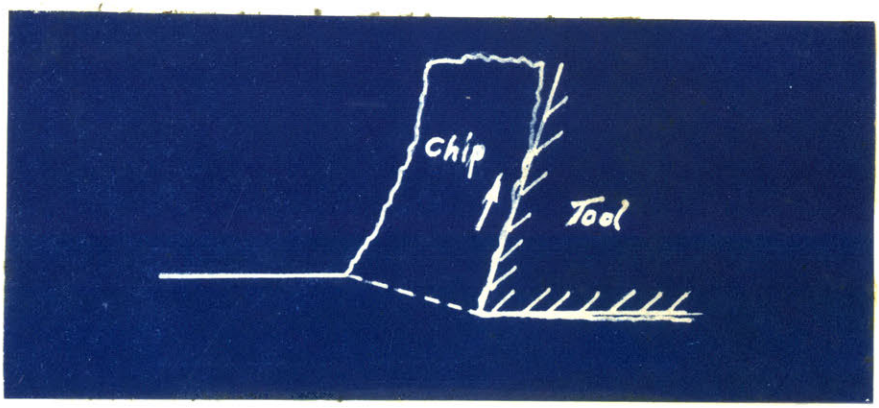


Figure 8.

Tool-Chip Contact

a somewhat exaggerated picture of the microgeometry at the tool-chip contact area, showing a large number of small contact points, each of which naturally forms a little thermocouple. Motion of the chip causes the contact areas to change continuously. Temperature at each of the little junctions, which modern friction theory assumes to be small welds, will in general be different. This means that the emf across these junctions will also vary widely, but there is no way of measuring these individual emf's, since they are all effectively in parallel. The low temperature points will act as partial short circuits for the high temperature ones.

The degree of such short-circuiting depends on the relative resistances between the points, that is the resistivity of the tool and work materials and the geometry of the contacts. Further short-circuiting is possible where the clearance face of the tool makes contact with the workpiece. Inertia in measuring instruments superimposes a time-integration on the thermocouple voltage-averaging taking place at the tool. It is clear therefore that the final result can only represent some sort of average temperature, the exact nature of the averaging process remaining unknown.

Using a similar thermocouple technique Bowden (4) and his group in Cambridge, developed a smethod for measuring temperature peaks in sliding contact of two dissimilar metals, using very small specimens and cathode ray oscilloscope recordings. Thus they could detect instances during sliding when one junction predominated, undisturbed by short-circuiting. The surprising result observed was that even at relatively slow speeds and low pressures some temperature peaks correspond to the melting point of the lower melting material and that this also proved the limiting temperature at higher speeds and pressures. It therefore seems reasonable to expect that under the much more severe conditions in metal cutting, even at very low speeds, there will be some junctions at the melting point of the work material. Accordingly any attempts to measure peak temperatures would seem to have little practical value, as this would always indicate the same value, regardless of speed. Since speed is known to have a very important effect on tool life, it is obvious that life is not a function of the maximum temperature, but of an average temperature.

The important question, of course, is whether the average temperature as determined by the thermocouple measurement is the same as the average temperature which is assumed to control the tool life. Lacking an alternative they are usually taken to be the same. Only a long series of tedious life-temperature tests can answer this question; there is very little such data in the literature, beyond the important paper by Shallbroch and Schaumann (27).

An important experimental limitation in this measurement arises from the built-up edge. When the presence of a built-up edge prevents direct contact between the tool and chip, the calibration conditions no longer exist and the emf measured loses its meaning. The very small, invisible built-up edges, which Shaw and Strang (32) have shown to be present even under the most favorable cutting conditions, need not cause concern, because as long as such a layer of work material is thin enough to prevent a large temperature gradient across it, the results are not affected. A large built-up edge, besides being unstable and altering cutting conditions, introduces a material of unknown thermo-electric properties and a large temperature gradient across it, for which no correction is possible. The thermo-color technique, however, might be a practical way to investigate this particular point.

The magnitude of the thermal emf generated under cutting conditions is an important factor, since it determines the instrumentation required and the accuracy obtainable. As might be expected from their greater dissimilarity, carbide tools give an emf about three times as great as high speed steel tools when cutting steel. This gives carbide a considerable

advantage in helping to cut down the influence of extraneous errors. The shape of the emf-temperature calibration curve can also have an important effect on results. A typical curve is shown in Figure 9 below. In the ideal case, the useful range of temperature covers the shape between (2) to (3), but in practice all possible combinations have been observed. Obviously when working in the range between (1) and (2) or (3) and (5) ambiguous results are possible and accuracy greatly reduced. As actual calibration curves will show, such difficulties do not appear with carbide tools.

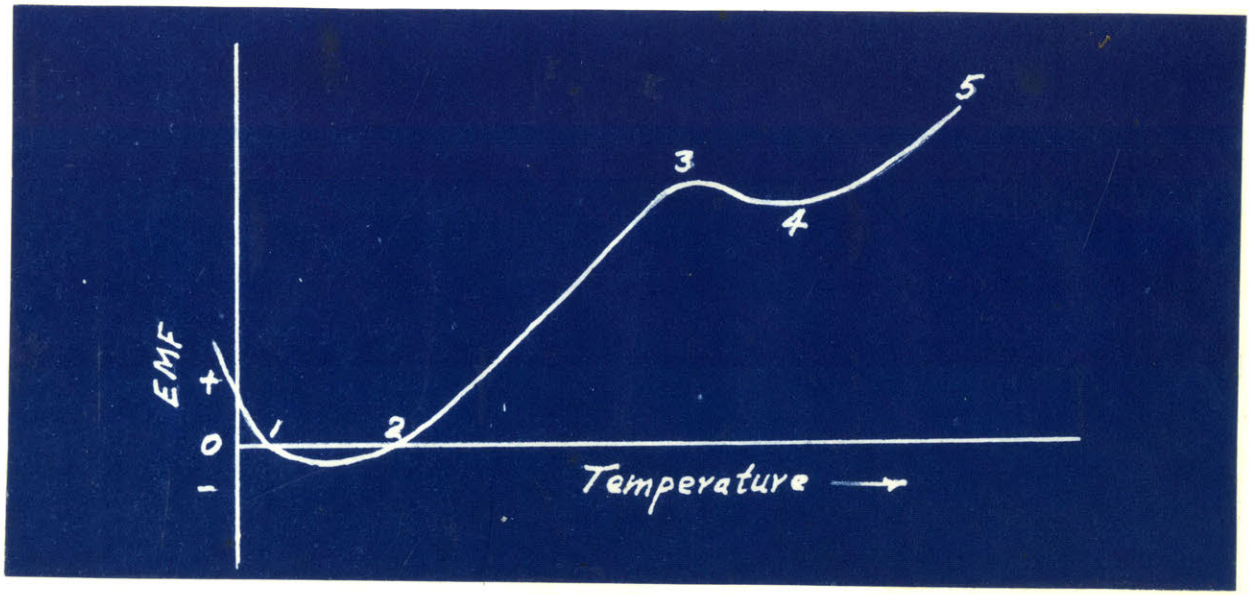


Figure 9.

Representative Temperature Calibration Curve.

A seemingly foolproof method of getting rid of all calibration troubles was proposed by Reichel and Gottwein (11) and was widely accepted in German industry. This is the so-called two-tool method illustrated on the following page. Here two geometrically identical tools are made to cut the workpiece simultaneously. Assuming the

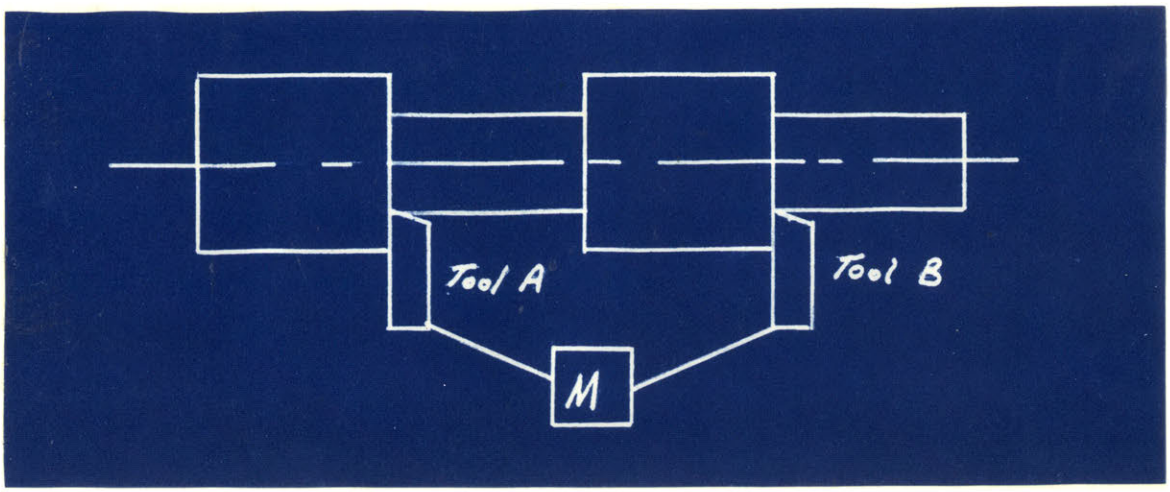


Figure 10.

Two-Tool Thermocouple method.

temperatures at the two tools to be the same, the emf produced between them is indepehdent of the thermo-electric properties of the work material, which therefore does not need to be determined. Only a calibration of the two tool materials is needed. As Lang (14) came to recognize much later, the method falls down on its basic assumption, in that temperatures at the two tools will not usually be the same, especially when they are of widely different materials, which is desirable from the thermo-electric viewpoint. This can be attributed to the varying coefficients of friction, and the different thermal conductivities of various materials.

As Shore pointed out in his original thesis, it is sufficient from a thermo-electric viewpoint if either the tool or the work are insulated ffom the machine. In this work, it turned out that insulating the workpiece alone proved entirely adequate.

## CALIBRATION OF TOOL-WORK THERMOCOUPLES

If temperature measurements of different experiments are to be reduced to a common denominator, it must be done in terms of degrees of temperature. Measuring thermal emf values alone can only serve for comparison, for a single tool-work combination, and even then can be misleading if the calibration happens to be non-linear.

Accurate calibration of the tool-work thermocouple combination is a surprisingly difficult job. The reason is chiefly a geometric one, in that neither material is likely to be in wire form, and any attempt to convert them to wire, could change their thermoelectric properties. Thus the usual standardized techniques for thermocouple calibration cannot be used.

Under the circumstances the most obvious method is to bring the tool and work into intimate contact (no oxide films) at one point, heat this junction, and measure the resulting emf, as well as that of a reference couple placed at the same junction. This method will be termed direct calibration.

There are several ways in which the tool and work materials might be brought together with the necessary good contact. One is to actually take a cut, on a lathe or drill press for instance, and stop the machine mid-cut and perform the calibration on the machine. This has the advantage of assuring a very clean contact, but suffers from the fact that machine tools are not easily converted to furnaces. Heating the junction uniformly and making sure the reference couple measures the same temperature are the principal difficulties.

Another method would be to clamp the two materials together with a C-clamp. This allows small contact areas, but is liable to be clumsy and unreliable if calibration up to high temperatures (1500°F) is intended.

A third method, and one used for part of the present work, depends on silver soldering the two materials together and burying the reference couple in the soldered joint, or immediately next to it. This is the method used for all "direct" calibrations. Making a satisfactory joint is the most difficult part of the procedure. An objection to the method lies in the fact that in silver soldering the temperature of the two pieces must be at least 1600°F, even if only for a short time (about 10 seconds), and that this can bring about metallurgical changes which might alter the thermoelectric properties. The silver itself should introduce no errors as long as it remains at a uniform temperature. This condition is not hard to meet, since the layer need not be much more than .010" thick and silver is a good conductor, Figure 11 shows a schematic diagram of the set-up.

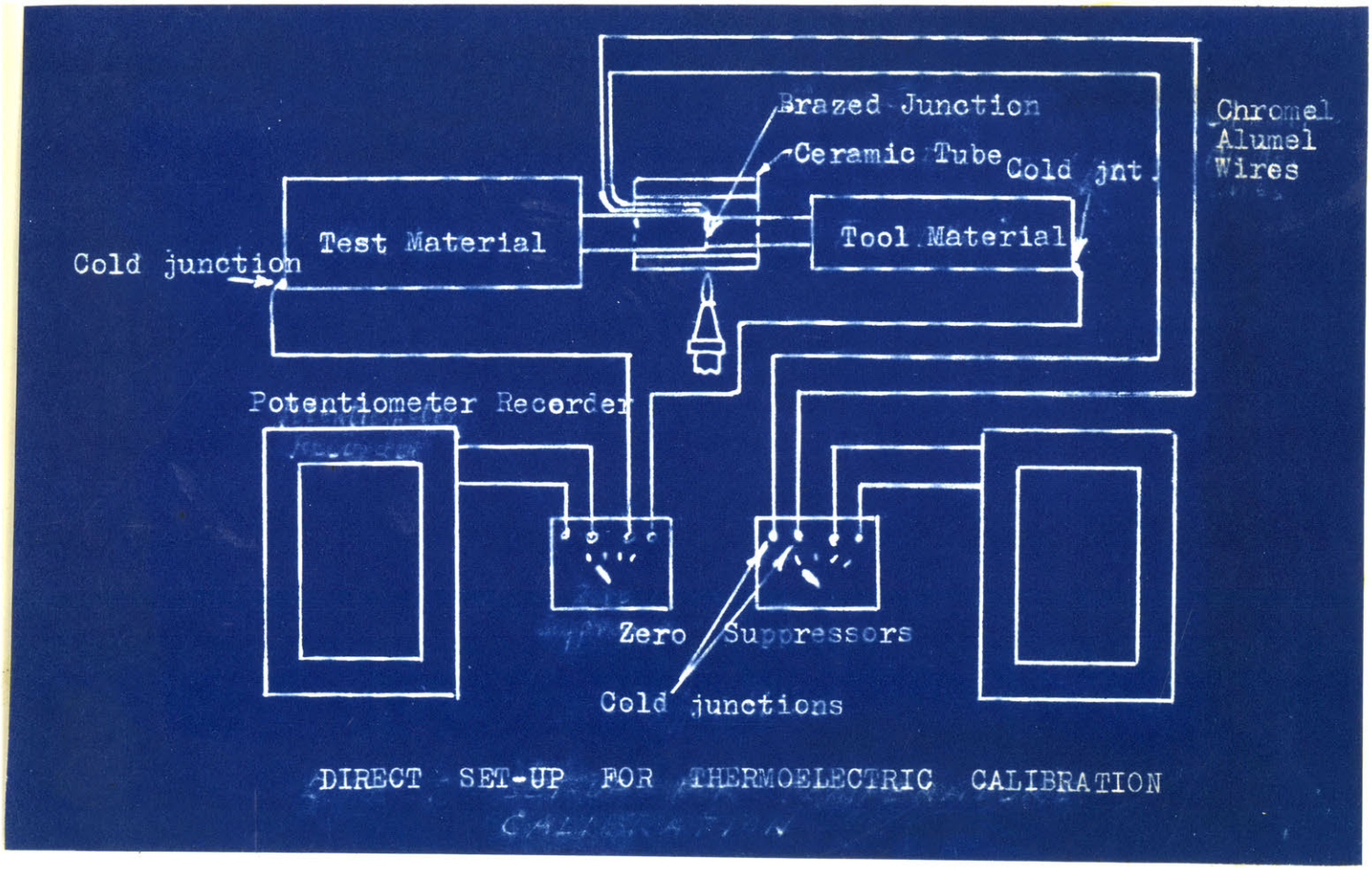


Figure 11.

A fourth method would be to insert the ends of the two materials, this time not joined together, and the reference couple, into a bath of molten metal. If the liquid metal could be maintained at a uniform temperature, to avoid introducing thermal emf's of its own, this would seem to be a simple method. However, heating should be fast enough to allow the cold ends of the test pieces to remain so.

One of the major difficulties in direct calibration is to keep the reference couple at the same temperature as the tool-work junction. This is because of the relatively high temperature gradients involved at this

point. Fortunately in this respect the calibration is self-checking when readings are taken both during heating and cooling cycles. If the reference couple is too exposed then it will read too high on the heating cycle and too low on the cooling cycle, resulting in the appearance of an hysterisis loop, as indicated below. Should the position of the couple be reversed then a loop such as that drawn dotted will result.

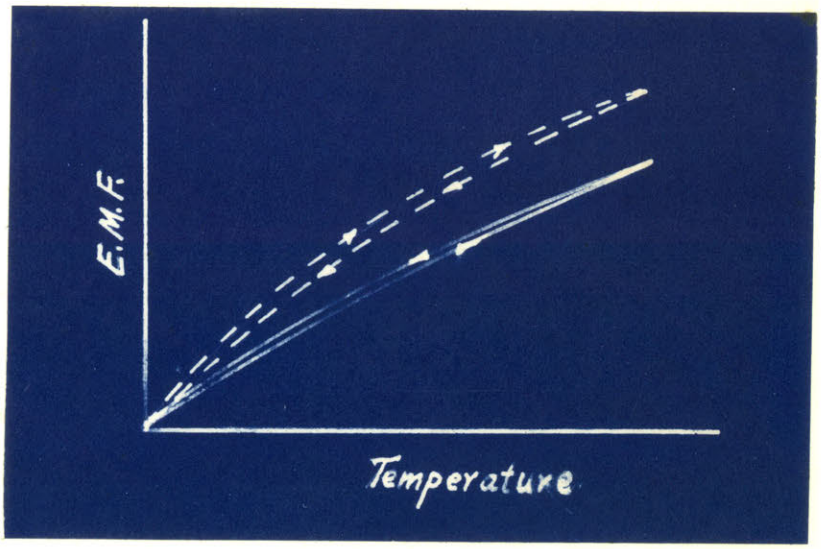


Figure 12.

Possible Shapes of Temperature Calibration curves.

Experience has shown that in neither case is it safe to draw an average line through such a hysterisis loop, due to non-linearity of the effect. Lack of such a loop, in addition to repeatability, is a good indication of the precision of the calibration.

Indirect Calibration

There are several objections to the direct calibration method as outlined above. One is the large number of heating and cooling cycles

the tool material is subjected to whenever a series of materials is to be calibrated. A more important objection is the relative cumbersomeness of the direct method and the time consumed, which allows no more than two calibrations in one day.

Both these objections can be overcome by recalling that according to the laws of thermo-electricity the thermal emf between the thermal emf's of these two materials against a third or standard material. Such a standard material can be chosen quite arbitrarily, but obviously a reproducable, thermodynamically stable material is indicated. Nothing could be simpler, therefore, than to use one of the two wires of the reference couple itself (e.g. chromel-alumel) as the reference. For use with carbide tools alumel is an ideal reference material, since it has a low emf compared to carbide. This then allows the use of the simple

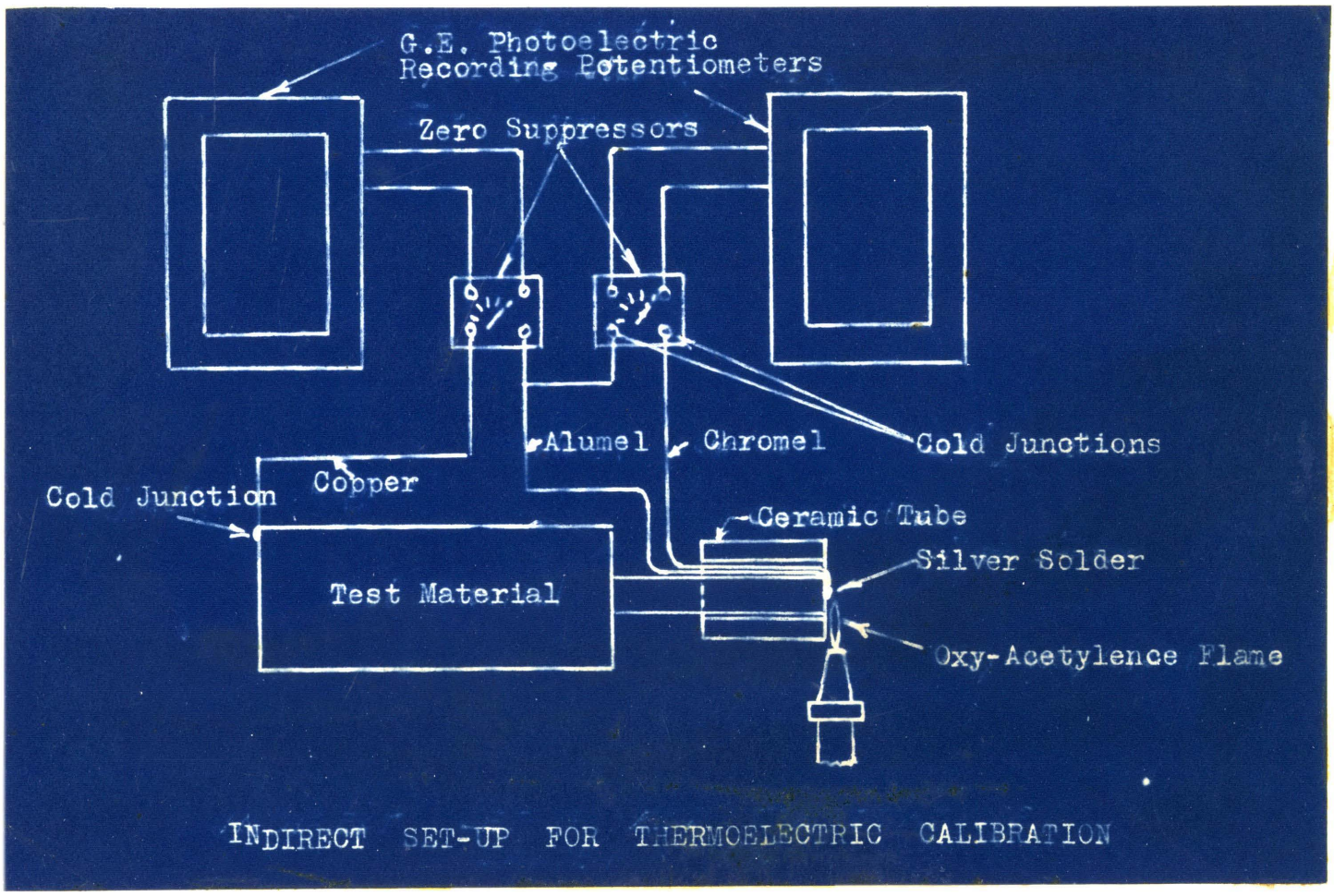


Figure 13.

set-up shown on the previous page, which can be prepared in a fraction of the time required for direct calibration.

Except for the first one, all the methods for heating in the direct method are also applicable here. The method used for all the indirect calibrations in this work was to insert a chromel-alumel couple in a little bead of silver solder at the tip of the test material and then heat the junction with a bunsen burner. For a permanent set-up, however, the liquid metal bath probably would prove superior and simpler. It also would eliminate the problem of momentary high temperatures when applying the silver solder. It turned out that Bickel (1) had developed a very similar technique, even to using alumel as the reference material. In calibrating he clamped the wires to the test piece, rather than use solder, but as a result could not calibrate above 1000°F. The silver solder technique allows a temperature of 1500°F to be reached in calibration in three minutes, the cooling cycle taking about 10 minutes. This is a very important advantage when only small pieces of material are available for calibration, as with a small total heat input it is possible to keep the cold end of the test piece at room temperature. When this is not possible, a separate thermometer or thermocouple is needed at the "cold" end to measure the temperature, and then correction can be made for the emf between the test piece and the copper connecting wire. This, of course, calls for another calibration of test-piece vs. copper emf. As the correction is a small one this can be done accurately enough by observing the emf between room temperature and boiling water. Automatic recording potentiometers are essential for such fast calibration. Figure 14 shows the experimental set-up used.


Figure 14

Overall view of Indirect Calibration set-up. Work piece is mounted on stand in front of oxy-acetylene torch. G.E. photoelectric Recording Potentiometers record emf of chromel-alumel couple and alumel-work couple. Brown self balancing potentiometer used to measure temperature at cold end of work piece, to allow necessary corrections to be applied.

The question arises as to whether it is legitimate to calibrate unstrained work material, when during cutting the chip has undergone severe straining. Trigger (41) attempted to check this by pressing a hard steel ball into a soft steel piece under high pressure, but could detect no emf between the two. Pigott and Richardson (31).checked it by noting that a furnace calibration with parts merely clamped together gave the same results as a calibration performed with a tool stopped in mid-cut on a lathe. However, a much simpler and more accurate check can be made by dipping the end of the workpiece as well as a chip formed from it into a bath of molten metal and see if there is an emf between the two.

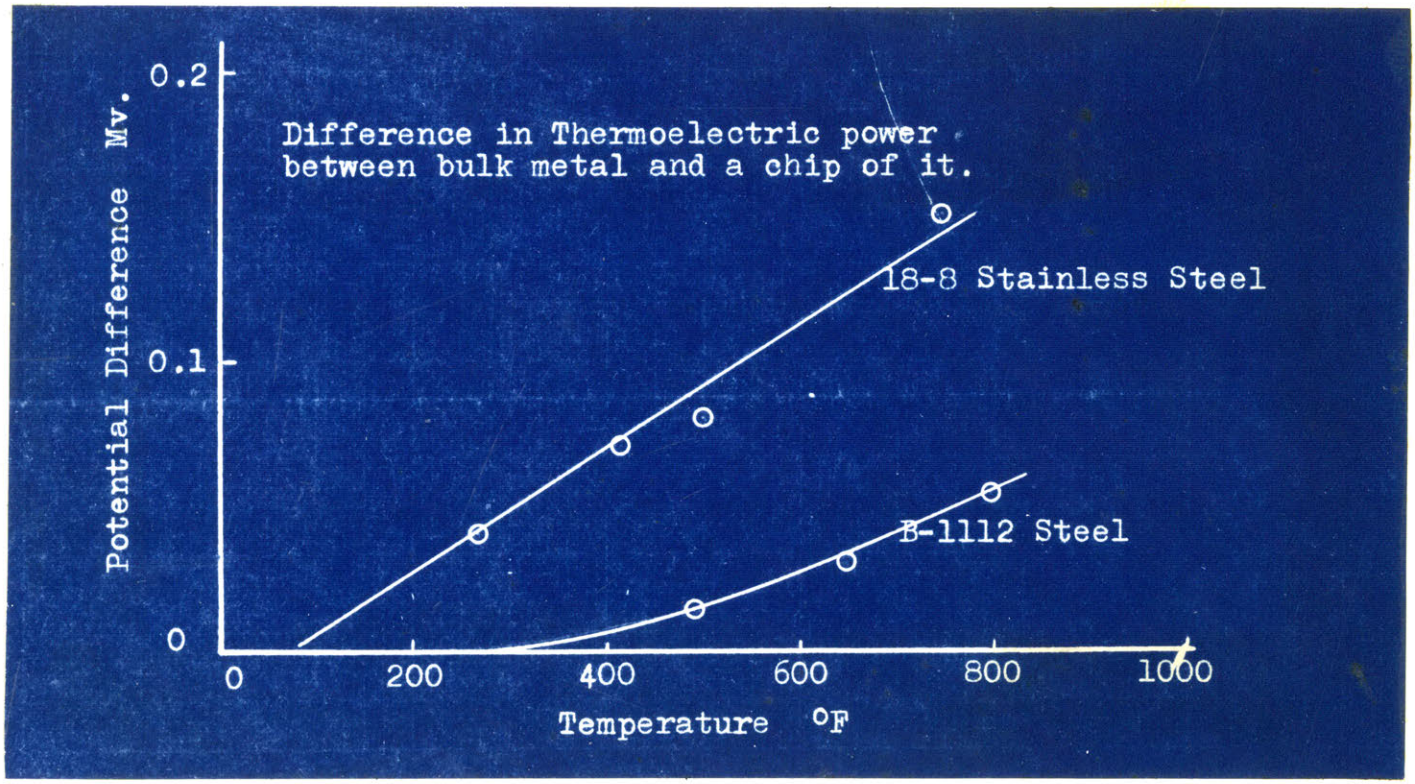


Figure 15.

EMF between bulk material and chips from the same material.

The results obtained such an experiment, for 18-8 and B1112 steels are shown in Fig. 15. Assuming the chip to have the correct thermoelectric properties, rather than the bulk metal, the polarities are such that with high speed steel tools the bulk metal calibration curves give results that are slightly too high, with carbide tools the opposite being true.

It is clear that with those materials capable of producing continuous chips, a very simple calibration set-up is possible, with the specimen consisting merely of a long enough chip. Such a set-up is sketched in the diagram below.

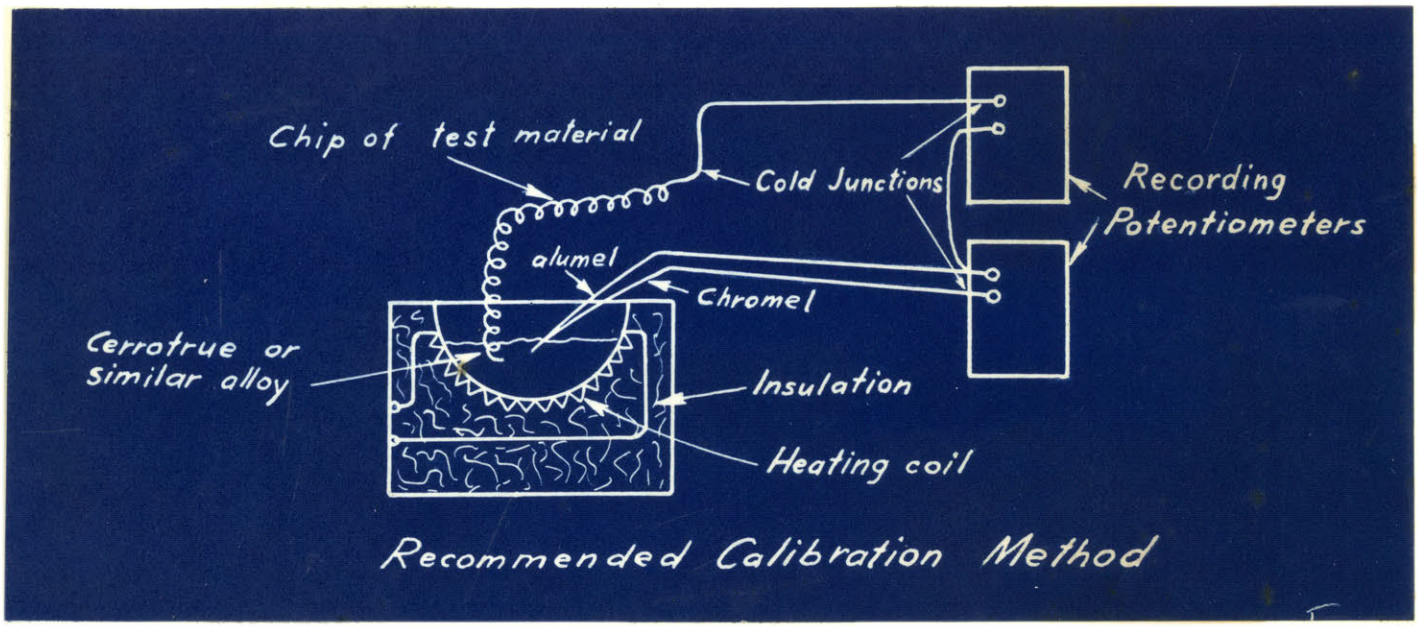


**Figure 16.**

Simple Calibration method when chips are available.

The question whether the indirect calibration method can give as good results as the direct is resolved by noting the comparison of the two methods, in the case of 4340 steel vs. high speed steel, as shown

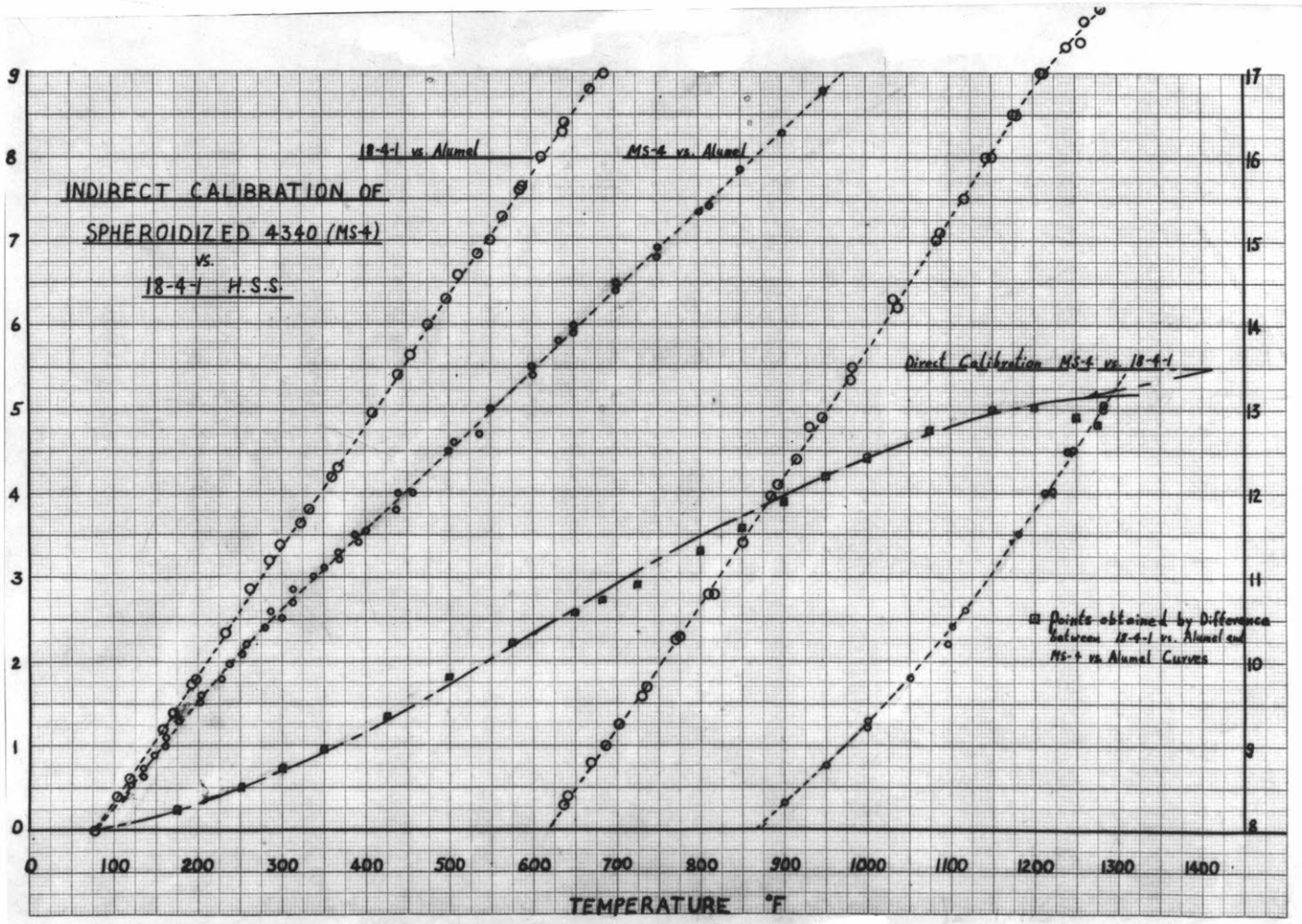


Fig. 17

INDIRECT CALIBRATION OF 4340 STEEL VS. 18-4-1 HIGH SPEED STEEL

18-4-1 vs. Alumel (large circles) 4340 vs. Alumel (small circles) plotted in two sections (see L.H. and R.H. scales) to increase accuracy. Squares used to represent difference between the two curves. Dashed line is traced from previous direct calibration of 4340 vs. 18-4-1.

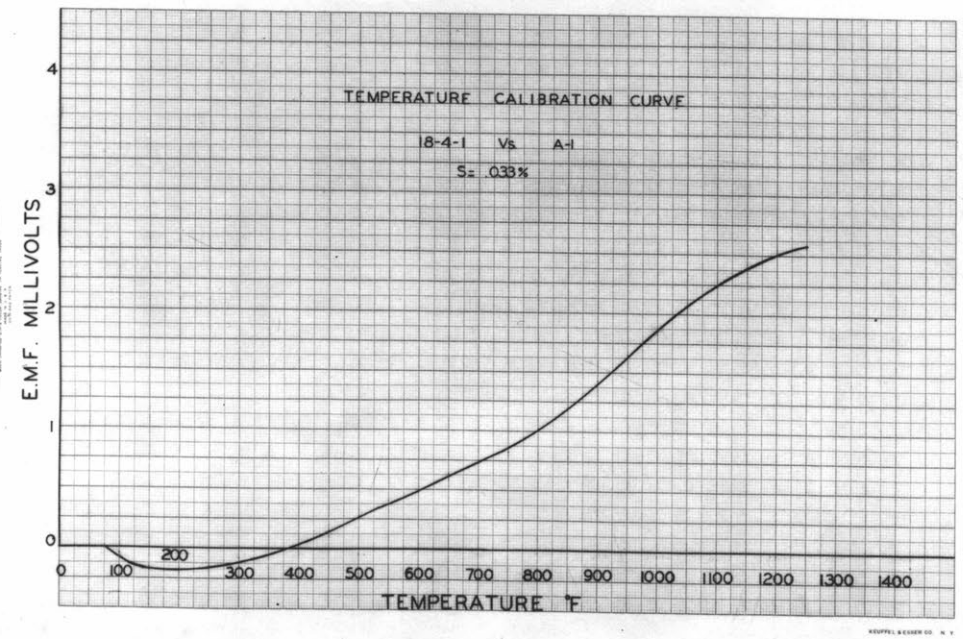
TEMPERATURE CALIBRATION CURVE
18-4-1 Vs. A-1
S= .033%
E.M.F. MILLIVOLTS
TEMPERATURE °F
0 100 200 300 400 500 600 700 800 900 1000 1100 1200 1300 1400
0 1 2 3 4

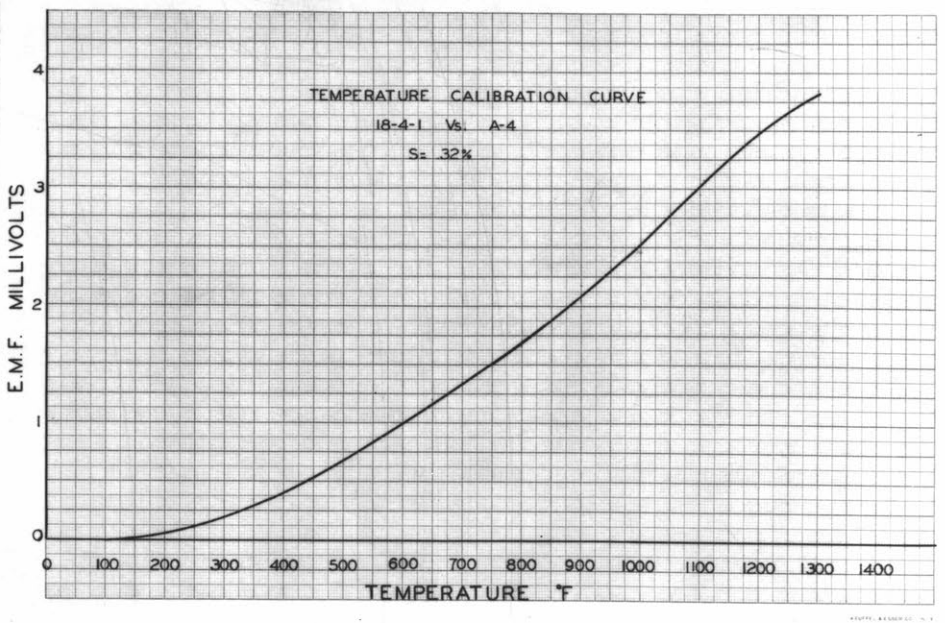
TEMPERATURE CALIBRATION CURVE
18-4-1 Vs. A-4
S= .32%
E.M.F. MILLIVOLTS
TEMPERATURE °F
0 100 200 300 400 500 600 700 800 900 1000 1100 1200 1300 1400
0 1 2 3 4

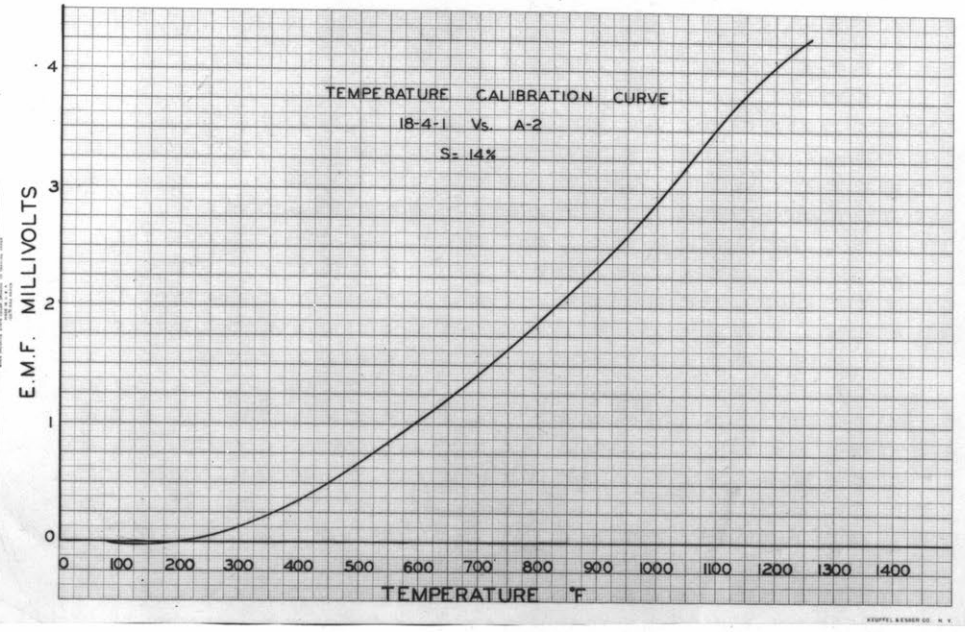
TEMPERATURE CALIBRATION CURVE
18-4-1 Vs. A-2
S= .14%
E.M.F. MILLIVOLTS
TEMPERATURE °F
0 100 200 300 400 500 600 700 800 900 1000 1100 1200 1300 1400
0 1 2 3 4

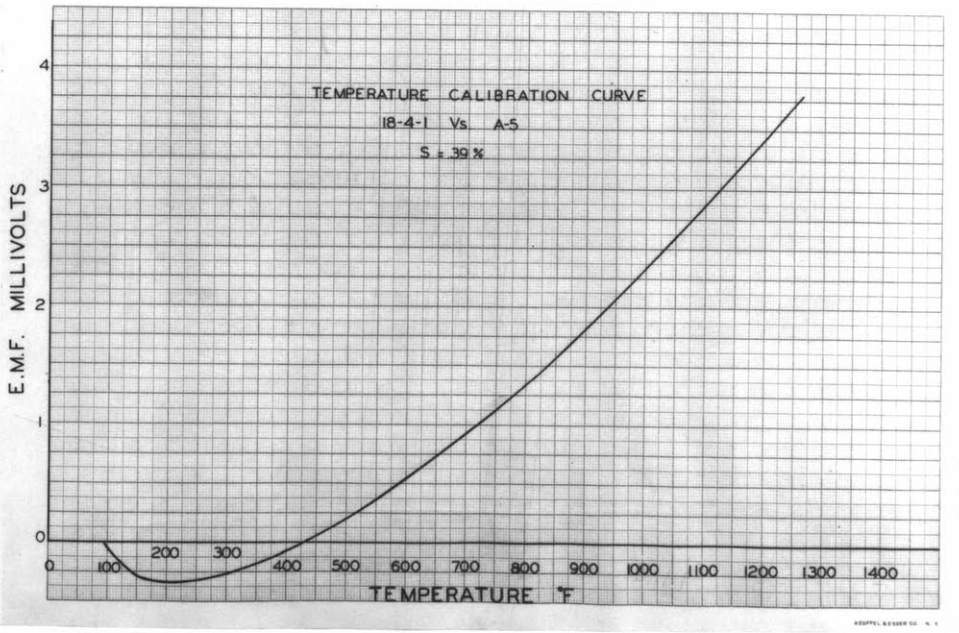
TEMPERATURE CALIBRATION CURVE
18-4-1 Vs. A-5
S = .39%
E.M.F. MILLIVOLTS
TEMPERATURE °F
0 100 200 300 400 500 600 700 800 900 1000 1100 1200 1300 1400
0 1 2 3 4

Fig.18

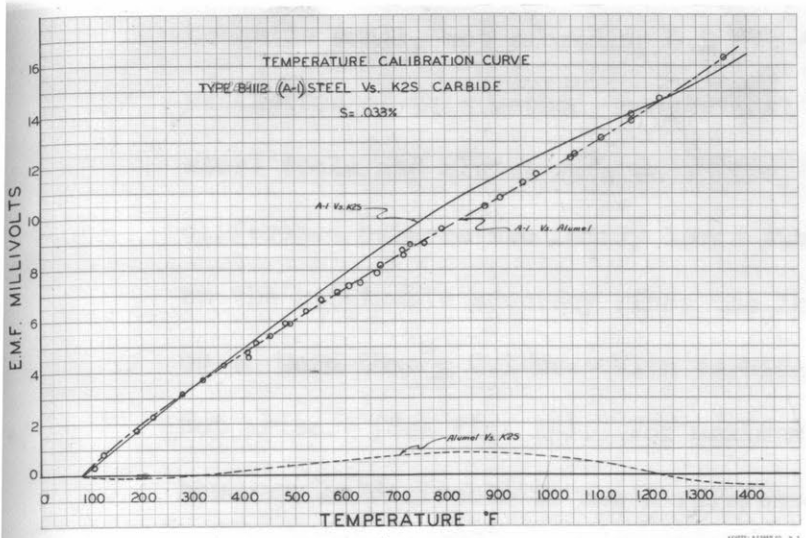


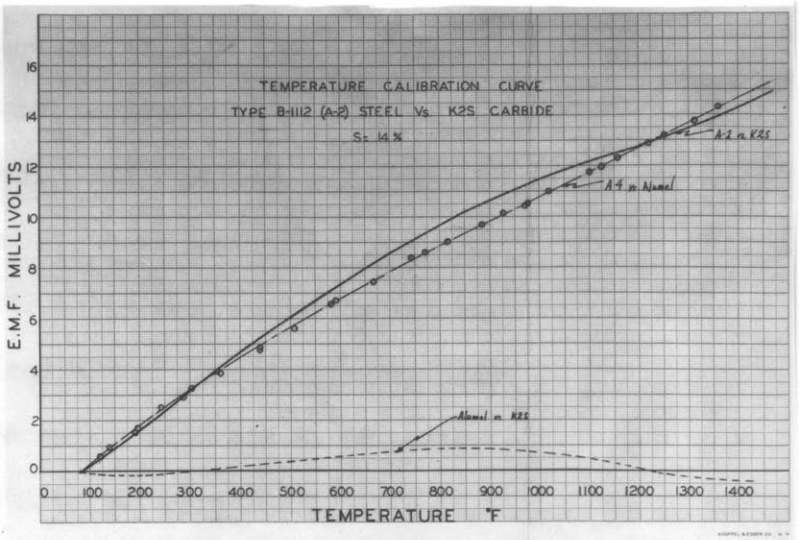


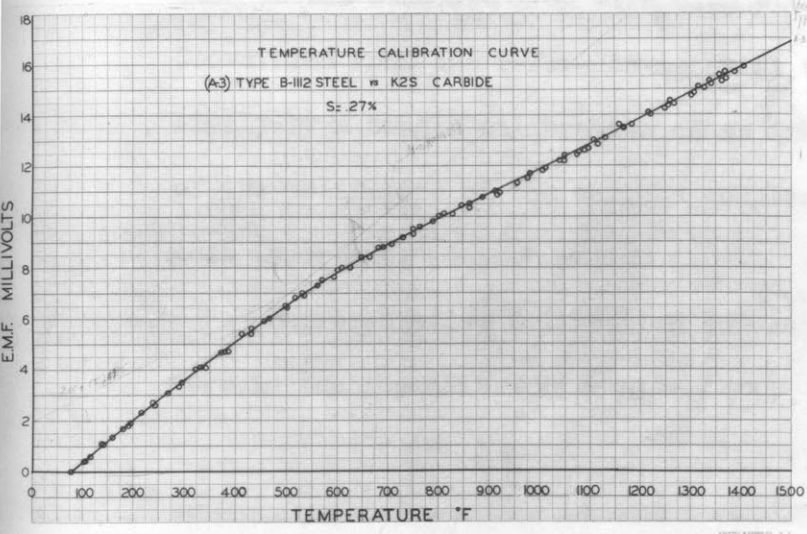


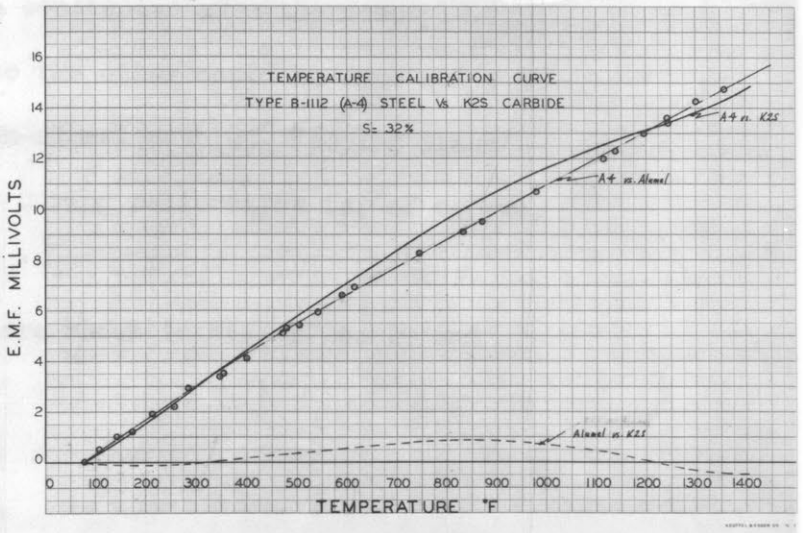


**Fig. 19**

TEMPERATURE CALIBRATION CURVES OF TYPE B-1112 STEELS CONTAINING VARIOUS AMOUNTS OF SULPHUR, AS SHOWN, VS. K2S CARBIDE.

Curve with 0.27% Sulphur steel obtained by direct calibration, all others by indirect calibration.

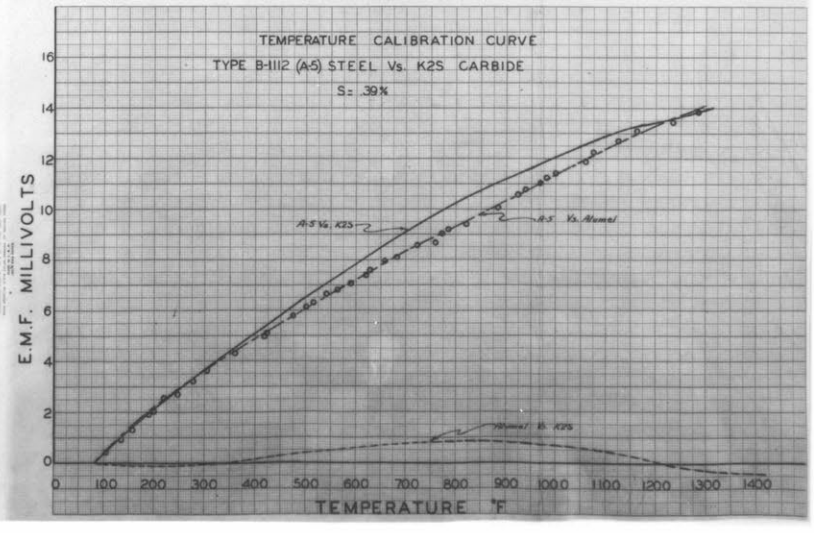

in Fig. 17. The maximum difference between the two methods is seen to be quite small, not exceeding 0.2 MV. The graphs also show one of the weaknesses of this method, namely that when dealing with high speed steel tools and alumel reference wire, the final result depends on the difference between two fairly large numbers, which naturally cuts down on the attainable accuracy since the instruments used cannot be relied on to more than ± 0.1 Mv. With carbide and alumel this difficulty does not arise. (See Fig. 19). For maximum accuracy with H.S.S. it would, however, be desirable to use a reference material more nearly like it, such as the standard iron wire used with constantan as a thermocouple. Conversion from one reference material to the other could be done quite simply by a single calibration of an iron-alumel couple. Keeping track of the polarities of the various couples during calibration is, of course, most important.

Representative Calibration curves are shown in Fig. 17 to 19 and more in the Appendix. (Fig.70 to 73).

EFFECT OF METALLURGICAL STRUCTURE ON THERMOELECTRIC PROPERTIES AND ALLOY CONTENT.

The effect of heat treatment on thermo-electric properties of steels is of particular interest here, since it may have a direct influence on the results obtained in metal cutting. Not much work seems to have been done along these lines in the past. Dupuy and Portevin (7) measured the thermal emf's of a large number of steel alloys against copper, but only between $0^{\circ}C$ and $-78^{\circ}C$ and between $0^{\circ}C$ and $100^{\circ}C$. They were unable to draw consistent conclusions from their results. This is not surprising, since curvature of the calibration curves can result in misleading interpretations when measurements are made at just three fixed temperatures. With modern instrumentation far more complete data could have been obtained with equal effort.

The result obtained from a large series of calibrations was that hardness alone, or the degree of tempering, has a definite effect on the thermal emf's, which usually, but not always, decrease with increased hardness (as measured against 18-4-1 High Speed Steel). This result is rather surprising since all the results, such as that shown in Fig. 20, were obtained by direct calibration (i.e. with a silver soldered junction), and the soldering must have raised the junction past the transformation point before any calibration took place. Yet in each case the curves were repeatable in successive heating cycles, as well as after resoldering the junctions several times. While this may merely indicate that any possible change took place during the first brazing, this makes the clear differences between samples of steel which differed only in their heat treatment even more surprising. This point would bear further investigation

as there appears to be no logical explanation of this.

In checking the effect on Spheroidized 4340 of several brazing and heating cycles the heated end of such a sample was inserted in a bath of molten cerrotru at 600°F together with a sample previously unheated, and the emf between the two measured. The resulting emf of 0.05 Mv is quite negligible.

In all these tests a long bar of 18-4-1 high speed steel served as the reference. Repeated checks showed that even after 50 heating and cooling cycles there was no noticable change in its thermo-electric properties. This probably means that changes, if any, took place during the first brazing. This was confirmed later when the reference bar and an unheated tool were both dipped in molten Cerrotru at 700°F and an emf of 0.25 Mv was measured between the two, introducing a corresponding uncertainty in the results.

## TEMPERATURE MEASUREMENT WITH CARBIDE TOOLS

The high thermal emf values between Tungsten carbide tool materials and steel would seem to make carbides ideal materials to use in thermoelectric temperature tests, since both measurement and calibration become simpler and less subject to errors when voltages become large. However, in practice difficulties arise because the cost involved makes it impractical to use solid carbide tools of the size required in the present test set-ups. The usual procedure is to make up tools by brazing a carbide insert or tip onto a soft steel shank. If the end of the steel shank is used as the cold junction connection, which is the simplest method of course, it is clear that another source of emf is added to that of the tool-work junction in the thermoelectric circuit. As soon as the carbide shank interface becomes heated above room temperature, an emf is generated at this point. Trigger's (41) solution was to make a tool as shown in the sketch below, in which contact is made with the carbide tip

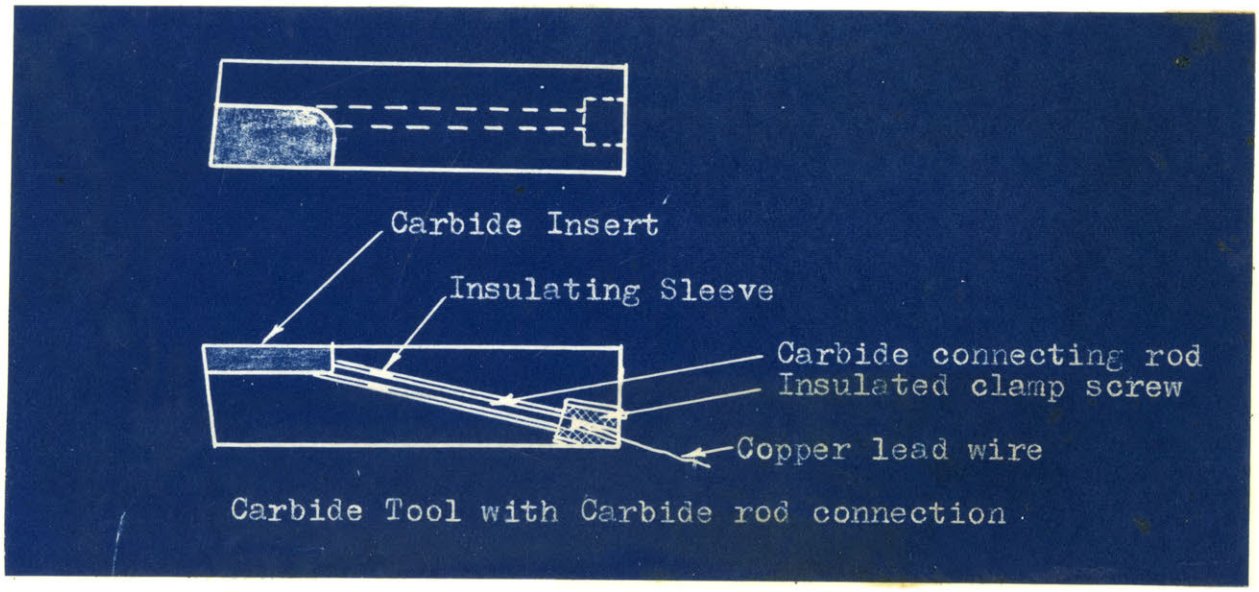


Figure 21.

by means of a rod made of the same batch of carbide as the tip, and therefore presumed to have identical thermoelectric properties. It is not difficult to maintain the cold end of this rod at room temperature, unless very long continuous cuts are taken. The disadvantage of this method lies in the expense of the special tool shanks, the extra effort involved when tools are changed, and most seriously the considerable expense involved in having both rods and tips made from the same batch of carbide.

Theoretically this method is still open to objections, since quite regardless of the method used to establish contact with the carbide tip, a temperature differential along the brazed section will give rise to parasitic currents, such as have been sketched in the diagram below,

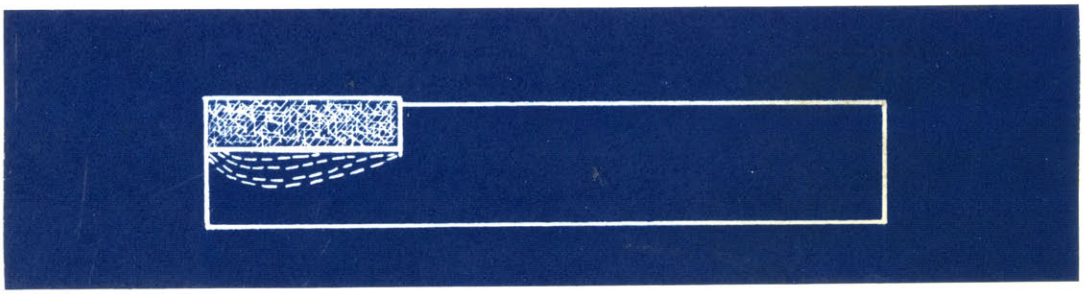

Figure 22.

and which can reduce the net emf output. Experiments have shown that with small tips this effect is not important, but work by Sze (MIT thesis, 1950) indicated that with a 2 inch long strip of carbide considerable trouble can be expected. The simplest solution to this problem would be if carbides could be brazed or cemented to the shanks with a non-conducting

material. However, none of the cements experimented with proved capable of holding the carbide properly. The solution actually used is described below.

In order to obtain an idea of the order of magnitude of the effectiveness of the carbide rod, a cutting experiment was run with a tool such as shown in Fig. 21. The recording potentiometer was connected alternately to the end of the carbide rod and to the tool shank by means of a SPDT microswitch. The results are plotted in Fig. 23. At the higher speeds, with the accompanying higher temperatures, it is quite evident how the emf at the carbide-tool shank interface builds up to reduce the indicated emf, when connection is made to the steel tool shank. At the same time the output as measured from the end of the carbide rod remains fairly constant, in fact rises slightly with time in one case. As might be expected, the difference between the two methods becomes greater as the cutting speed is increased. The effect is also made relatively large by the thin section of the carbide tip, only .090 inches thick. Parasitic currents do not seem to have influenced these results.

All of these precautions become relatively unimportant when only very short test runs are made and relatively thick carbide tips are used. In that case, there is not enough time for the brazed junction to be heated above room temperature and therefore no emf can develop there. Since nearly all the experiments reported on in this thesis were very short ones, and since the higher the speed (and temperature) the shorter the run, it appeared justifiable to ignore the elaborate precautions and make the cold junction connection with the shank of the tool. The carbide tips used were all 1/8 inch thick and some of the high speed runs less than 2 seconds in duration.

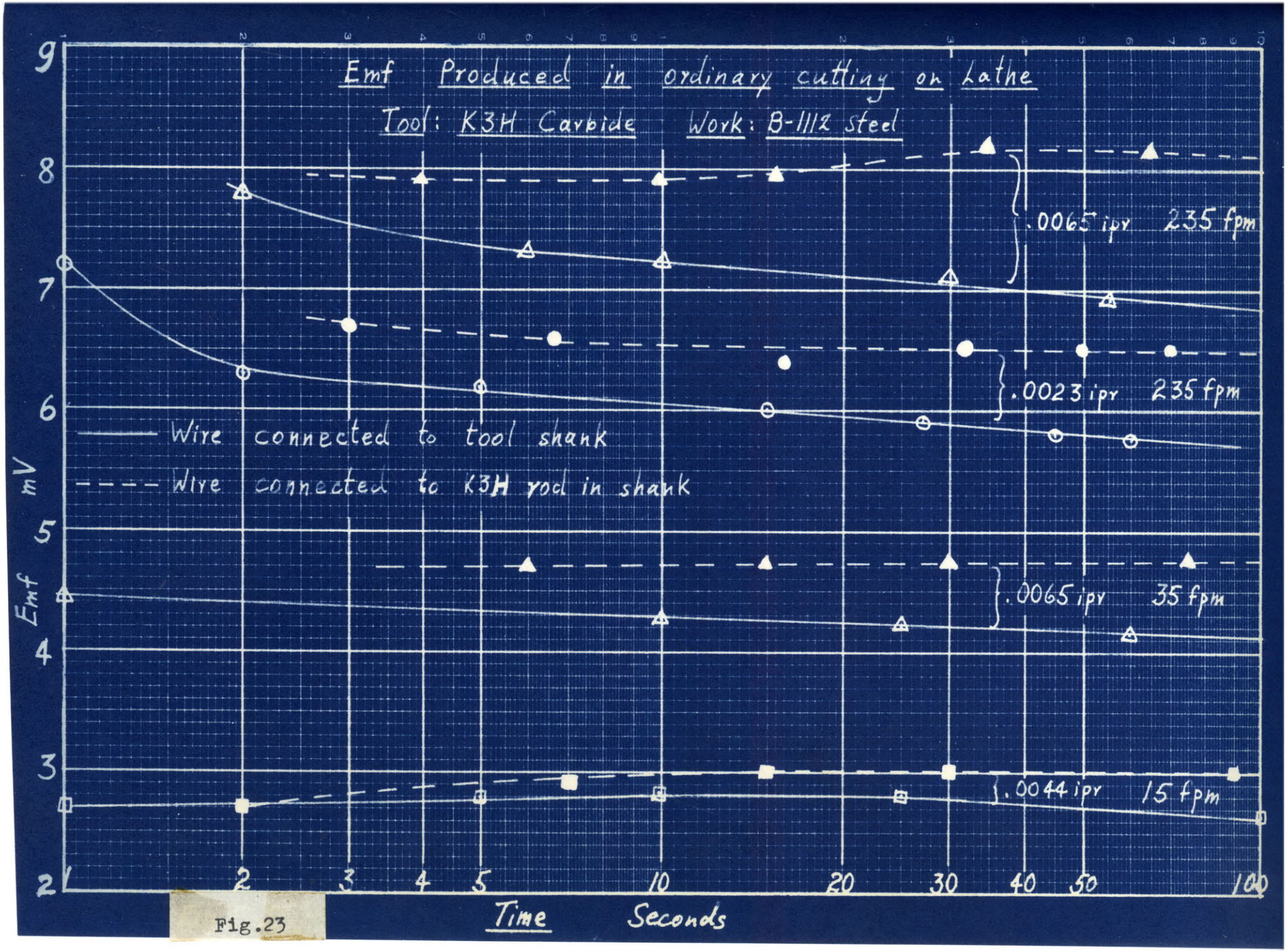
Emf Produced in ordinary cutting on Lathe
Tool: K3H Carbide Work: B-1112 steel
.0065 ipr 235 fpm
.0023 ipr 235 fpm
.0065 ipr 35 fpm
.0044 ipr 15 fpm
Wire connected to tool shank
Wire connected to K3H rod in shank
Emf mV
Time Seconds
9
8
7
6
5
4
3
2
1
2
3
4
5
10
20
30
40
50
100

Fig.23

Probably the best solution to the difficulties of measuring with carbide tips is to use Bickel's artificial tool junction (see p.11). In fact Alumel wire has thermoelectric properties so similar to some carbides that in some cases a single alumel wire clamped or soldered at the far end of a tool tip is sufficient to eliminate all troubles.

## THE EXPERIMENTAL SET-UP

Practically all the cutting experiments reported on in this thesis were orthogonal type cuts, performed on a Monarch CK 12" lathe, in the Machine Tool Laboratory of M.I.T. As work materials are usually available only in the form of solid bars, it is necessary to reduce them to tubes in order to cut under the orthogonal (2-dimensional) conditions desired for simplified analysis. This was accomplished by means of a special trepanning or grooving tool mounted upside-down on the rear of the tool cross-slide. One of the advantages of this method over straight boring out of a tube is that it leaves a solid piece of metal in the center which not only makes the set-up much more rigid by allowing the use of a tail-stock center, but leaves enough material for running other tests on the material, such as a tensile test. It also provides greater control over concentricity and wall thickness.

A specially designed dynamometer (see Fig.1) was used to measure the vertical (cutting) force and the horizontal transverse (feed) force, there being presumably no component along the tool axis when cutting under orthogonal conditions. Cutting temperatures were measured by the tool-work thermocouple method. A sketch of the entire set-up is shown in Fig. 23, while Fig. 24 shows a photograph.

The accuracy of force measurement is limited only by that of the calibration and that of the amplifying and recording system. However, superimposed on this, and effectively limiting the attainable accuracy, are small random fluctuations in forces observed during a run, caused in part by inhomogenuities in the work material and slight variations in chip formation. The built-up edge, which is completely absent only in exceptional

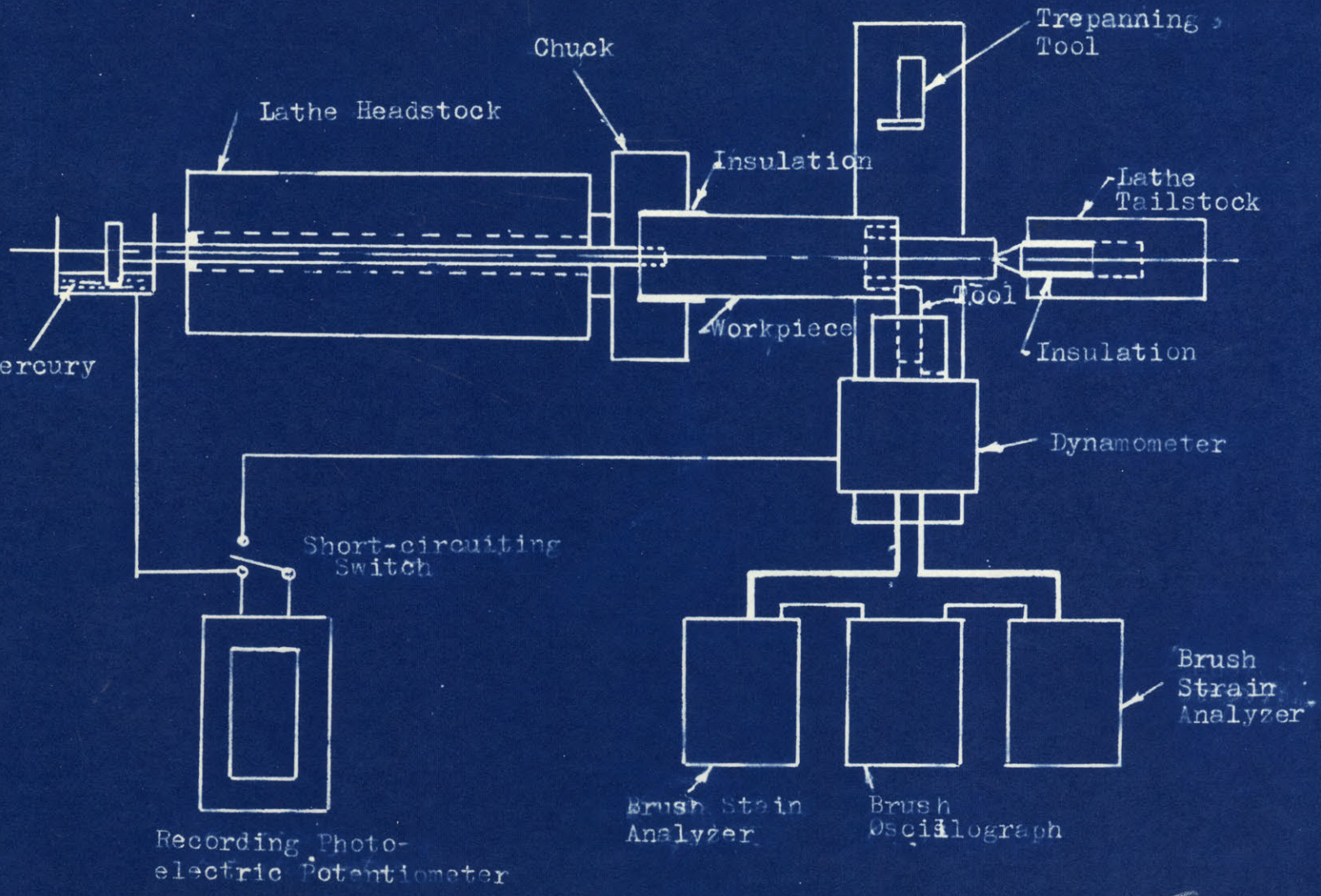


SCHEMATIC DIAGRAM OF LATHE SET-UP FOR TEMPERATURE AND FORCE MEASUREMENTS IN ORTHOGONAL CUTTING

Fig. 23

Fig. 2?

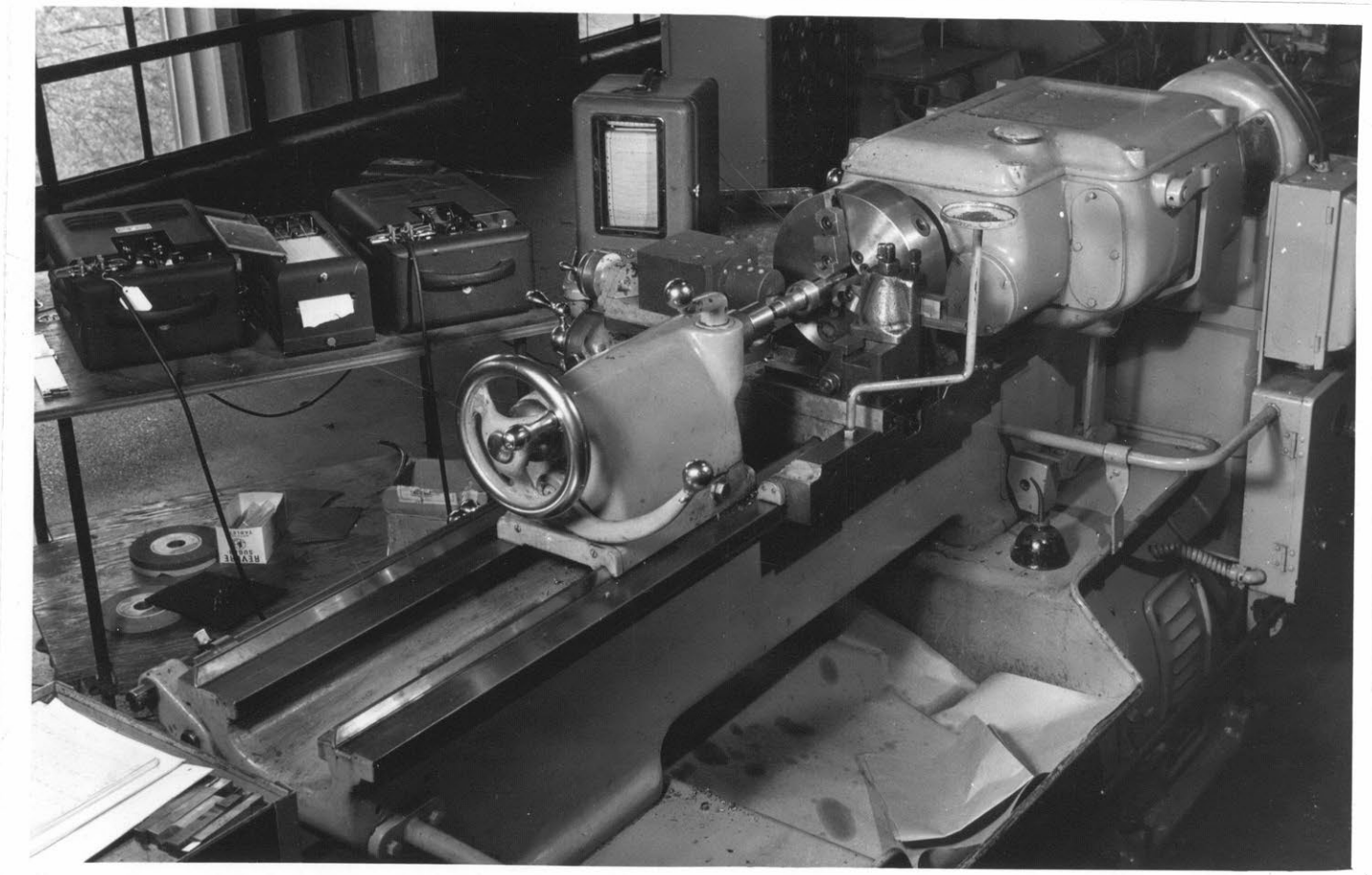

Figure 24

Monarch 12" Ck. Lathe set-up with Model L-4 Lathe Dynamometer on compound slide, grooving tool on rear of cross-slide, insulated live center in tailstock. Brush Strain Analyzers used to record cutting forces. G.E. photoelectric Recording Potentiometer used to measure tool-work emf.

circumstances, and which often is produced under random conditions, is probably the chief villain when it comes to precise metal cutting measurements of all kinds. With this in mind the force measurement has a probable error of 10% associated with it, although occasional errors twice as great are possible. Usually in such cases it is standard procedure to cut down the probable error by taking mean values of a large number of tests. Unfortunately this course could not be followed here for two reasons. One was the very limited amount of material available of some specimens (bars 1 7/8" diam. only 7" long) from which runs under as many different conditions as possible were desired. The other was that even when more material was available the time involved in repeating several hundred runs several times was prohibitive, so that in this case available precision was sacrificed in favor of covering a very wide range of conditions. The alternate procedure adopted was to repeat a few runs chosen at random. Repetition was usually within 10%, and few differences exceeded 20%. It seems clear that claims of 2% accuracy in metal cutting forces can rest only on a statistical basis.

The width of cut was usually determined by measuring the width of the chip with a micrometer, which is simpler than measuring the wall thickness of the tube being cut, and the loss in accuracy, from 1/2% to 2%, is not important.

The chip contact length is difficult to measure accurately, since it can be obtained only be observation of a tool after a cut. Unless the boundary is unusually well defined .001" is the maximum attainable accuracy; when a large built-up edge is present the measurement becomes not much more than a guess. This subject is also discussed in detail later.

The thermo-electric voltages were measured with a G. E. Photo-electric recording Potentiometer, probably the best instrument available for this kind of work. It has a response speed up to 4 cycles/sec., chart speed of 3"/min., and ranges adjustable from 0.2 to 50 millivolts full scale, with an accuracy of 3% in the useful range (above 1 Mv). This is entirely adequate since slight variations during a cut usually exceed this value. Even a small built-up edge can have a considerable effect on the voltage measured, and is the real limitation of this measurement. Under favorable conditions errors can be kept within 5%, but with a large built-up edge can easily reach 10 times this value. In some cases the removal of a built-up edge by adding a good cutting fluid increased the indicated emf by 50%, although a temperature reduction is what one would normally expect.

There exists at the present time no really satisfactory method for measuring the chip-length ratio. Two methods were used in this work. The better of the two depends on cutting a groove into the surface of the workpiece, parallel to its axis, which results in notches in the side of the chip. The distance between successive notches divided by the circumference of the work is the desired ratio. Unfortunately chips are not always continuous for an entire revolution of the work, especially when cutting at slow speeds and heavy depths of cut, and sometimes a good cutting fluid can produce tightly curled chips that are mechanically broken off at short intervals. In such cases the best method is to weigh a known length of chip and from its known width, density and the depth of cut calculate the uncut length of the chip, the ratio between the two giving the desired result. Such measurements require a certain amount of

skill and patience, especially when chips must be annealed and straightened before they can be measured. The accuracy of these measurements is estimated at 10 to 20%, although as before the averaging of a large number of readings can cut this down appreciably.

It should be pointed out that in nearly all calculations the rake angle of the tool must be known. It is obvious, therefore, that any built-up edge large enough to affect the geometry at the point will introduce errors into all subsequent calculations. The average shear stress and normal stress on the shear plane are the quantities most sensitive to errors in rake angle, and this accounts for the relatively large fluctuations observed in these values under some conditions.

The significant cutting variables, as calculated from equations (a) to (m), from cutting data on low carbon Bessemer steel containing various amounts of sulphur (.033 to 0.39%) as well as 18-8 stainless steel are shown plotted in Fig. 76 to 99 in the Appendix.

## ANALYTIC APPROACH TO CUTTING TEMPERATURES

A theory describing the temperature development in the metal cutting process would be a very useful tool. The object of a complete theory would be ability to predict tool temperatures from known cutting geometry and physical constants of the tool and work materials. If successful, it should enable proper correlation of experimental data, and, perhaps even more important, aid in a more rational tool design. It should enable predictions to be made from a limited amount of experimental data.

The basic work on heat transfer that has made this analyisis possible is due to Blok (3) who originated the idea of calculating the temperature underneath a moving friction slider by looking at the problem as one involving both stationary and moving heat sources, and to Jaeger (13) who performed a much more detailed mathematical analysis of the same problem. Chao and Trigger (6) were the first to apply these ideas to the special and more complicated case of metal cutting. However, their paper contained several errors and incorrect assumptions. Some of these were corrected by Shaw (29). The analysis below is an attempt to present as rational a picture as seems possible at the present time.

As Blok already pointed out, a mathematically exact solution for the temperature under a moving slider seems impossible at the present time. However, a good approximation is possible if the average temperature of the slider is calculated as a stationary heat source problem and that of the plane on which the sliding takes place as a moving heat source problem. By equating these average temperatures, it becomes possible to calculate the percentage of the frictional heat going into the plane and the slider, after which the temperature is easily found. There now follows a discussion of these two problems and then the results will be applied to the case of metal cutting.

THE MOVING HEAT SOURCE PROBLEM

Mathematically exact solutions were obtained by Jaeger (13) for the case of a perfectly insulating slider sliding on a semi-infinite plane z=0, as indicated in the sketch below. Solutions are given both for the band source ($m \gg l$) and the square source ( $m = l$ ), an appreciable difference between them existing only at low speeds ($L < 5$). In

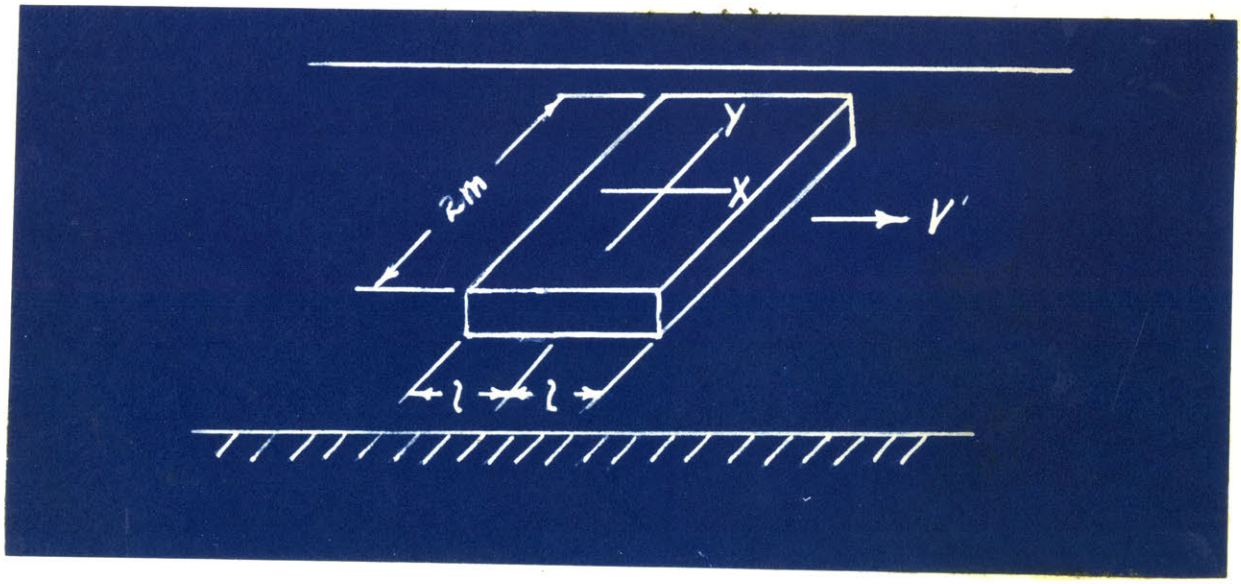


Figure 25.

metal cutting only the band source is of interest. The solution for the temperature immediately underneath the slider is in terms of a dimensionless velocity parameter L which is defined by

$$L = \frac{V' l}{2K} \qquad (1)$$

where these and other heat transfer symbols are listed in Table I. Unfortunately two solutions are required, depending whether L is greater or less than 5. In the latter case the factors $\mathcal{F}$ and $f_m$ are introduced as plotted functions of L, in order to avoid a complicated expression. The results are given for both $\theta$ and $\theta_m$, the average and maximum temperatures

respectively.

| $L > 5$ | | $L < 5$ | |
|---|---|---|---|
| $\theta = \frac{4}{3\sqrt{\pi}} \frac{ql}{k\sqrt{L}}$ | (2) | $\bar{\theta} = .636 \frac{Kq\bar{f}}{k V'}$ | (4) |
| $\theta_m = \frac{2}{\sqrt{\pi}} \frac{ql}{k\sqrt{L}}$ | (3) | $\theta_m = .636 \frac{Kqf_m}{k V'}$ | (5) |

Where the functions $\bar{f}$ and $f_m$ are plotted in Fig. 35, after Jaeger. For very small values of L there exists a third solution, but this is of no interest in the case of metal cutting and it tends towards the solution for a stationary heat source. The graphical functions of $\bar{f}$ and $f_m$, especially $\bar{f}$, can be represented with an accuracy almost equal to the ability to read the graph by the following equations:

$$\bar{f} = 2.40 \sqrt{L} \quad \text{and} \quad f_m = 3.3 \sqrt{L}$$

With this in mind these equations can be rewritten as follows:

| $L > 5$ | | $L < 5$ | |
|---|---|---|---|
| $\bar{\theta} = 0.754 \frac{ql}{k\sqrt{L}}$ | (2a) | $\bar{\theta} = 1.52 \frac{Kq\sqrt{L}}{kV'} = 0.76 \frac{ql}{k\sqrt{L}}$ | (4a) |
| $\theta_m = 1.130 \frac{ql}{k\sqrt{L}}$ | (3a) | $\theta_m = 2.10 \frac{Kq\sqrt{L}}{k V'} = 1.05 \frac{ql}{k\sqrt{L}}$ | (5a) |

From this it is evident that as long as only $\bar{\theta}$ is of interest it will be safe to use equation (2a) over the entire range of L in metal cutting problems, the error not exceeding 3% as long as $L > 0.2$, which will be the case in all practical problems. Fortunately $\theta_m$ is not of major interest, since here the error involved in using equation (3a) instead of (3 and 5) can be as much as 15%.

TABLE I

Symbols used in Heat Transfer analysis.

| | | |
|---|---|---|
| $K$ | Thermal Diffusivity | $in^2/sec$ |
| $k$ | Thermal Conductivity | $Btu/in^2/sec/(^oF/in)$ |
| $c$ | Specific heat | $Btu/lb^oF$ |
| $\rho$ | Density | $lb/in^3$ |
| $\theta$ | Temperature in degrees | Fahrenheit |
| $\theta_o$ | Room Temperature in degrees | Fahrenheit |
| $V'$ | Sliding Velocity | in/sec |
| $q$ | Energy flow | $Btu/in^2/sec$ |
| $L$ | Dimensionless Velocity Parameter (due to Jaeger) | |
| $t$ | Time | seconds |
| $J$ | Mechanical Equivalent of heat | 778 ft-lb/Btu or 9340 in-lb/Btu |
| $\overline{\theta}_s$ | Average Temperature of the shear plane | |
| $\overline{\theta}_t$ | Average Temperature at the Tool-Chip interface | |

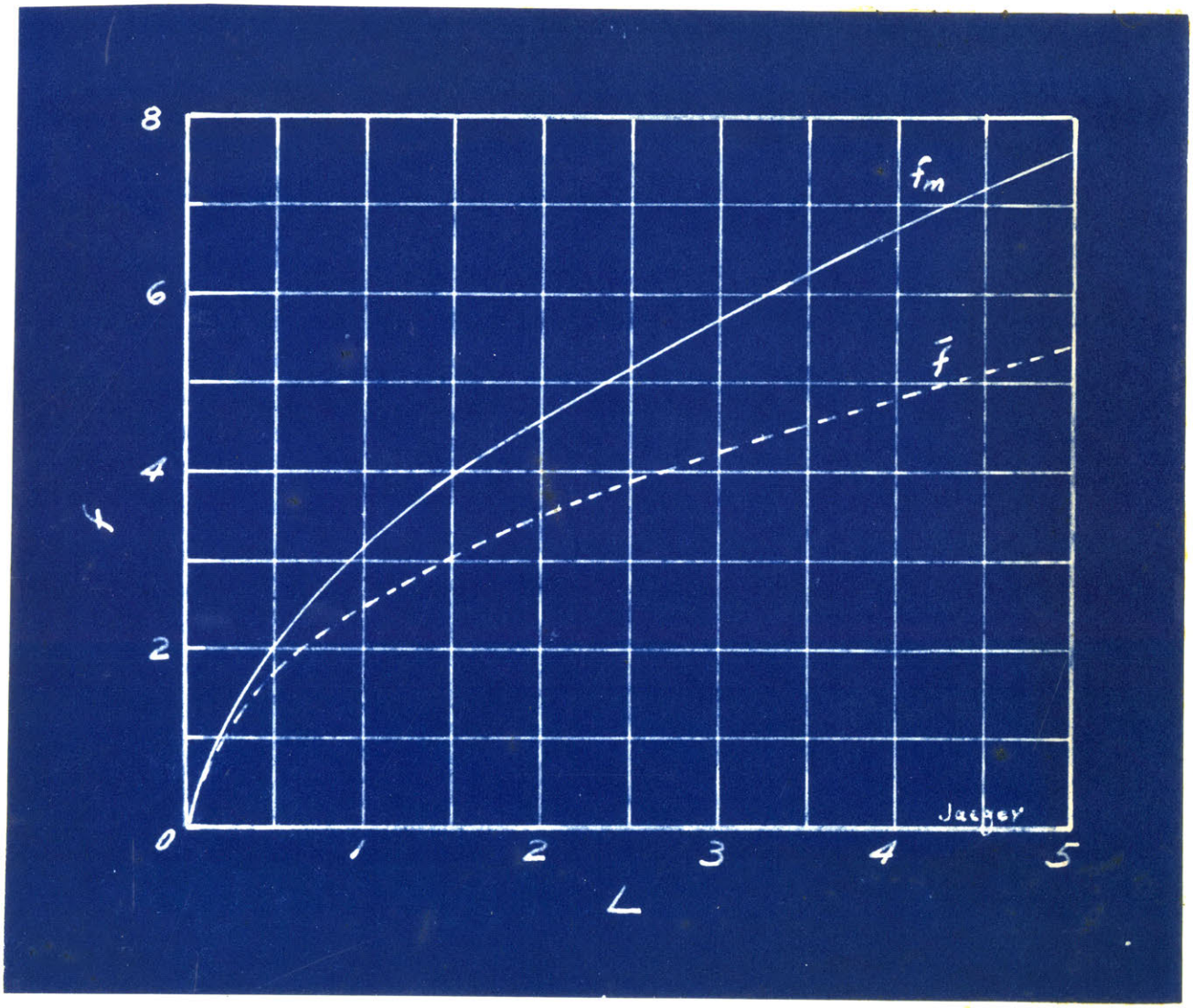


Figure 26.

Plot of Temperature factors f vs. parameter L.

Jaeger also determined the temperature distribution underneath the slider, and his result, plotted in non-dimensional form, as a function of L, is shown in Fig. 27 for a slider of width 2$l$, travelling from right to left. It will be noted that at higher speeds the maximum temperature is almost under the heel of the slider. It must be recalled that all these results assume the slider a perfect insulator. While this temperature distribution is not used directly in further computations, it is

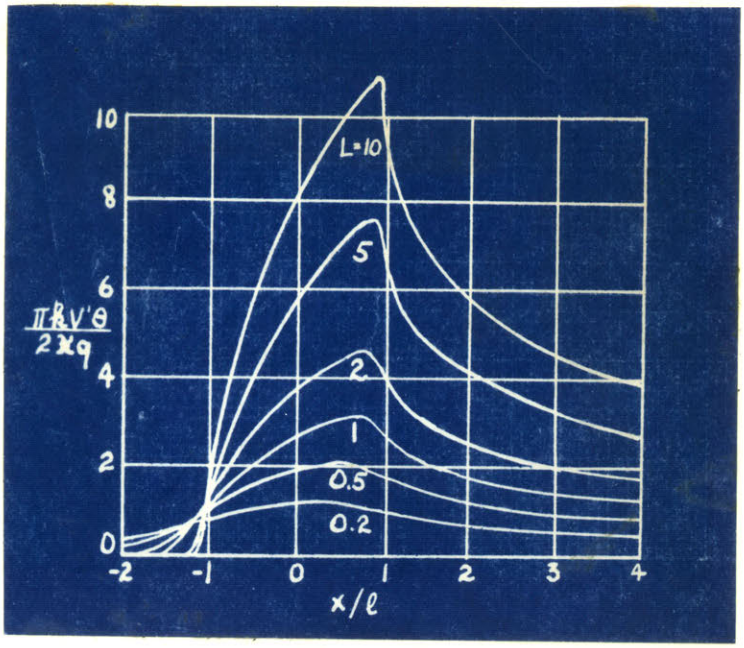


Figure 27.

Temperature distribution underneath a friction slider.

necessary in order to clarify the thinking on this problem, and for checking the validity of assumptions made later on. The same is true of a second set of calculations due to Jaeger, in which he determined the temperature distribution below the plane, underneath the heel of the slider. His plot, again in non-dimensional form, is shown in Fig. 28,

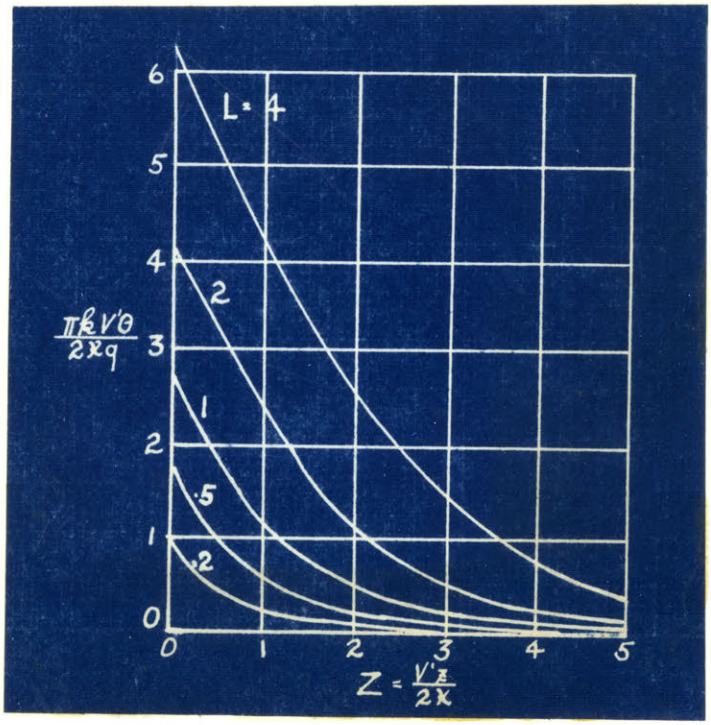


Figure 28.

Temperature distribution underneath the heel of the slider.

with the temperature plotted against the parameter Z, defined by $Z = \frac{V'z}{2K}$, where z is the depth below the surface, for several values of the parameter L.

Another contribution of Jaeger's was calculation of the effect of non-uniform heat generation under the slider. The rather unexpected result was that the effect of such non-uniformity on both the maximum and average temperatures under the moving slider was a very slight one. In the case of L = 1, substituting a strength distribution varying linearly from zero in the rear to a maximum at the front of the slider, but with the total energy remaining the same as in the constant case, the average temperature is increased by about 4% and the maximum temperature increased by 4.5%. The position of the maximum is shifted, however, from a point 1/8 of the slider width from the rear to a point 1/3 of the slider width from the front.

Other calculations of Jaeger's, such as the effect of non-uniform velocities, are of no interest in the metal cutting problem.

## THE STATIONARY HEAT SOURCE PROBLEM

The stationary heat source problem differs from the usual heat transfer calculations in that it is the temperature that is to be caclulated from a known value of heat flow, rather than vice versa. The basic formulation of this problem is again due to Blok and Jaeger (loc.cit.). The starting point is the integration of the Fourier equation

$$K\nabla^2\theta + \frac{K}{k}\, q = \frac{d\theta}{dt}$$

for the case of an instantaneous amount of heat Q liberated at point $(x' , y' , z' )$ in an infinite body. The resulting equation for the temperature at any point $(x,y,z)$ in the body at time t after the liberation of Q is, according to Carslaw (5)

$$\theta\,(x,y,z,t) = \frac{Q\,K}{8k\,(\pi Kt)^{3/2}}\, e^{-\frac{r^2}{4Kt}} \qquad (6)$$

where $r^2 = \left[(x-x')^2 + (y-y')^2 + (z-z')^2\right]$

This solution will now be applied to the case of a uniform stationary heat source, applied over the rectangle $-l < x' < l$ , $-m < y' < m$, on the surface of a semi-infinite body, z = 0 in the diagram below.

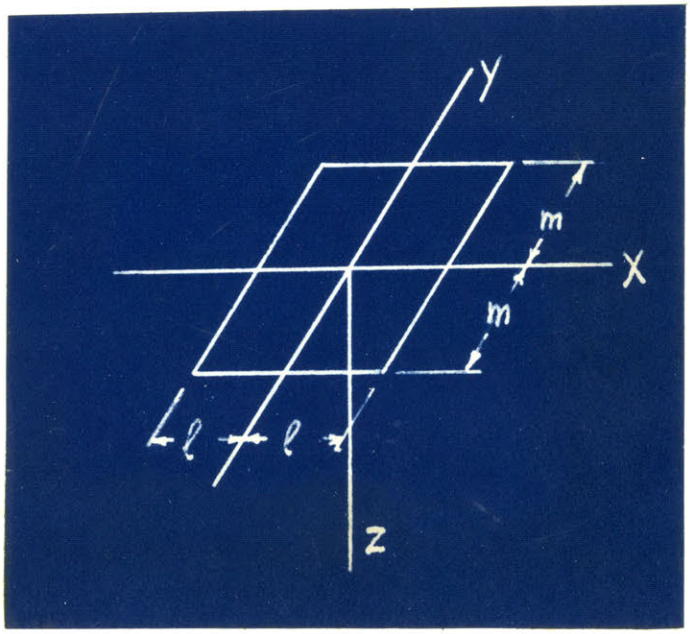


Figure 29.

For this case the constant 8 in the denominator of (6) becomes 4, since in a semi-infinite body heat transfer can take place in only one direction and since the surface z = 0 will be assumed to be a perfect insulator, except over the area where heat is applied. Heat will be assumed be supplied at the rate of q units per unit time per unit area. Commencing at time t = 0 when the body is at zero temperature the temperature at any point in the body at any time is given by

$$\theta\,(x,y,z,t) = \frac{qk}{4k(\pi K)^{3/2}} \int_{-l}^{l} dx' \int_{-m}^{m} dy' \quad \frac{dt'}{(t-t')^{3/2}}\, e^{-\frac{r^2}{4K(t-t')}} \qquad (7)$$

Where r is as defined above.

The time integral can be solved by letting $T^2 = 1/(t-t')$, so that $dt = -2\,dT/T^3$ and equation (7) can be rewritten:

$$\theta\,(x,y,z,T) = \frac{qk}{2k(\pi K)^{3/2}} \int_{-l}^{l} dx' \int_{-m}^{m} dy' \quad e^{-\frac{r^2T^2}{4K}} \quad (-dT) \qquad (8)$$

for finite values of t this leads to the Gauss error integral, however, when $t \to \infty$, the case of interest here, the last integral reduces to $\frac{\sqrt{\pi K}}{\sqrt{r^2}}$, so that the steady state solution is

$$\theta\,(x,y,z) = \frac{q}{2\pi k} \int_{-l}^{l} dx' \int_{-m}^{m} \frac{dy'}{\sqrt{(x-x')^2 + (y-y')^2 + z^2}} \qquad (9)$$

In the expression for $\sqrt{r^2}$ the value of z' is zero (plane source). The integration of this equation (9) is considerably simplified if it is desired to obtain temperature values in the surface plane, z = 0, only. Fortunately this is the area of interest in this problem, so that the final expression to be integrated is

$$\theta\,(x,y,0) = \frac{q}{2\pi k} \int_{-l}^{l} dx' \int_{-m}^{m} \frac{dy'}{\sqrt{(x-x')^2 + (y-y')^2}} \qquad (10)$$

This integration, carried through in detail in the Appendix, leads to the result

$$\theta(x,y) = \frac{q}{2\pi k}\left[ |x-l| \sinh^{-1}\frac{y-m}{x-l} - |x+l| \sinh^{-1}\frac{y-m}{x+l} - |x-l| \sinh^{-1}\frac{y+m}{x-l} \right.$$

$$+ |x+l| \sinh^{-1}\frac{y+m}{x+l} + |y-m| \sinh^{-1}\frac{x-l}{y-m} - |y-m| \sinh^{-1}\frac{x+l}{y-m}$$

$$\left. - |y+m| \sinh^{-1}\frac{x-l}{y+m} + |y+m| \sinh^{-1}\frac{x+l}{y+m} \right] \quad (11)$$

The multiplying factors of the $\sinh^{-1}$ terms are all absolute quantities, corresponding to the fact that the denominator of (10) represents a positive radius. This is an important point. The maximum temperature is at the point $x = y = 0$, and is given by

$$\theta_{max}(0,0) = \frac{qm}{k}\frac{2}{\pi}\left[\frac{l}{m} \sinh^{-1}\frac{m}{l} + \sinh^{-1}\frac{l}{m}\right] \quad (12)$$

The minimum temperature in the surface of the source is at the point $(l, m)$ and is exactly $1/2\ \theta_{max}$. Expressions for $\theta$ at different points in the surface are given in the Appendix; they are all functions of the ratio $m/l$, which is termed the aspect ratio. It is seen that equation 11 is symmetrical about both x and y axis.

The nature of the temperature distribution in the plane z = 0 and also along the z-axis is shown in the sketch below.

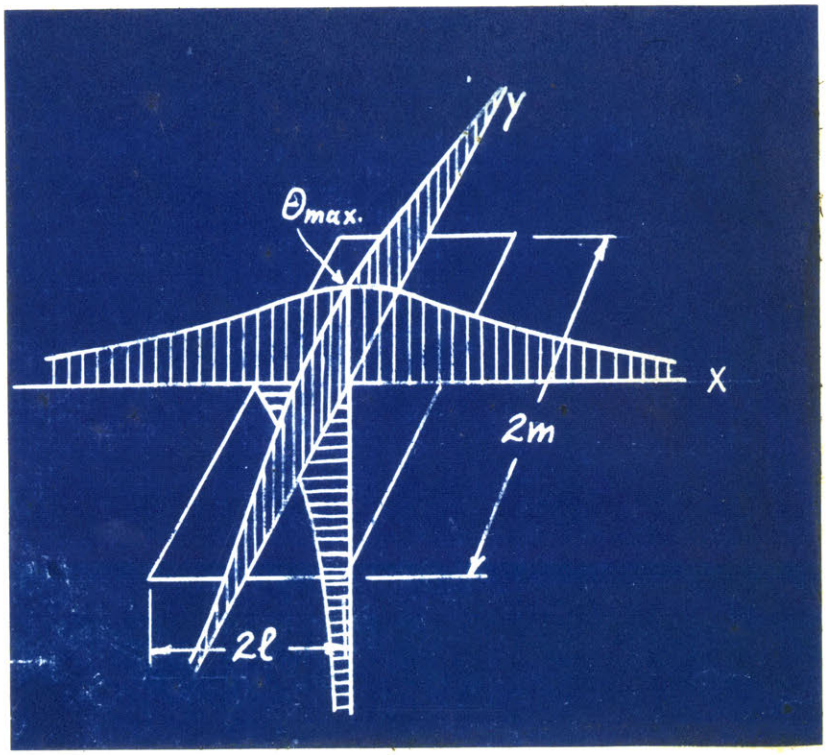


Figure 30.

Temperature distribution on surface heated by stationary source 2ℓ x2m. Further values of temperature along both the X and Y axis are shown plotted in dimensionless form, as functions of the aspect ratio m/ℓ , in Figures 31 and 32.

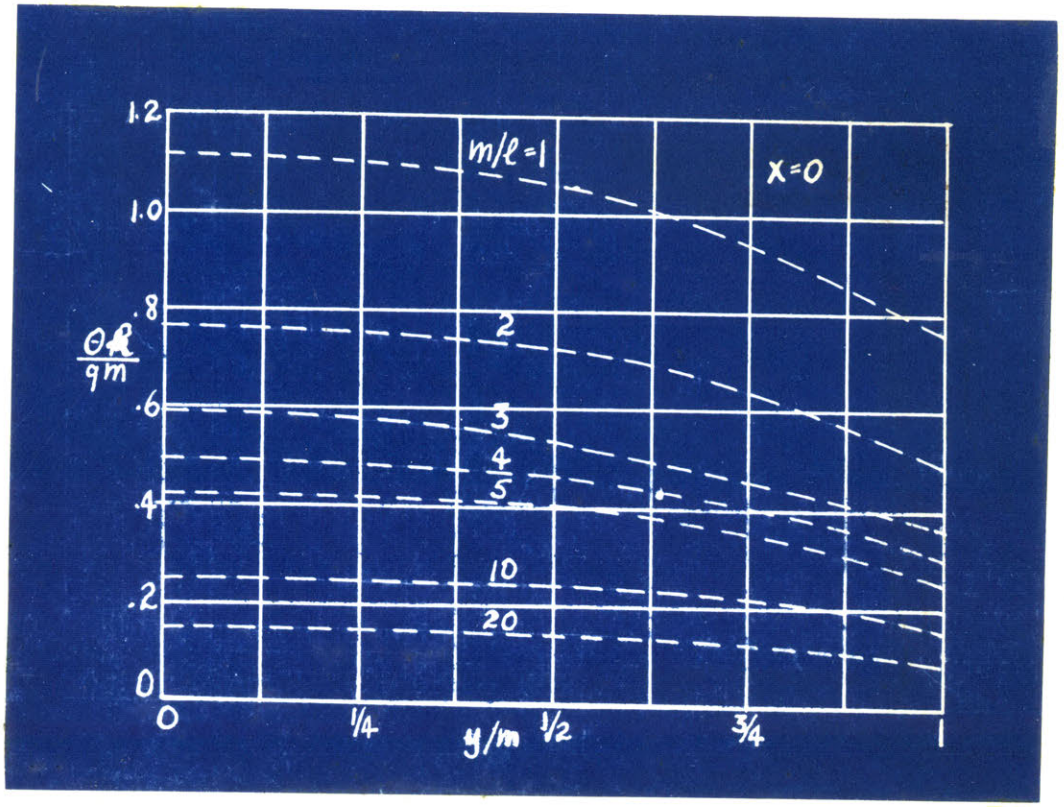


Figure 31.

Temperature distribution along the Y-axis

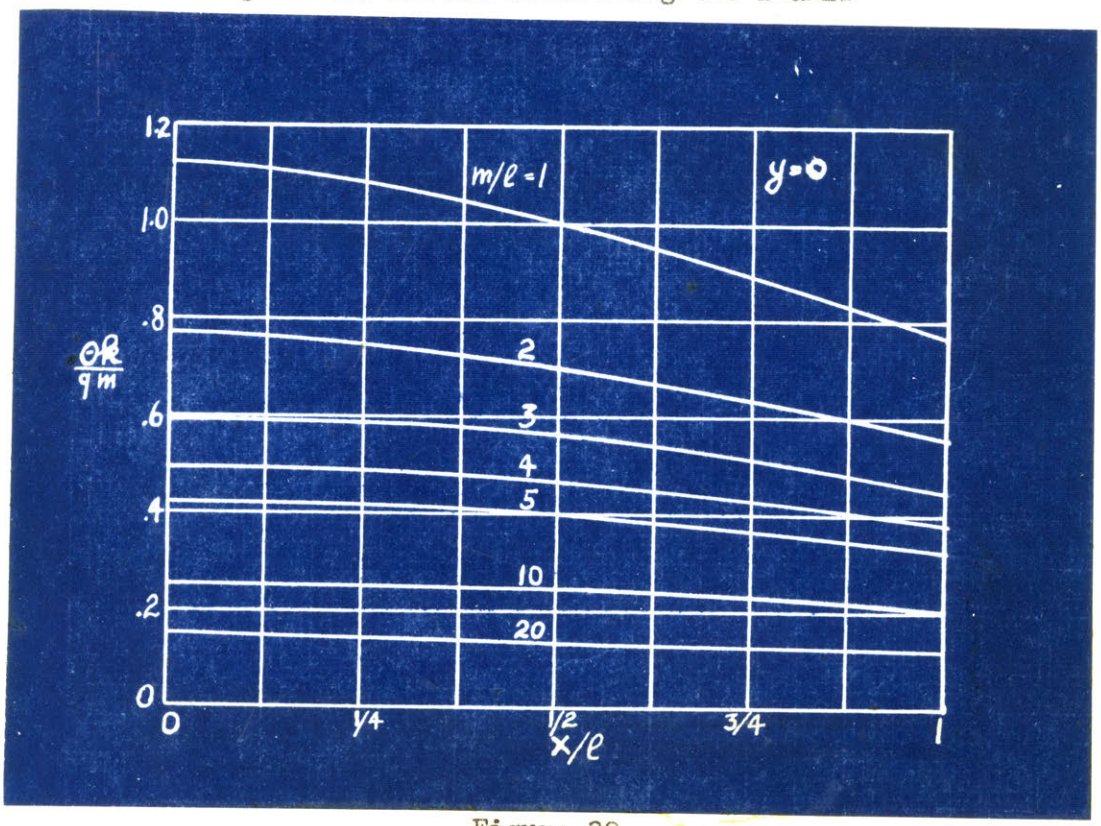


Figure 32.

Temperature distribution along the X-axis.

It is possible theoretically to integrate equation (9) completely and thereby get a general solution for the temperature at any point (x, y, z) in the body. However, a simple explicit solution seems obtainable only when z = 0. Since the temperature below the surface is of some interest in the metal cutting problem it was calculted as a function of (z) for the two most interesting fixed values of x and y, namely (x = y = 0) and (x = $\ell$ , y = 0). The results, again plotted in dimensionless form, are shown in Figures 32 and 34, for three different values of the aspect ratio m/l. The necessary integration of equation (9) was performed in two steps. The first was a straightforward integration with respect to x, which leads to one or two $\sinh^{-1}$ terms, depending on the x and y values chosen for evaluation. The integration of these terms with respect to y can then be carried out graphically for different values of z and m/l, by simply plotting and measuring the area under the curve.

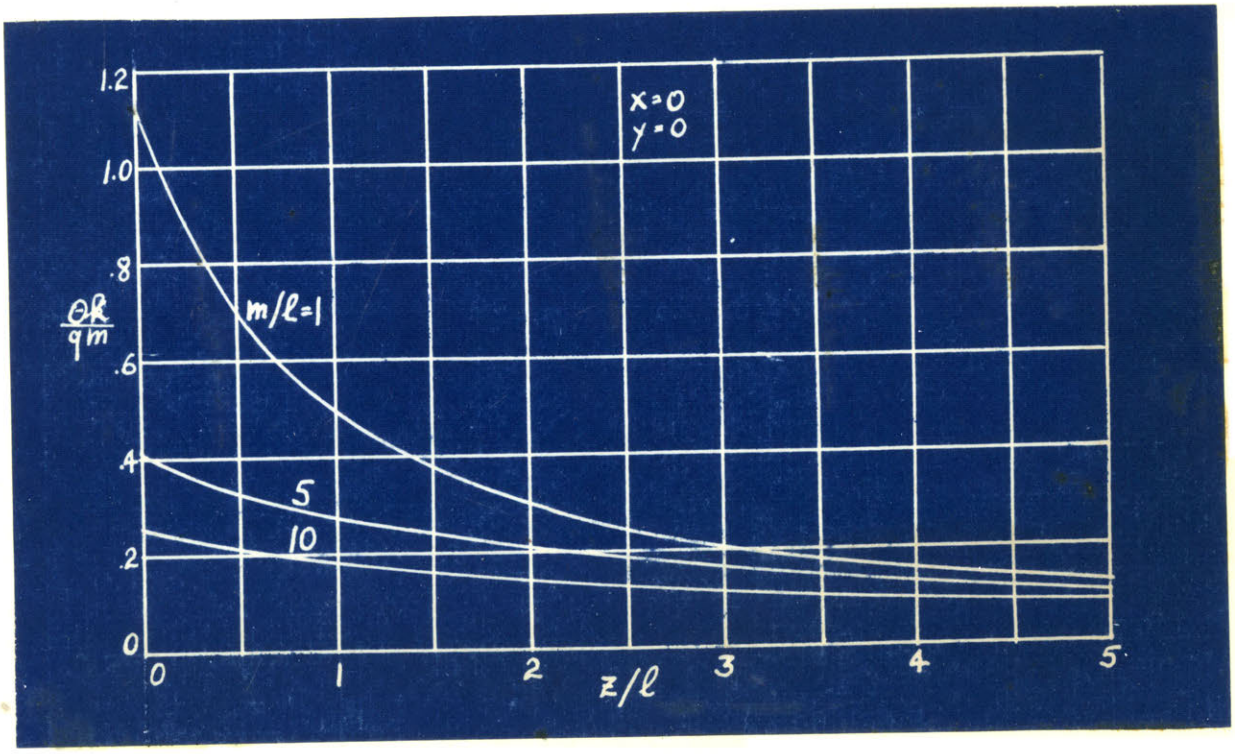


Figure 33.

Temperature distribution along the z-axis underneath point (0,0)

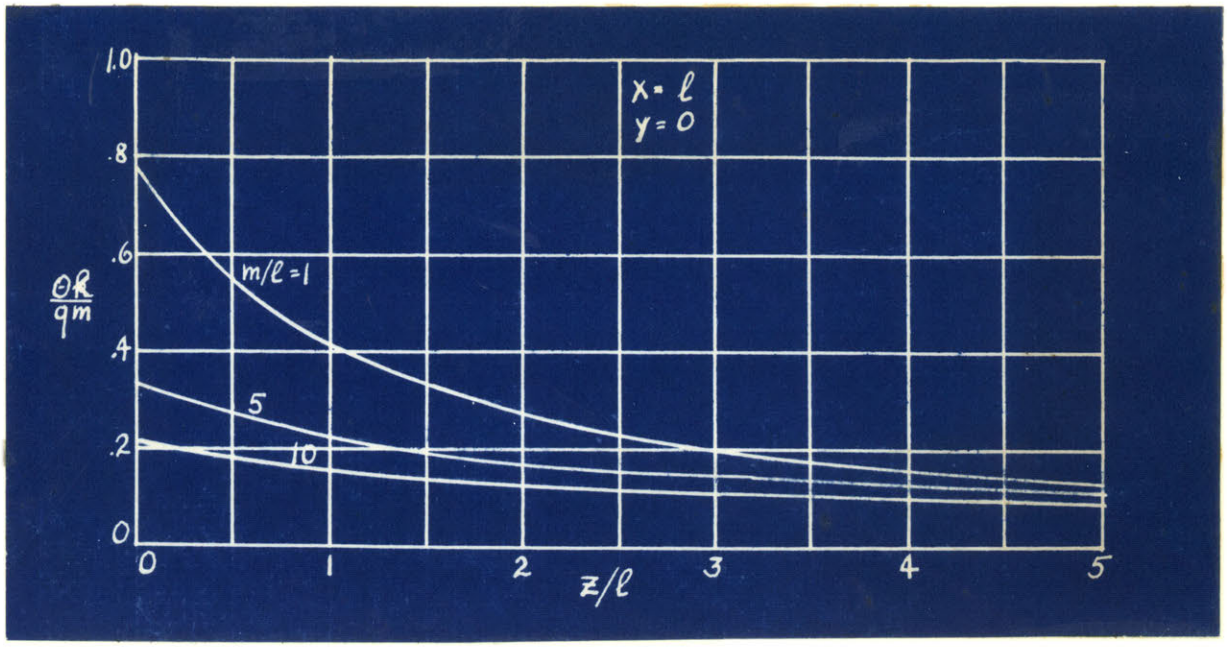


Figure 34.

Temperature distribution underneath point (ℓ ,0)

Another method by which steady state temperatures inside a body may be found from known boundary conditions is the Southwell relaxation method. Even when the problem is simplified by treating it as a two-dimensional one this is still a rather tedious procedure, although capable of taking into account variable boundary conditions and irregular shapes. Use of this technique was made in one case, to determine the temperature distribution in the plane y = 0, when m/l = 5. The resulting isotherms are shown in the diagram below. Comparison with the exact solution of Fig. 33 shows that this is only a fair approximation.

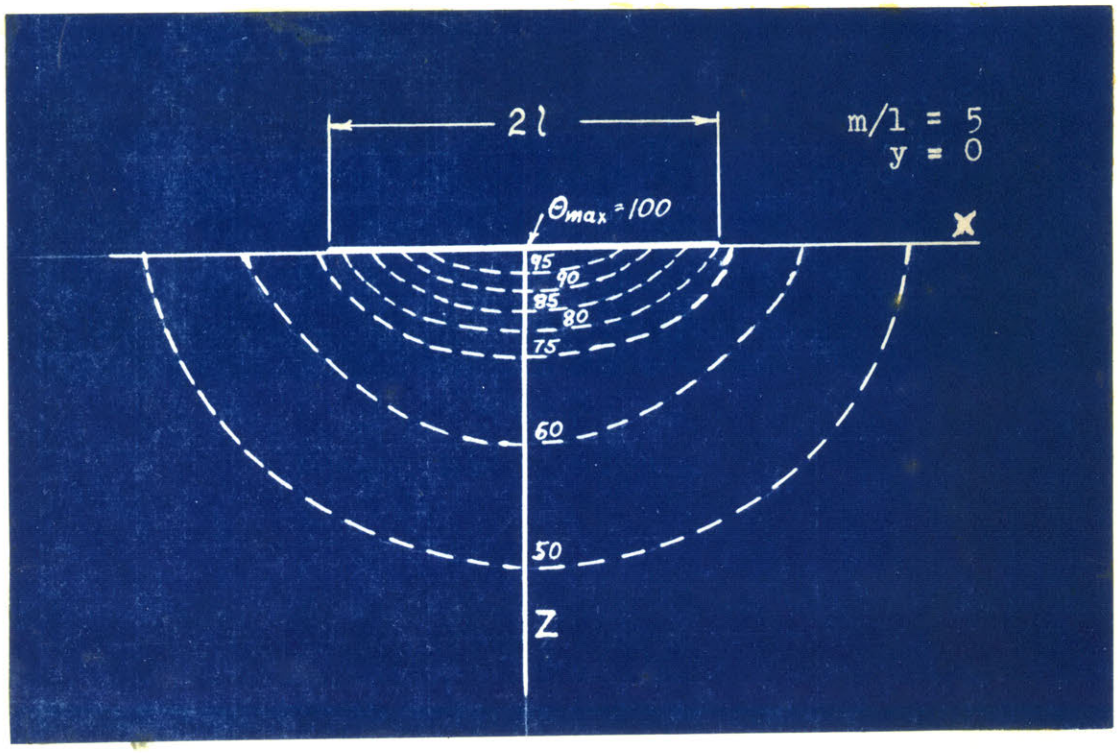


Figure 35.

Temperature distribution in the plane y=0 when m/l = 5 (Approximate).

It will prove interesting to see what the temperature variation in the surface is when the heat input q is not uniformly distributed. The simplest case is a linear distribution of q in the x-direction, constant in the y-direction, of which four types can be imagined, as shown in Fig. 36 a,b,c,d). The maximum in each case is taken as 2q, since then

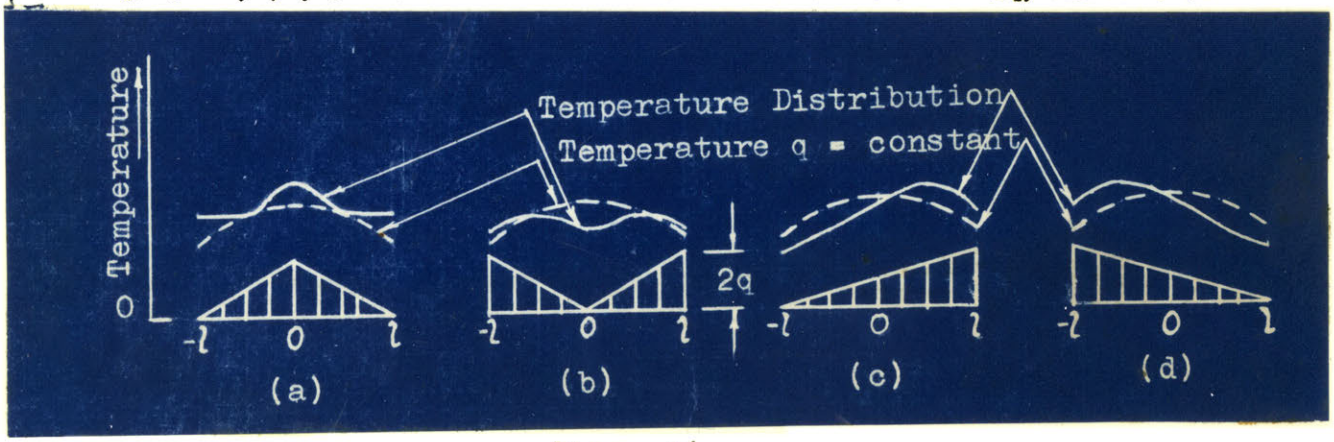


Figure 36.

Triangular heat distributions.

the total heat input is equal to that of the constant case whose solution was given on previous page. Equation (9) must now be rewritten for each of the above cases:

$$\theta = \frac{1}{2\pi k}\ 2q\ (1-\left|\frac{x}{l}\right|) \int_{-l}^{l}\int_{-m}^{m} \frac{dx'dy'}{\sqrt{(x-x')^2+(y-y')^2}} \qquad (13a)$$

$$\theta = \frac{1}{2\pi k}\ 2q\ \left|\frac{x}{l}\right| \int_{-l}^{l}\int_{m}^{m} \frac{dx'dy'}{\sqrt{(x-x')^2+(y-y')^2}} \qquad (13b)$$

$$\theta = \frac{1}{2\pi k}\ 2q\left[1+\left(\frac{x}{l}\right)\right] \int_{-l}^{l}\int_{-m}^{m} \frac{dx'dy'}{\sqrt{(x-x')^2+(y-y')^2}} \qquad (13c)$$

$$\theta = \frac{1}{2\pi k}\ 2q\left[1-\left(\frac{x}{l}\right)\right] \int_{-l}^{l}\int_{-m}^{m} \frac{dx'dy'}{\sqrt{(x-x')^2+(y-y')^2}} \qquad (13d)$$

Integrating these equations to obtain a general solution for $\theta(x,y)$ is rather difficult. However, it is not difficult to obtain solutions at any given point, for a fixed ratio $m/l$ , by numerical integration. In particular, it is quite simple to obtain solutions to cases b,c,d, after case (a) has been evaluated. The accuracy of the numerical integration can be checked quite easily by using it to evaluate the case of constant heat input q, for which the exact solution was obtained above, and in the case reported below, the agreement was found to be within 2%. In the table III results are tabulated for $\theta(0,0)$ and $\theta(\frac{l}{2},0)$, $\theta(l,0)$ when $m/l = 1$(square source), for each of the four distributions above. For reference purposes, results for the constant case are included. The temperatures are shown to scale in Fig. 36, including, for reference again, the temperature distribution for q = constant.

TABLE III

| Heat Distribution | $\theta(0,0)$ | $\theta(\frac{l}{2},0)$ | $\theta(-l,0)$ |
|---|---|---|---|
| Constant q Btu/in$^2$/sec | 1.123 qm/k | 1.062 qm/k | .766 qm/k |
| Triangular 2q (Fig.36a) | 1.39 qm/k | 1.08 qm/k | 1.06 qm/k |
| Triangular 2q (Fig.36b) | .84 qm/k | .99 qm/k | .87 qm/k |
| Triangular 2q (Fig.36c) | 1.10 qm/k | 1.26 qm/k | 1.01 qm/k |
| Triangular 2q (Fig. 36d) | 1.10 qm/k | .79 qm/k | .58 qm/k |

The interesting result is that quite drastic changes in the heat distribution pattern have relatively small effects on the temperature distribution and magnitude, compared to the case with constant heat input. In addition, when $m/l$ increases, the importance of the shape of the heat distribution will decrease further.

The quantity of primary interest further in this analysis is not the actual temperature distribution, but the mean temperature $\bar{\theta}$ over the area $-l < x < l$, $-m < y < m$. This value may be obtained by integrating equation (11) over this entire area and dividing by the area. Fortunately the symmetry of the problem allows the reduction of the 8 terms in equation (11) to two, the 4th and 8th terms being chosen to avoid any possible sign ambiguities. With this in mind we can write

$$\bar{\theta} = 4 \left( \frac{q}{2\pi k} \right) \left( \frac{1}{4lm} \right) \int_{-l}^{l} dx \int_{-m}^{m} \left[ (x+l) \sinh^{-1} \frac{y+m}{x+l} + (y+m) \sinh^{-1} \frac{x+l}{y+m} \right] dy \quad (14)$$

This integration, which is carried through in detail in Appendix, leads to the result:

$$\bar{\theta} = \frac{2}{\pi} \frac{qm}{k} \left\{ \frac{l}{m} \sinh^{-1} \frac{m}{l} + \sinh^{-1} \frac{l}{m} + \frac{1}{3} \frac{m}{l} + \frac{1}{3} \left( \frac{l}{m} \right)^2 - \frac{1}{3} \left[ \left( \frac{l}{m} \right)^2 + 1 \right] \sqrt{1 + \left( \frac{m}{l} \right)^2} \right\} \quad (15)$$

This is obviously not a very convenient function to use and has therefore been plotted in terms of a shape factor $\bar{S}$, as a function of the aspect ratio $m/l$, in a manner defined by the equation below:

$$\bar{\theta} = \frac{qm}{k} \bar{S} \qquad (18)$$

Similarly the maximum temperature given in equation (12) may conveniently be expressed in terms of another shape factor $S_m$ defined by

$$\theta_m = \frac{qm}{k} S_m \qquad (19)$$

Both shape factors are plotted in Fig. 46, for values of m/l from one to twenty. When $m/l > 20$ it is possible to simplify the expressions for $\bar{S}$ and $S_m$:

$$\bar{S} = \frac{2}{\pi} \left(\frac{l}{m}\right) \left[ \log \frac{2m}{l} + \frac{1}{3} \left(\frac{l}{m}\right) + \frac{1}{2} \right], \quad m/l > 20 \qquad (15a)$$

$$S_m = \frac{2}{\pi} \left(\frac{l}{m}\right) \left[ \log \frac{2m}{l} + 1 \right], \quad m/l > 20 \qquad (12a)$$

It should be recalled at this point that all the above equations represent exact steady state solutions for a semi-infinite body insulated everywhere except the area of heat supply, and assuming a reference temperature of zero degrees.

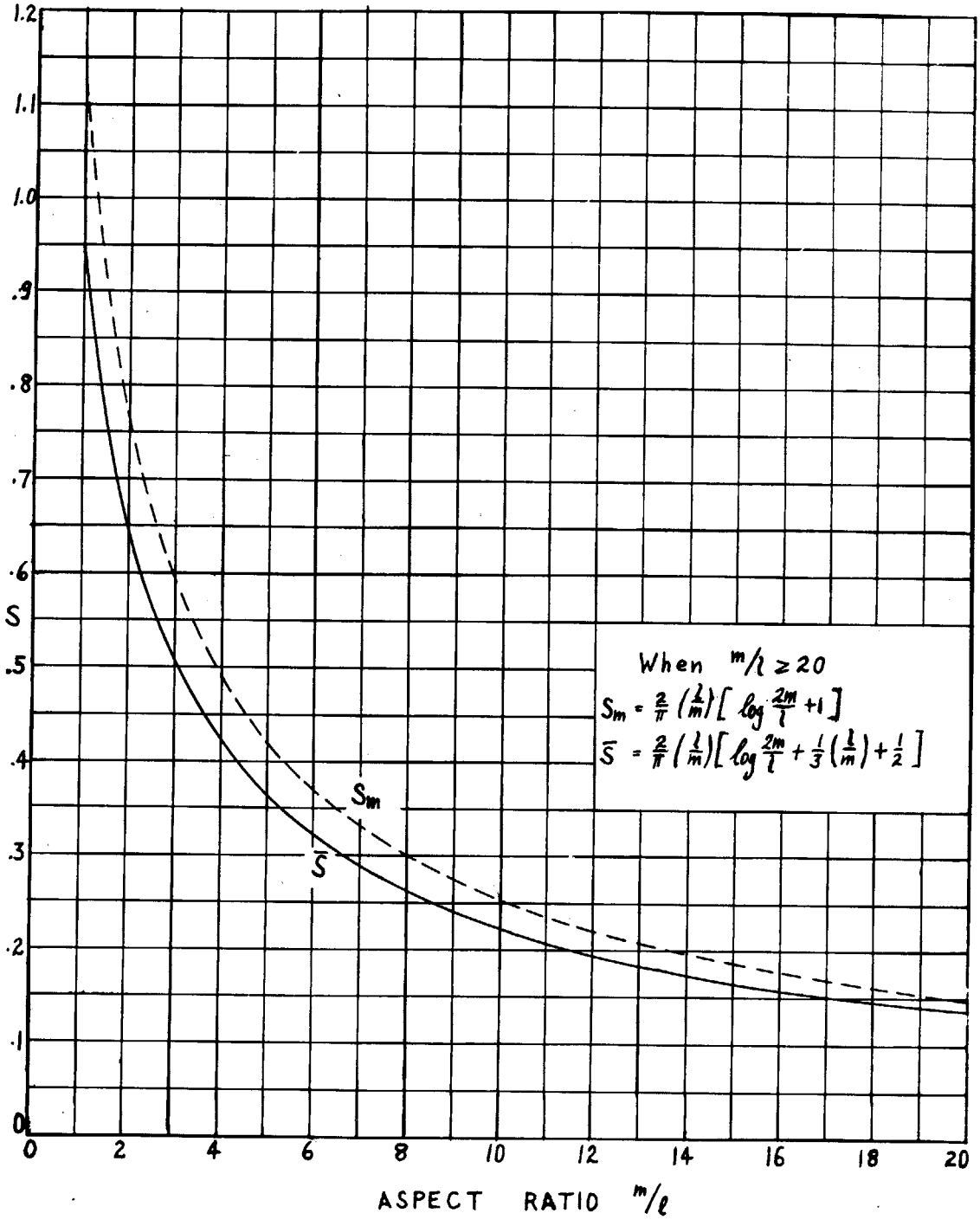
1.2
1.1
1.0
.9
.8
.7
.6
S
.5
.4
.3
.2
.1
0
0
2
4
6
8
10
12
14
16
18
20
ASPECT RATIO m/ℓ
When m/ℓ ≥ 20
$S_m = \frac{2}{\pi}\left(\frac{1}{m}\right)\left[\log\frac{2m}{\ell}+1\right]$
$\bar{S} = \frac{2}{\pi}\left(\frac{1}{m}\right)\left[\log\frac{2m}{\ell}+\frac{1}{3}\left(\frac{1}{m}\right)+\frac{1}{2}\right]$
$S_m$
$\bar{S}$

Fig. 37

COMBINING STATIONARY AND MOVING HEAT SOURCE SOLUTIONS

The basic idea behind finding the temperature under a slider with finite conductivity, which is due to Blok (loc.cit.), is to combine the solutions for stationary and moving heat sources in order to find the unknown division of the heat generated in the plane of contact. However, this cannot be done exactly because the calculated temperature distributions along the slider are quite different for the two cases. The sketch below is typical of the temperature distributions that can be expected.

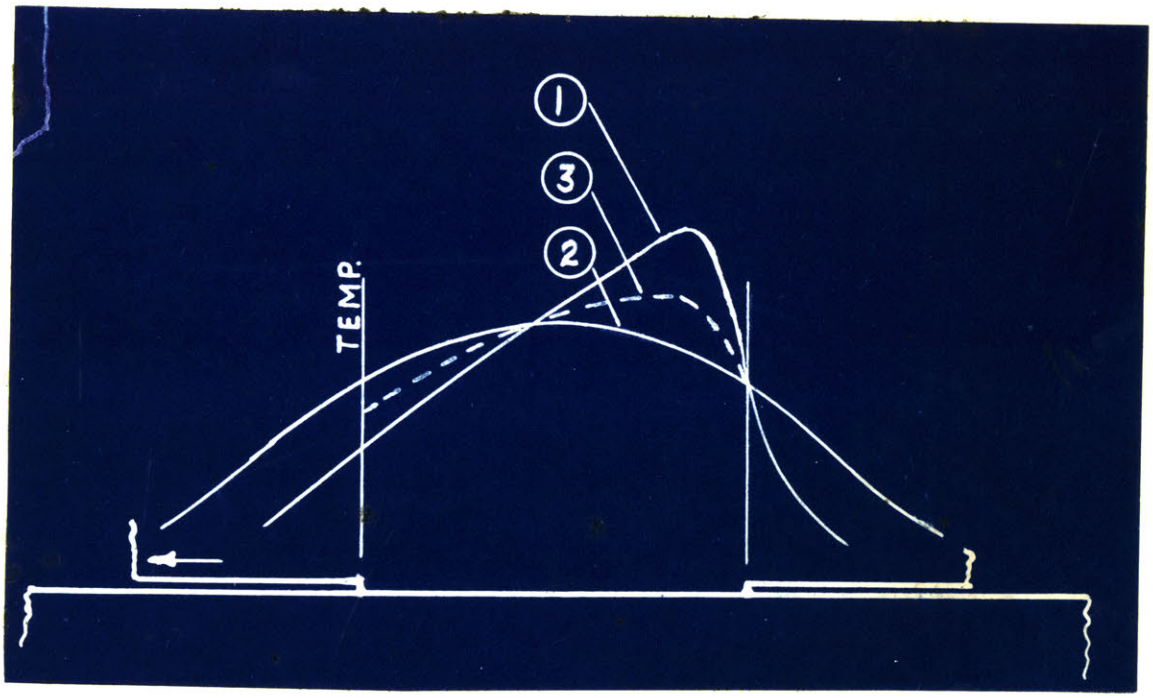


Figure 38.

Sketch indicating temperatures underneath a moving slider.

The curves were taken from Figures 32 and 27 and adjusted to have about the same mean temperatures. Curve (1) represents the temperature in the plane underneath the slider while curve (2) represents the temperature in

the face of the slider. Obviously neither can be the correct solution since such temperature differences invite heat transfer between the two bodies, tending to equalize at the mean temperature indicated by curve (3). In other words, there is heat transfer back and forth between plane and slider which can be regarded as super-imposed on the constant frictional heat flowing into the two directions. The shape of (3) depends largely on the shape of (1) which is a function of the speed parameter (L), the rise towards the rear of the slider increasing with the speed. However, especially at high speeds, complete equalization of temperatures is not likely to occur, so that the actual temperature of the slider will be between (2) and (3) while that in the plane will be somewhere between (1) and (3). This point is not subject to any simple experimental verification, since sliders small enough to insure uniform pressure will be too small to allow insertion of satisfactory surface thermocouples, and using the thermoelectric voltage between the slider itself and the plane will give only average values.

There appears therefore no practical alternative to equating the mean temperatures of the two types of solutions in order to solve for the heat flow.

At very slow speeds ( $L < 0.2$) Figures 27 and 32 shows that the difference between the two solutions tends to disappear, so that the ambiguity mentioned above also disappears. Unfortunately this region is of no great practical interest.

TABLE II

Symbols used in Metal Cutting Analysis.

| | |
|---|---|
| $\alpha$ | Rake angle of an orthogonal tool, degrees. |
| $\beta$ | Friction angle on the cutting face of the tool, degrees |
| $\gamma$ | Shear Strain the chip has undergone |
| $\mu$ | Coefficient of friction between the chip and tool |
| $\phi$ | Shear angle, angle between shear plane and direction of tool travel |
| $\tau$ | Shear stress, average over the shear plane $lb/in^2$ |
| $F_c$ | Cutting force in lbs or lb/in width, as specified |
| $F_t$ | Thrust force in lbs or lb/in width, as specified |
| $t_d$ | Depth of cut, inches |
| $V_t$ | Cutting velocity ft/min |
| $V_t'$ | Cutting velocity in/sec |
| $V_c'$ | Chip velocity in/sec |
| $r_c$ | Chip length ratio |
| b | Width of cut, inches |
| a | Length of contact between chip and tool, perpendicular to edge, inches |
| $F_f$ | Friction force parallel to tool face, lbs or lb/in width as specified |
| u | Total energy required in cutting process $in\text{-}lb/in^3$ |
| $u_f$ | Energy consumed in friction on tool face $in\text{-}lb/in^3$ |
| $u_s$ | Energy consumed in shearing the metal $in\text{-}lb/in^3$ |
| $S_n$ | Normal stress on the shear plane $lb/in^2$ |

## ENERGY IN THE METAL CUTTING PROCESS

Before any of the foregoing theory can be applied to metal cutting, it is necessary to consider the energy distribution in the cutting process. The total energy may be thought of as being used up in five different processes:

1. Surface energy required to form a new surface.
2. Change in momentum of the metal crossing the shear plane.
3. Friction along the clearance face of the tool.
4. Shearing the metal as it crosses the shear plane.
5. Friction along the cutting face of the tool.

The first two items can be shown to be insignificant compared to the rest. For a sharp tool the third item is also very small; this is the only case analyzed here. With dull tools friction on the clearance face can become quite appreciable but the effect is very difficult to treat quantitatively.

There remain then the shear and friction energies, with orders of magnitude of 3:1, which are of primary interest in temperature calculations. That all the friction energy is converted to thermal energy is unquestioned, but with shear energy the case is not so clear. Some of the latter may be expected to be retained as latent energy of latice deformation in the chip, only the remainder appearing as heat energy. The relative amounts involved can be determined only by experiment. Taylor and Quinney (40) observed that in plastic twisting of a steel bar only 85 to 90% of the work done was recoverable as thermal energy, the remainder obviously accounted for by latice deformation. Extrapolation of Taylor and Quinney's data indicates that as strains increase, the

percentage of work retained as latent energy decreases, so that some sort of energy saturation takes place in plastically deformed material at high strains. This is very important, because of the large strains encountered in metal cutting. Additional weight to this viewpoint is given by some careful work of Epifanov and Rebinder (8), who found that when drilling Aluminum all but 2-3% of the total input energy appeared as heat. Calorimeter studies made by Schmidt (34), although with a different end in view, also support this view.

If the shear energy is taken as 75% of the total energy input, then this would indicate that in metal cutting approximately 3-4% of the shear energy remained in the form of latent energy of lattice deformation. Since this amount is too small to seriously affect temperature calculations it will be omitted in the calculations to follow. Should the need arise it is, of course, a very simple matter to subtract 3-4% from the shear energy before making temperature calculations.

APPLICATION OF THEORY TO THE CUTTING PROCESS

Since this analysis will concern itself with sharp tools only, the following sketch shows the two areas of heat generation in metal cutting.

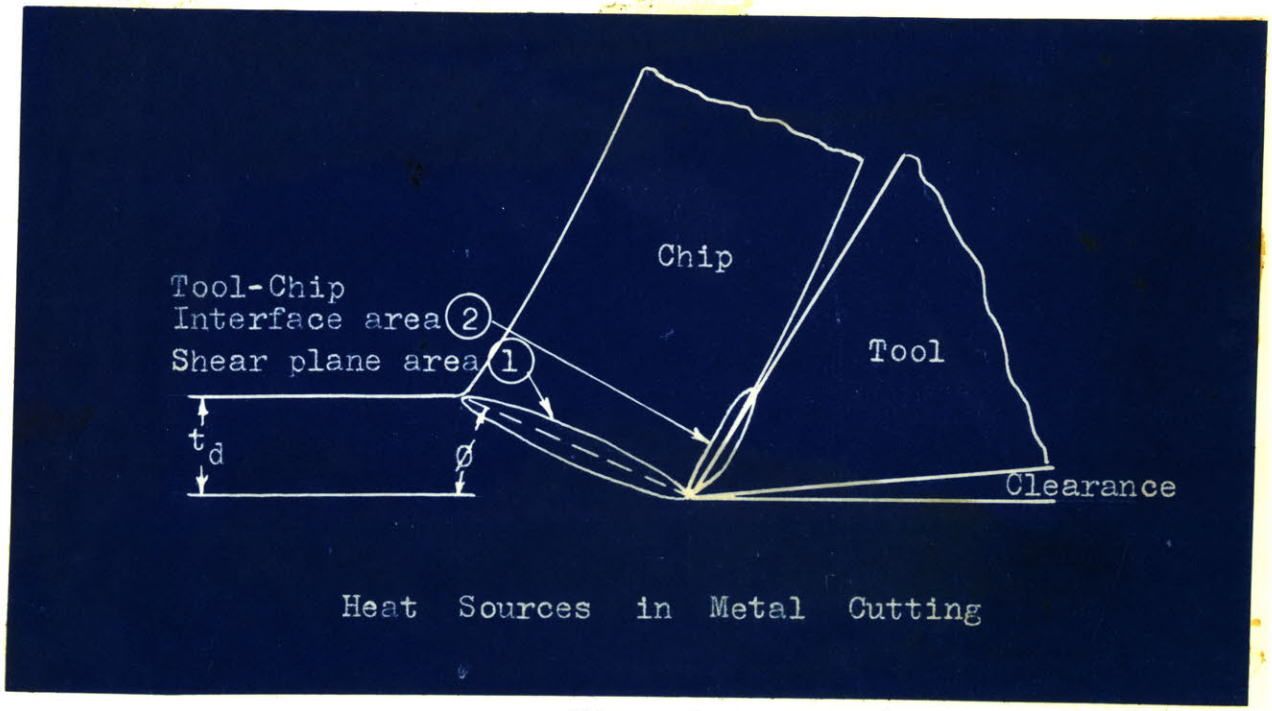


Figure 39.

The shear plane is designated (1) and equations and constants concerning it will carry the subscript 1, while the subscript (2) will be used in describing relations at the chip-tool interface.

The Shear Plane (1).

As pointed out above, all the shear energy will be assumed transformed into thermal energy. From a temperature distribution viewpoint, the value of the shear energy along the shear plane is of interest. It is usually assumed to be constant, so that the temperature of the chip leaving the shear plane will be uniform across the section. In a recent term paper (1952) in this laboratory A. Chorev measured both the shear stress $\tau$ and the shear strain $\gamma$ across the shear plane by making micro-hardness measurements. Using annealed copper he found that while the shear stress varied,

only from 29,400 lb/in$^2$ to 28,000 going from the tool cutting edge to the end of the shear plane, the corresponding strain varied from 1.90 to 1.10. Since the shear energy is the product of $\tau\gamma$, this would indicate the following energy distribution:

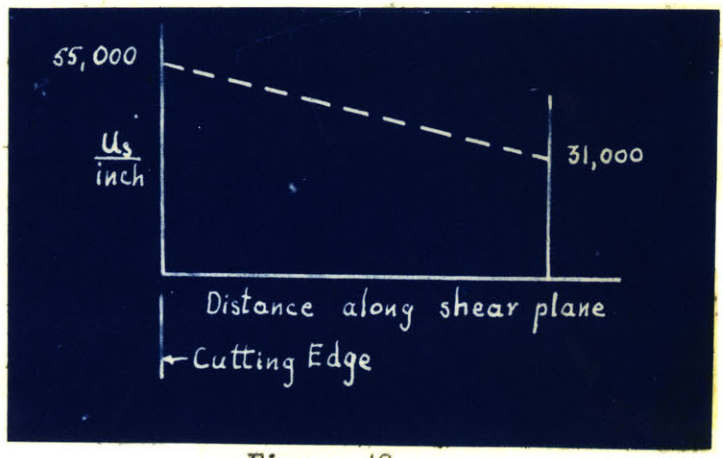


Figure 40.

Energy distribution along the shear plane for annealed copper.

While this obviously indicates non-uniform distribution, similar experiments for steel are lacking and for that reason an average value will be used in the subsequent calculations.

With this in mind, the rate of shear energy liberation $q_1$ Btu/in$^2$/sec can be written in terms of an average shear force $F_s$ lbs:

$$q_1 = \frac{F_s V_s'}{t_d \cot\phi \; b \; 12J} \qquad (20)$$

But since

$$u_s = \tau\gamma = \frac{F_s V_s'}{b \; t_d \; V_t'} \qquad (21)$$

$$q_1 = u_s \frac{V_t'}{12J \cot\phi} \qquad (22)$$

Since heat can flow in either direction perpendicular to the shear plane, only a certain fraction, which will be called $R_1$, will flow into the chip. Obviously the remaining fraction $(1-R_1)$ will flow back into the work material. The average temperature of the chip leaving the shear plane, $\bar{\theta}_s$

can then be written, from the first law of thermodynamics.

$$\bar{\theta}_s = R_1 q_1 \frac{b\, t_d \csc\phi}{c_1 \rho_1 V_t' b\, t_d} + \theta_o \qquad (23)$$

or substituting the value of $q_1$ from Equation

$$\bar{\theta}_s = R_1 u_s \frac{\sec\phi}{c_1 \rho_1 12J} + \theta_o \qquad (23a)$$

where $\theta_o$ is the room or reference temperature, and the remaining symbols listed in Table II. When, as is usually the case, (c) varies with temperature it is necessary to use for ($c_1$) the integrated mean value between $\theta_o$ and $\bar{\theta}_s$. To make this simpler, the integrated mean value from a room temperature value of 75°F is shown plotted along with the instantaneous values in Fig.43. Obviously $\bar{\theta}_s$ cannot be calculated until $R_1$ has been determined. This will now be done by considering the same problem as one of a moving heat source of strength $(1-R_1)\, q_1$, sliding with respect to the metal below the shear plane. In that case we can write from equation (2a) another approximate expression for the average shear plane temperature $\bar{\theta}_s$:

$$\bar{\theta}_s = (1-R_1)\, q_1 \frac{0.754\, t_d \csc\phi}{2 k_1 \sqrt{L_1}} + \theta_o \qquad (24)$$

Where in accordance with equation (1) $L_1$ is defined by

$$L_1 = \frac{V_s' t_d \csc\phi}{4 K_1} = \frac{\gamma V_t' t_d}{4 K_1} \qquad (25)$$

By equating the two expressions for the average shear plane temperature (23a) and (24) it is possible to solve for $R_1$, with the result

$$R_1 = \frac{1}{1 + \frac{.664\gamma}{\sqrt{L_1}}} \qquad (26)$$

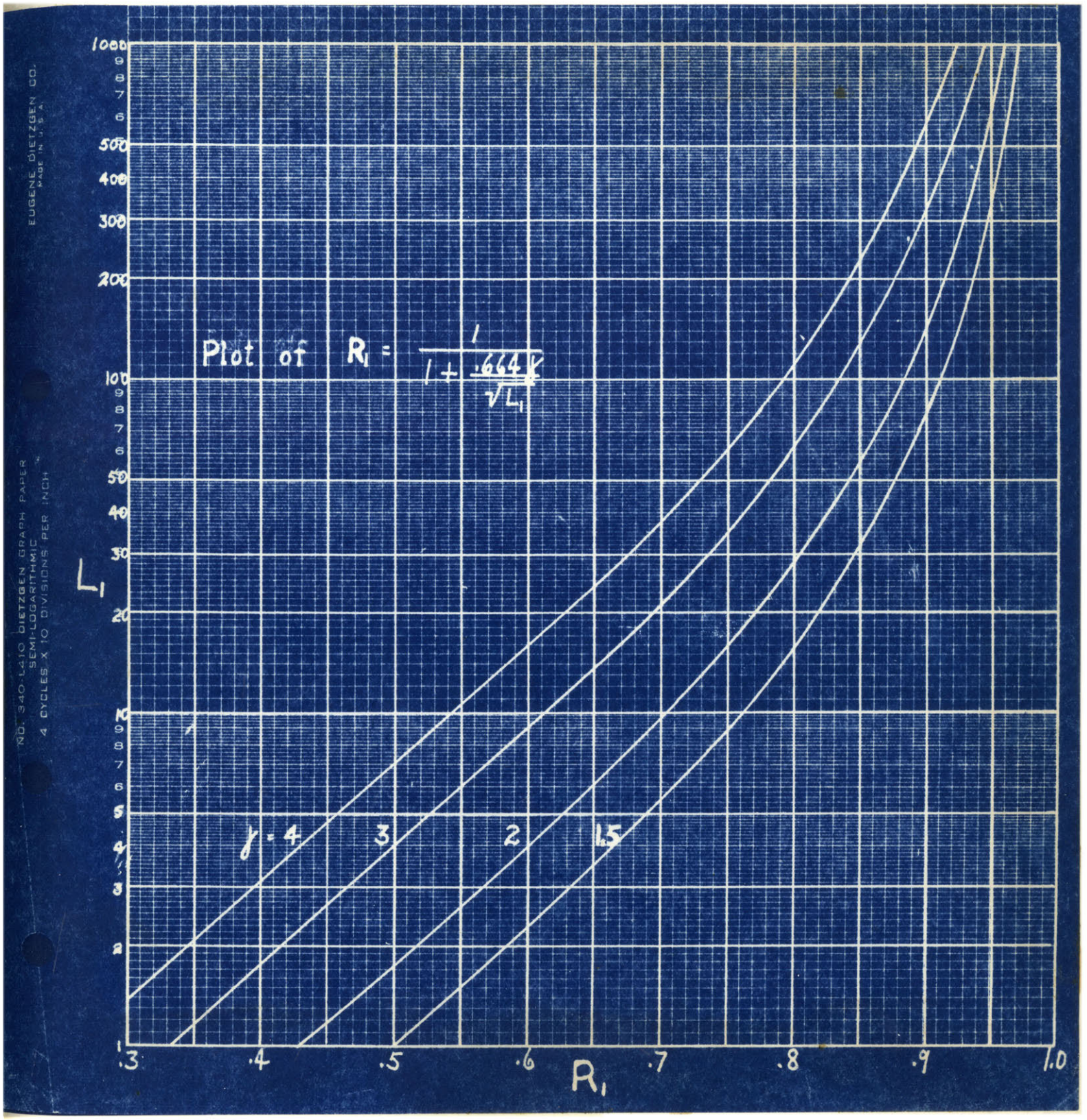
Plot of $R_1 = \frac{1}{1 + \frac{.664}{\sqrt{L_1}}}$
$L_1$
$R_1$
γ = 4
3
2
1.5
1000
500
400
300
200
100
50
40
30
20
10
5
4
3
2
1
.3
.4
.5
.6
.7
.8
.9
1.0
EUGENE DIETZGEN CO.
MADE IN U.S.A.
NO. 340-1410 DIETZGEN GRAPH PAPER
SEMI-LOGARITHMIC
4 CYCLES X 10 DIVISIONS PER INCH

Fig.50

For convenience in use, this equation has been plotted as a function of $L_1$ for several values of $\gamma$, in Fig. 50. There is nothing in this equation to indicate any practical limitation on $R_1$, except that equation (2a) is not valid of $L_1 < 0.2$, and the same restriction applies to equation (26). At low speeds and feeds this value of $L_1$ may be approached under actual cutting conditions, and with the usual values of the shear strain $\gamma$ results in values of $R_1$ as low as 0.25. This may at first glance appear unusual, since presumably heat has an equal opportunity to travel in either direction from the shear plane, which would limit $R_1$ to a minimum of 0.5. However, at slow speeds the greater mass of metal surrounding the lower portion of the shear plane allows greater heat transfer in this direction, so that equation (26) appears to fit the physical picture quite well.

Shaw (29) arrived at a similar solution, but projected the shear plane in the direction of the surface being cut. The difference between $R_1$ calculated by the two methods is less than 5% under a wide range of actual cutting conditions. For a tool with 20° rake angle the difference becomes negligible.

With $R_1$ determined from (26) $\bar{\theta}_s$ is most easily calculated from equation (23a), so that

$$\bar{\theta}_s = \theta_o + u_s \frac{1}{1 + \frac{.664\gamma}{\sqrt{L_1}}} \quad \frac{\sec \phi}{c_1 \rho_1 12J} \qquad (27)$$

Since in most cases an approximate value of $K_1$ or $L_1$ is sufficient to give satisfactory values of $R_1$, it is possible to find $\bar{\theta}_s$ directly, without a trial solution, by plotting the enthalpy (h) of the work material as a function of temperature, where (h), as usual, is defined as $h = \int_0^{\theta} c_p d\theta$, in Btu/lb. This can be done by noting that

$$\frac{R_1 u_s \sec\phi}{12 \rho J} = h_s - h_o \qquad (23b)$$

THE TOOL-CHIP INTERFACE (2)

Since it is one of the determining factors in tool life, the most significant temperature in the metal cutting process is that at the cutting face of the tool, and it is this value that will now be calculated. The value of $\bar{\theta}_s$ enters these calculations since the chip is 'preheated' by the shear process before it comes in contact with the tool.

As pointed out previously, this problem will be attacked as one consisting of a stationary heat source providing heat to the tool over the chip contact area, and the same area acting as a moving heat source with respect to the chip flowing past it.

The moving heat source problem is a relatively straightforward one. The amount of heat $q_2$ Btu/in$^2$/sec created by the friction on the tool face will be given by

$$q_2 = \frac{F_f V_c'}{12J\ a\ b} \qquad (28)$$

where the symbols are given in Table II: Of this total energy a fraction $R_2$ will be assumed to go to the chip, the remaining fraction $(1-R_2)$ to the tool. Then, in accordance with equation (2a) the average temperature rise $\bar{\theta}_f$ of the chip surface, due to its rubbing against the tool, is given by

$$\bar{\theta}_f = R_2 q_2 \frac{.754\ a}{2\ k_2\sqrt{L_2}} \qquad (29)$$

where in accordance with equation (1) $L_2$ is given by

$$L_2 = \frac{V_c' a}{4\ K_2} \qquad (30)$$

where $k_2$ and $K_2$ are the thermal conductivity and diffusivity respectively of the work material at the final average chip temperature. As in the

shear plane calculations, q has been assumed constant over the contact area. The mean temperature of the chip along the tool face contact area will be the sum of the shear and friction effects:

$$\bar{\theta}_t = \bar{\theta}_s + \bar{\theta}_f = \theta_s + R_2 q_2 \frac{.376\ a}{k_2 \sqrt{L_2}} \qquad (31)$$

To find $R_2$ we again make use of the technique of calculating $\bar{\theta}_t$ from the conditions of a stationary heat source $(1-R_2)\ q_2$ acting on the tool face.

A convenient approximation to the true picture is to assume an orthogonal tool having zero rake and clearance angles, such as shown in the sketch below. If these angles on an actual cutting tool remain small,

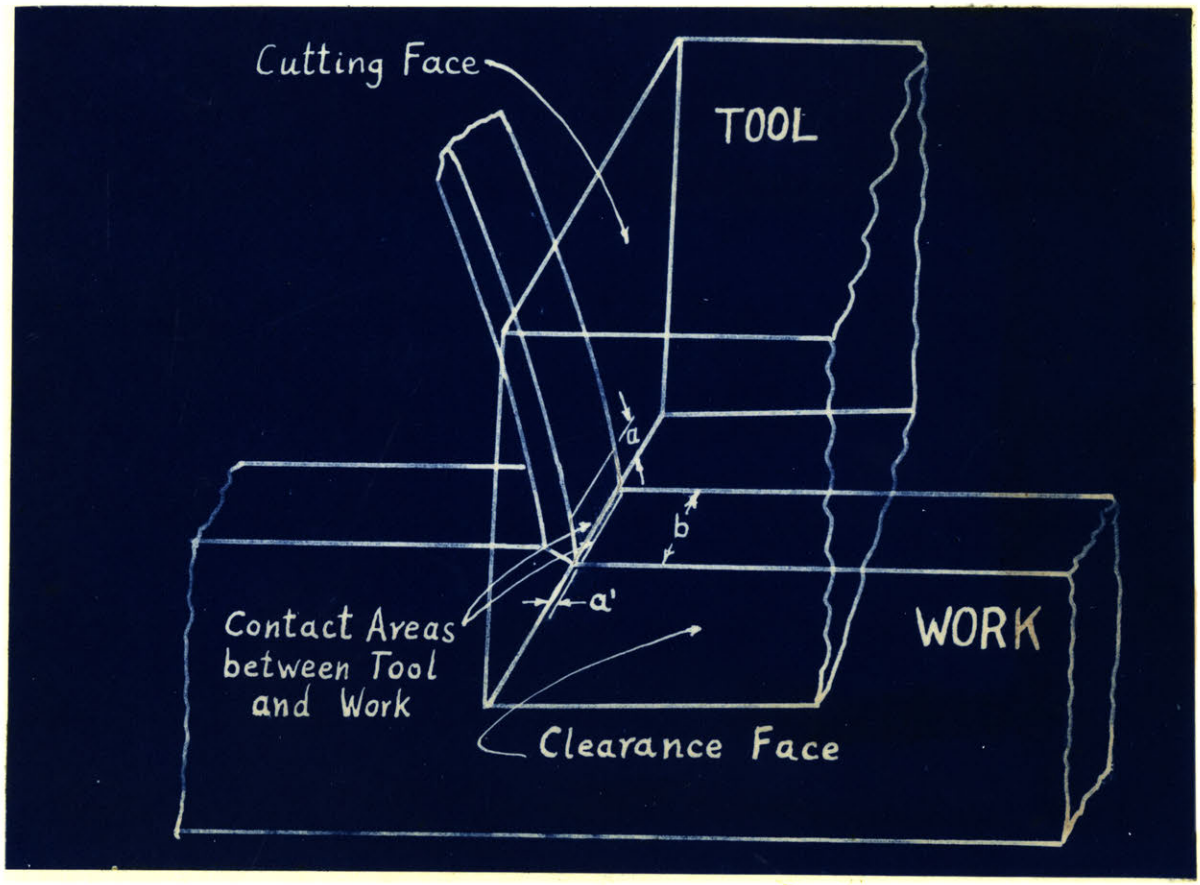


Figure 42.

Sketch of chip formation showing tool contact areas.

below $10^{\circ}$, the assumption should be a good one. For other tool shapes it would probably be most convenient to determine shape factors relating them to square tools, by making use of the relaxation method. This is always a somewhat tedious procedure, especially when it has to be carried out in three dimensions, even if the methods have been worked out (22). The contact area under consideration is a'b on the above diagram. The effect of the very small contact area a' .b on the clearance face will be discussed later, but is disregarded for the time being.

If both the cutting and clearance faces of the tools are considered perfect insulators except at the areas of contact, and if the tool is large compared to contact areas, assumptions later justified, then the method of heat images allows us to use the solutions for a semi-infinite body, since the latter is unchanged by inserting an insulating layer in the plane $x = 0$ or $y = 0$ (see Fig. 29). Thus equations (31) and (15) can be applied directly as long as the contact area is interpreted as

$$2m = b \qquad (32a)$$

$$l = a \qquad (32b)$$

Should the tool be cutting a corner instead of near the center, a picture corresponding more nearly to commercial use, the same reasoning allows the use of the semi-infinite body solution for this 1/8 infinite body, only that in this case $m = b$ and $l = a$. Although a factor of two is involved in the interpretation of m between the two cases, later calculations will show that the difference in tool temperature is only a few per cent.

All the experimental work was done under orthogonal cutting so that equations (32a) and (32b) most closely approximate the facts, and applying

equation (18) we can write

$$\bar{\theta}_t = \theta_o + (1-R_2)\, q_2 \frac{b/2}{k_3} \bar{S} \qquad (33)$$

where $k_3$ is the conductivity of the tool material, assumed a constant. The aspect ratio from which $\bar{S}$ is found in Fig. 46 is given by $m/\ell = b/2a$. In the unusual but not impossible case of $m/\ell < 1$, one merely uses the reciprocal value in finding $\bar{S}$.

By now equating the two expressions (33) and (31) for $\bar{\theta}_t$ it is possible to solve for $R_2$ and obtain

$$R_2 = \frac{q_2 \frac{b\bar{S}}{2k_3} - (\theta_s - \theta_o)}{q_2 \frac{b\bar{S}}{2k_3} + q_2 \frac{.376\, a}{k_2\sqrt{L_2}}} \qquad (34)$$

This can be rewritten in a simpler form, but with less physical meaning associated with the terms:

$$R_2 = \frac{1 - (\theta_s - \theta_o)\frac{2k_3}{q_2 b\bar{S}}}{1 + \frac{.752\, k_3\, a}{k_2 b\, \bar{S}\sqrt{L_2}}} \qquad (34a)$$

With this value of $R_2$ substituted into equation (29), $\bar{\theta}_f$ is readily obtained. Since $\bar{\theta}_t$ is the result of adding $\bar{\theta}_s$ and $\bar{\theta}_f$, a complete expression for $\bar{\theta}_t$ in terms of the measurable variables entering into the problem and parameters $L_1$, $L_2$, $\bar{S}$, $q_2$, calculated from them, follows from equation (31):

$$\bar{\theta}_t = \theta_o + u_s \frac{1}{1 - \frac{.664\sqrt{}}{\sqrt{L_1}}} \frac{\sec\phi}{c_1\rho_1 12J} + q_2 \frac{q_2 \frac{b\bar{S}}{2k_3} - \frac{u_s \sec\phi}{(1 - \frac{.664\sqrt{}}{\sqrt{L_1}})\, c_1\rho_1 12J}}{q_2 \frac{b\bar{S}}{2k_3} + \frac{.376\, a}{k_2\sqrt{L_2}}\, q_2} \frac{.376a}{k_2\sqrt{L_2}} \qquad (35)$$

It should be clear that values of the Tool tip temperature calculated from (35) can be no better than the assumptions made in the analysis, the measurements of forces and geometry, and knowledge of the thermal properties of tool and work materials. Just how important these various factors are will now be examined in some detail.

Sample Calculations

Although equation (35) is in concise form, it is not the most convenient one for obtaining a solution. In order to illustrate the most practical procedure for calculating $\bar{\theta}_t$ two illustrative examples will now be carried through, chosen at random from the data available.

Example 1:

Low Carbon ffee machining steel, with sulphur content 0.32%, .11%C
Tool: K2S Carbide, 20° Rake angle, 5° Clearance angle
Orthogonal cutting.
Quantities measured during test:
Cutting Speed $V_t$ = 445 ft/min $V_t'$ = 89 in/sec
Depth of cut $t_d$ = .0023"
Width of cut $b$ = .151"
Chip contact length a = .009"
Chip length ratio $r_c$ = .51
Cutting force $F_c$ = 80 lb.
Thrust force $F_t$ = 28 lb.
Quantities calculated from this data; from equations ( a) to ( m), p. 6 .
Average Shear strain $\gamma$ = 1.91
Shear energy $u_s$ = 153,000 in-lb/in$^3$
Shear angle $\phi$ = 30°
Chip velocity $V_c'$ = 45.4 in/sec
Friction force $F_f$ = 350 lb/in

Steps of solution:
1. Estimate $\bar{\theta}_s$, take 500°F
2. Look up value of $K_1$ at this temperature in Fig. (44): .020 in$^2$/sec
3. Calculate $L_1$ from $L_1 = \dfrac{V_t t_d}{4K_1} = 48.8$
4. Use the plot of equation (26) in Fig. 41 to find $R_1$ corresponding to $L_1$ = 48.8 and $\gamma$ = 1.91. $R_1$ = .84
5. Calculate $(\bar{\theta}_s - \theta_o)$ from equation (27), conveniently written as

$$(\bar{\theta}_s - \theta_o) = \frac{R_1 u_s \sec\phi}{2640} \frac{1}{c_1}$$

where $c_1$ is written separately so as to leave it the last operation on the slide rule. This enables $c_1$ to be chosen directly from the integrated mean curve of Fig. 43 to match the value of $\bar{\theta}_s$ resulting.

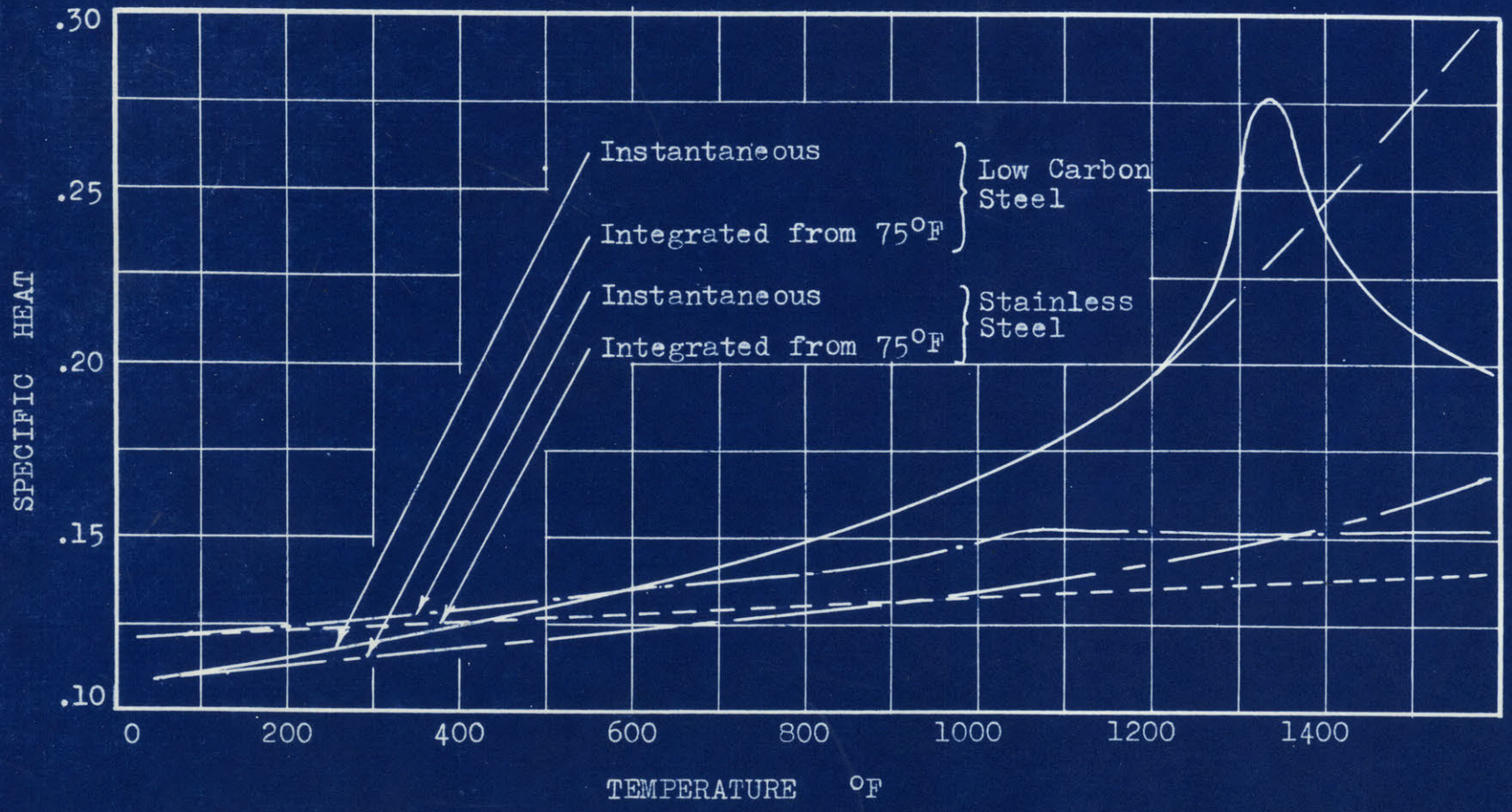


Fig.43
Instantaneous specific heats and values integrated from 75°F of Low Carbon Steel (.08C,.31 Mn) and Stainless Steel (19.1 Cr,8.1 Ni) Instantaneous values from 1948 Metals Handbook (p.314)

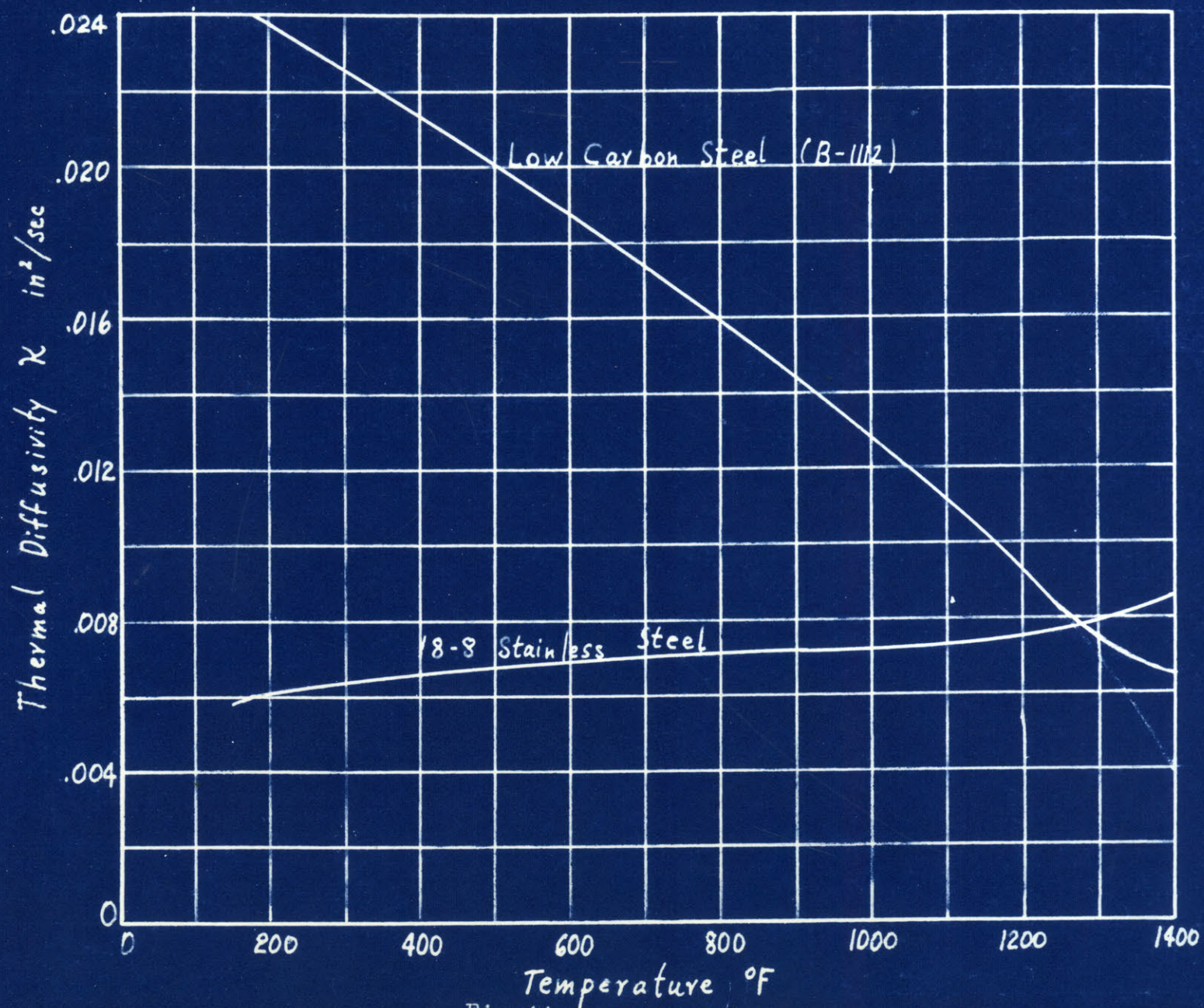
.024
.020
.016
.012
.008
.004
0
Thermal Diffusivity $\kappa$ in²/sec
Low Carbon Steel (B-1112)
18-8 Stainless Steel
0
200
400
600
800
1000
1200
1400
Temperature °F

Fig.44

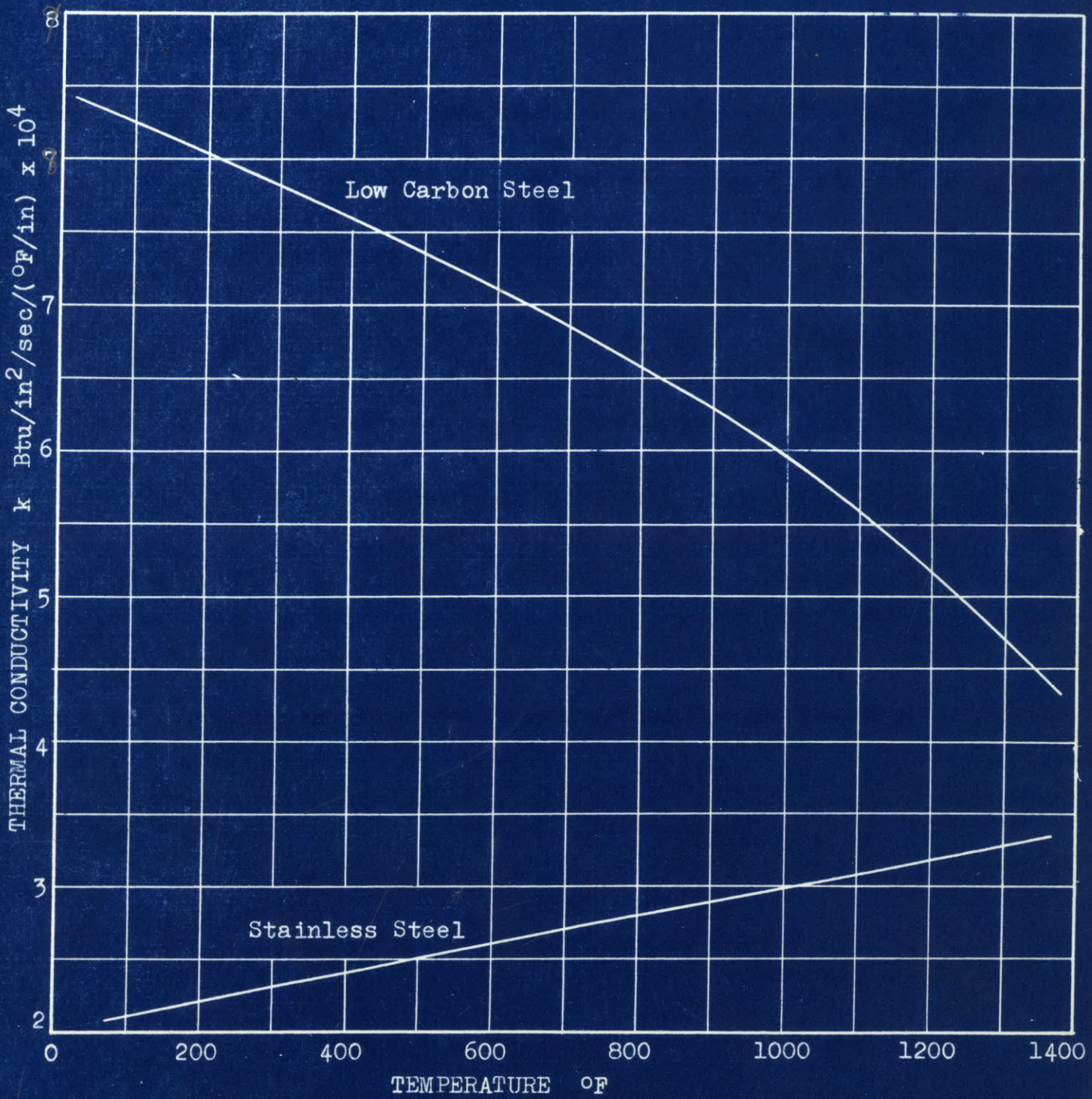


Variation of Thermal Conductivity with Temperature of Low Carbon Steel (.08C,.31 Mn) and Stainless Steel (19.1 Cr,8.1Ni). (From 1948 Metals Handbook).

Fig.45

Since the effect of $K_1$ on $R_1$ is not too strong, especially at high speeds, a second trial solution is needed only if the first guess missed by a large amount. In this case $c_1 = .120$, so that

$$(\bar{\theta}_s - \theta_o) = 468^\circ$$

With room temperature assumed ataa constant $75^\circ$ this makes

$$\bar{\theta}_s = 543^\circ F$$

This is close enough to the original estimate of $500^\circ$ to eliminate the need for a second solution.

6. Estimate $\bar{\theta}_t$ at $800^\circ F$ (since the measured value was $735^\circ F$)
7. Evaluate $K_2$ and $k_2$ at $800^\circ F$ from Fig. 44 and 45

$$K_2 = .016 \text{ in}^2/\text{sec} \qquad k_2 = 6.6\text{x}10^{-4} \text{ Btu/in}^2/\text{sec}/(^\circ F/\text{in})$$

8. Calculate $L_2 = \dfrac{V_c' a}{4K_2} = 6.38$, from equation (30)
9. Calculate the aspect ratio $m/\ell = b/2a = 8.4$
10. Evaluate the shape factor from Fig. 37 $\bar{S} = .255$
11. Calculate D, defined by $D = \dfrac{F_f V_c'}{24{,}800} = .64$

(This is evaluated separately purely for convenience in finding B and $q_2$)

12. Calculate B, defined by $B = \dfrac{D}{k_2 \sqrt{L_2}} = 384$
13. Calculate $q_2$ from equation (28), now rewritten as

$$q_2 = \frac{2.64\, D}{a} = 188 \text{ Btu/in}^2$$

14. Calculate A, again for convenience, defined by

$$A = q_2 \frac{b\bar{S}}{2k_3}$$

where $k_3$, the conductivity of the K2S carbide is taken as $7.63\text{x}10^{-4}$ Btu/sec/in$^2$/($^\circ$F/in)

$$A = 4730$$

15. Calculate $R_2$ from equation (34), now written more conveniently

$$R_2 = \frac{A - (\bar{\theta}_s - \theta_o)}{A + B} = .84$$

16. Calculate $\bar{\theta}_f$ from equation (29), now rewritten as $\bar{\theta}_f = R_2 B = 322^\circ$
17. Calculate $\bar{\theta}_t$ from equation (31),

$$\bar{\theta}_t = \bar{\theta}_s + \bar{\theta}_f = 865^\circ F$$

18. Compare with assumed value of $\bar{\theta}_t$, 800°F. The only quantity seriously affected by the difference between the two is $k_2$, and therefore B. The effect on $R_2$ is negligible. Repeating steps #12 to 17, results in an increase in $\bar{\theta}_f$ and $\bar{\theta}_t$ of 10°, which is negligible.
19. Compare this result with the measured temperature of 735°F.

Example 2:

Steel: 18-8 Stainless Steel (Austenitic)
Tool: 18-4-1 High Speed Steel, 15° rake angle, 5° clearance angle orthogonal cutting.
Quantities measured during test:

Cutting speed: $V_t$ = 140 ft/min $V_t'$ = 28 in/sec
Depth of cut $t_d$ = .0065"
Width of cut b = .134"
Chip contact length a = .034"
Chip length ratio $r_c$ = .54
Cutting force $F_c$ = 275 lbs
Thrust force $F_t$ = 115 lbs

Quantities calculated from this data:

Average shear strain: $\gamma$ = 1.92
Shear energy $u_s$ = 202,000 in-lb/in$^3$
Shear angle $\phi$ = 31.5°
Chip velocity $V_c'$ = 15.3 in/sec
Friction force $F_f$ = 1400 lb/in

Steps of solution:
1. Estimate $\bar{\theta}_s$ at 600°F
2. Evaluate $K_1$ at this temperature for 18-8 Steel, Fig. 44 $K_1$ = .0068 in$^2$/sec.
3. Calculate $L_1 = \dfrac{V_t t_d}{4K_1} = 13.0$
4. Using Curves of Fig. 41 find $R_1$ = .735
5. Calculate

$$(\bar{\theta}_s - \theta_o) = \frac{R_1 u_s \sec\phi}{2640} \frac{1}{c_1}$$

where $c_1$ is 0.127 (integrated mean value from 75°, Fig. 43) at 600°F, from which

$$(\bar{\theta}_s - \theta_o) = 560°F \text{ or}$$

$$\bar{\theta}_s = 635°F$$

This is close enough to the assumed value of 600°.

6. Estimate $\bar{\theta}_t$, using measured values as well as past experience as a guide, to be 1200°F.
7. Evaluate $K_2$ and $k_2$ at this temperature from curves in Fig. 44 and 45

$$K_2 = .075 \text{ in}^2/\text{sec} \qquad k_2 = 3.15 \text{ Btu/in}^2/\text{sec}/(^\circ\text{F/in})$$

8. Calculate $L_2$ from equation (30) $\quad L_2 = 17.4$
9. Calculate the aspect ratio $m/l = b/2a = 1.97$
10. Evaluate the shape factor from Curve in Fig. 37 $\quad \bar{S} = .65$
11. Calculate D $\quad D = \dfrac{F_f V_c'}{24{,}800} = .865$
12. Calculate B $\quad B = \dfrac{D}{K_2\sqrt{L_2}} = 660$
13. Caldulate $q_2 = \dfrac{2.64D}{a} = 67.3 \text{ Btu/in}^2$
14. Calculate A, where $k_3$ is the conductivity of High Speed Steel, taken as $3.4 \times 10^{-4}$ Btu/in$^2$/sec/(°F/in) $\quad A = q_2 \dfrac{6\bar{S}}{2}_3 = 8600$
15. Calculate $R_2$ from $\quad R_2 = \dfrac{A - (\bar{\theta}_s - \theta_o)}{A + B} = .866$
16. Calculate $\bar{\theta}_f = R_2 B = 572^\circ$
17. Calculate $\bar{\theta}_t = \bar{\theta}_s + \bar{\theta}_f = 1207^\circ\text{F}$
18. If the estimate of $\bar{\theta}_t$ in Step #6 had been off by more than 100° a second trial would have been required.
19. Compare with experimentally measured temperature of 1135°F.

ASSUMPTIONS MADE IN APPLYING EXACT ANALYSIS OF SEMI-INFINITE PLANE TO CONDITIONS IN A SQUARE TOOL.

If a simple square orthogonal tool is used, or if angles do not depart too far from that condition, there are only two assumptions necessary to apply the exact analysis of a semi-infinite body to a square tool, as long as the manner of heat supply is known (assumed here as constant over the area of application).

The first is the assumption of steady state conditions. As Pahlitzsh and Helmerdig (19) have shown, this is an important factor only at distances removed from the source. In the plane of the source steady state termperatures are reached almost instantaneously.

The other assumption is far more important in that it assumes negligible heat flow from the source, anywhere but into the body of the tool on the chip. Obviously this can only be an approximation, since actually heat will be lost by conduction, radiation and convection at various points of the tool. An attempt will now be made to estimate the amount of such losses and the effect they are likely to have. It should be borne in mind that only losses occuring close to the chip-tool contact area can have any serious effect on the temperature at that area.

The first area of loss to be considered will be the small contact area between the tool and work along the clearance face, just behind the cutting edge (see area a' .b in Fig. 42. Exact calculations are not possible, because the length of this area a' is difficult to estimate, although visual studies of cutting and tool wear indicate that for sharp tools it will be less than .001 inches. To find out how much heat can be lost here, data will be taken from an actual cutting test, and for three

assumed values of a' and corresponding temperatures, the amount of heat the work can absorb from such a source calculated from Jaeger's moving heat source solution. All values are taken for a tool one inch wide.

Example 1:

Cutting speed $V_t$ = 445 ft/min = 89 in/sec.
Length of contact on cutting face $a \doteq .009"$
Average temperature on cutting face $\bar{\theta}_t = 830^\circ F$
Approx. heat input to tool on cutting face: $(1-R_2)q_2 a = .27$ Btu/in/sec
Approx. thermal conductivity of work: $k_4 = .0007$
Approx. temp. of work surface preheated by shear wofk: $500^\circ F$
Approx. thermal diffusivity of work: $K = .020$ in$^2$/sec

| | a' = .001 | a' = .0005" | a' = .0001" |
|---|---|---|---|
| $L_3 = \frac{a'V_t}{4K}$ | = 1.1 | .55 | .11 |

From (2a) $(830-500) = \frac{q_4 \cdot .754 \frac{1}{2}(a')}{k_4 \sqrt{L_3}}$ where $q_4$ is the amount of heat transferred Btu/in$^2$/sec

| | | | |
|---|---|---|---|
| $(a'q_4)$ = | .64 Btu/in/sec | .21 | .021 |

There are several conclusions that can be drawn from these results. If generation of additional frictional heat over the clearance contact area a' is neglected then these results imply that either the temperature differential is less than the $330^\circ F$ assumed (830-500), or that a' is less than .0005". That this length is indded less than .001" was demonstrated by radioactive experiments described below. Otherwise, a reasonable balance between $q_4$ and the total heat supplied to the tool (.27 Btu/in/sec) is not maintained. It should be recalled that this calculation is for the amount of heat the work is capable of receiving, rather than what the tool is capable of supplying. For instance, lack of temperature

equilibrium across a', in other words a tool surface hotter than the work surface underneath it, would also cut down the calculated heat transfer $q_4$, from the tool to the work. In cutting, a certain small amount of heat as also bound to be generated at the clearance contact area which can be expected to provide at least part of the heat passed on to the work. Unfortunately there appears no way at present of assaying these conditions accurately. A study of Fig. 35 will show that only a complete change in the heat flow pattern could account for any significant flow across the Z-axis for such a very short distance from the origin. No such drastic distortion was noted by Bickel (2) in his thermocolor measurements. The result he gave for a tool giving a slight wear crater is shown in Fig. 43. Although experimental data was not given in great detail there does not seem to be any evidence that much heat is lost across the clearance face contact area.

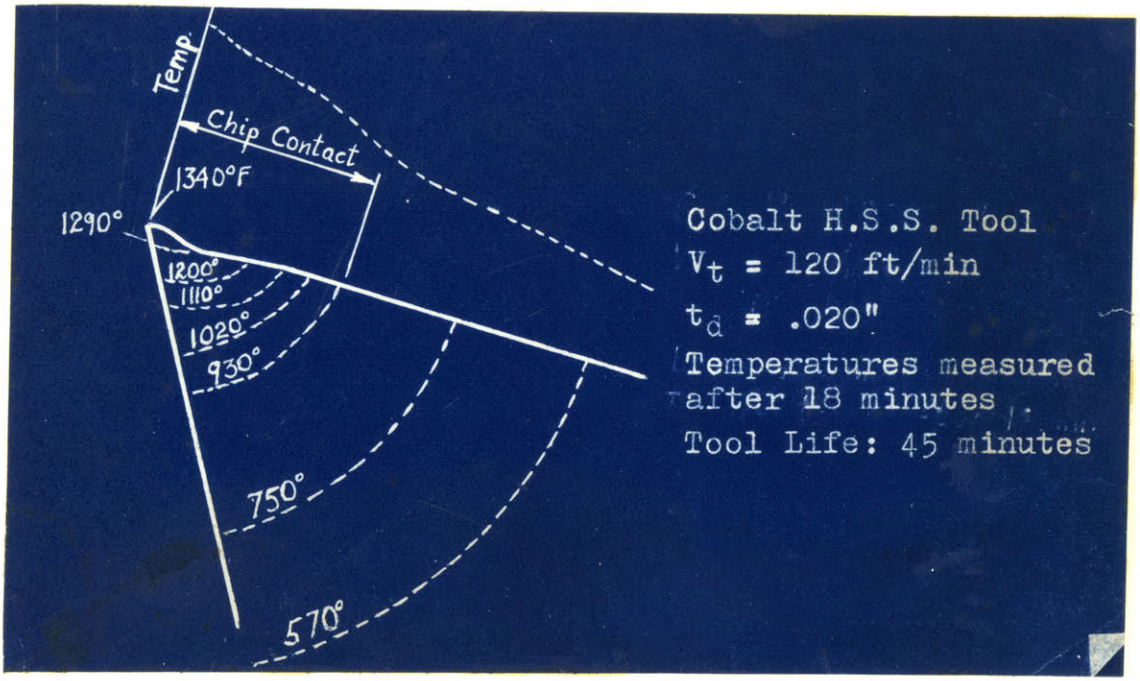


Figure 46.

Bickel solution for temperature along cutting face.

As Fig. 33 shows the temperature gradients in the tool are not very great once steady state conditions are reached, and this adds to the view that whatever heat transfer exists across the clearance face, contact area has a negligible effect on tool temperatures.

Due to the enclosed space along the clearance face, convention can be expected to take place principally from the cutting face. If the latter is horizontal, as it usually is on a lathe, then the heat transfer coefficient for free convection from the surface can be taken from McAdams (17) as $h_c = 0.38\ (\Delta\theta)^{.25}$ Btu/ft$^2$/hr, so that the heat lost from an area (A) with a temperature differential with the surroundings of $\theta$, is given by

$$q_{conv.} = 0.38\ A\ (\Delta\theta)^{1.25} \quad \text{Btu/hr} \qquad (37)$$

An approximate map of isotherms surrounding the chip contact area of the tool cutting face of the same case discussed above is given in Fig. 44, calculated with the help of equation(37)and Fig. 32. Subdividing this

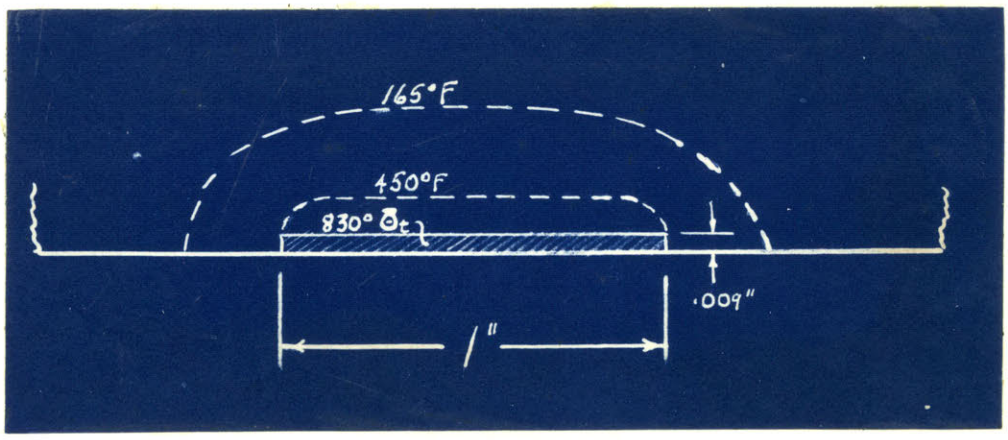


Figure 47.

Approx. map of isotherms surrounding chip contact area.

into regions small enough to work with average temperatures, it is possible to use equation (37) to arrive at an estimate of the amount of thermal energy lost by convection. This total amounts to only about 0.0001 Btu/in/sec, which is an insignificant fraction of the energy supplied to the tool (0.27 Btu/in/sec). Over the range of temperatures involved in metal cutting, the radiation losses are of the same order as the convection losses, and can be disregarded for the same reason.

Since as a rule the chip contact area is small compared with the dimensions of the tool body, the assumption of the latter as being infinite in directions away from the cutting edge is probably a good one, although correction could be made in longer runs if the temperature of the tool sides increased much above room temperature. The effect is merely to raise the base or reference temperature by just that amount.

Summarizing now, it seems fair to state that the exact solution of temperature distribution in a semi-infinite body, insulated except over a finite area over which thermal energy is supplied, can be applied well within engineering accuracy to the case of a finite approximately square tool.

There is one common commercial practice which complicates this picture, and that is the use of liquid coolants. However, as Pahlitzsch and Helmerdig (19) showed, such a coolant must be applied very close to the cutting edge if the temperature at this point is to be affected significantly. The main body of the tool is cooled very easily, of course. This view is supported by Pigott and Richardson's (31) work who found that at speeds above 100 ft/min fluids had very little effect on the measured temperatures. R.J.S. Pigott (20) showed that the speed

at which fluids remained effective in cutting down temperatures could be increased considerably if the fluid is forced into the wedge formed between work and clearance of the tool by means of high pressure jets. This agrees with the work of Lauterbach and Ratzel (15) who demonstrated by some neat experiments that for low speeds at least, cutting fluids penetrate to the cutting face from the clearance face.

In order to learn more about the action of cutting fluids, in particular their effective working area on the tool, some experiments were run in which the fluid was made radioactive. Both steel and aluminum were cut on a planer type of set-up, shown in Fig. 48, and the fluid used was Amyl Iodide, $CH_3(CH_2)_3CH_2I$, chosen because it is an effective cutting fluid (as demonstrated by both force and surface finish measurement) and contains 64% by weight $I_{131}$, a highly active (8-day half-life) isotope of Iodine.

The tests were performed by adding a few drops of the active fluid after the cut had started and thoroughly scrubbing the tool afterwards with cotton soaked in Methylene Iodide, to remove any traces of unreacted fluid remaining on the surface. As a control, similar tools were allowed to cut either dry or with ordinary Amyl Iodide as cutting fluid and then had some radioactive fluid dropped on afterwards, and washed off like the other tools after 1 minute.

To measure the amount and location of radioactivity as accurately as possible, a small piece of very thin (.0007") Kodak NTB nuclear strip film was wound around the tool, held in place by scotch tape. After being exposed for 10 days, in cans kept dry with silica gel, the films were developed in concentrated D-19 developer for 20 minutes.

A typical result is shown in Fig. 46a, where B-1112 steel had been cut with a 15° rake angle 18-4-1 High Speed Steel Tool, at a speed of 2 1/8 in/min, at a depth of cut of 0.010".

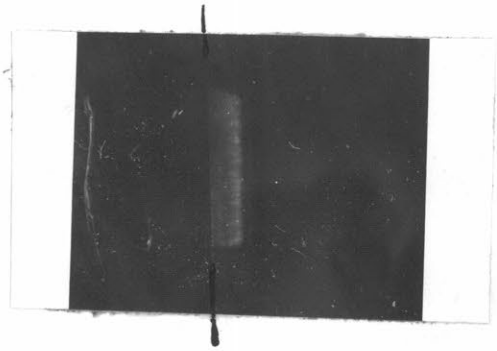

Figure 46a

Autoradiograph of a Tool, using Radioactive Amyl Iodide as cutting fluid. Cutting edge marked by ink line, with cutting face to right of edge. Magnification 4x.

Although exact measurements are difficult to make the activity shown above is estimated to correspond to about $3 \times 10^{-6}$ g/cm$^2$ of Iodine, which is equivalent to about ten monolayers of iodine compounds, presumably ferric iodide.

However, it is quite clear that the fluid was active over the entire cutting face, right down to the cutting edge. Since no trace of activity was visible on the clearance face in any of the tests, it is clear that if there is any area on the clearance face at the cutting edge, where pressure and temperature are high enough to cause decomposition of the cutting fluid, such an area must be less than .001" wide.

## THE EFFECT OF CHIP LENGTH (a) ON TOOL TEMPERATURE

Of all the quantities measured in the cutting process, the greatest uncertainty exists in the determination of (a), the length along the tool face over which the chip makes contact. It is natural, therefore, either to improve this measurement, or lacking this possibility, to blame any discrepancies between calculated and measured temperatures on the value of (a). Whether this is reasonable or not will now be explored.

The reason for the difficulty in measuring (a) lies in the fact that it cannot be measured directly during a cut, but must be obtained from observation of the tool after a cut. As a rule it is not difficult to distinguish the area of the tool which has had contact with the chip from the part that has not. With steel tools such observation is aided if the tool is first given a very thin copper plate, by rubbing a little acidified copper sulphate solution over the surface. With Carbide tools this method fails, but the tarnishing of a polished tool face, where the chip has rubbed over it, is quite obvious. This means regrinding the tool after every test. The actual measurement was made with a Spencer Microscope having a reticule in the eyepiece, with divisions corresponding to .002 inches on the tool, and visually integrating the ragged edges. Trigger and Chao (6) proposed photographing the contact area and measuring enlarged pictures, but such refinement seems quite unwarranted at present.

Obviously any such measurement as just described can give only the total length over which contact has taken place sometime during a test, and therefore represents more of an upper limit than a true contact area. The difference between what may be regarded as a true area, and it is

not yet established whether this is the same for force transmission and temperature calculations, is to a large extent due to a built-up edge. Even the very small built-up edge that is nearly always present can have a disturbing effect. This accounts for the considerable effect a good cutting fluid has on the contact length, and the fact that (a) usually decreases with speed, in fact with anything that reduces friction between chip and tool, such as increasing the sulphur content in low carbon steel.

In order to assay the importance of (a), seven runs were chosen at random from the large amount of data available, the temperature calculated from equation (35) and then repeated with different values of (a). The results are shown in Figure 47, where to gain a quick oversight the values of (a) actually observed are marked with an x. In addition, a circle (O) marks the point where the temperature corresponds to that measured by the tool-work thermocouple method.

The conditions for the runs plotted in Figure 47 are given in Table III.

Table III

| Run | Work Material | Tool | Rake angle | Cutting Speed ft/min | Depth of Cut inches |
|---|---|---|---|---|---|
| 18F | 18-8 Stainless | K2S Carbide | 20° | 616 | .0065 |
| 4F | " | " | " | 616 | .0023 |
| 16F | " | " | " | 86 | .0065 |
| 24F2 | " | 18-4-1 High Speed | 15° | 277 | .0023 |
| 4E | Low Carbon Steel 32%S | K2S Carbide | 20° | 445 | .0023 |
| 11F | 18-8 Stainless | " | " | 15 | .0044 |
| 22F | " | 18-4-1 High Speed | 15° | 15 | .0023 |

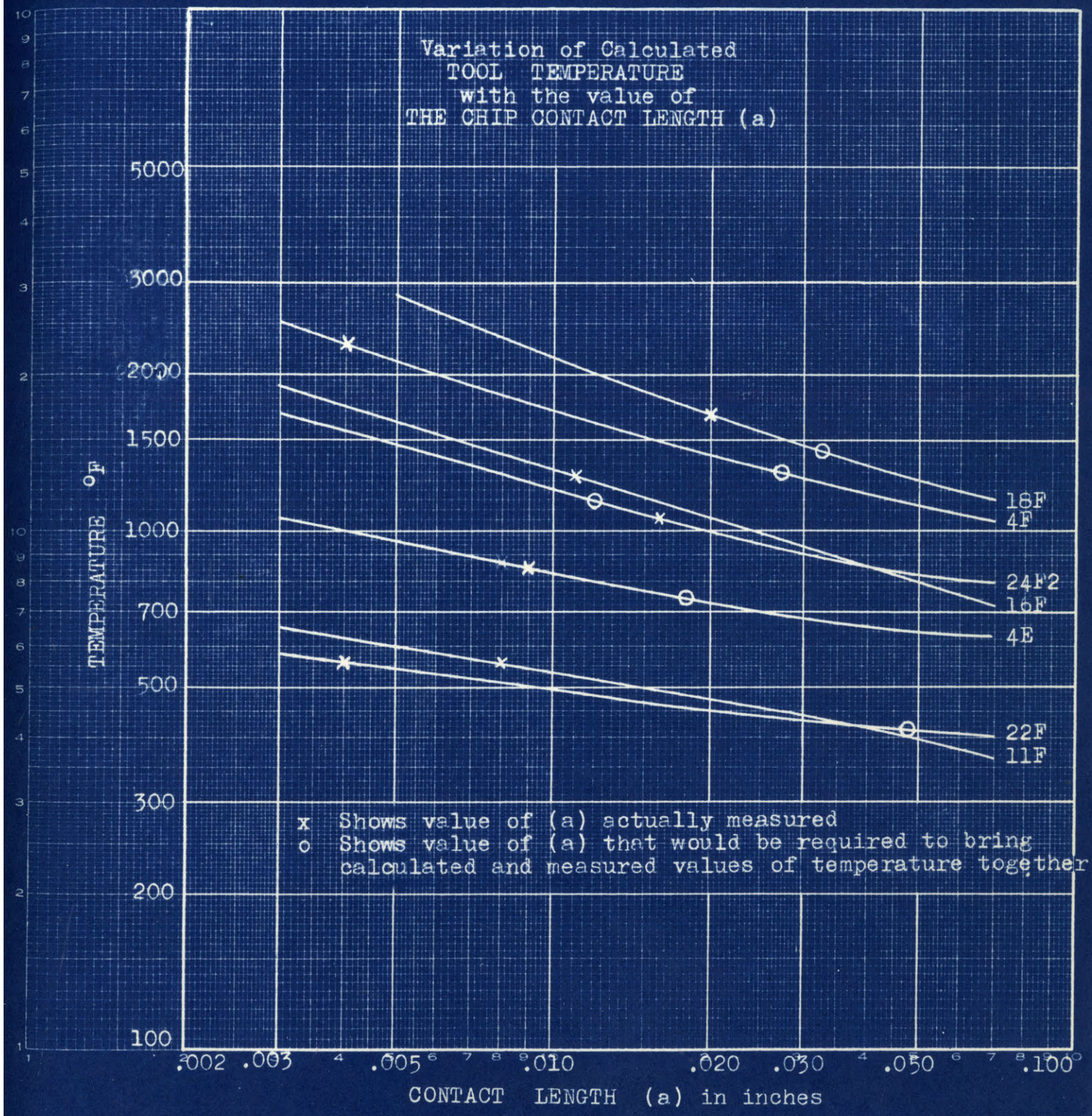
Variation of Calculated
TOOL TEMPERATURE
with the value of
THE CHIP CONTACT LENGTH (a)
TEMPERATURE °F
5000
3000
2000
1500
1000
700
500
300
200
100
18F
4F
24F2
16F
4E
22F
11F
x Shows value of (a) actually measured
o Shows value of (a) that would be required to bring calculated and measured values of temperature together
.002
.003
.005
.010
.020
.030
.050
.100
CONTACT LENGTH (a) in inches

Fig.47

It is clear from the curves of Fig. 47 that the effect of changes in (a) on calculated temperatures is not too great, especially at low speeds. However, it should be kept in mind that percentage error in measuring (a) increases as (a) becomes smaller.

Experimentally observed values of (a) obtained under a wide variety of conditions, for both 18-8 Stainless steel and low carbon steel containing different amounts of sulphur are plotted in figures (48 a, b, c). The more erratic the curves the more certain one can be that a built-up edge was present. On the whole it can be said with a fair degree of certainty that when (a) is less than twice the depth of cut there is no appreciable built-up edge, and that when (a) is more than four times the depth of cut that there will be an appreciable depth of cut. This, of course, is just a rule of thumb.

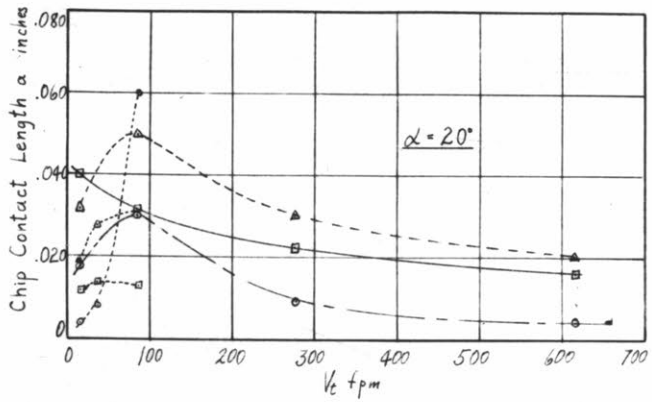


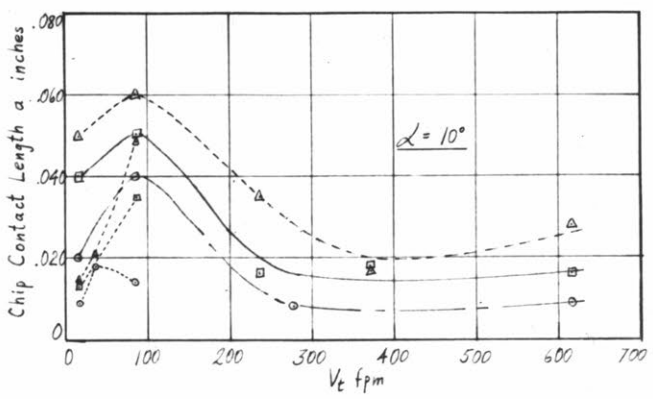


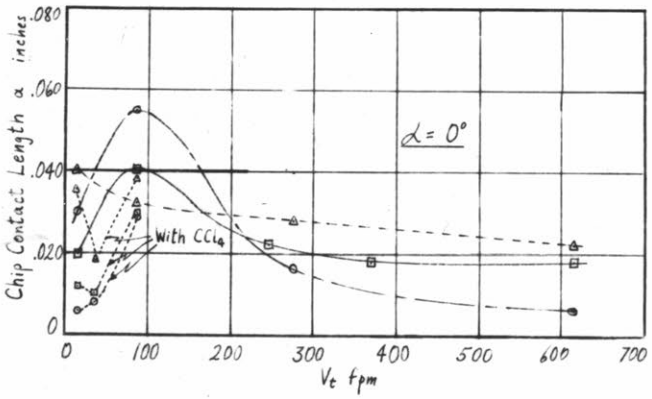


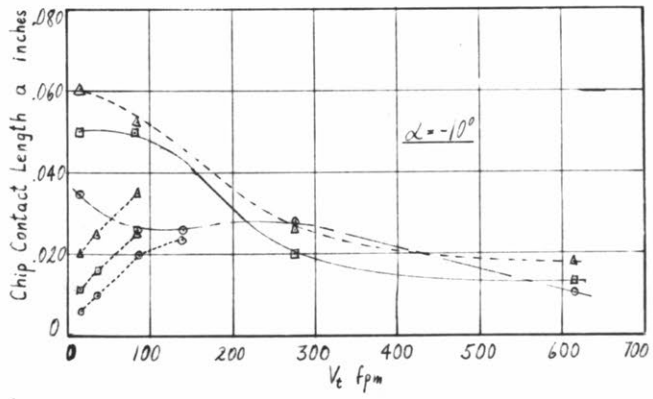


CHIP CONTACT LENGTHS VS. CUTTING VELOCITY CURVES

ORTHOGONAL CUTTING

WORK MATERIAL: 2½" Diam. Bar 18-8 Stainless Steel as receieved

TOOL MATERIAL: K2S Tungsten-Titanium Carbide
Rake angles: As shown on graphs
Clearance angle: 5°
Width of cut: 1/8" approx.

FLUID: None
Low Speed Tests repeated using Carbon-tetrachloride.

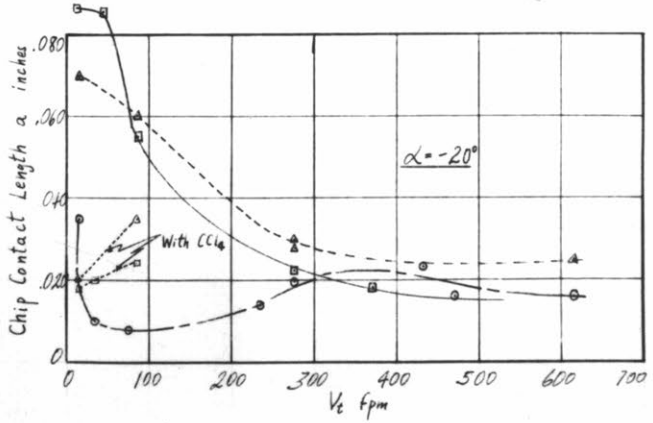


Fig. 48a

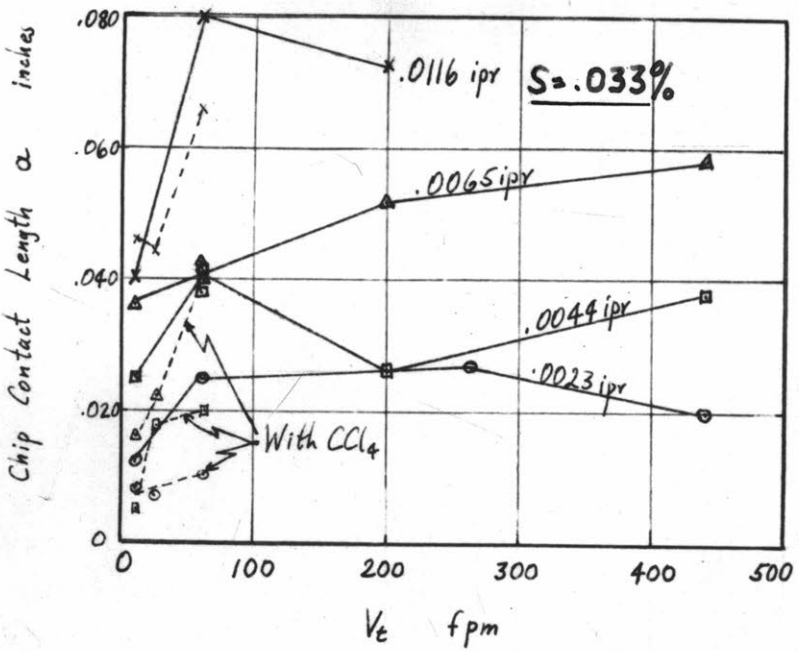


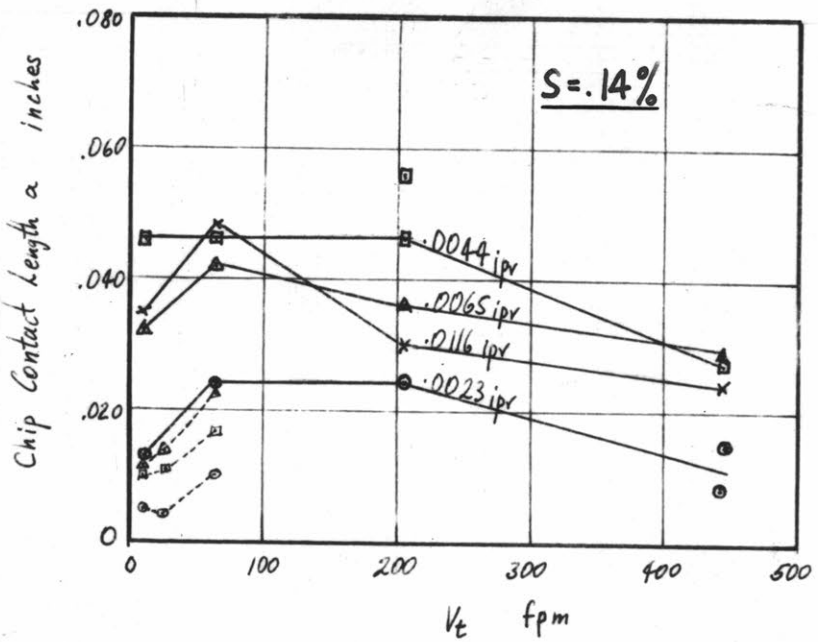


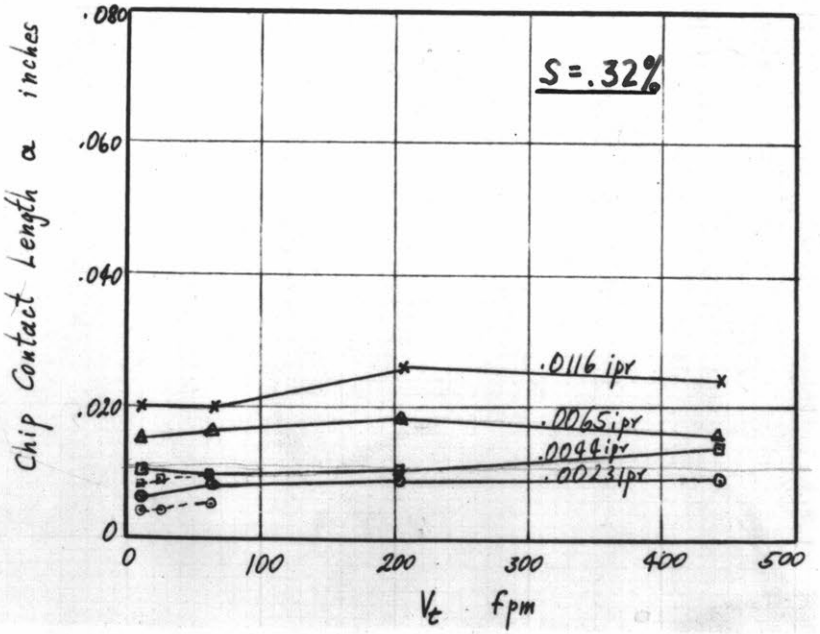


CHIP CONTACT LENGTH VS. CUTTING SPEED CURVES
ORTHOGONAL CUTTING

WORK MATERIAL: 1 7/8" Diam. bars of type B-1112 steel containing various amounts of sulphur.

TOOL MATERIAL: K2S Tungsten-Titanium Carbide
Rake angle: 20°
Clearance angle: 5°
Width of cut: 1/8" approx.

FLUID: None
Some low speed tests repeated using Carbon-tetrachloride (dotted lines)

Fig.48b

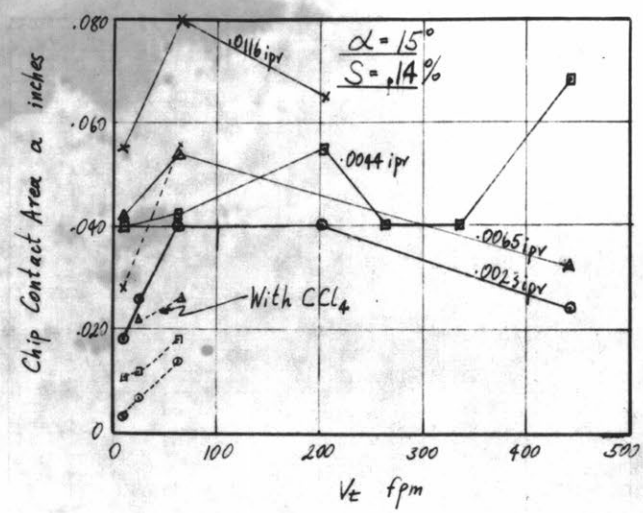


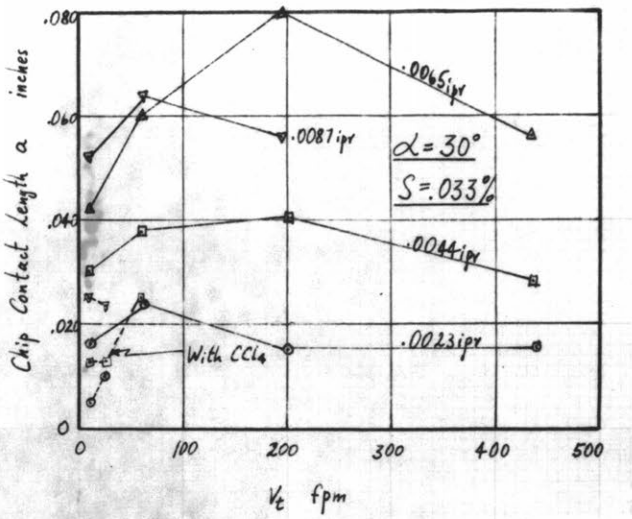


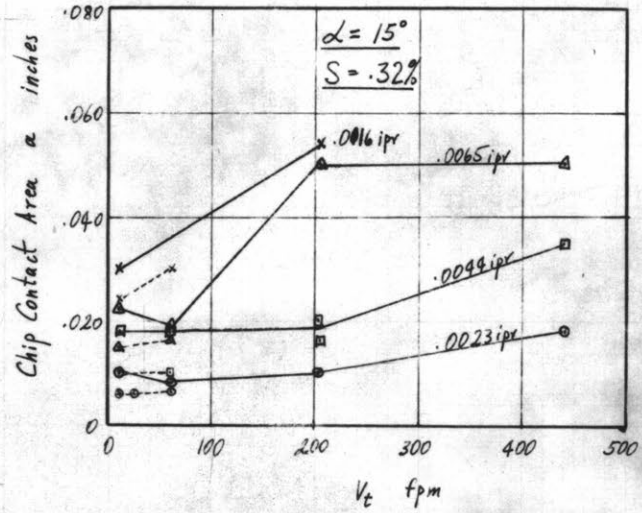


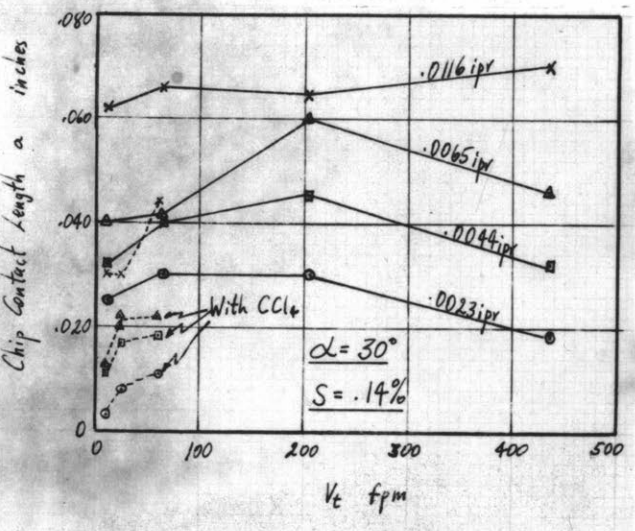


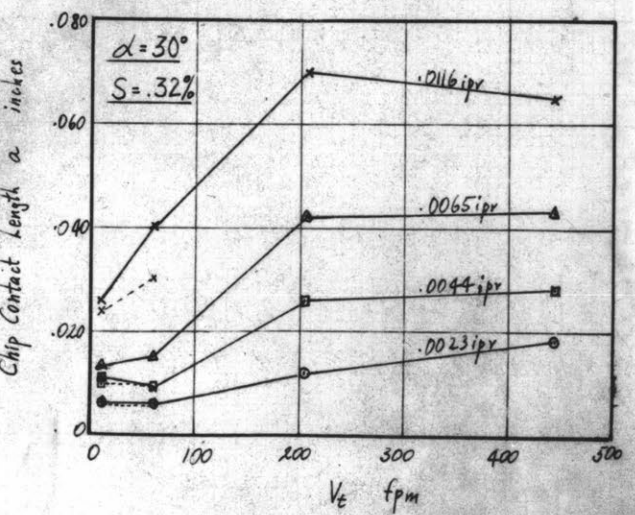


CHIP CONTACT LENGTH VS. CUTTING SPEED CURVES
ORTHOGONAL CUTTING

WORK MATERIAL: 1 7/8" Diam. bars of type B-1112 steel containing various amounts of sulphur.

TOOL MATERIAL: 18-4-1 High Speed Steel
Rake angle: 15° and 30° as shown
Clearance angle: 5°
Width of cut: 1/8" approx.

FLUID: None
Some low speed tests repeated using Carbon-tetrachloride cutting fluid.

Fig.48c

THE EFFECT OF WIDTH OF CUT ON TOOL TEMPERATURE

Besides direct comparison between calculated and measured tool tip temperatures the two most convenient means of checking on the validity of equation (35) is to compare experimental and calculated data for trends when either the depth of cut ($t_d$) or the width of cut (b) is changed. The convenience lies in the fact that in both cases cutting conditions do not change too much except for the desired difference in geometry, and what changes do occur are easily visualized.

To check on the effect of width of cut, a piece of B-1112 steel was cut with a $20^\circ$ Rake angle K2S Carbide Tool over a wide range of speed and at two different feeds, under orthogonal conditions. Use of a trepanning tool made it possible to generate wall thicknesses (b) down to .010", short of course, to prevent buckling. The temperatures as measured by the tool-work thermocouple method are shown plotted as dotted lines in Fig. 49. The unusual shape of the 84 ft/min curve for .0044" depth of cut, is due to built-up edge formation.

The corresponding calculated temperatures were obtained from force measurements made on the A-3 (.27% S) low carbon steel, very similar to B-1112, at widths of cut around 0.14". They are plotted as solid lines in Fig. 49, and arrows from the depth of cut figures connect corresponding calculated and experimental values. In two cases, both for $t_d$ = .0023", when $V_t$ = 15 and 226 ft/min, the theoretical and experimental values are so close together as to preclude separate curves. In the other cases the absolute agreement is not so good, but the shape of the curves is similar enough to give a good check on the geometrical quantities in equation (35).

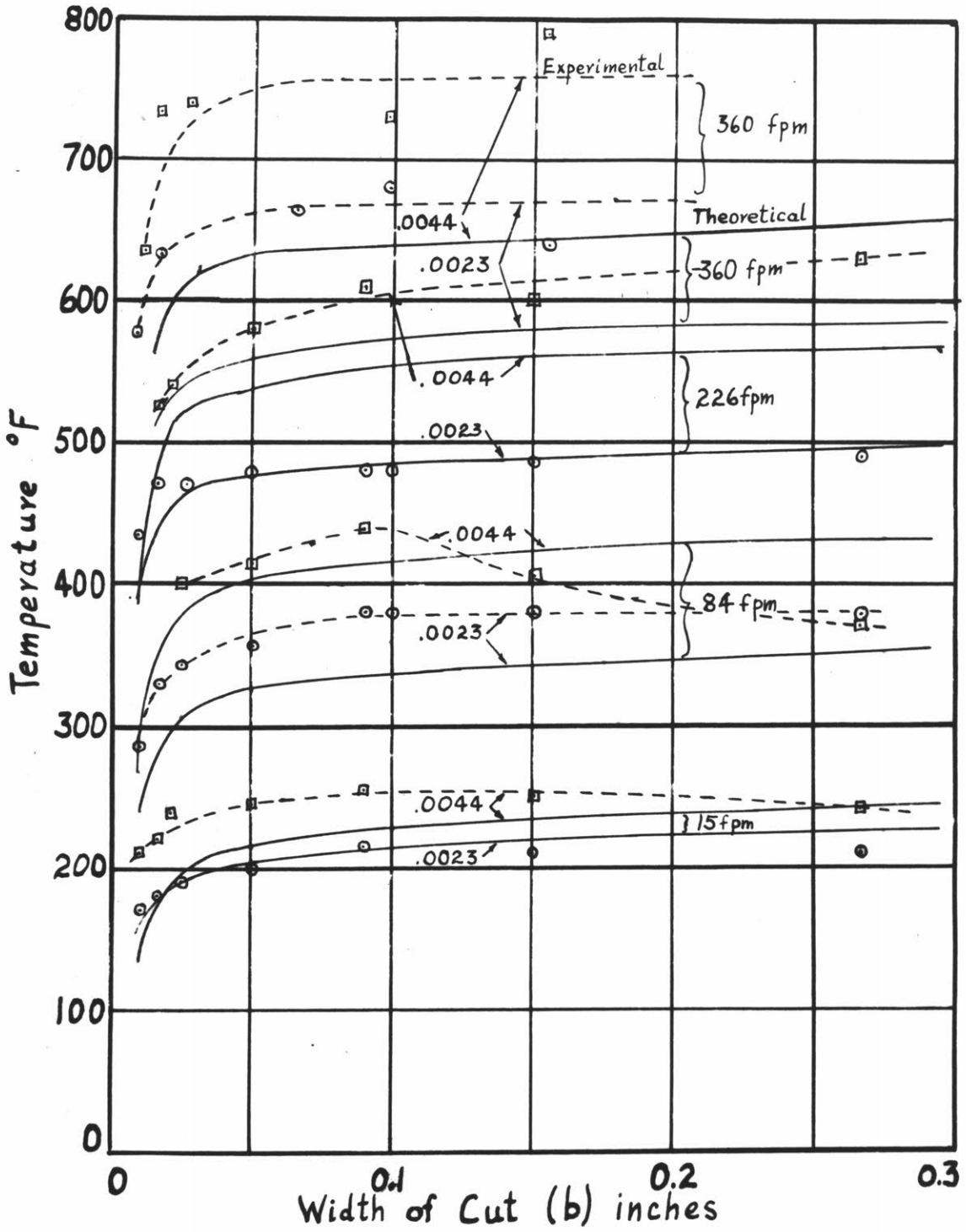


VARIATION OF CUTTING TEMPERATURES WITH WIDTH OF CUT

Orthogonal Cutting

Material: B-1112 Steel
Tool: K2S Carbide, 20°Rake angle, 5° Clearance angle

Calculated Temperatures: Solid Lines
Feeds: .0023 and .0044 inches/rev.

Measured Temperatures: Dotted Lines
● .0023 inches/rev. feed
□ .0044 inches/rev. feed

Fig.49

When (b) becomes very small the radiation and convection from the workpiece would be expected to become noticeable and act to reduce experimental values. That such was not observed may be due to the slight strain hardening of the material at the inside and outside diameters due to previous machining, which would have a negligible effect at large values of (b). Within the limits of the dynamometer used (max.sensitivity 1 lb) forces were found to be exactly proportional to (b), but at least 10 times this sensitivity would be required to check on this proportionality accurately when (b) becomes as small as 0.010".

EFFECT OF DEPTH OF CUT ON TOOL TEMPERATURE

Although the depth of cut was varied in several hundred tests, only two representative series are shown in Fig. 50. The experimental values are indicated by circles (o) connected by dotted lines, while calculated values are drawn as solid lines, with a solid dot (o) indicating the depth of cut at which the basic data for making the calculations was obtained. In making these calculations it was assumed that nothing changes with depth of cut except the geometry and the forces, both in direct proportion. No account was taken of the size effect (increased apparent strength at lower depths of cut) nor of any change in thermal properties that might accompany the change in calculated temperature. The effect is small enough to justify the considerable simplification of the calculations that results.

In the case of low carbon free machining steel (.32% S) the agreement between experimental and calculated temperatures is very good inddeed, both as regards absolute values and the shape of the curves. The reason for the

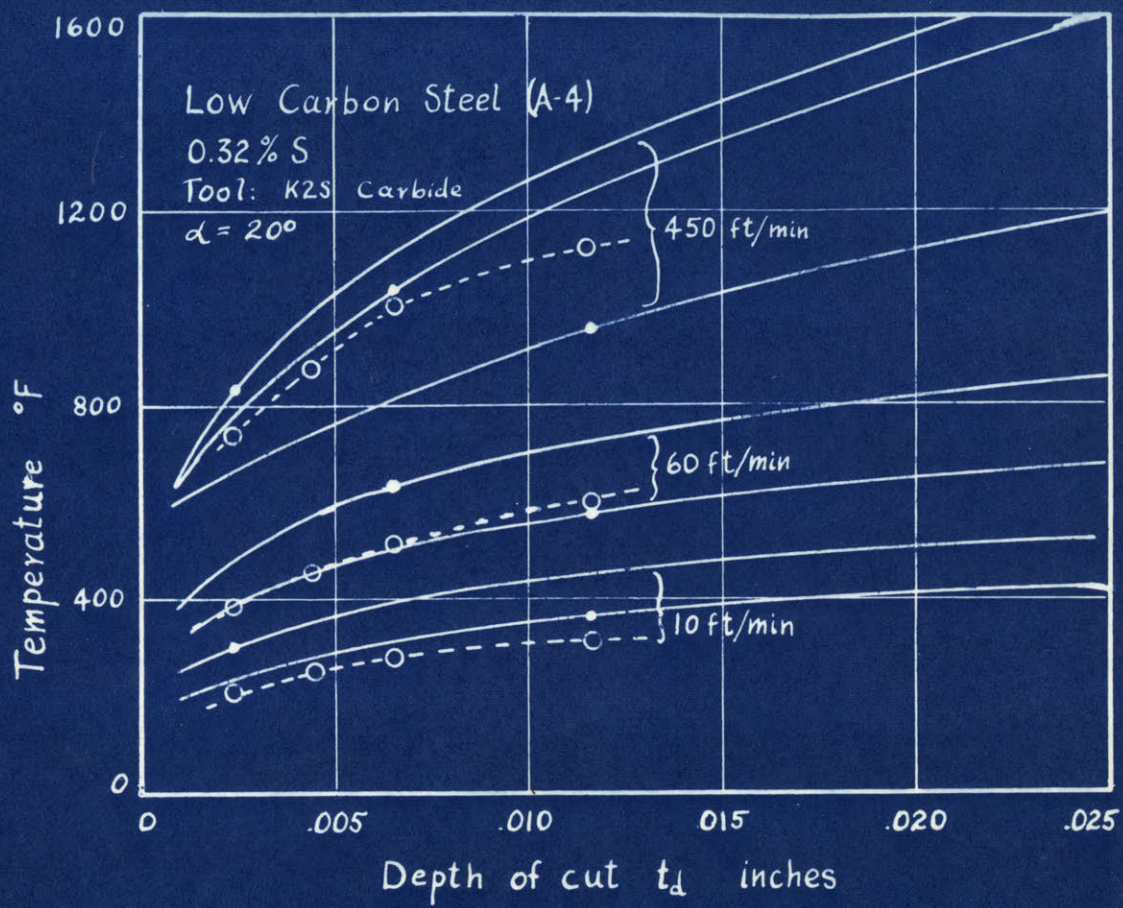
Low Carbon Steel (A-4)
0.32% S
Tool: K2S Carbide
α = 20°
450 ft/min
60 ft/min
10 ft/min
Temperature °F
1600
1200
800
400
0
0
.005
.010
.015
.020
.025
Depth of cut $t_d$ inches

(a)

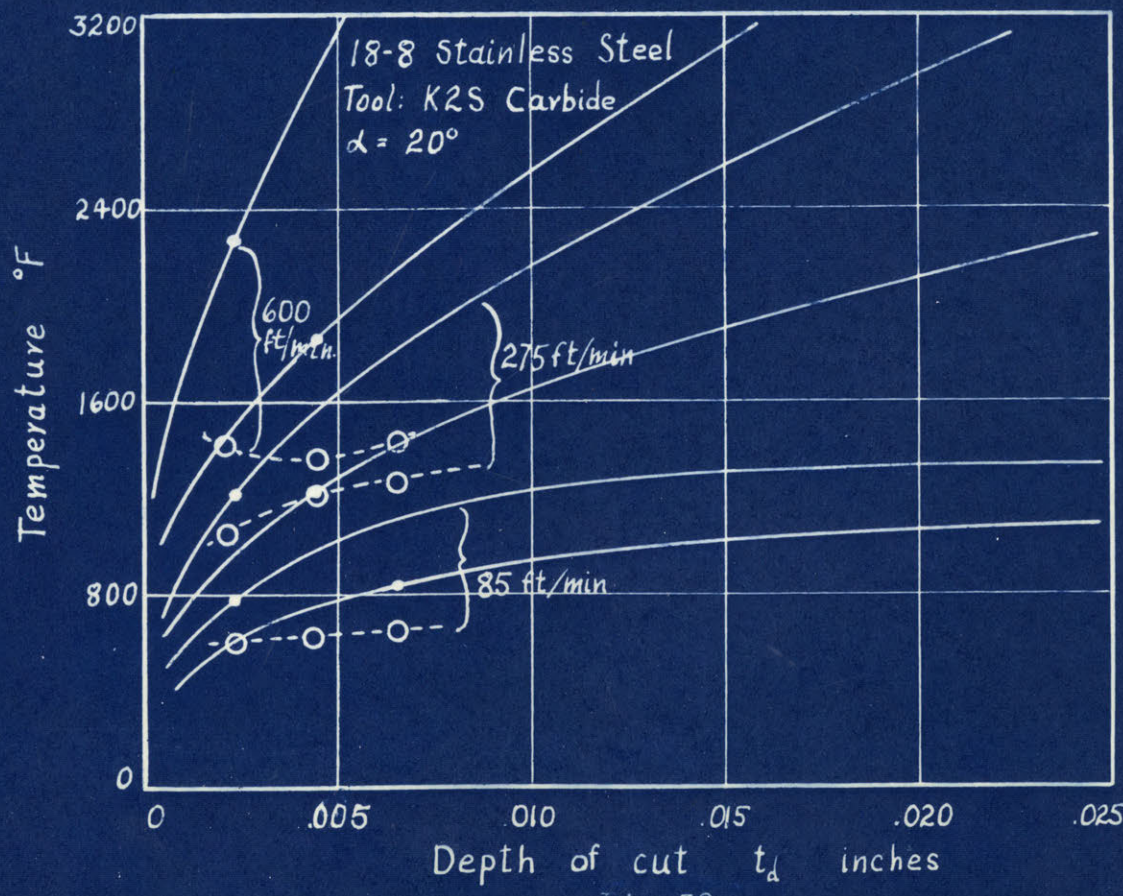
18-8 Stainless Steel
Tool: K2S Carbide
α = 20°
600 ft/min.
275 ft/min
85 ft/min
Temperature °F
3200
2400
1600
800
0
0
.005
.010
.015
.020
.025
Depth of cut $t_d$ inches

(b)

Fig. 50

difference between the theoretical curves lies in the above mentioned size effect and the lack of proportionality between depth of cut and length of chip contact. It is interesting to observe that the lower the cutting speed the larger the depth of cut at which calculated and measured temperatures agree.

Similar data taken with 18-8 Stainless Steel show far less agreement between theory and experiment, as is evident in Fig. 50. Reference to Fig. 62 shows far less regular behaviour in the variation of temperature with speed and feed, in some cases increased feed resulting in lower temperatures. This can be ascribed in large part to the irregular formation of a built-up edge, which makes good thermo-electric measurements impossible. The lack of proportionality of chip contact length and depth of cut, as evident in Fig. (48a,b,c) lends further support to this view. The discrepancy at the high speed of 600 ft/min cannot be explained in this manner, but is discussed later. Comparison with the low carbon steel shows that with stainless steel sensitivity of temperature to increased depth of cut is about twice as great (note different scales).

In general, curves such as these may be very helpful in correlating allowable cutting speeds to depth of cut whenever tool temperatures are the limiting factor. Thus tool life studies made at one depth of cut may be converted to other depths. If this can be substantiated by experimental studies of tool life, it would prove a very useful concept.

## THE EFFECT OF THERMAL PROPERTIES OF WORK MATERIALS ON CUTTING TEMPERATURES

It is clear from the number of times they enter into equation (35) that the thermal properties of the work material will have an important bearing on the temperatures reached in the cutting process. The two properties considered here as the primary ones are conductivity and specific heat, since the diffusivity is a function of these two, as long as the very small changes of density with temperature are ignored.

The clearest picture of the effect that changes in thermal properties can have, is to take actual cutting data and then change values of conductivity and specific heat by arbitrary ratios wherever they appear in the calculations, and assume that nothing else changes. In this manner the shape of the conductivity curves is maintained. What happens to calculated temperature when the conductivity is changed is shown in Fig. 51, while Fig. 52 gives a similar picture of the effect of specific heat, both sets of values calculated from a series of arbitrarily chosen runs, the conditions of which are listed in the Table V below,

Table V

| Run | Work Material | Cutting Speed ft/min . | Depth of Cut $t_d$ inches | Tool Material | Rake angle |
|---|---|---|---|---|---|
| 4E | Low Carbon Steel with Sulphur | 445 | .0023 | K2S Carbide | 20° |
| 16E | content of .32% | 62 | .0065 | " | " |
| 28E | " | 445 | .0116 | " | " |
| 4F | 18-8 Stainless | 616 | .0023 | " | " |
| 18F | " | 616 | .0065 | " | " |
| 22F | " | 15 | .0023 | 18-4-1 HSS | 15° |
| 36F | " | 15 with $CCl_4$ fluid | .0065 | " | " |
| 24F2 | " | 277 | .0023 | " | " |
| 7F | " | 86· with $CCl_4$ fluid | .0023 | K2S Carbide | 20° |

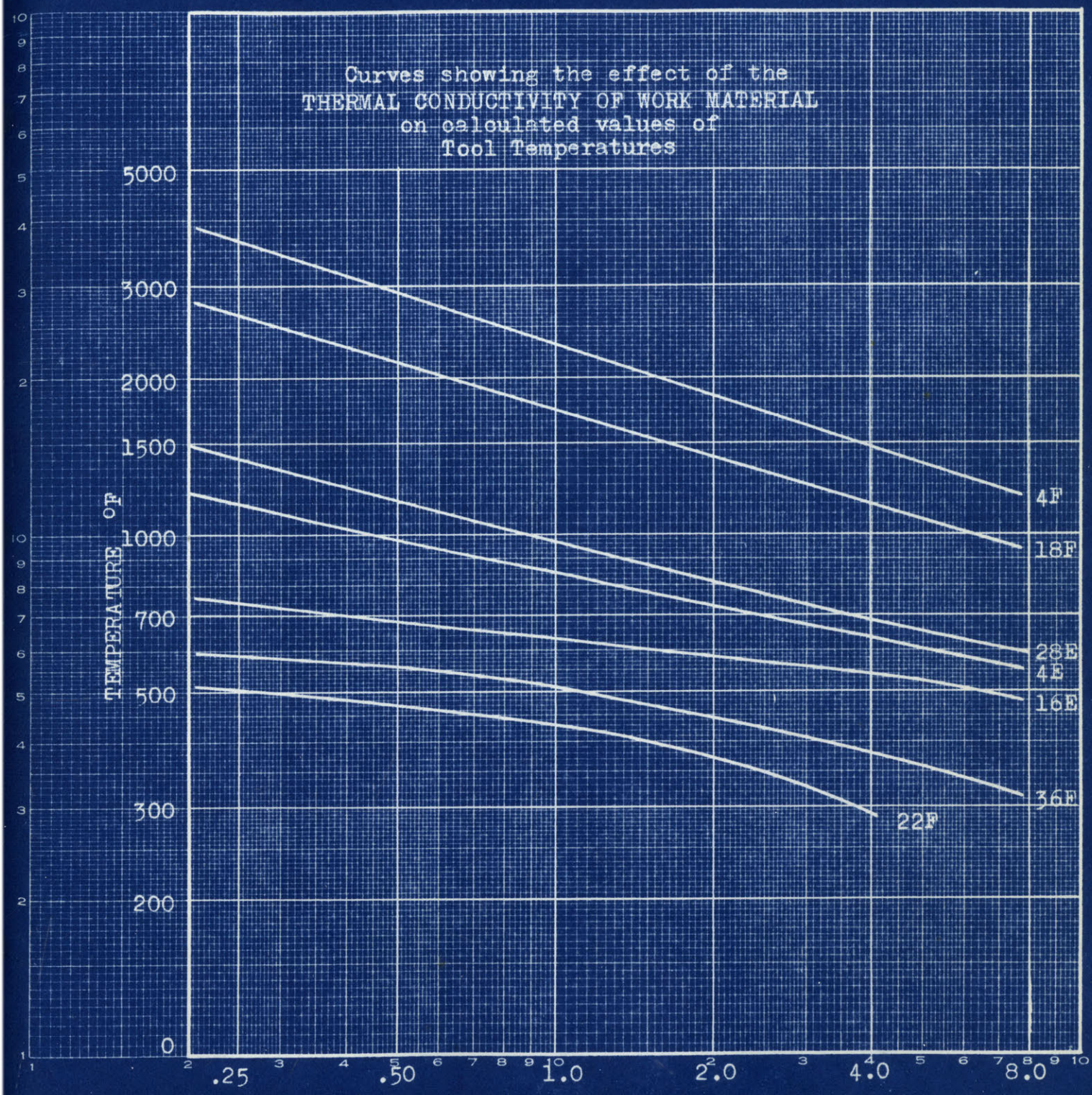
Curves showing the effect of the
THERMAL CONDUCTIVITY OF WORK MATERIAL
on calculated values of
Tool Temperatures
TEMPERATURE °F
5000
3000
2000
1500
1000
700
500
300
200
0
4F
18F
28E
4E
16E
36E
22F
.25
.50
1.0
2.0
4.0
8.0
Ratio
ASSUMED VALUES OF ORDINATES OF CONDUCTIVITY CURVE
KNOWN VALUES OF ORDINATES OF CONDUCTIVITY CURVE

Fig.51

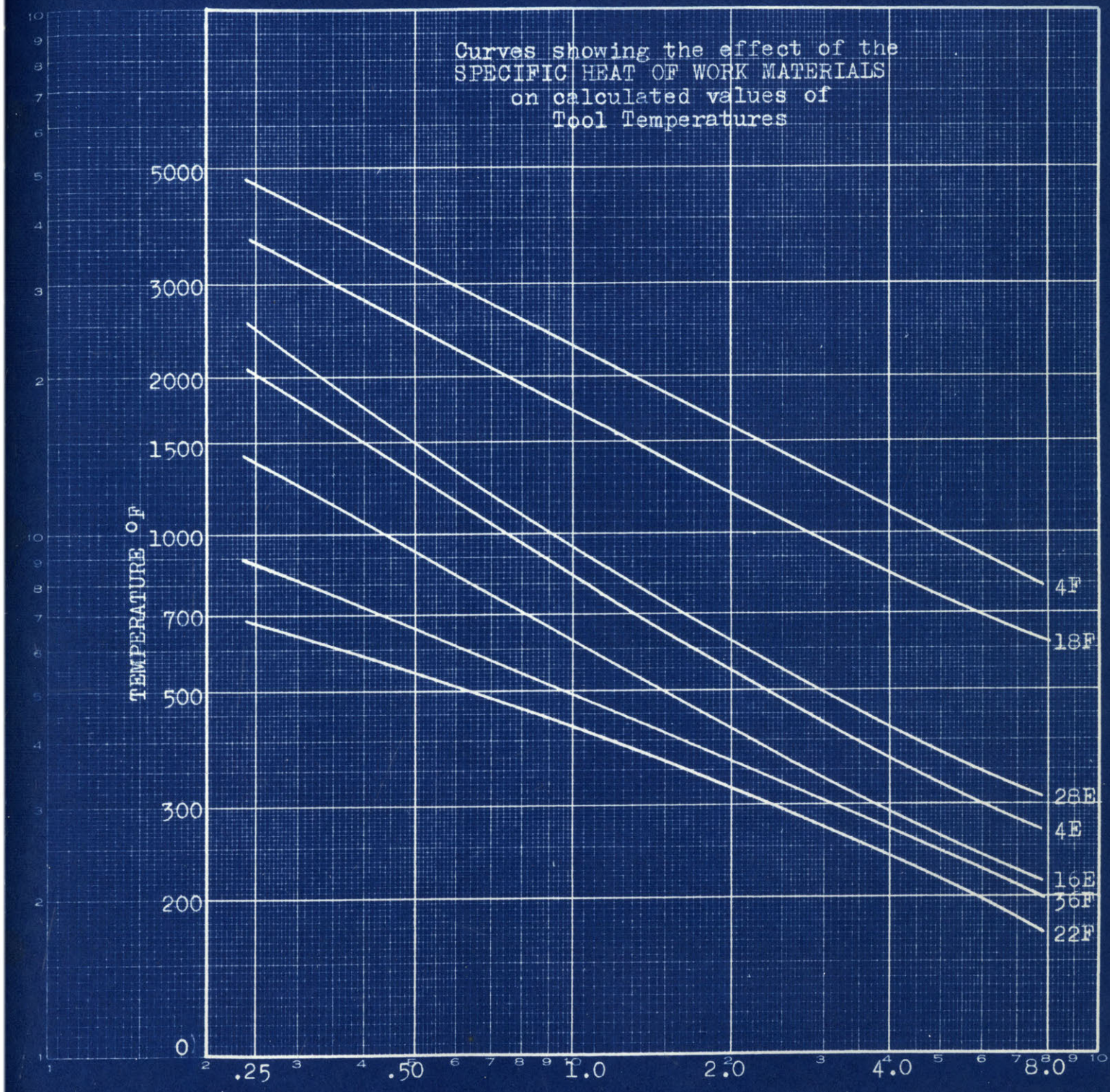
Curves showing the effect of the
SPECIFIC HEAT OF WORK MATERIALS
on calculated values of
Tool Temperatures
TEMPERATURE °F
5000
3000
2000
1500
1000
700
500
300
200
0
4F
18F
28E
4E
16E
36F
22F
.25
.50
1.0
2.0
4.0
8.0
Ratio
Assumed values of ordinates of specific heat curve
Known values of ordinates of specific heat curve

Fig. 52

Just as one would expect, increased conductivity results in lower calculated temperatures, the effect becoming most noticeable at the higher temperatures, and approximately linear when plotted on log-log paper. These curves also give an idea of the effect inexact conductivity data has on calculated temperature. Thus an error of 20%, which is quite possible, corresponds to a change in calculated temperature of only $10^{\circ}$ at $600^{\circ}$F, $50^{\circ}$ at $1000^{\circ}$F and $100^{\circ}$ at $1500^{\circ}$F. This shows the importance of exact conductivity values just in the range where they are the hardest to determine.

To obtain an idea of the role conductivity is likely to play in cutting various materials a series of approximate values is listed below, all relative to the conductivity of Iron.

| Material | Relative Conductivity |
|---|---|
| Copper | 6.5 |
| Magnesium | 3.1 |
| Aluminum Alloys | 2.4 |
| Brass | 2.0 |
| Iron | 1.0 |
| Monel Metal | .45 |
| Stainless Steel(18-8) | .30 |
| Titanium | .26 |
| Tungsten | .18 |

Interesting is the large range covered, 25:1 from Copper to Titanium.

The steep slopes of Fig. 52 indicate clearly the large effect specific heat has on calculated temperature, and thus presumably also on the actual temperatures. An error of only 10% in the value of specific heat corresponds to a change in calculated temperature of $30^{\circ}$ at $600^{\circ}$, $60^{\circ}$ at $1000^{\circ}$, and $90^{\circ}$ at $1500^{\circ}$F, which points up the importance of knowing this quantity as accurately as possible and also emphasizes the difficulty encountered by having to deal with instantaneous specific heat values rather than the steady state values one usually measures.

It should be noted from Figures 51 and 52 that the relative effect of thermal properties appears to be quite independent of the kind of material calculations are started with, nor does the speed or feed chosen appear to make much difference.

It is important to realize that when specific heats of different materials are compared, (c) is always multiplied by the density ($\rho$) in equation (35), so that it is the product of these two, the heat capacity, that is the quantity of primary interest. The curves of Fig. 52 can still be applied as a reference by simply substituting heat capacity ratios for the specific heat ratios in the abscissa. Again, for purposes of comparison, a table of ($\rho c$) for various materials is given below.

| Material | Heat Capacity ($\rho c$) Btu/in$^3$ $^o$F |
|---|---|
| Carbon Steel | .037 |
| Stainless Steel | .037 |
| Copper | .029 |
| Tungsten | .024 |
| Titanium | .018 |
| Magnesium | .016 |
| Aluminum | .016 |

THE EFFECT OF TOOL PROPERTIES ON ITS TEMPERATURE

According to the theory, as developed here, the only properties of a tool that influence the temperature at the tip, except for geometry, are the coefficient of friction and the thermal conductivity. It is obvious that, other things being equal, a tool with a higher coefficient of friction will generate more heat and therefore will become hotter than one with a lower coefficient.

The effect of thermal conductivity was calculated from equation (35) for the runs listed in Table V, and the results are plotted in Figure 53. Perhaps the most interesting result is that when cutting a material like free machining steel, with its relatively high conductivity, the effect of the tool conductivity is very small, an effect more pronounced at the higher speeds. To take a typical case: where a perfectly insulating tool gave a temperature of 1000°F, one with the high conductivity of $12 \times 10^{-4}$ Btu/sec/in$^2$/(°F/in) corresponded to 930°, a difference of only 70°F. Obviously in this case exact calculations do not depend on precise knowledge of tool conductivity.

However, when cutting a material of poor conductivity, such as Stainless Steel or Titanium, the effect of tool conductivity is much more pronounced, and, other things being equal, points to the advantage a tool with high conductivity has. In an example the change from a perfectly insulating tool to one with a conductivity of $12 \times 10^{-4}$ was observed to reduce the calculated temperature from 980°F to 680°F, a drop of 300°F.*

*There exists in the current literature no data on conductivity of tool materials other than that around room temperature, so that for lack of better values these were used in all calculations made here. It is hoped that this deplorable gap in information will be soon filled, so that more accurate calculations will be possible.

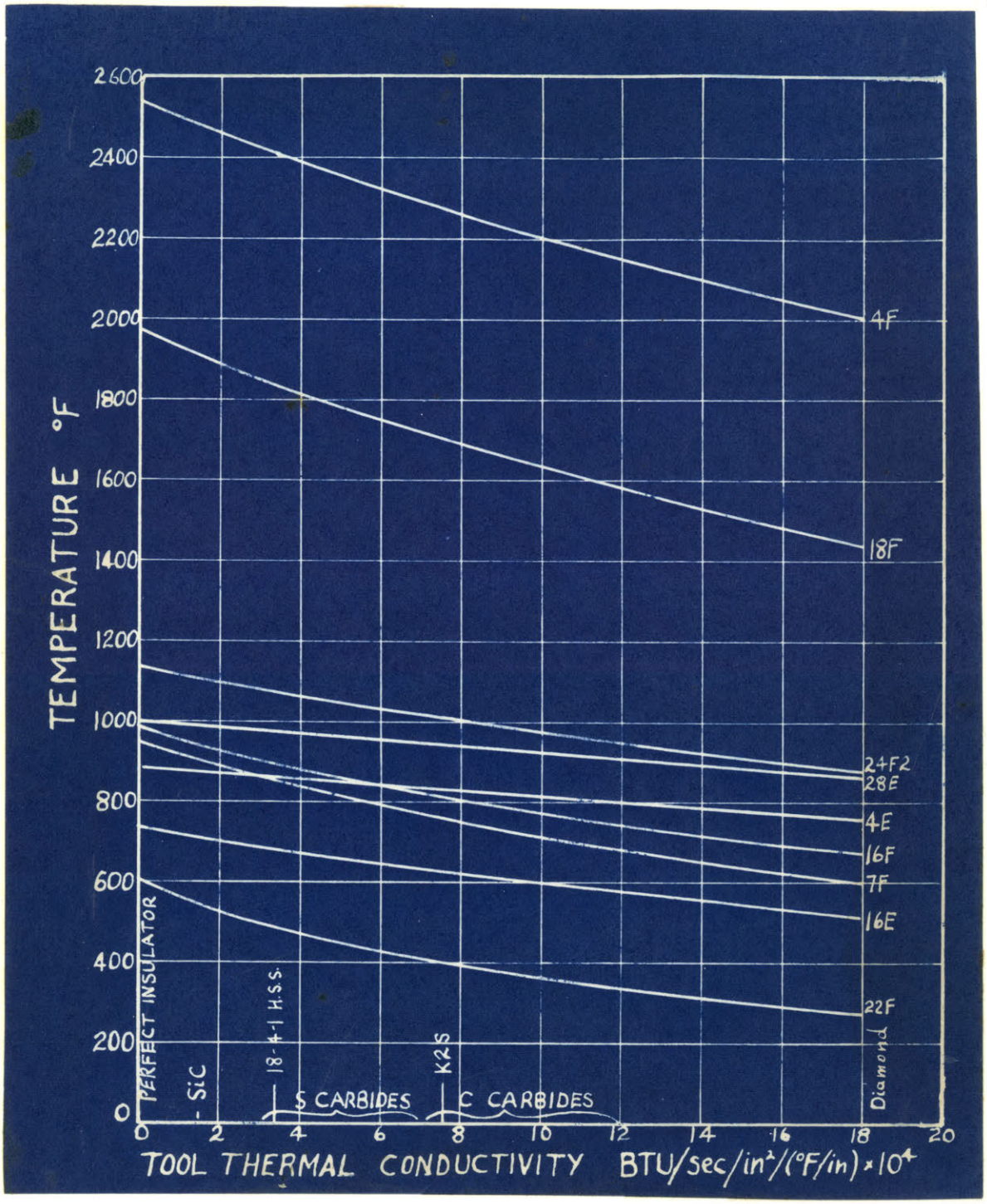


Figure 53.

Graph showing the effect of Tool Thermal Conductivity on Calculated Tool Tip Temperature.

Experiments have shown (see Figures 76-78) that in machining steel 18-4-1 High Speed Steel Tools have a coefficient of friction 25 to 50% greater than those of K2S carbide. This one would expect from the greater

hardness of the carbide. Since, in addition, the conductivity of K2S carbide is about twice that of the H.S.S. it is only natural to expect carbide tools to run cooler than H.S.S. cutting under similar conditions. Furthermore, the above results would indicate that the difference would be more pronounced when dealing with 18-8 Stainless Steel, rather than free, machining steel. These conclusions were substantiated by experiment. Reference to Fig. (74a,b) in the Appendix shows that when machining the low carbon steels at 100 ft/min the temperatures are slightly higher when cutting with H.S.S. Tools, although at 400 ft/min the picture is reversed for not very clear reasons. In the case of 18-8 Stainless Steel reference to Figures (62) and (75a) shows that, as predicted, the temperatures are far higher when cutting with the H.S.S. Tool. A typical figure is 230°F difference between carbide and H.S.S. at 100 ft/min, at a .0023" depth of cut. We can conclude from this that even if the ability of carbides to stand up at higher temperatures is not considered at all, there would be a considerable advantage in using carbide tools to machine 18-8 type stainless steels, or materials with similar properties.

THE EFFECT OF CUTTING SPEED ON TEMPERATURE

Of all quantities influencing cutting temperatures the one having the greates practical significance, because of the control we have on it, is the cutting speed. Under many conditions, though not all, useful cutting speed is determined by the temperature attained at the tool tip that gives a reasonable tool life. It is therefore most interesting to see whether the velocity parameters in equation (35) adequately represent the temperature changes that are observed experimentally. As will be shown in detail below, the answer appears to be that they do, within limits that are imposed in part by the approximations of the analysis and in part by lack of accurate knowledge of the physical properties of tool and work materials.

With free machining low carbon steel (S = .32%) the agreement between temperatures measured by the tool-work thermocouple method and those calculated from force measurements and physical properties is seen to be quite satisfactory. They are shown plotted as dotted and solid lines respectively, in Fig. 54. Theoretical values are consistently higher than measured values, the difference varying from 30° to 100°F, which is well within experimental accuracy and the various approximations made in the analysis.

Cutting 18-8 Stainless steel under the same conditions as the free machining steel gave results that are not in quite such good agreement, see Fig 55. It is interesting to compare these curves with those shown in Fig. 56, which are also for Stainless Steel, but cut with a High Speed Steel tool instead of K2S carbide. Here the agreement between theory and experiment is so much better that one might conclude that incomplete data on the conductivity of the K2S Carbide were the sole cause of the 200°F

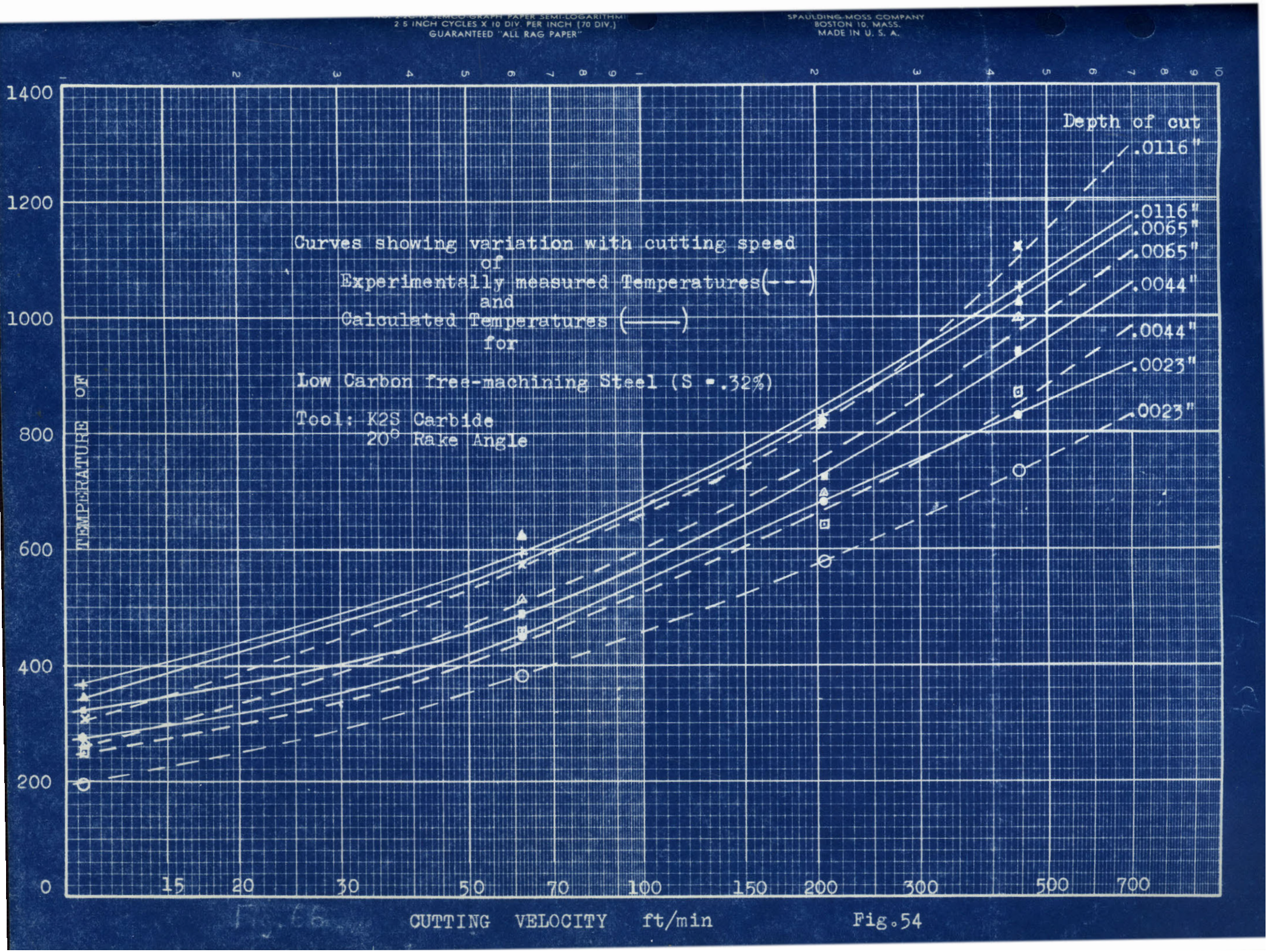
2 5 INCH CYCLES X 10 DIV. PER INCH (70 DIV.)
GUARANTEED "ALL RAG PAPER"
SPAULDING-MOSS COMPANY
BOSTON 10, MASS.
MADE IN U. S. A.
Curves showing variation with cutting speed
of
Experimentally measured Temperatures(- - -)
and
Calculated Temperatures (———)
for
Low Carbon free-machining Steel (S = .32%)
Tool: K2S Carbide
20° Rake Angle
Depth of cut
.0116"
.0116"
.0065"
.0065"
.0044"
.0044"
.0023"
.0023"
TEMPERATURE OF
1400
1200
1000
800
600
400
200
0
15
20
30
50
70
100
150
200
300
500
700
CUTTING VELOCITY ft/min

Fig.54

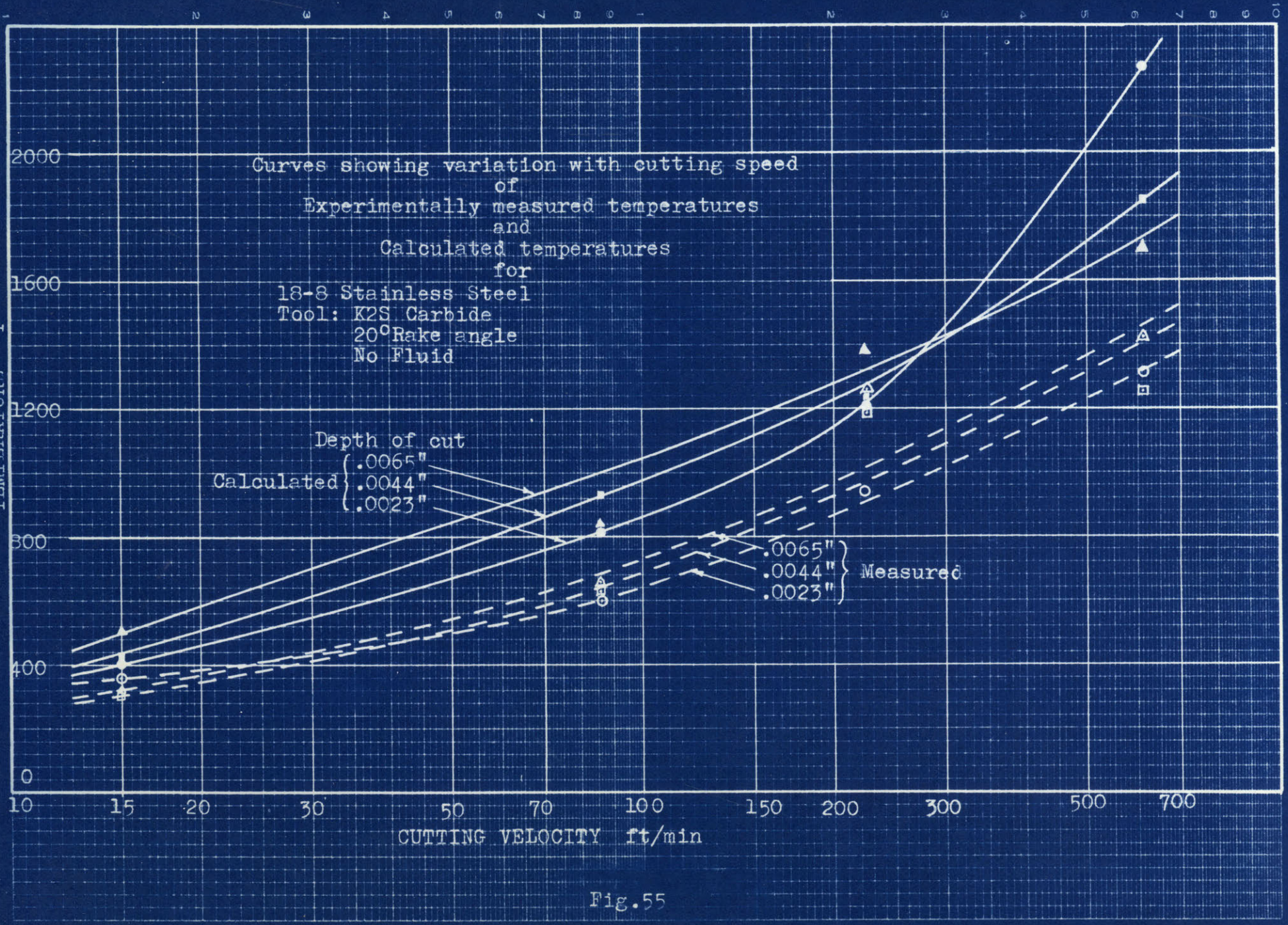
Curves showing variation with cutting speed
of
Experimentally measured temperatures
and
Calculated temperatures
for
18-8 Stainless Steel
Tool: K2S Carbide
20° Rake angle
No Fluid
Depth of cut
Calculated
.0065"
.0044"
.0023"
Measured
.0065"
.0044"
.0023"
TEMPERATURE °F
2000
1600
1200
800
400
0
10
15
20
30
50
70
100
150
200
300
500
700
CUTTING VELOCITY ft/min

Fig.55

discrepancy noted above. However, there are probably other factors also, such as incomplete knowledge of the properties of High Speed Steel, because otherwise a similar large discrepancy would also be expected with the free machining steel. On the whole, it seems fair to conclude that within present knowledge of the thermal properties of tool and work materials, experimental errors, and approximations made in the temperature analysis, the agreement between theory and experiment is entirely satisfactory.

It will be of some theoretical interest to observe the fractions of the final cutting temperature due to shear and to friction, and how the relative proportions vary with cutting speed. For that reason the values for both $\bar{\theta}_s$ and $\bar{\theta}_f$, their sum $\bar{\theta}_t$, and the experimental values for $\bar{\theta}_t$ for two different sets of conditions are shown plotted separately in Fig. 56 below.

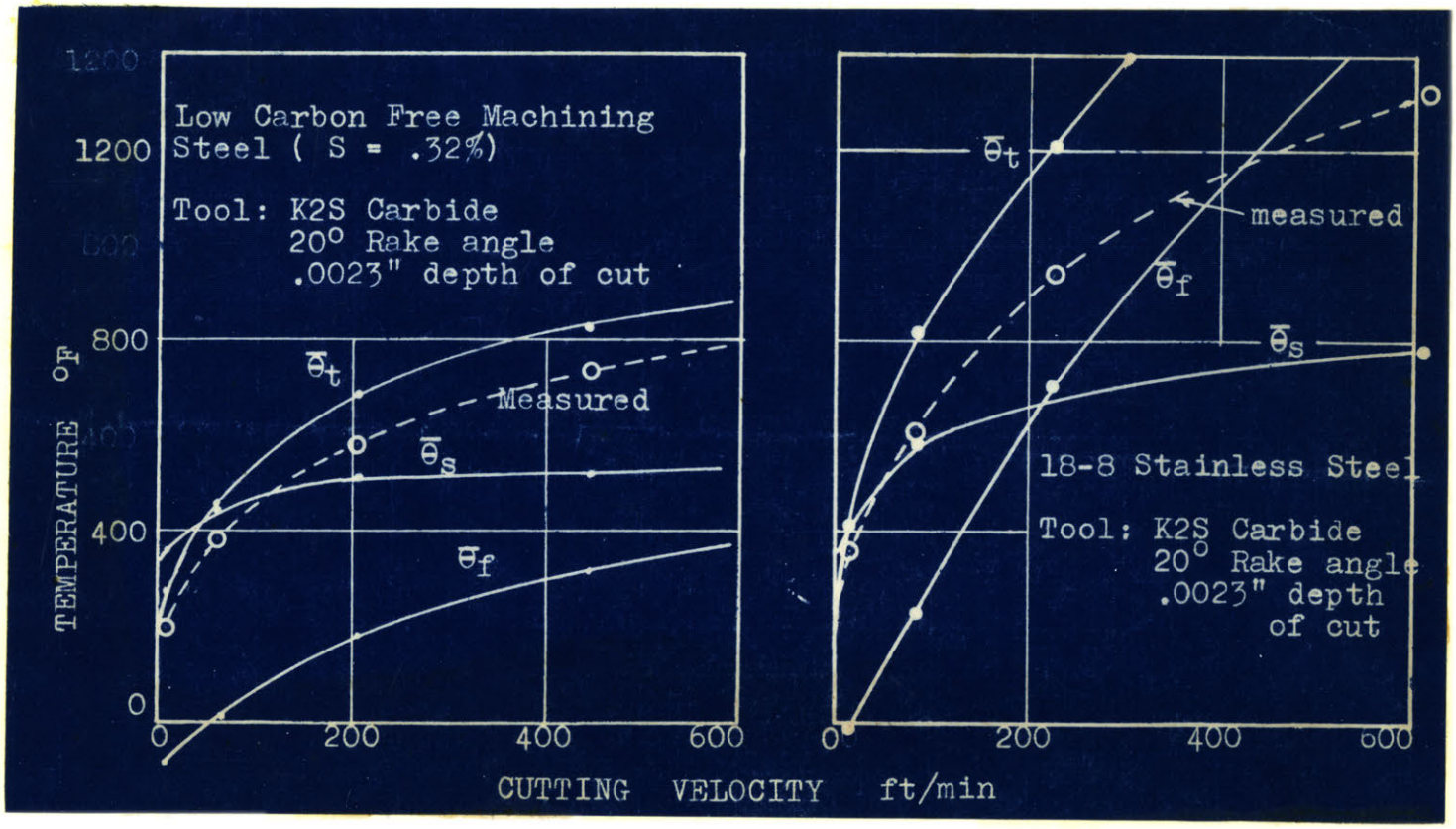


Figure 56.

$\bar{\theta}_s$, $\bar{\theta}_f$, $\bar{\theta}_t$ plotted as functions of cutting speed.

Of particular interest is the fact that above 100 ft/min the shear plane temperature does not increase much with speed. At very low cutting speeds the friction temperature becomes negative, which implies that all of the frictional and some of the shear energy goes to the tool.

These temperature variations are functions of $R_1$ and $R_2$, the fractions of shear and friction energy respectively that go into the chip. To see how $R_1$ and $R_2$ vary with speed, a few representative curves are shown in Fig. 58, for the same conditions as those in Fig. 57.

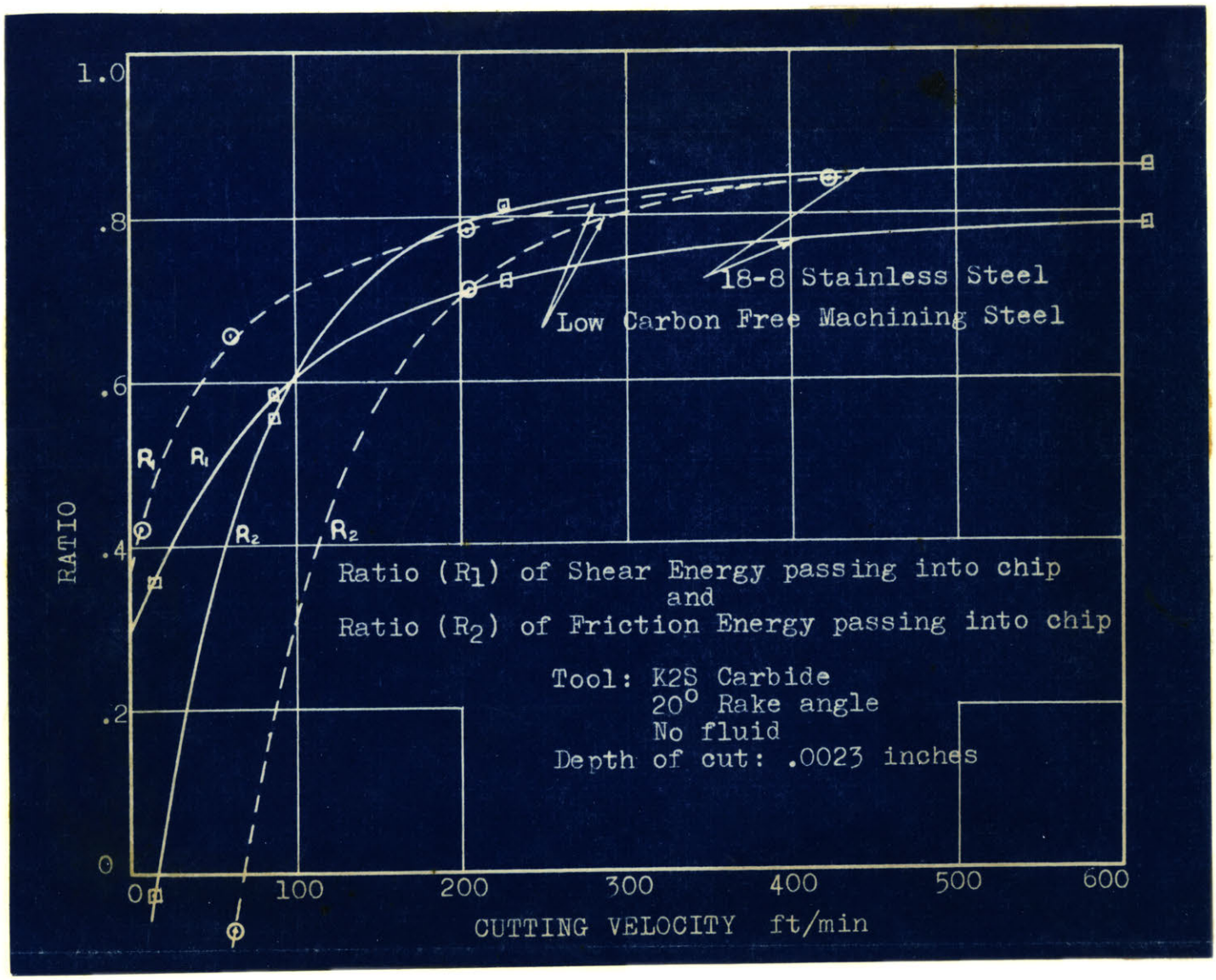


Figure 58.

Variation of $R_1$ and $R_2$ with cutting speed.

Probably more interesting than the above values of $R_1$ and $R_2$ are the actual energies going into the chip, tool, and workpiece, which can be found from the simple expressions below.

$$u_{chip} = R_1 u_s + R_2(u-u_s) \qquad (40)$$

$$u_{work} = (1-R_1)u_s \qquad (41)$$

$$u_{tool} = (1-R_2)(u-u_s) \qquad (42)$$

How the properties of the total cutting energy as calculated from these expressions, for the same conditions as plotted in Fig. 57 and 58, is shown in Fig. 59. The fraction of energy going into the work is seen to be rela-

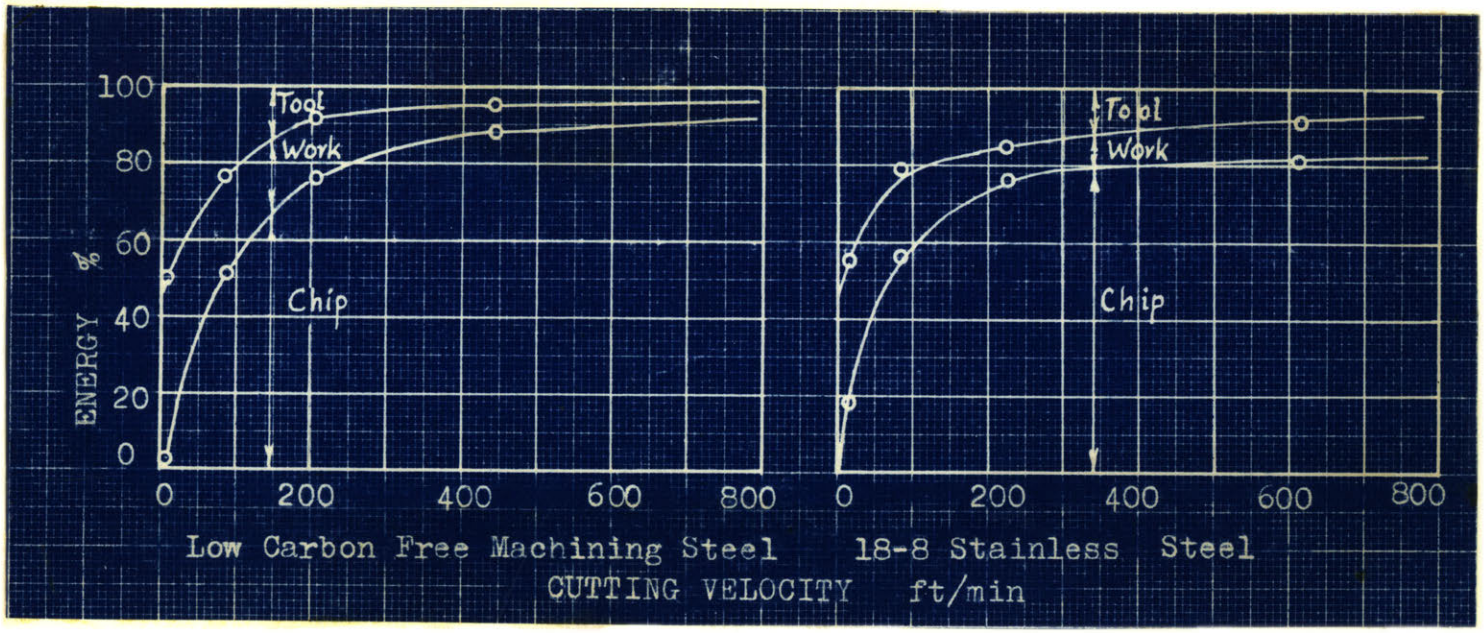


Figure 59.

Energy distribution as a function of cutting speed.

tively constant, while that going into the chip increases with speed, at the expense of that going into the tool. This is most fortunate, of course, since otherwise high speed machining would be impossible.

Cutting temperatures measured under a wide variety of conditions both for low carbon steels with varying amounts of sulphur content and 18-8

Stainless steel are plotted in Figures 60 to 62. Fig. 63 is a cross plot showing the variation of temperature with rake angle of the tool. Except at the lower speeds where built-up edge makes exact measurement impossible the temperature is seen to increase as the rake angle becomes more negative, the result of the increased amount of shear work required for cutting.

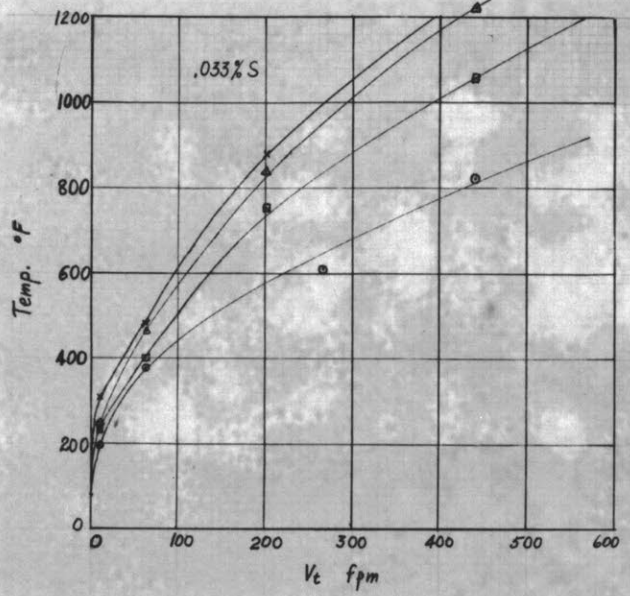


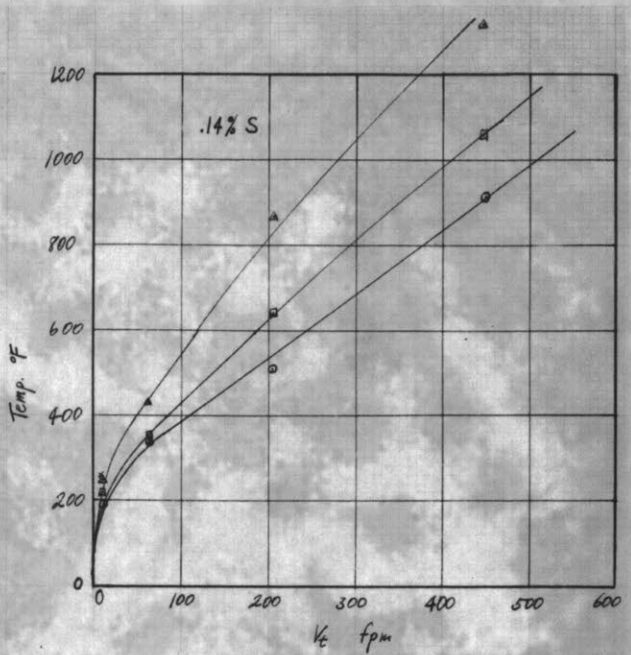


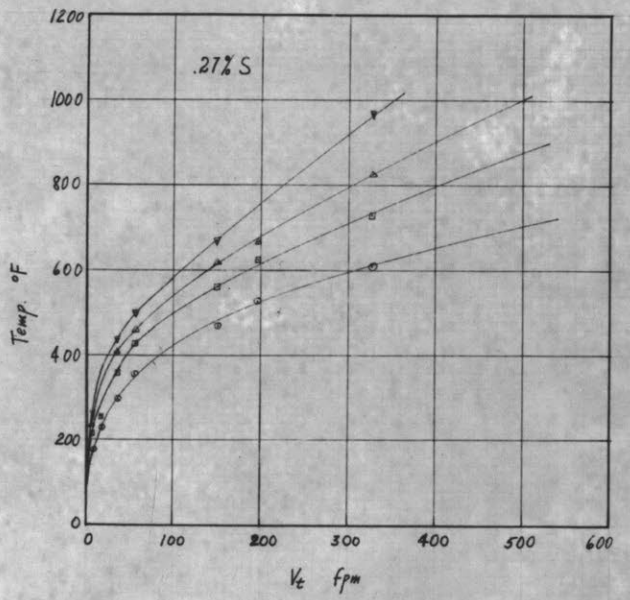


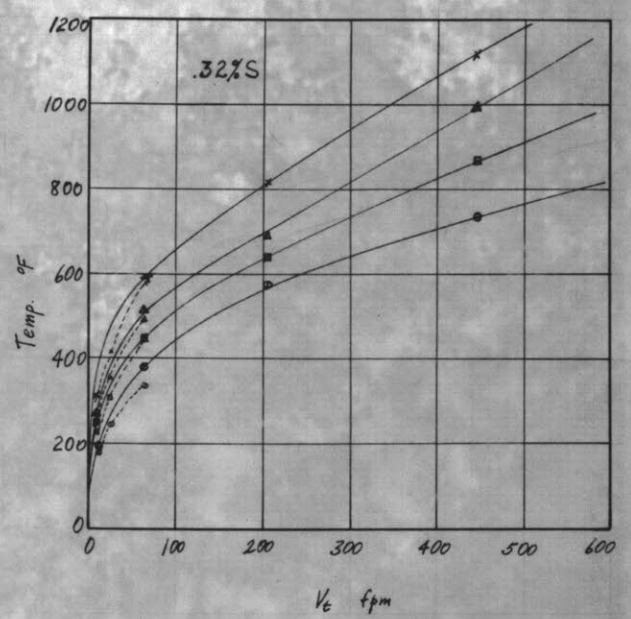


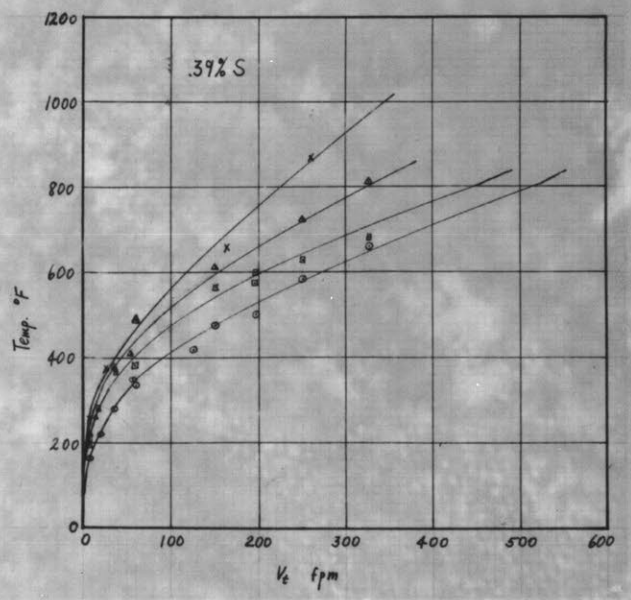


Fig.60

TEMPERATURE VS. CUTTING SPEED CURVES
ORTHOGONAL CUTTING

WORK MATERIAL: 1 7/8" Diam.bars of type B-1112 steel containing various amounts of sulphur.

TOOL MATERIAL: K2S Tungsten-Titanium Carbide
Rake angle: 20°
Clearance angle: 5°
Width of cut: 1/8" approx.
Feeds as shown by code: .0023 ipr
.0044 ipr
.0065 ipr
.0087 ipr
.0116 ipr

FLUID: None
Some low speed tests repeated using Carbon-tetrachloride (dotted lines).

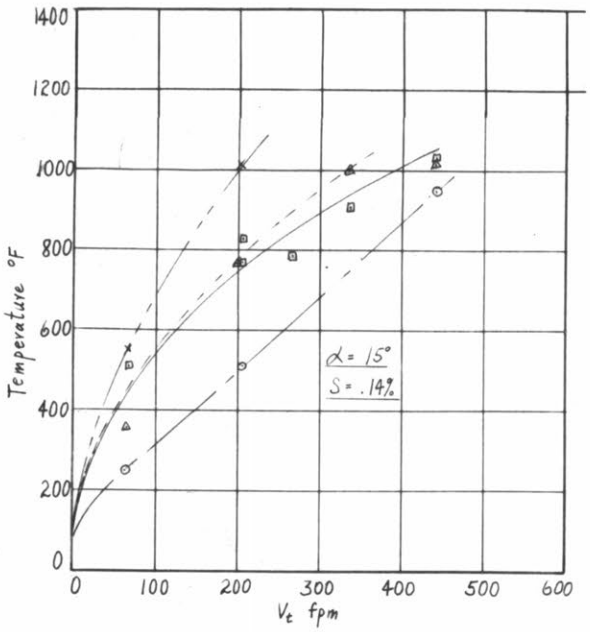


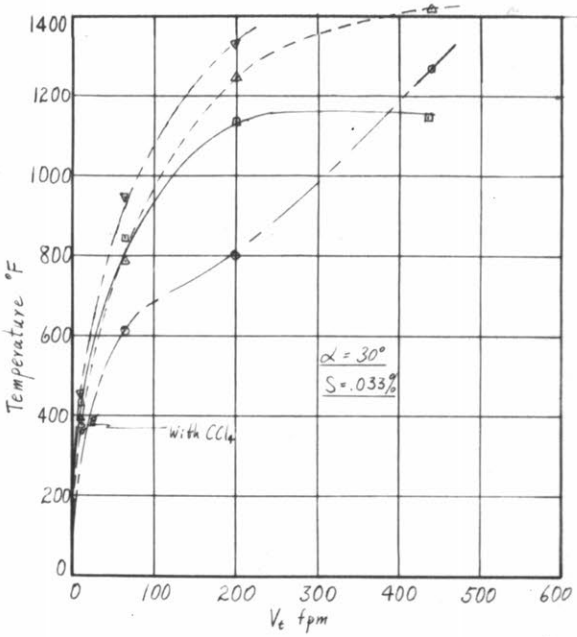


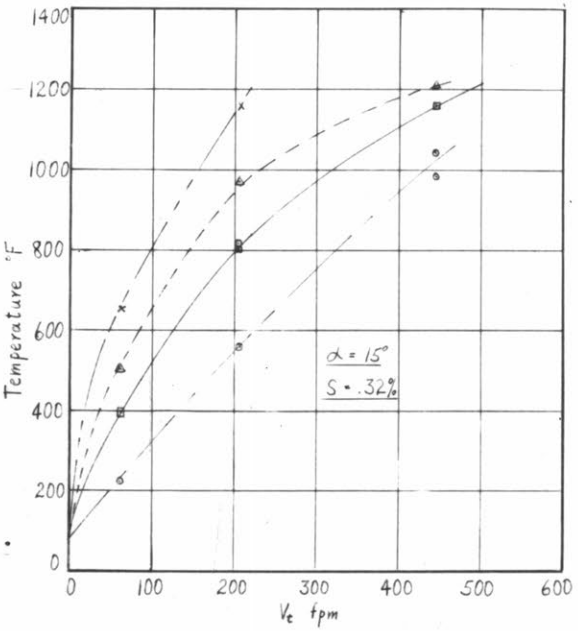


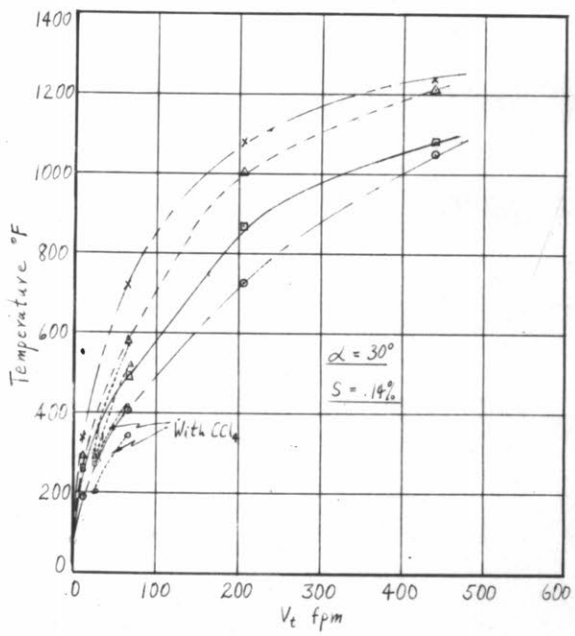


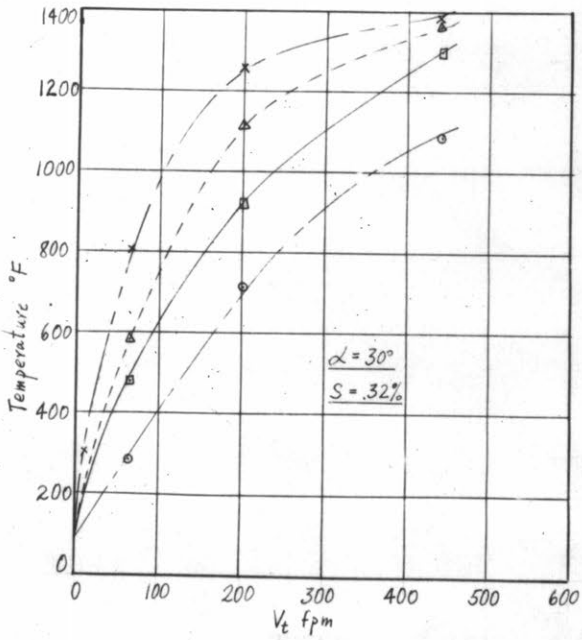


**Fig.61**

CUTTING TEMPERATURE VS. CUTTING VELOCITY

ORTHOGONAL CUTTING

WORK MATERIAL: 1 7/8" diam. bars of type B-1112 steel containing various amounts of sulphur.

TOOL MATERIAL: 18-4-1 High Speed Steel
Rake angle: 15° and 30° as shown.
Clearance angle: 5°
Width of cut: 1/8" approx.
Feeds as shown by code:
- ⊙ .0023 ipr
- □ .0044 ipr
- △ .0065 ipr
- ▽ .0087 ipr
- x .0116 ipr

FLUID: None
Some low speed runs repeated using Carbon-tetrachloride (dotted lines)

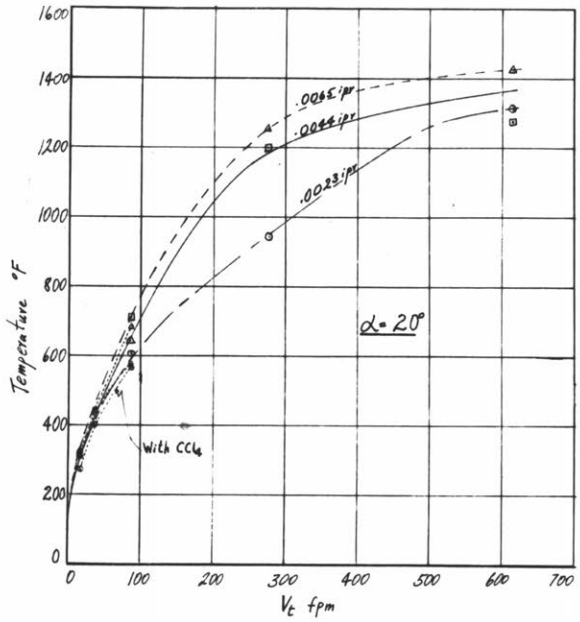


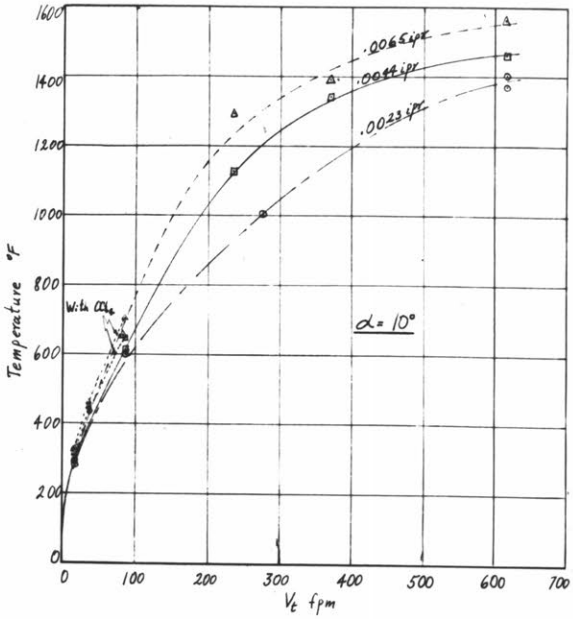


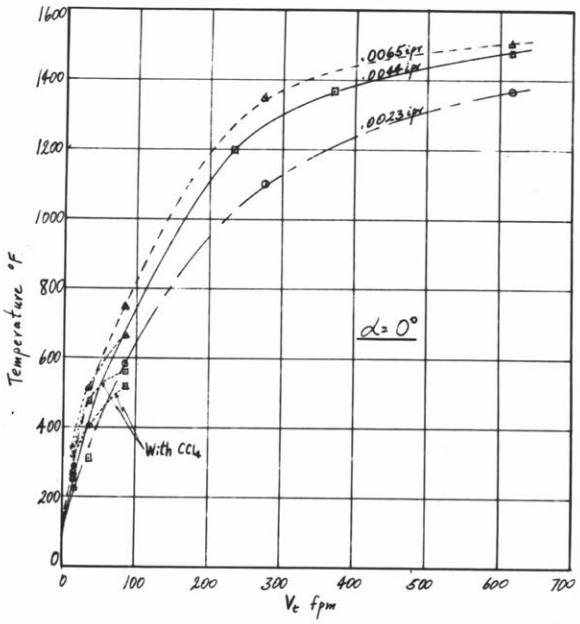


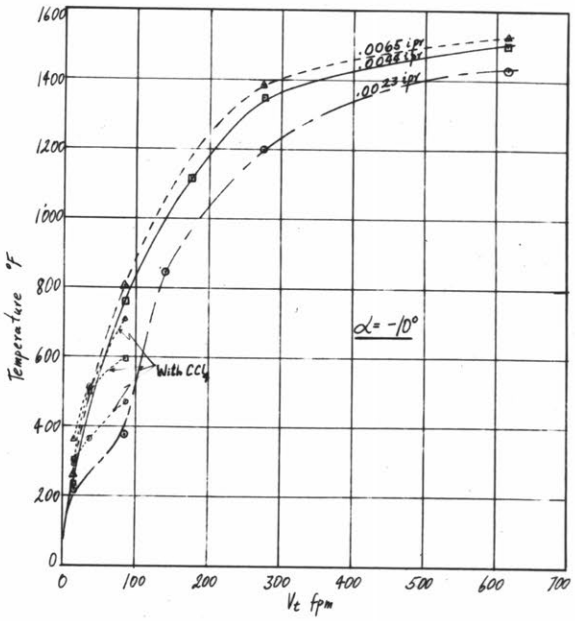


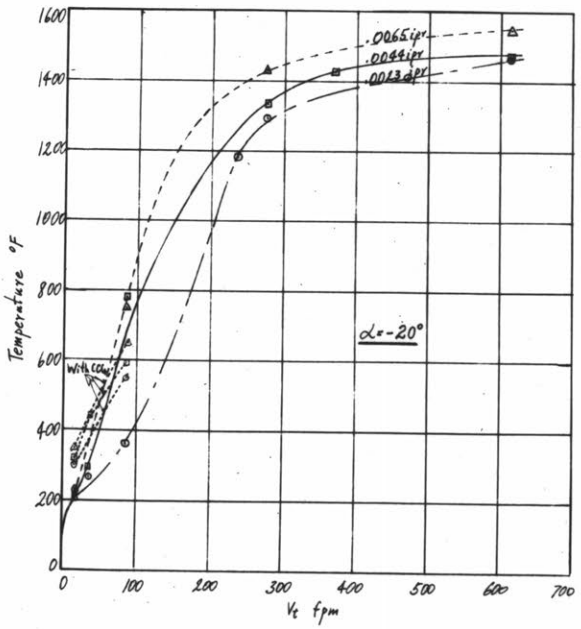


**Fig.62**

TEMPERATURE VS. CUTTING SPEED CURVES

ORTHOGONAL CUTTING

WORK MATERIAL: 2½" Diam. bar 18-8 Stainless Steel as received.

TOOL MATERIAL: K2S Tungsten-Titanium Carbide

Rake angles as shown on graphs
Clearance angle: 5°
Width of cut: 5/32" approx.
Feeds as shown on graphs

FLUID: None used for main tests.
Low speed runs repeated using Carbon-tetrachloride as fluid, as shown on graphs in dotted lines.

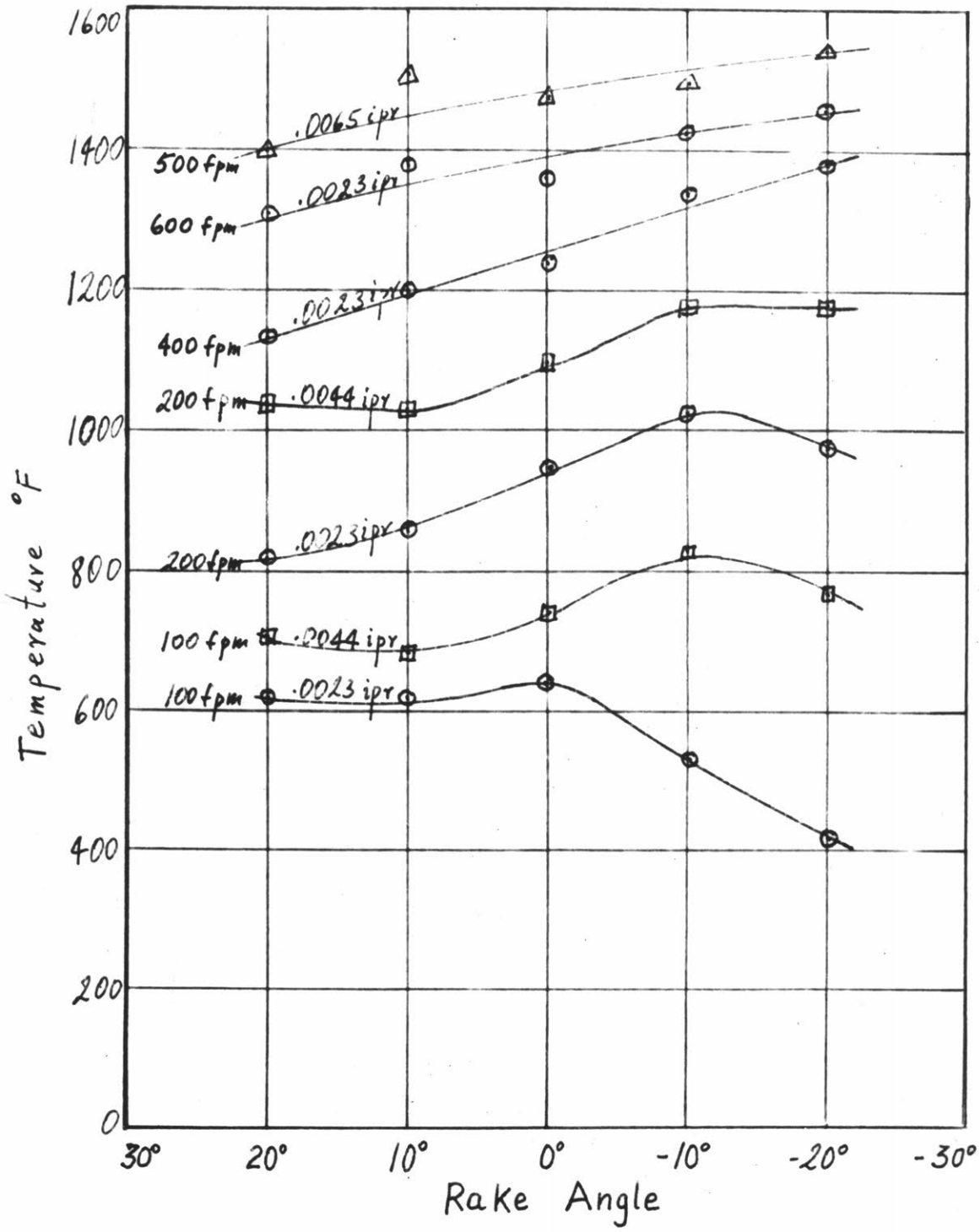


CUTTING TEMPERATURE VS. RAKE ANGLE

ORTHOGONAL CUTTING

WORK MATERIAL: 2 1/2" diam. bar 18-8 Stainless Steel, as received.

TOOL MATERIAL: K2S Tungsten-Titanium Carbide
Clearance Angle: 5°
Speeds and feeds as shown.
Width of cut: 1/8" approx.

FLUID: None

Fig.63

TEMPERATURE DISTRIBUTIONS IN THE CUTTING PROCESS

The manner in which temperature distributes itself over the cutting area is of considerable practical interest. For instance, for a given total energy input and average temperature tool life will be less if there is a steep temperature gradient over the cutting face, than if there is a more uniform distribution. It is the parts of the tool at the maximum temperature which, as a rule, will limit tool life and cutting speeds.

Unfortunately distributions are very difficult to measure directly. Only two methods have been developed so far. The one due to Lang and Bickel was discussed on page 8 and Bickel's result for temperature along the cutting face given in Fig.46. This single curve was the result of several months work, obviously far from a routine test, but it shows quite clearly that for the case in question at least, the peak temperature is developed at the tool tip. The severe cratering that is observed so often behind the cutting edge has led many observers to conclude that maximum temperature is developed behind the edge. For instance, Trent, as quoted by Tangerman (38) believes that at 150 ft/min cutting speed, the maximum temperature is reached about .020" behind the cutting edge, this distance reducing to .005" at 300 ft/min, this apparently based on no other evidence than the cratering. The analysis made here does not give a clear answer to this problem. The temperature distribution in chip and tool face is drawn in Fig. 64 below, similar to Fig.38 , only that curve (2) starts with a maximum at the cutting edge, which corresponds to the solution for a stationary heat source applied to the tool. It should be recalled that solution for the averaged cutting temperature $\overline{\theta}_t$ was

obtained by equating the mean temperatures of curves (1) and (2), where (1) represents the moving heat source solution applied to the chip.

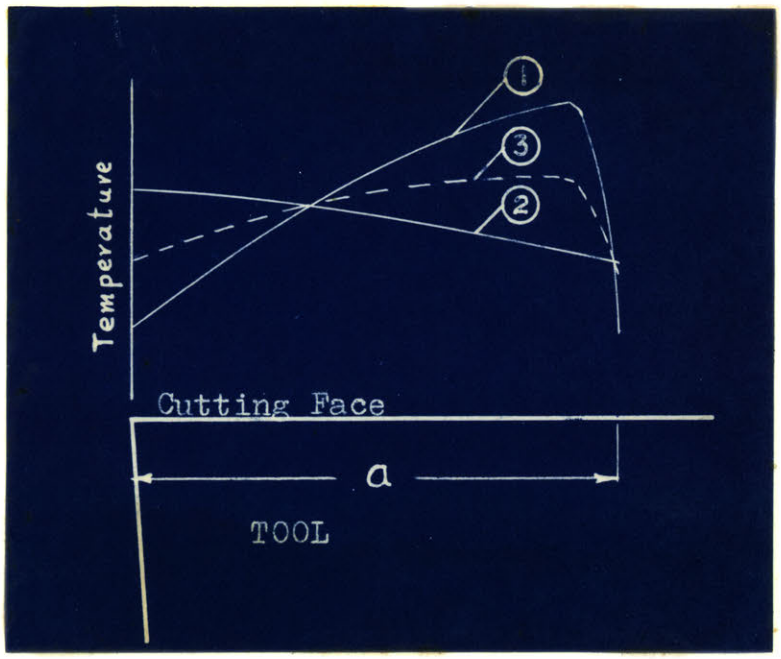


Figure 64.

Theoretical temperature distributions at Tool cutting face.

If curve (3) is taken as the mean between (1) and (2) then the finite time required for temperature equilibrium to be reached between two bodies leads to the conclusion that the actual temperature of the tool will lie somewhere between curves (2) and (3). Although the shape of (2) is independent of speed, reference to Fig.27 shows that curve (1) becomes steeper as the speed increases. From this one can draw the qualitative conclusion that at low speeds the maximum temperature will lie at the tip, while at higher speeds a maximum temperature behind the cutting edge is likely. A quantitative treatment of this problem would seem to be a very difficult one.

The only other experimental work done of temperature distribution was by Schwerdt (37), who using a tool not unlike Bickel's (loc.cit.) measured surface temperatures by means of a very elaborate radiation detection device.

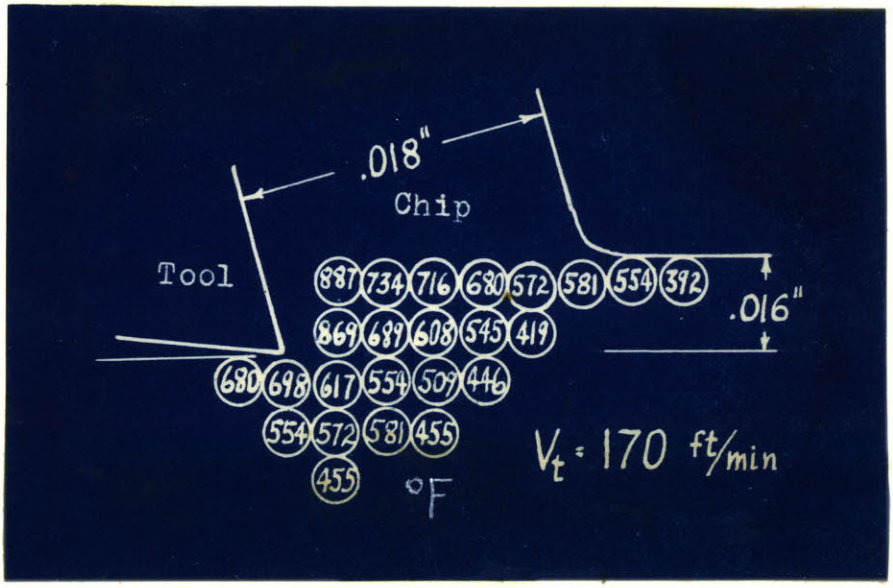


Figure 65.

Radiation temperature measurements due to Schwerdt.

Schwerdt's picture, does seem to give clear evidence that the temperature in the shear plane is not uniform and increases from a maximum at the tool edge to a minimum at the outside surface. The ratio between the two is about 1.5, and thus of the same order of magnitude at the variation of shear energy across the shear plane noted in Fig. for the case of annealed copper (1.75). It is most unfortunate in this connection that the bulk of Schwerdt's data was never published.

Due to insufficient supporting evidence this energy distribution factor across the shear plane was not taken into account in the analysis developed here. If found generally valid, it would increase the important maximum shear plane temperature about 20 to 25% above the average now used, and this would increase the calculated tool tip temperature by about 70°

to 120°F, depending on conditions. This effect is therefore large enough to warrant further investigation into the energy distribution across the shear plane.

## THE PROBLEM OF MACHINING TITANIUM

Titanium, newest of engineering materials, has been called the glamour metal. However, it is hardly regarded as such in the machine shop. Although its hardness is not unreasonably high (Rc 31) attempts to machine it at normal speeds always result in quick tool breakdown. Reasonable tool life seems possible only at speeds far below even those used for Austenitic Stainless Steel (18-8) and can be compared only with high temperature alloys such as Timken Alloy (16-25-6).

Since the short tool lives appear to be due to high cutting temperatures, it will be interesting to see if the analysis presented here offers an explanation for the behaviour of Titanium in machining. In discussing Titanium it is convenient to compare it with 18-8 Stainless steel, since they have many properties in common (e.g. they require about the same total energy per unit volume to machine), although there are some significant differences that will be examined later. As a glance at Fig. 66 shows, cutting temperatures, as measured by the tool-work thermocouple method, are seen to be a good deal higher with Titanium alloy. Although the absolute difference between them decreases at high temperature, small differences at these high values can be expected to have a significant effect on tool life. For reference purposes, temperature curves for Low carbon free machining steel are also shown in Fig. 66. These temperature curves agree approximately with comparative tool life data (42).

Analysis of data obtained from cutting Titanium reveals a set of properties that are nearly all designed to give high cutting temperature. The first item to be noted is that while total energy to cut unit volume is about the same as for 18-8 Stainless Steel, the fraction of it used up

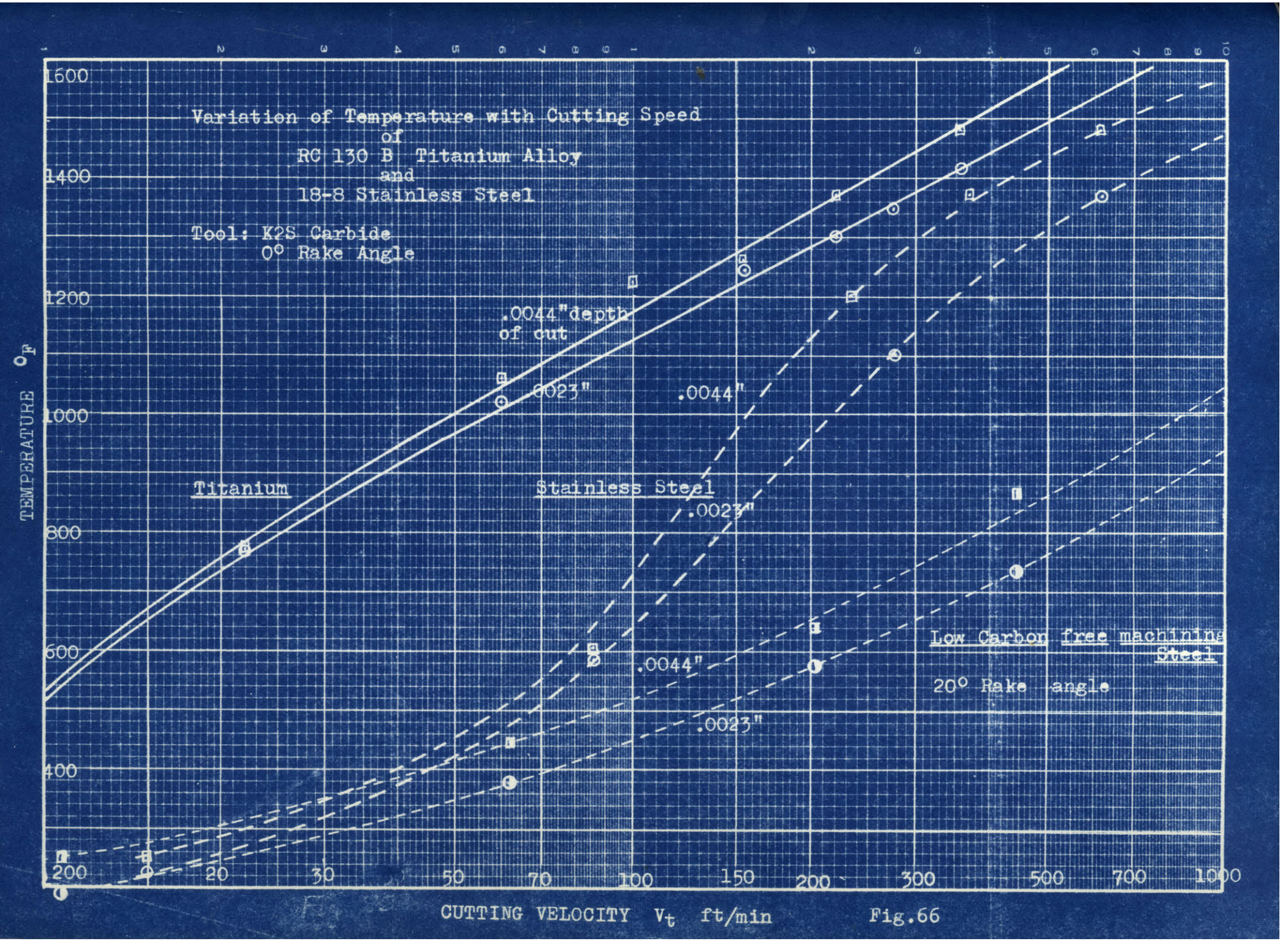
Variation of Temperature with Cutting Speed
of
RC 130 B Titanium Alloy
and
18-8 Stainless Steel
Tool: K2S Carbide
0° Rake Angle
.0044" depth of cut
.0023"
.0044"
.0023"
Titanium
Stainless Steel
.0023"
.0044"
Low Carbon free machining Steel
20° Rake angle
TEMPERATURE °F
1600
1400
1200
1000
800
600
400
200
20
30
50
70
100
150
200
300
500
700
1000
CUTTING VELOCITY $V_t$ ft/min

Fig.66

in friction energy at the tool face is much higher for Titanium, 55% instead of 35% being representative values. This is not due to any great difference in the coefficient of friction (they are about the same), but arises from the much higher relative chip velocity, which is due to the unusually high chip length ratios (and shear angles)noted in cutting Titanium. Chip length ratios greater than 0.9 are easily obtained at the higher cutting speeds, and we thus have the rather unexpected result that high chip length ratios can be harmful from the standpoint of machinability. Increased tool face temperatures are then to be expected from the increased work done at that point.

The second factor to be noted is the unusually short contact length between chip and tool, usually less than 1/3 of that observed with 18-8. Thus the greater frictional energy mentioned above is developed over a smaller area, resulting in still higher temperatures.

The single most important factor influencing cutting temperatures of Titanium is its unusually low heat capacity, less than 1/2 that of Stainless Steel. As was noted on page 87, this alone can account for a very much higher tool-chip interface temperature.

A fourth factor entering the picture is the thermal conductivity of Titanium. Not much is known about this quantity at present, except that at room temperature it is about 10% below that of Stainless Steel. However, from the fact that tool temperatures calculated from this one value have unreasonably high values at high speeds, one would expect thermal conductivity of Titanium to increase with temperature. It is hoped that future experiments will verify this conclusion.

In view of these uncertainties, the agreement between temperatures obtained experimentally by the tool-work thermocouple method and those

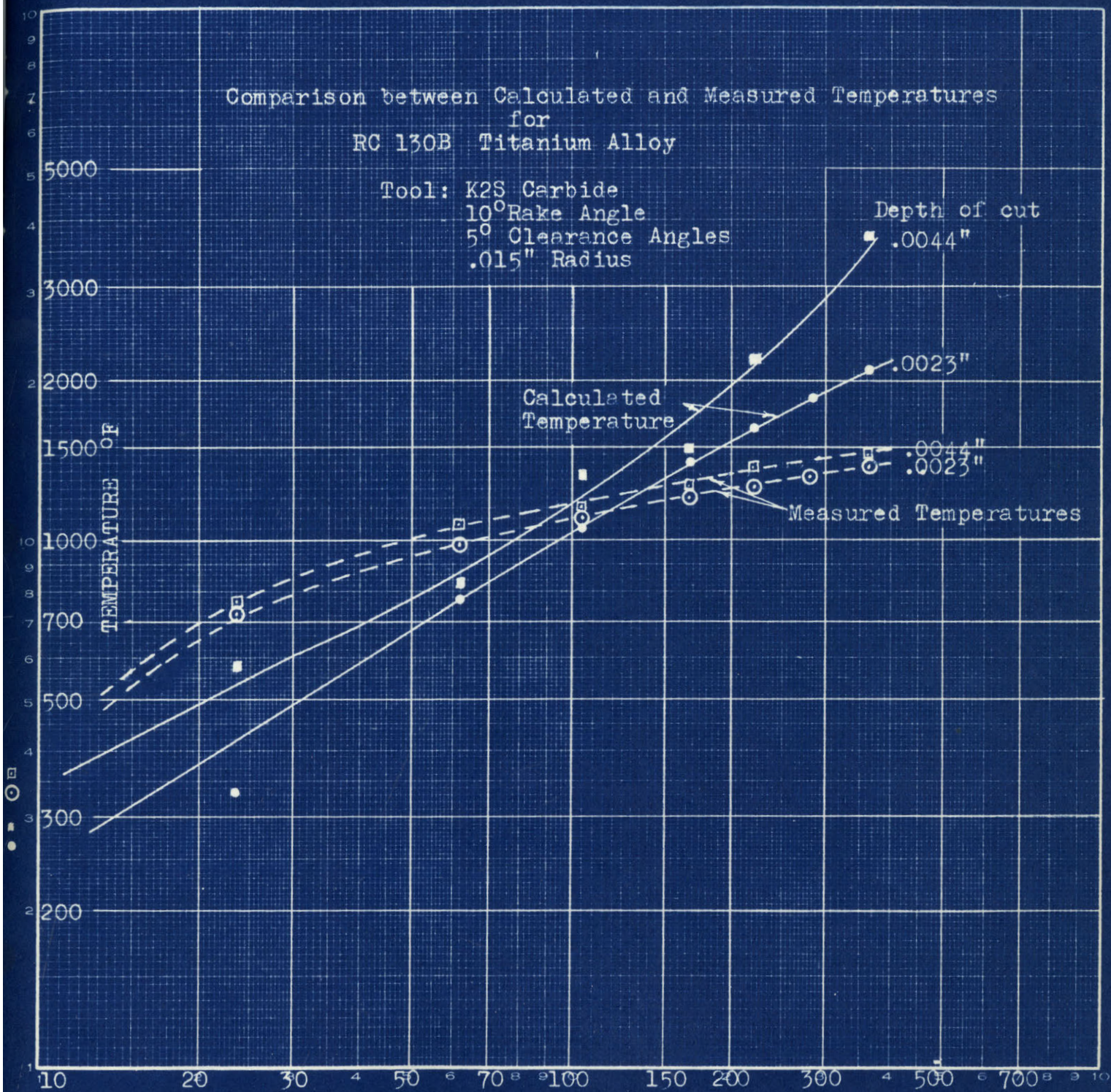
Comparison between Calculated and Measured Temperatures
for
RC 130B Titanium Alloy
Tool: K2S Carbide
10° Rake Angle
5° Clearance Angles
.015" Radius
Depth of cut
.0044"
.0023"
Calculated
Temperature
.0044"
.0023"
Measured Temperatures
TEMPERATURE °F
5000
3000
2000
1500
1000
700
500
300
200
10
20
30
50
70
100
150
200
300
500
700
CUTTING VELOCITY $V_t$ ft/min

Fig.67

calculated from equation (35), and shown plotted on Fig. 67, is not unreasonable.

One of the most striking phenomena observed whn machining Titanium is the case with which one can obtain red-hot chips over appreciable periods of time without damaging the tool. This appears even more unusual when it is observed that chips begin to come off red at speeds as low as 50 ft/min, corresponding to a tool tip temperature of about 950°F, while stainless steel chips fail to turn color even when machining at the very high speed of 900 ft/min, which corresponds to a tool tip temperature of over 1500°F. The answer to this paradox lies in the fact that it is the average chip temperature, and not that at the tool face, which determines whether or not a chip appears red on its top surface.

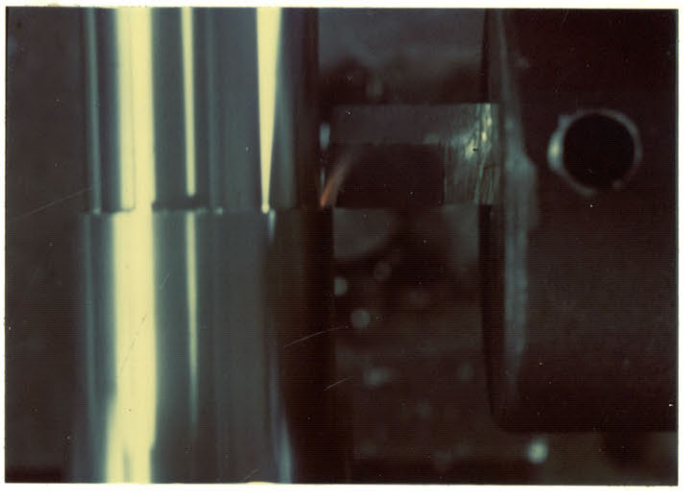

Figure 68.

Kodachrome of red-hot Titanium chip; Zero degree tool rake angle. Cutting speed 160 ft/min., 0044"/rev feed (depth of cut). Exposure of 20 seconds accounts for blurred edge and fact that the cooled off weaving chip is not visible.

This average temperature of the chip, $\bar{\theta}_c$, can be calculated quite readily from the energy per unit volume going into the chip, $u_c$, given in equation (40) page .

The average temperature of the chip is then given by

$$\bar{\theta}_c = \frac{u_c}{J(c\rho)_{chip}} \qquad (43)$$

The interesting results of such a calculation are shown in Fig. 69, where both $u_c$ and $\bar{\theta}_c$ are plotted as functions of cutting speed, for 18-8 and Titanium, at a .0044" depth of cut and with a $0^o$ rake angle carbide tool. Titanium was cut in the conventional manner, while the Stainless Steel was cut orthogonally. The results show that while the total energy going

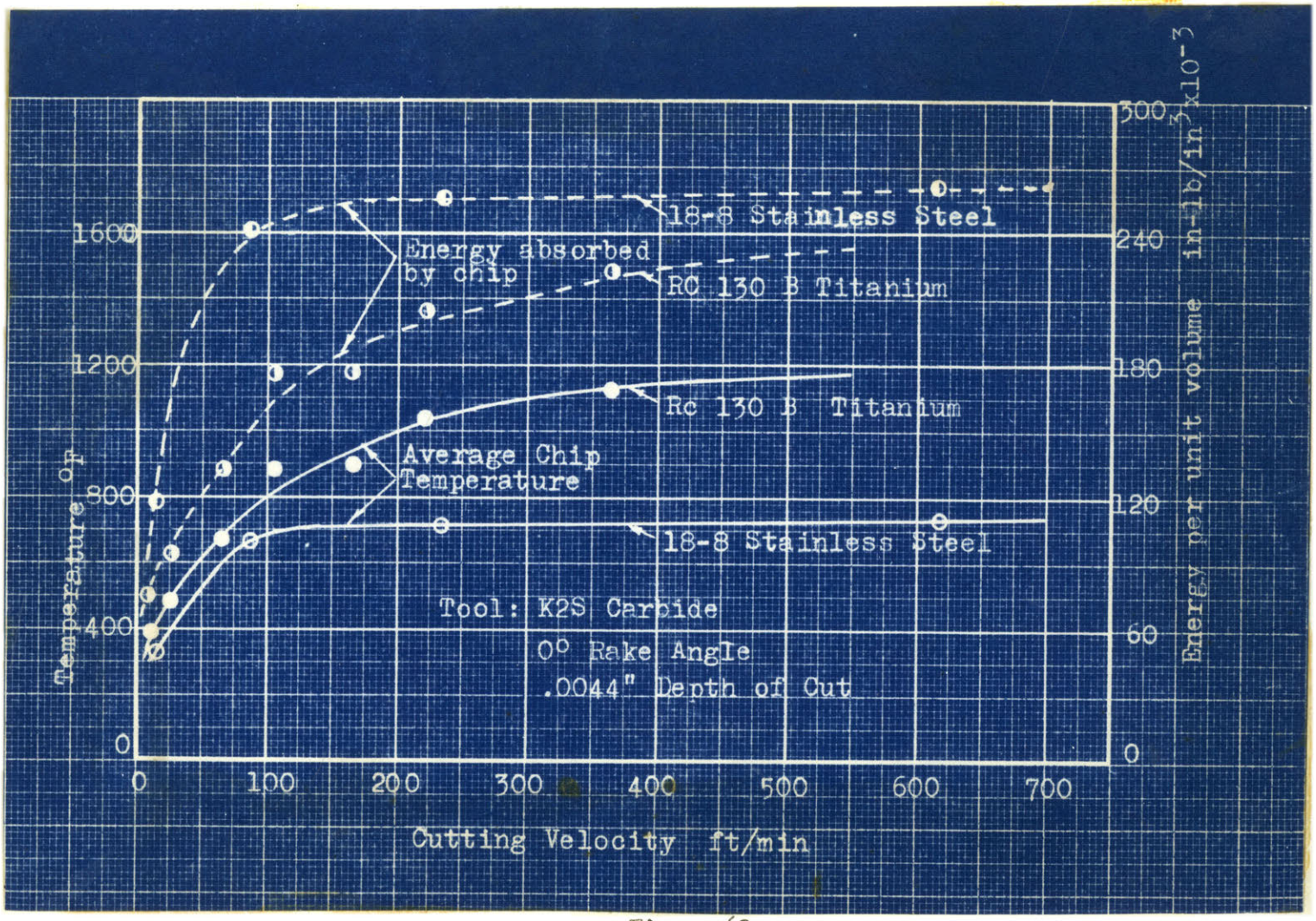


Figure 69.

Chip energy and average temperature of Titanium and 18-8 Steel.

into the stainless steel chip is a good deal higher than that of Titanium, the much lower heat capacity ( $\rho c$) value of the latter results in a much higher calculated average chip temperature.

The conclusions to be drawn from this discussion is that the temperature analysis presented in this thesis is capable of giving a rational explanation of the phenomena observed in the cutting of Titanium, and offers a clear explanation of why this material is so difficult to machine.

ACKNOWLEDGEMENTS

Thanks are due primarily to Professor Milton C. Shaw as Thesis advisor; without him this thesis would never have been written. Of the many members of the faculty who have given advice and assistance, Professor Brandon G. Rightmire should be cited for his insight into some very knotty problems. Discussions with Mr. N. Cook and other members of the Metal Cutting Laboratory always proved a source of ideas. Mr. Eliahou Dabora and Mr. Robert Schiesser had the patience and skill to attack a mountain of routine measurements and calculations, without making any detectable errors. Mr. W. Walsh helped conduct some of the temperature calibrations. Dr. E. Rabinowitz was most helpful in making quantitative radioactivity calculations. Mr. John Leach and members of the Machine Tool Laboratory did a very fine job making most of the experimental equipment.

## BIBLIOGRAPHY


1. Bickel, E., Die Zerspanungsforchung an Werkzengmaschinen Laboratorium der E.I.H., Industrielle Organisation 1950, No. 4.

2. Bickel, E. and Widmer, W., Die Temperaturem an der Werkzengschneide, Industrielle Organisation, 1951, No. 8.

3. Blok, H., Theoretical Study of Temperature Rise at Surfaces of Actual Contact Under Oiliness Lubricating Conditions, Proc. of Gen. Disc. on Lubrication, Inst. of Mech. Eng., London, England 1938, pp. 222-235.

4. Bowden, F. P. and Tabor , Friction and Lubrication of Solids.

5. Carslaw, H. L. and Jaeger, J. C., Conduction of Heat in Solids, Clarendon Press, 1947.

6. Chao, B. T. and Trigger, K. J., Cutting Temperatures and Metal-Cutting Phenomena, A.S.M.E. paper 50-A-43, 1950.

7. Dupuy, E. L. and Portevin, A. M., The Thermo-Electric Properties of Special Steels, Journal Iron & Steel Inst, 91, 1915, pp. 306-335.

8. Epifanov, G. I. and Rebinder, P. A., Energy Balance of the Metal Cutting Process, Doklady Akademii Nauk SSRR, 66, 1949. pp. 653/6. Brutcher Translation No. 2394.

9. Ernst, H. and Merchant, M. E., Mechanics of the Metal Cutting Process, J. Appl. Phys., 16, 1945, pp 267-275, 318-324.

10. Gottwein, K., Die Messung der Schneidentemperatur beim Abdrehen von Flusseisen, Maschinenban, 4, 1925, pp. 1129-1135.

11. Gottwein, K. and Reichel, W., German Patent DRP 617855.

12. Herbert, E. G., The Measurement of Cutting Temperatures, Proc. Inst. of Mech. Engineers, 1, 1926, pp. 289-329.

13. Jaeger, J. C., Moving Sources of Heat and the Temperature at Sliding Contents, Proc. Royal Soc. New S. Wales, 76, 1942, pp. 203-224.

14. Lang, M., Prüfen der Zerspanbarkeit durch Messung der Schnittemperatur, Carl Hanser Verlag, Munich, 1949.

15. Lauterbach, W. E. and Ratzel, E. A., An Investigation of the Flow and Effect of a Cutting Oil in Machining Operations, Lubrication Engineering, 7, 1, 1951, pp. 15-19.

16. Loewen, E. G., Marshall, E. R. and Shaw, M. C., Electric Strain Gage Tool Dynamometers, Proc. Soc. of Experimental Stress Analysis, VIII, 2, pp. 1-16.

17. McAdams, W. H, Heat Transmission, McGraw-Hill, New York, 1942.

18. Outwater, J. O. and Shaw, M. C., Surface Temperatures in Grinding, Trans. A.S.M.E., 74, January 1952, pp. 73-86.

19. Pahlitzsch, G. and Helmerdig, H., Das Temperaturfeld am Drehmeissel Warmetechnisch betrachtet, Z.d.V.D.I., 81, 1943, pp. 564/71, 691/98.

20. Pigott, R. J. S., Little High Pressure Jets from Below Cool Cutting Better, Am. Machinist, 96, 2, January 21, 1952, pp. 281-286.

21. Reichel, W., Abgekurtztes Standzeitermittlungsverfahren fur spangebende Werkzeuge, Mash. Ban., 11, 1932, page 473.

22. Rohsenow, W., Notes on the Relaxation Method applied to heat transfer, M.I.T., 1951.

23. Rumford, Benjamin, An Inquiry Concerning the Source of the Heat which is Excited by Friction, Phil. Trans. Royal Soc., 18, 1798, pp. 278-287.

24. Schallbroch, H., Schnittemperaturmessung mittels Strahlungsempfanger, Z. VDI, 83, 1939, pp. 438/39.

25. Schallbroch, H. and Balzer, H., Schnittkraft und Drehmomentmesser fur Werkzeugmaschinen, Werkstattbuch, Heft 9, Springer 1943, Berlin.

26. Schallbroch, H. and Lang, M., Messung der Schnitttemperatur mittels temperature anzeigender Farbanstriche, VDI, 87, No.1/2, January 9, 1943.

27. Schallbroch, H. and Schaumann, H., V.D.I., 81, 1937, pp. 325/30.

28. Schaumann, H., Die Schuittemperatur im Drehvorgang, und ihre Anwendung als Zerspanbarkeitskennziffer, Dissertation, T. H. Munchen, 1937.

29. Shaw, M. C., Metal Cutting Principles , M.I.T. Notes, 1951.

30. Shaw, M. C., Cook, N. H. and Smith, P. A., The Mechanics of Three-dimensional Cutting Operations, A.S.M.E. Preprint 51A-61, 1951.

31. Shaw, M. C., Pigott, J. D. and Richardson, L. P., The Effect of the Cutting Fluid upon Chip-Tool Interface Temperature, Trans. A.S.M.E., 1951, pp. 45/56.

32. Shaw, M. C. and Strang, C. D., Metal Transfer in the Cutting Process, J. Appl. Phys., 21, 1950, pp. 349/350.

33. Schmidt, A. O., Heat in Metal Cutting, Reprint from "Machining-Theory and Practice", A.S.M. 1950 , Cleveland.

34. Schmidt, A. O., Gilbert, W. W. and Boston, O. W., A Thermal Balance Method and Mechanical Investigation for Evaluating Machinability, Trans. A.S.M.E., CSM2, 1945, pp. 225/232.
Measurement of Temperatures in Metal Cutting, Trans. A.S.M.E., CSM8, 1946, pp. 47/49.

35. Schmidt, E., Das Differeuzverfahren zur Losung von Differenzialgleichungen der nichstationaren Warmeleitung, Diffusion und Impulsausbreitung, Forsch. Ing. Wes., 13, 1942, pp. 177/85.

36. Schmidt, E., Einfuehrung in die technische Thermodynamik, Berlin 1936, pp. 262/268.

37. Schwerd, F., Uber die Bestimmung der Temperaturfeldes beim Spanablauf, Z.d. V.D.I., 77, 1933, pp. 211/16.

38. Tangerman, E. S., Europe Studies Carbide Cutting, Am. Machinist, 96, 4, February 18, 1952, pp. 134/5.

39. Taylor, F. W., On the Art of Cutting Metals, Trans. A.S.M.E., 28, 1907, pp. 31-350.

40. Taylor, G. I. and Quinney, H., The Latent Energy Remaining in a Metal after Cold Working, Proc. Royal Soc., Series A, 143, 1934, pp. 307-326.

41. Trigger, K. S., Progress Report No. 1 on Tool-Chip Interface Temperatures, Trans. A.S.M.E., 70, 1948, pp. 91-98.

42. U. S. Air Force Machinability Report, Vol. 2, 1951.

43. Woxen, R., Tool-Life and Balance of Heat in Lathe Work, Proc. Royal Swedish Inst. of Eng. Research No. 142, 1937.

BIOGRAPHY

The author was born April 12, 1921 in Frankfurt a/M, Germany. Elementary education in Jena, Germany, completed at Bembridge School, Isle of Wight, England, in July 1937, with Oxford and Cambridge Joint Board Certificate. Arrived in U.S.A., with family, in October 1937. Began college February 1938, by entering the College of Engineering, New York University. Graduated cum laude in June 1941. Later received the S.M. degree in 1949, the Mechanical Engineer's degree in 1950, both from the Massachusetts Institute of Technology.

Working experience totalling five years with the Taft-Peirce Manufacturing Co., Woonsocket, R.I., as machinist, inspector, estimator, staff engineer, and research engineer, working chiefly in the field of gages and precision measurement. Two years in the U.S. Army Corps of Engineers.

# APPENDIX

Detailed derivation of equations (11),(15), and evaluations of equation (11) for various values of m and l.

$$\theta(x,y,0) = \frac{q}{2\pi k}\int_{-\ell}^{\ell} dx' \int_{-m}^{m} \frac{dy'}{\sqrt{(x-x')^2+(y-y')^2}} \qquad (10)$$

$$= \frac{q}{2\pi k}\int_{-\ell}^{\ell} \left[-\sinh^{-1}\frac{x-x'}{y-y'}\right]_{x'=-\ell}^{x'=\ell} dy$$

$$= \frac{q}{2\pi k}\int_{-\ell}^{\ell} \left[-\sinh^{-1}\frac{x-\ell}{y-y'} + \sinh^{-1}\frac{x+\ell}{y-y'}\right] dy$$

$$= \frac{q}{2\pi k}\left[(y-y')\sinh^{-1}\frac{x-\ell}{y-y'} + (x-\ell)\sinh^{-1}\frac{y-y'}{x-\ell} - (y-y')\sinh^{-1}\frac{x+\ell}{y-y'} - (x+\ell)\sinh^{-1}\frac{y-y'}{x+\ell}\right]_{y'=-m}^{y'=m}$$

$$= \frac{q}{2\pi k}\left\{|x-\ell|\sinh^{-1}\frac{y-m}{x-\ell} - |x-\ell|\sinh^{-1}\frac{y+m}{x-\ell} - |x+\ell|\sinh^{-1}\frac{y-m}{x+\ell} + |x+\ell|\sinh^{-1}\frac{y+m}{x+\ell}\right.$$

$$\left. + |y-m|\sinh^{-1}\frac{x-\ell}{y-m} - |y+m|\sinh^{-1}\frac{x-\ell}{y+m} - |y-m|\sinh^{-1}\frac{x+\ell}{y-m} + |y+m|\sinh^{-1}\frac{x+\ell}{y+m}\right\} \qquad (11)$$

Useful integrals of $\sinh^{-1}u$ functions, found by changing variables and integrating by parts, and where (a) and (p) are arbitrary constants are given below:

$$\int \sinh^{-1}\frac{x}{p}\,dx = x\sinh^{-1}\frac{x}{p} - \sqrt{p^2+x^2} \qquad (A)$$

$$\int \sinh^{-1}\frac{p}{\pm(x-a)}\,dx = +(x-a)\sinh^{-1}\frac{p}{\pm(x-a)} \pm p\sinh^{-1}\frac{\pm(x-a)}{p} \qquad (B)$$

$$\int x\sinh^{-1}\frac{p}{x}\,dx = \frac{1}{2}x^2\sinh^{-1}\frac{p}{x} + \frac{1}{2}p\sqrt{p^2+x^2} \qquad (C)$$

$$\int (a\pm x)\sinh^{-1}\frac{p}{a\pm x}\,dx = \pm\frac{1}{2}(a\pm x)^2\sinh^{-1}\frac{p}{a\pm x} \pm \frac{1}{2}p\sqrt{p^2+(a\pm x)^2} \qquad (D)$$

Equation (11) for certain specific values of $x$ and $y$ reduces to the following equations.

$$\theta(0,0) = \frac{qm}{k}\cdot\frac{2}{\pi}\left[\frac{\ell}{m}\sinh^{-1}\frac{m}{\ell} + \sinh^{-1}\frac{\ell}{m}\right] \qquad (12)$$

$$\theta(m,\ell) = \frac{qm}{k}\cdot\frac{1}{\pi}\left[\frac{\ell}{m}\sinh^{-1}\frac{m}{\ell} + \sinh^{-1}\frac{\ell}{m}\right] \qquad (12a)$$

$$\theta\left(\frac{\ell}{2},\frac{m}{2}\right) = \frac{qm}{k}\cdot\frac{1}{\pi}\left[\frac{\ell}{m}\sinh^{-1}\frac{m}{3\ell} + \sinh^{-1}\frac{\ell}{3m} + \frac{1}{4}\frac{\ell}{m}\sinh^{-1}\frac{3m}{\ell} + \frac{1}{4}\sinh^{-1}\frac{3\ell}{m}\right] + \theta(m,\ell) \qquad (12b)$$

$$\theta(\ell,0) = \frac{qm}{k}\cdot\frac{1}{\pi}\left[2\frac{\ell}{m}\sinh^{-1}\frac{m}{2\ell} + \sinh^{-1}\frac{2\ell}{m}\right] \qquad (12c)$$

$$\theta\left(\frac{3}{2}\ell,0\right) = \frac{qm}{k}\cdot\frac{1}{2\pi}\left[-\frac{\ell}{m}\sinh^{-1}\frac{2m}{\ell} + 5\frac{\ell}{m}\sinh^{-1}\frac{2m}{5\ell} - 2\sinh^{-1}\frac{\ell}{2m} + 2\sinh^{-1}\frac{5\ell}{2m}\right] \qquad (12d)$$

$$\theta(2\ell,0) = \frac{qm}{k}\cdot\frac{1}{\pi}\left[-\frac{\ell}{m}\sinh^{-1}\frac{m}{\ell} + 3\frac{\ell}{m}\sinh^{-1}\frac{m}{3\ell} - \sinh^{-1}\frac{\ell}{m} + \sinh^{-1}\frac{3\ell}{m}\right] \qquad (12e)$$

$$\theta\left(\frac{\ell}{2},0\right) = \frac{qm}{k}\cdot\frac{1}{2\pi}\left[\frac{\ell}{m}\sinh^{-1}\frac{2m}{\ell} + 3\frac{\ell}{m}\sinh^{-1}\frac{2m}{3\ell} + 2\sinh^{-1}\frac{\ell}{2m} + 2\sinh^{-1}\frac{3\ell}{2m}\right] \qquad (12f)$$

$$\theta(10\ell,0) = \frac{qm}{k}\cdot\frac{1}{\pi}\left[-9\frac{\ell}{m}\sinh^{-1}\frac{m}{9\ell} + 11\frac{\ell}{m}\sinh^{-1}\frac{m}{11\ell} - \sinh^{-1}\frac{9\ell}{m} + \sinh^{-1}\frac{11\ell}{m}\right] \qquad (12g)$$

$$\theta\left(0,\frac{m}{2}\right) = \frac{qm}{k}\cdot\frac{1}{2\pi}\left[2\frac{\ell}{m}\sinh^{-1}\frac{m}{2\ell} + 2\frac{\ell}{m}\sinh^{-1}\frac{3m}{2\ell} + \sinh^{-1}\frac{2\ell}{m} + 3\sinh^{-1}\frac{2\ell}{3m}\right] \qquad (12h)$$

$$\theta(0,m) = \frac{qm}{k}\cdot\frac{1}{\pi}\left[\frac{\ell}{m}\sinh^{-1}\frac{2m}{\ell} + 2\sinh^{-1}\frac{\ell}{2m}\right] \qquad (12i)$$

$$\theta\left(0,\frac{3}{2}m\right) = \frac{qm}{k}\cdot\frac{1}{2\pi}\left[-2\frac{\ell}{m}\sinh^{-1}\frac{m}{2\ell} + 2\frac{\ell}{m}\sinh^{-1}\frac{3m}{2\ell} - \sinh^{-1}\frac{2\ell}{m} + 5\sinh^{-1}\frac{2\ell}{5m}\right] \qquad (12j)$$

Note that the same expressions hold for equivalent points in other quadrants than the first.

$$\bar{\Theta} = \frac{qm}{k} \cdot \frac{1}{2\pi} \cdot \frac{1}{lm^2} \int_{-l}^{l} \int_{-m}^{m} \left[ (x+l) \sinh^{-1} \frac{y+m}{x+l} + (y+m) \sinh^{-1} \frac{x+l}{y+m} \right] dy\, dx \quad (14)$$

Let $I_1 = \int_{-l}^{l} \int_{-m}^{m} (x+l) \sinh^{-1} \frac{y+m}{x+l}\, dy\, dx$

$$= \int_{-l}^{l} \left[ (x+l)(y+m) \sinh^{-1} \frac{y+m}{x+l} - (x+l)^2 \sqrt{1 + \left(\frac{y+m}{x+l}\right)^2} \right]_{y=-m}^{y=m} dx$$

$$= \int_{-l}^{l} \left[ 2m (x+l) \sinh^{-1} \frac{2m}{x+l} - (x+l) \sqrt{(x+l)^2 + 4m^2} + (x+l)^2 \right] dx$$

$$= \left[ m(x+l)^2 \sinh^{-1} \frac{2m}{x+l} + 2m^2 \sqrt{4m^2 + (x+l)^2} + \frac{1}{3}(x+l)^3 - \frac{1}{3}\left[(x+l)^2 + 4m^2\right]^{\frac{3}{2}} \right]_{x=-l}^{x=l}$$

$$= \left[ 4ml^2 \sinh^{-1} \frac{m}{l} + 4m^2 l \sqrt{\left(\frac{m}{l}\right)^2 + 1} - 4m^3 + \frac{8}{3} l^3 - \frac{1}{3}\left[4l^2 + 4m^2\right]^{\frac{3}{2}} + \frac{8}{3} m^3 \right]$$

$$= 4m^2 l \left[ \left(\frac{l}{m}\right) \sinh^{-1} \frac{m}{l} - \frac{1}{3}\left(\frac{m}{l}\right) + \frac{2}{3}\left(\frac{l}{m}\right)^2 + \left[\frac{1}{3} - \frac{2}{3}\left(\frac{l}{m}\right)^2\right] \sqrt{\left(\frac{m}{l}\right)^2 + 1} \right] \quad (16)$$

Let $I_2 = \int_{-l}^{l} \int_{-m}^{m} (y+m) \sinh^{-1} \frac{x+l}{y+m}\, dy\, dx$

$$= \int_{-l}^{l} \left[ \frac{1}{2}(y+m)^2 \sinh^{-1} \frac{x+l}{y+m} + \frac{1}{2}(x+l) \sqrt{(x+l)^2 + (y+m)^2} \right]_{y=-m}^{y=m} dx$$

$$= \int_{-l}^{l} \left[ 2m^2 \sinh^{-1} \frac{x+l}{2m} + \frac{1}{2}(x+l) \sqrt{(x+l)^2 + 4m^2} - \frac{1}{2}(x+l)^2 \right] dx$$

$$= \left[ 2m^2 (x+l) \sinh^{-1} \frac{x+l}{2m} - 4m^3 \sqrt{1 + \left(\frac{x+l}{2m}\right)^2} + \frac{1}{6}\left[(x+l)^2 + 4m^2\right]^{\frac{3}{2}} - \frac{1}{6}(x+l)^3 \right]_{x=-l}^{x=l}$$

$$= 4m^2 l \sinh^{-1} \frac{l}{m} - 4m^3 \sqrt{1 + \left(\frac{l}{m}\right)^2} + 4m^3 + \frac{1}{6}\left[4l^2 + 4m^2\right]^{\frac{3}{2}} - \frac{4}{3} m^3 - \frac{4}{3} l^3$$

$$= 4m^2 l \left[ \sinh^{-1} \frac{l}{m} - \frac{1}{3}\left(\frac{l}{m}\right)^2 + \frac{2}{3}\left(\frac{m}{l}\right) + \left[\frac{1}{3}\left(\frac{l}{m}\right)^2 - \frac{2}{3}\right] \sqrt{\left(\frac{m}{l}\right)^2 + 1} \right] \quad (17)$$

Combining (14) with (16) and (17) gives

$$\bar{\Theta} = \frac{qm}{k}\,\frac{2}{\pi}\left\{\left(\frac{l}{m}\right)\sinh^{-1}\frac{m}{l} + \sinh^{-1}\frac{l}{m} + \frac{1}{3}\left(\frac{m}{l}\right) + \frac{1}{3}\left(\frac{l}{m}\right)^2 - \frac{1}{3}\left[1+\left(\frac{l}{m}\right)^2\right]\sqrt{1+\left(\frac{m}{l}\right)^2}\right\} \tag{15}$$

When $\frac{m}{l} \geq 20$ the following relations hold:

$$\sinh^{-1}\frac{l}{m} = \frac{l}{m}$$

$$\frac{l}{m}\sinh^{-1}\frac{m}{l} = \frac{l}{m}\log_e\frac{2m}{l}$$

$$\frac{1}{3}\left[1+\left(\frac{l}{m}\right)^2\right]\sqrt{1+\left(\frac{m}{l}\right)^2} = \frac{1}{3}\left[1+\left(\frac{l}{m}\right)^2\right]\left[\frac{m}{l}+\frac{1}{2}\frac{l}{m}\right] = \frac{1}{3}\frac{m}{l} + \frac{1}{2}\frac{l}{m} + \frac{1}{6}\left(\frac{l}{m}\right)^3$$

Substituting these expressions into (15) and noting that the $\frac{1}{6}\left(\frac{l}{m}\right)^3$ term is negligible, (15) becomes

$$\bar{\Theta} = \frac{ql}{k}\cdot\frac{2}{\pi}\left[\log_e\frac{2m}{l} + \frac{1}{3}\left(\frac{l}{m}\right) + \frac{1}{2}\right] \quad (\vartheta \geq 20) \tag{15a}$$

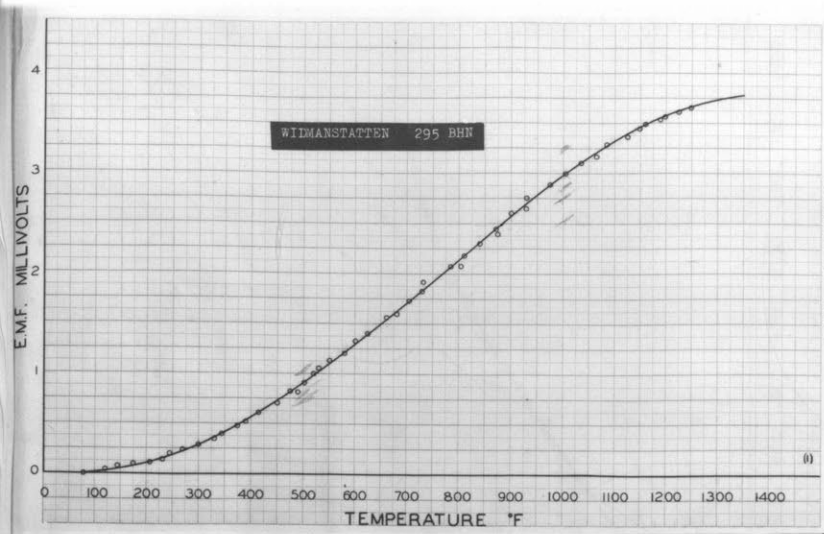


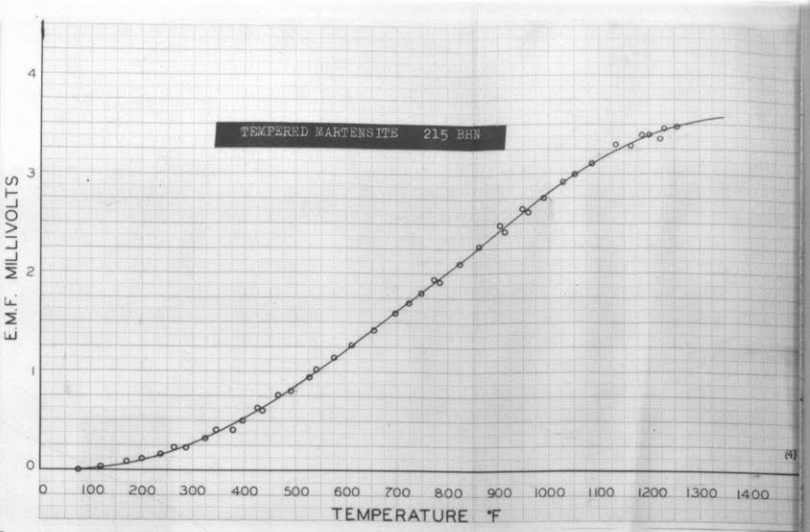


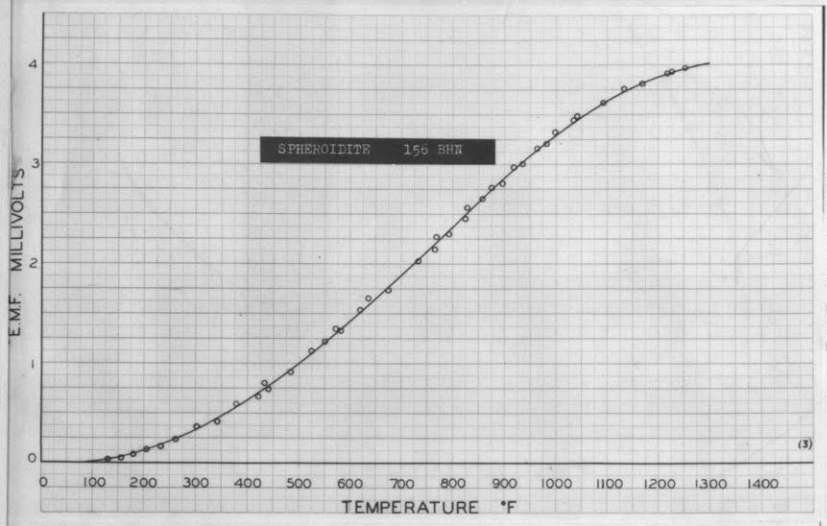


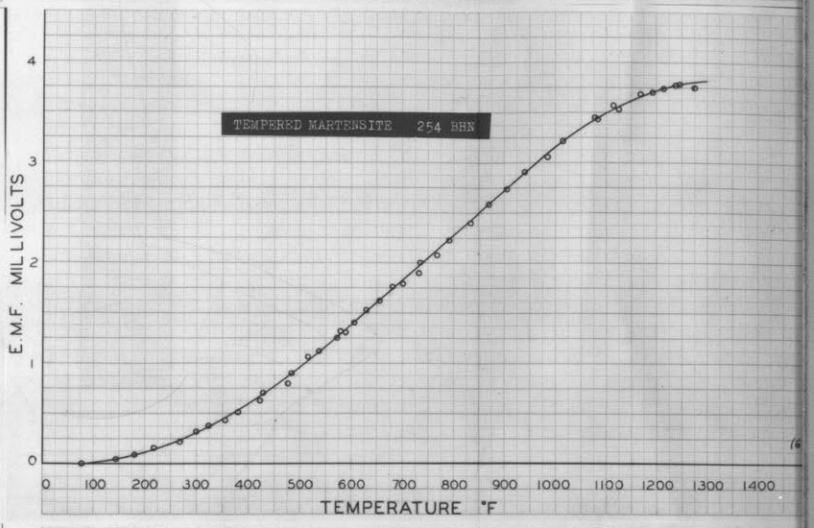


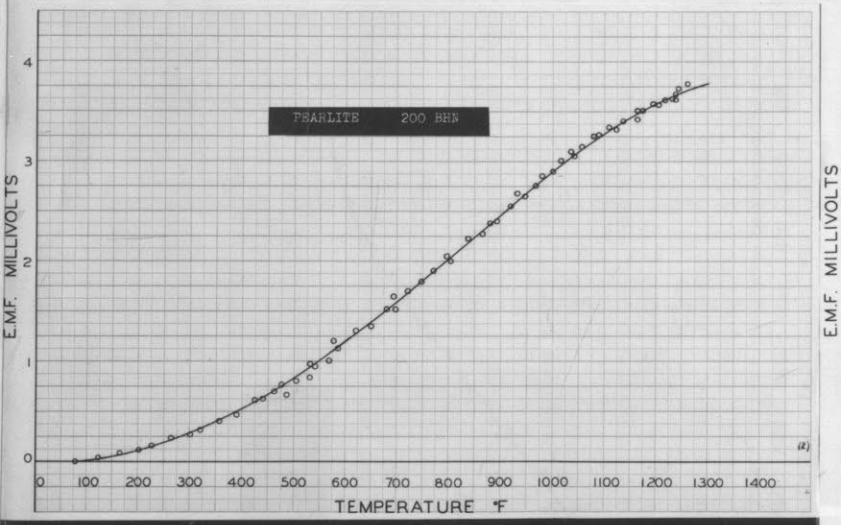


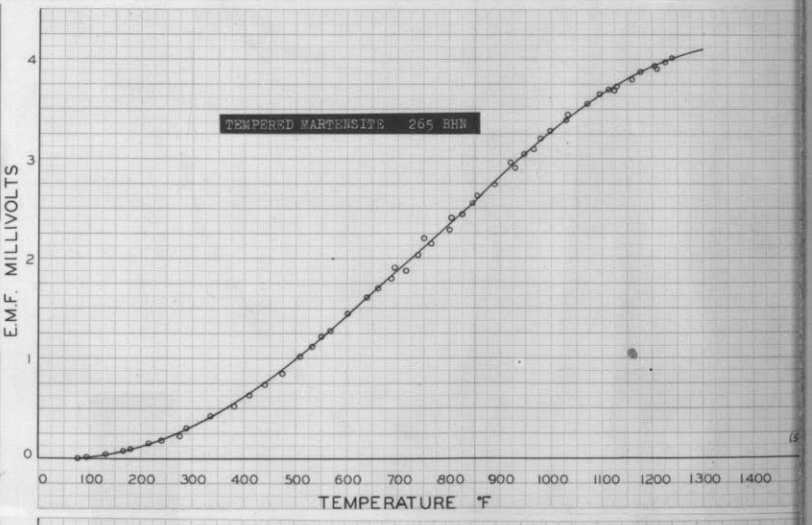


# TEMPERATURE CALIBRATION CURVES

## 8640 STEEL

## vs.

## 18-4-1 HIGH SPEED STEEL

Fig.70

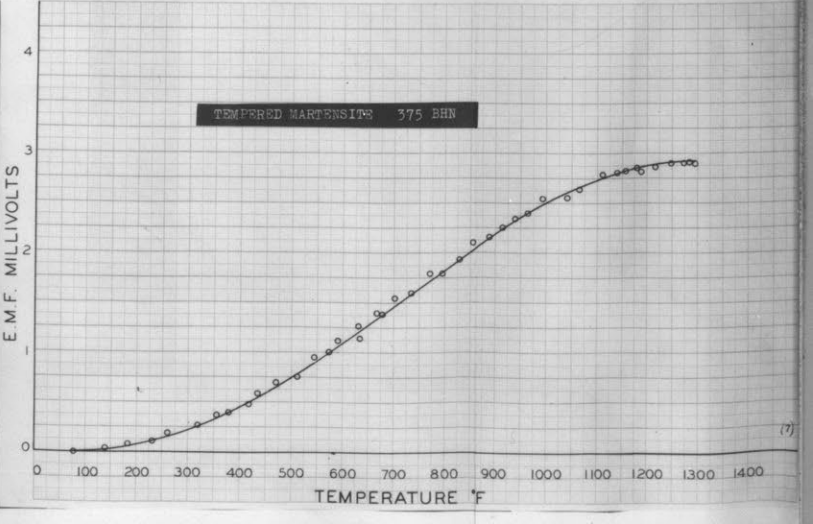

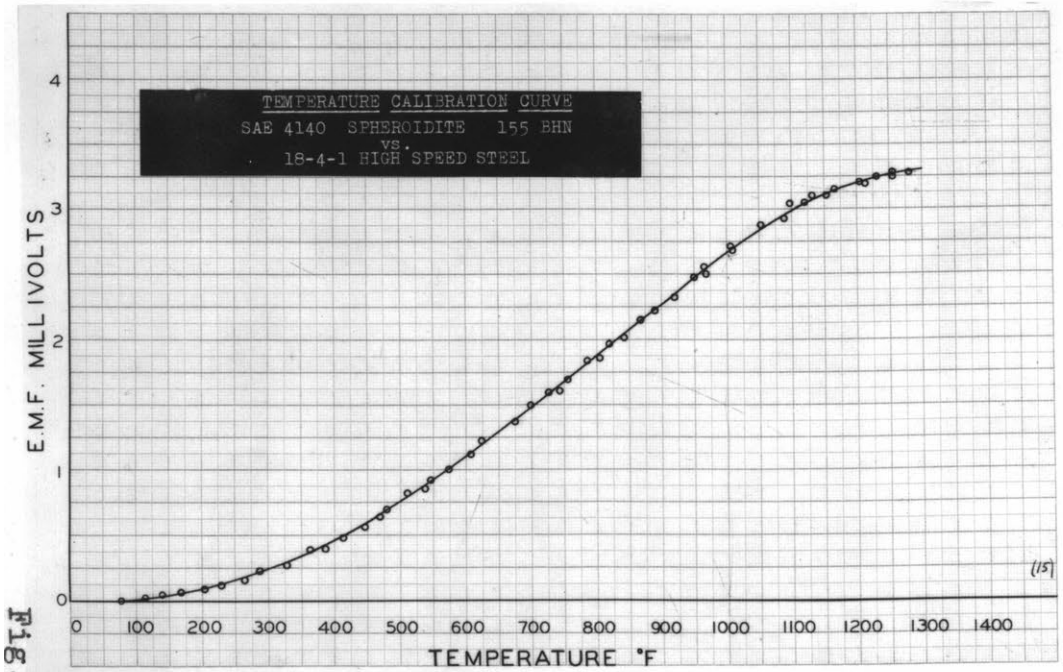
TEMPERATURE CALIBRATION CURVE
SAE 4140 SPHEROIDITE 155 BHN
vs.
18-4-1 HIGH SPEED STEEL
E.M.F. MILLIVOLTS
TEMPERATURE °F
(15)

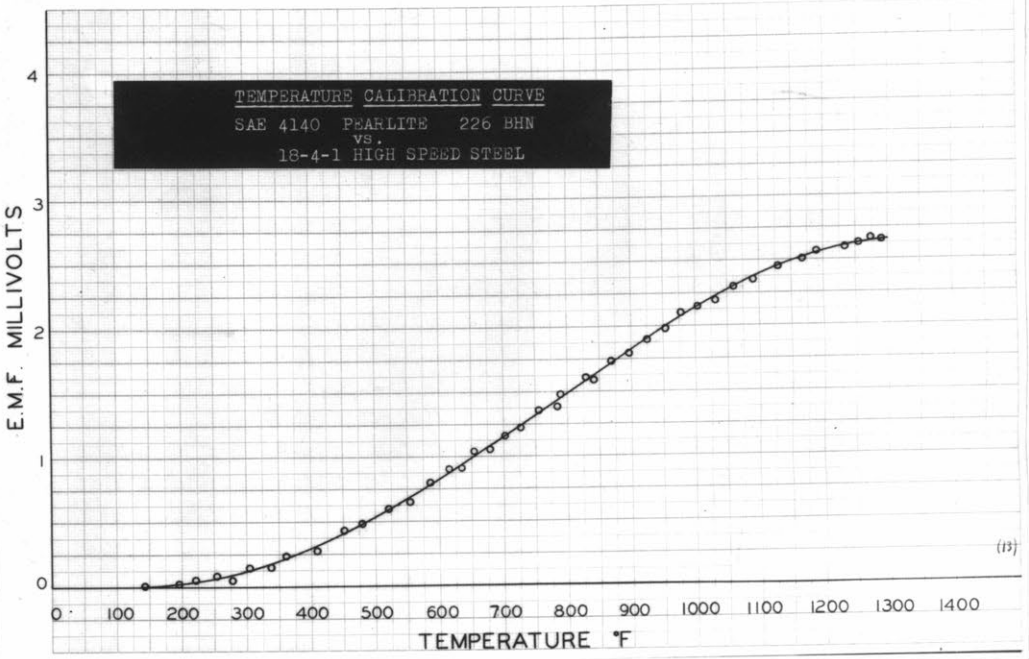
TEMPERATURE CALIBRATION CURVE
SAE 4140 PEARLITE 226 BHN
vs.
18-4-1 HIGH SPEED STEEL
E.M.F. MILLIVOLTS
TEMPERATURE °F
(13)

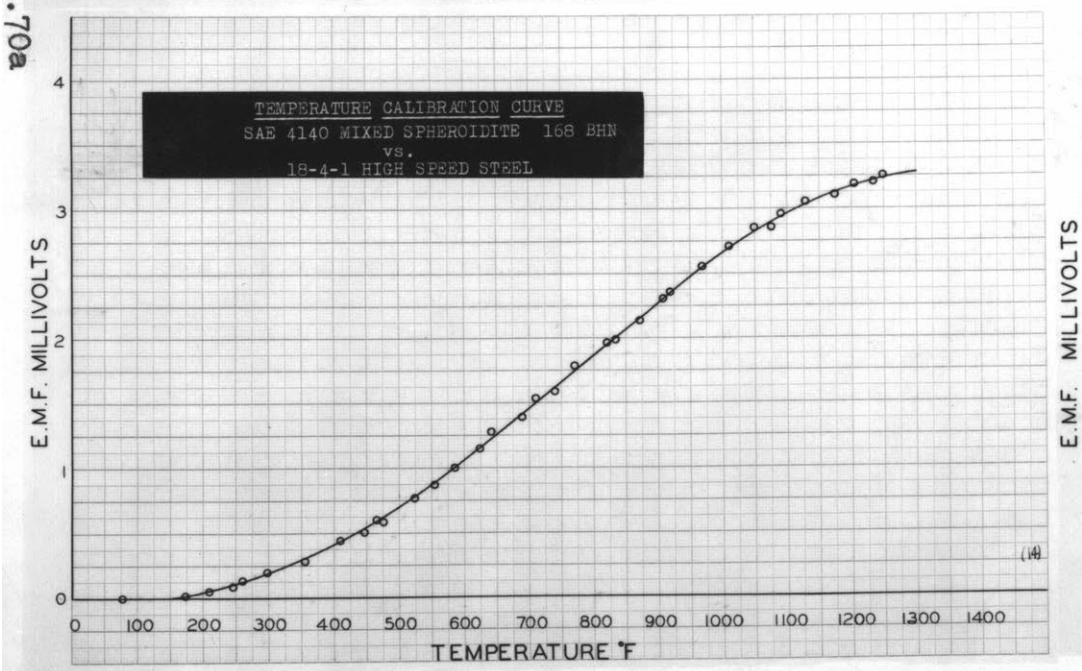
TEMPERATURE CALIBRATION CURVE
SAE 4140 MIXED SPHEROIDITE 168 BHN
vs.
18-4-1 HIGH SPEED STEEL
E.M.F. MILLIVOLTS
TEMPERATURE °F
(14)

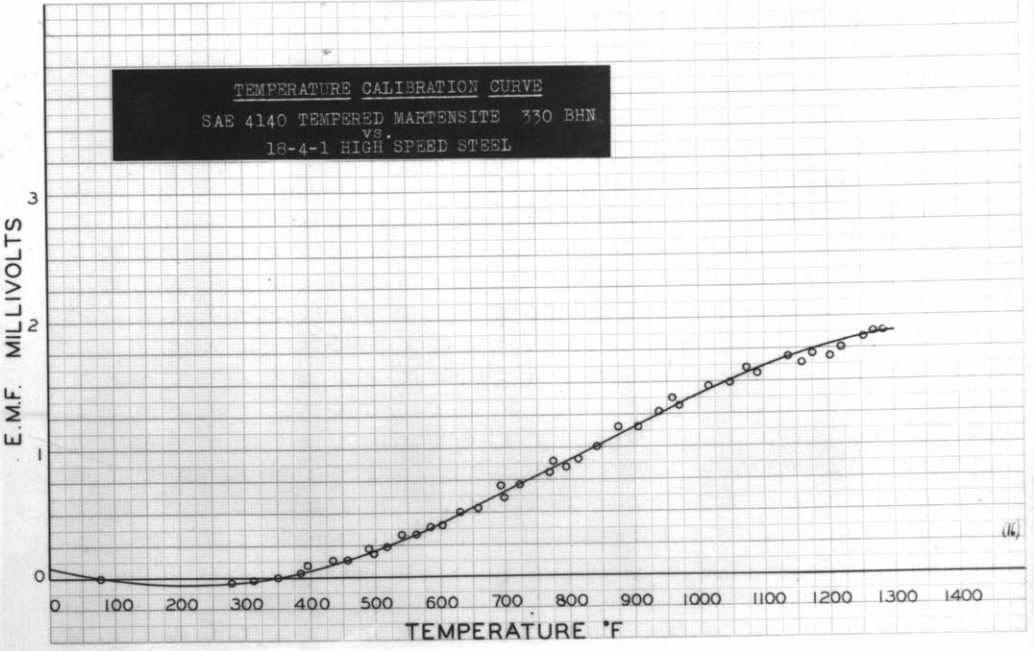
TEMPERATURE CALIBRATION CURVE
SAE 4140 TEMPERED MARTENSITE 330 BHN
vs.
18-4-1 HIGH SPEED STEEL
E.M.F. MILLIVOLTS
TEMPERATURE °F
(16)

Fig. 70a

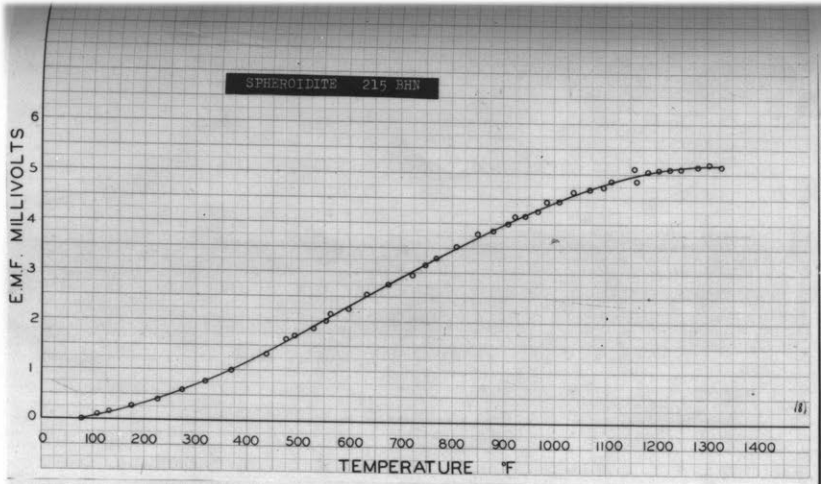


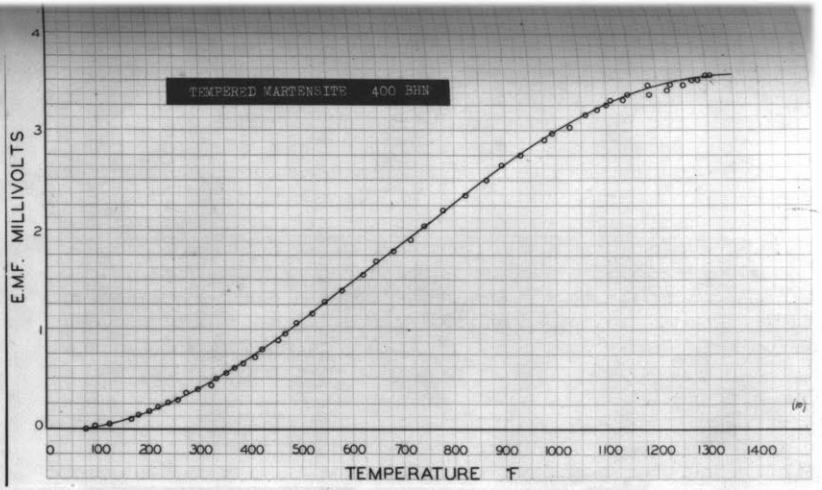


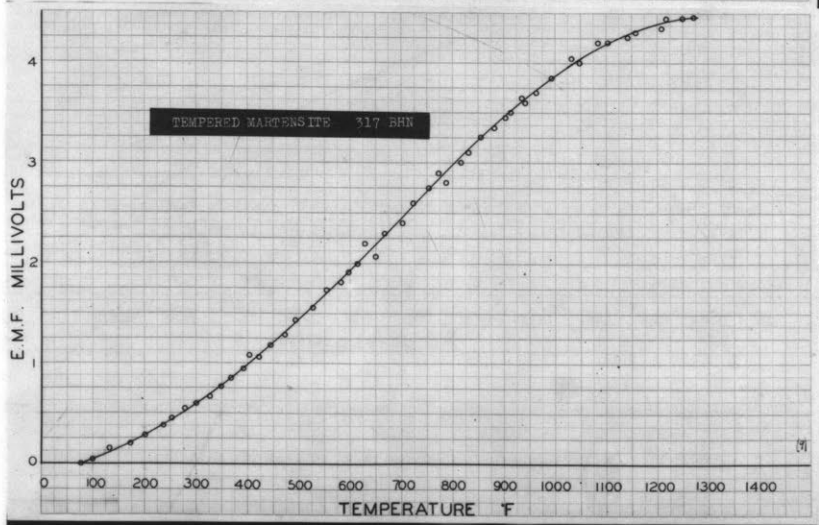


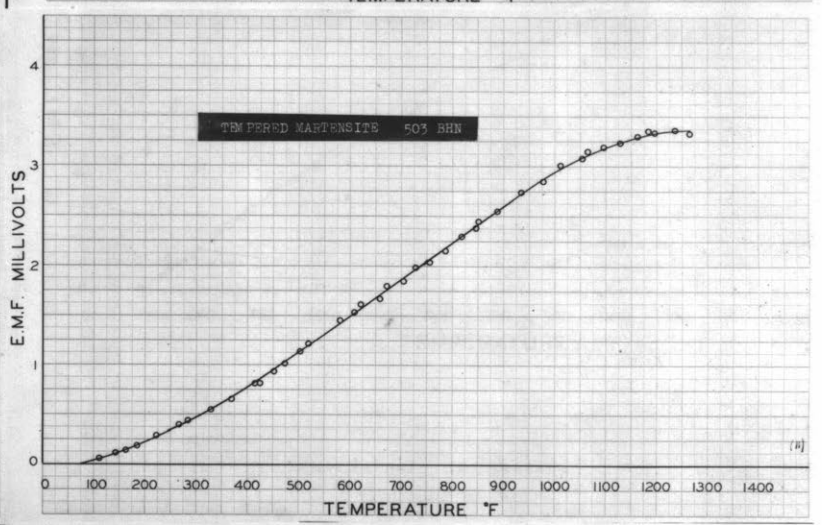


# TEMPERATURE CALIBRATION CURVES

## 4340 STEEL

vs.

## 18-4-1 HIGH SPEED STEEL

Fig. 71

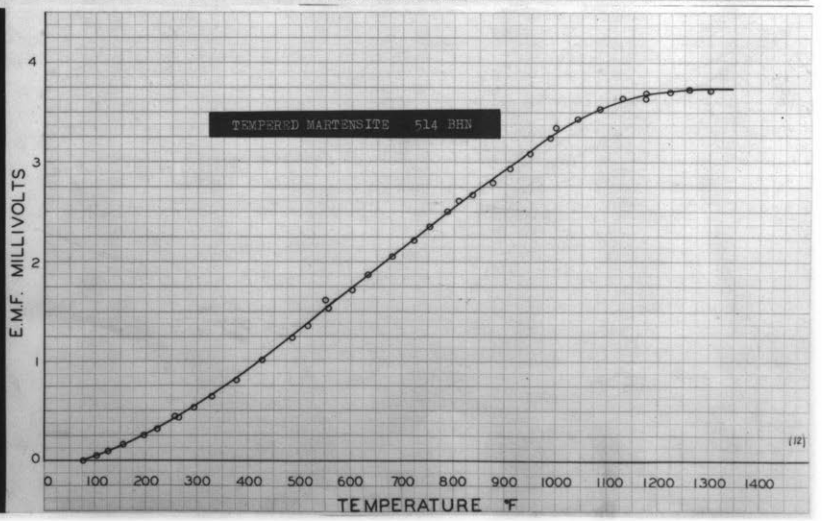

Fig. 72

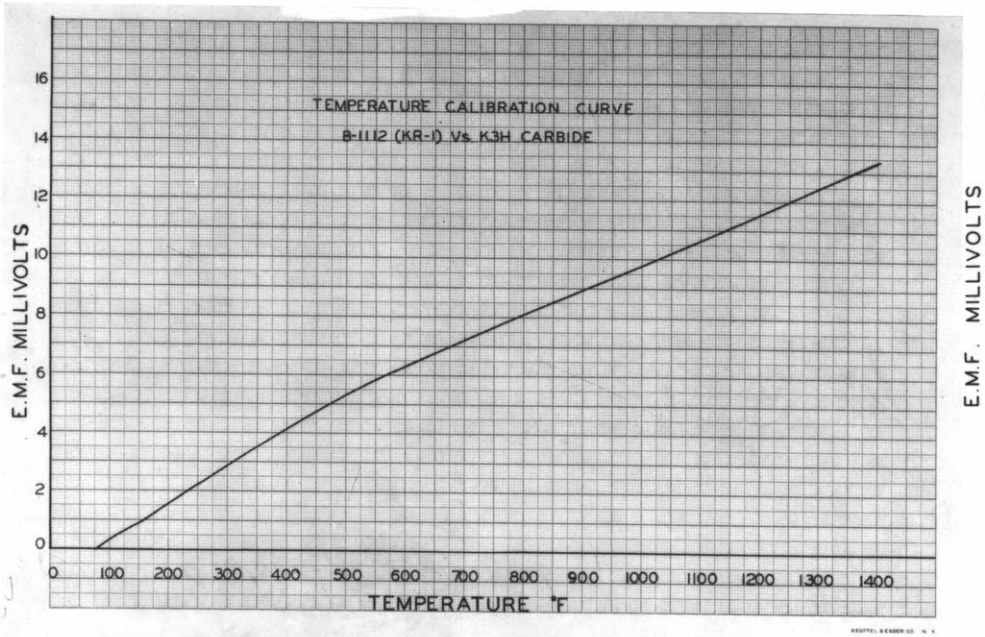
TEMPERATURE CALIBRATION CURVE
B-1112 (KR-1) Vs. K3H CARBIDE
E.M.F. MILLIVOLTS
TEMPERATURE °F

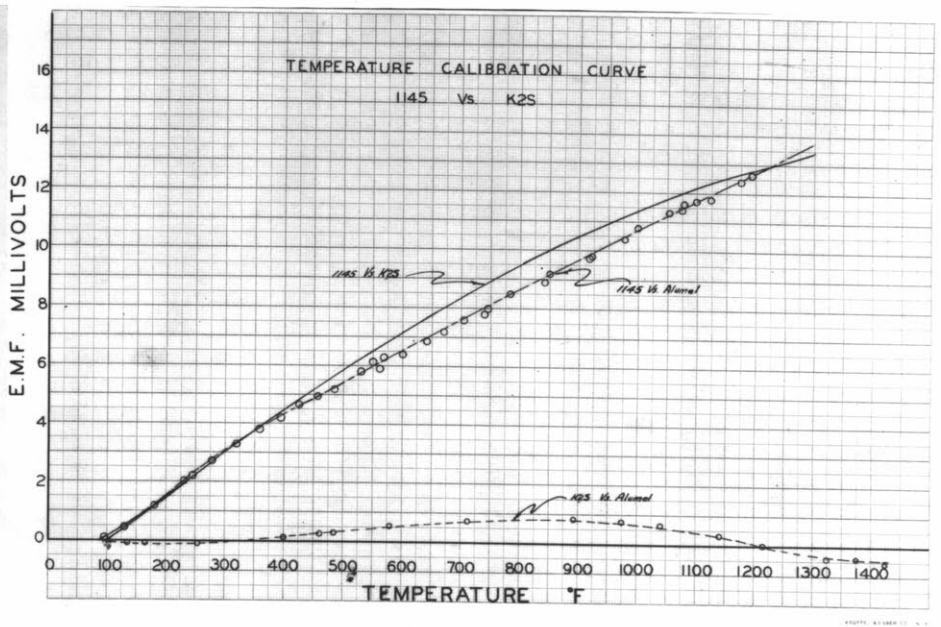
TEMPERATURE CALIBRATION CURVE
1145 Vs. K2S
E.M.F. MILLIVOLTS
TEMPERATURE °F

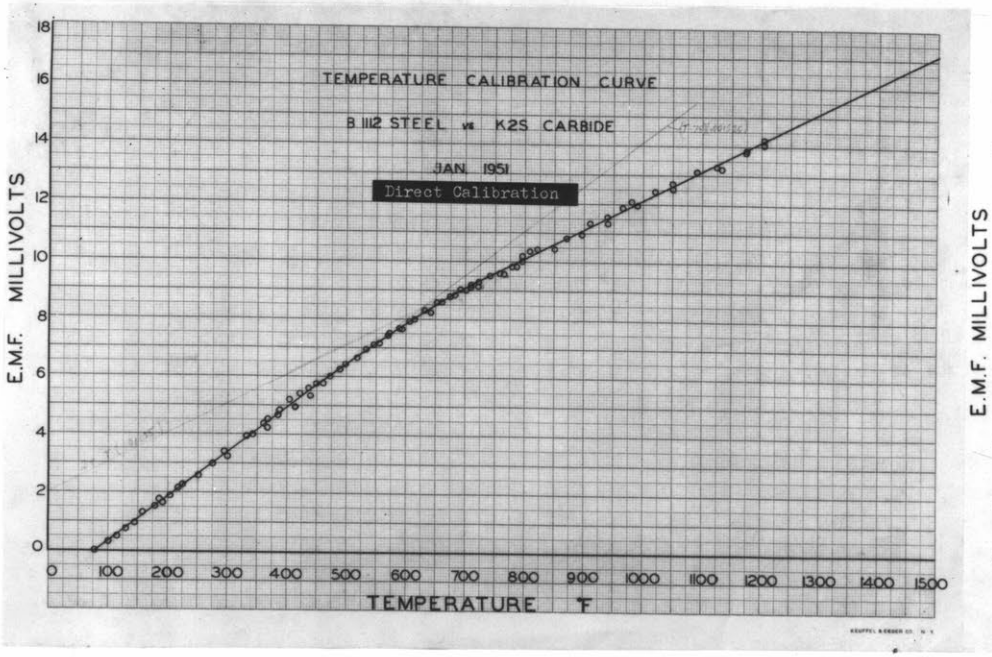
TEMPERATURE CALIBRATION CURVE
B 1112 STEEL vs K2S CARBIDE
JAN. 1951
Direct Calibration
E.M.F. MILLIVOLTS
TEMPERATURE °F

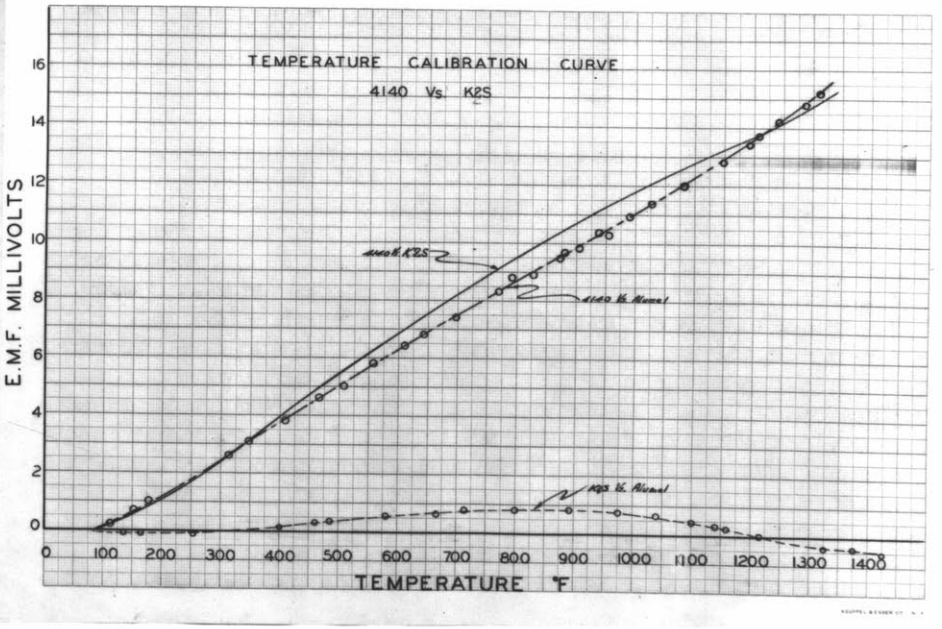
TEMPERATURE CALIBRATION CURVE
4140 Vs. K2S
E.M.F. MILLIVOLTS
TEMPERATURE °F

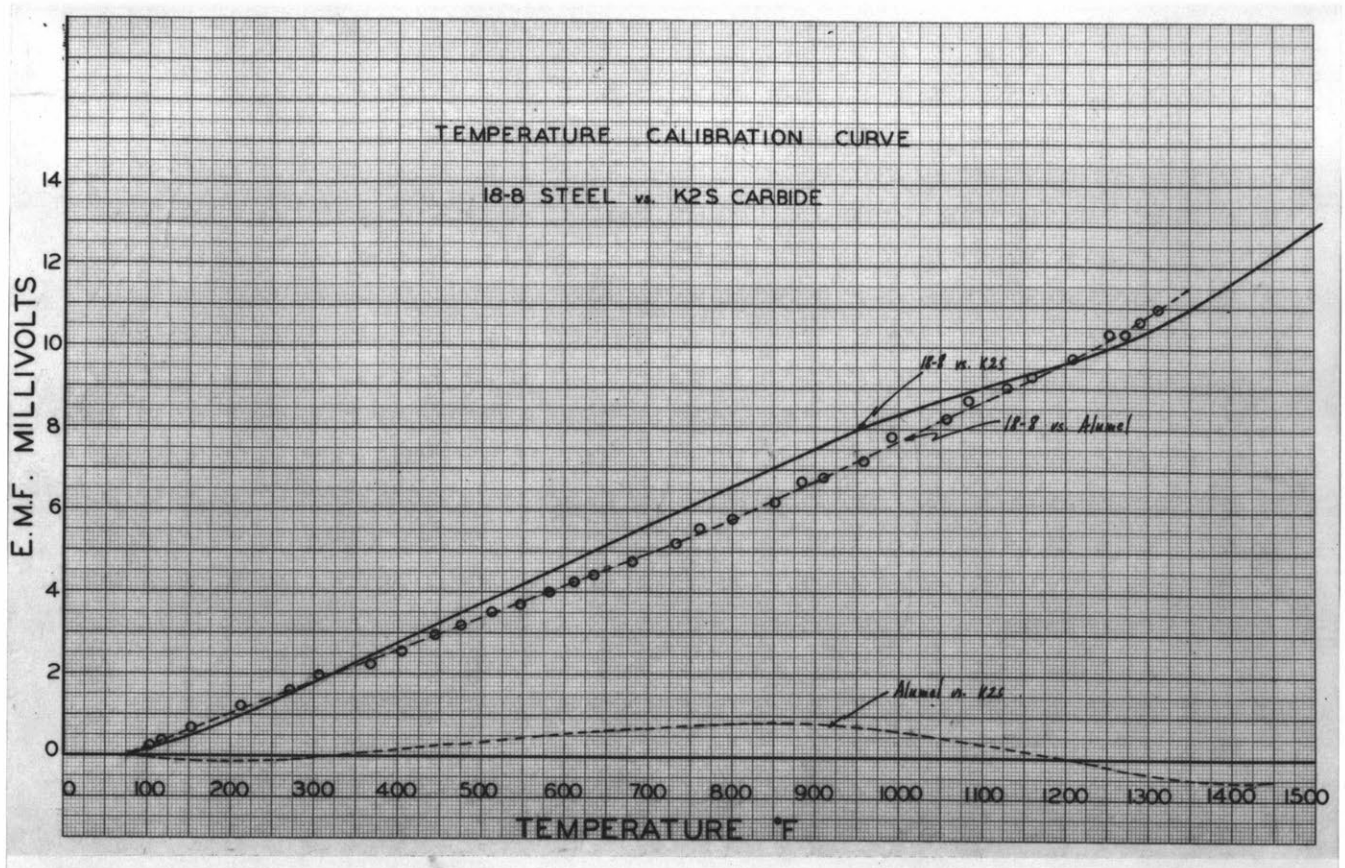


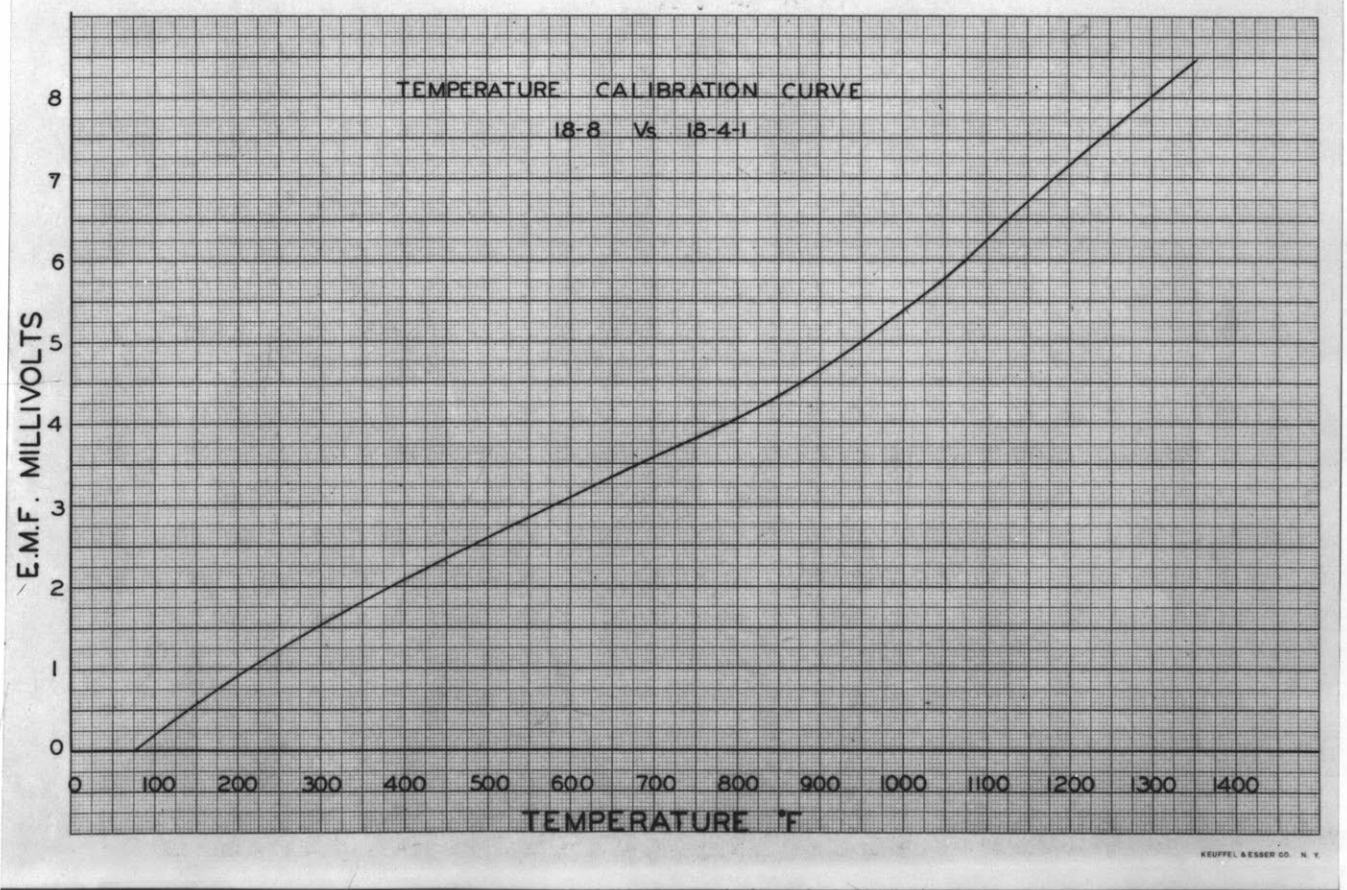


Fig.73

TEMPERATURE CALIBRATION CURVES OF 18-8 STAINLESS STEEL VS. K2S Carbide and 18-4-1 High Speed Steel. Alumel used as reference material in both cases.

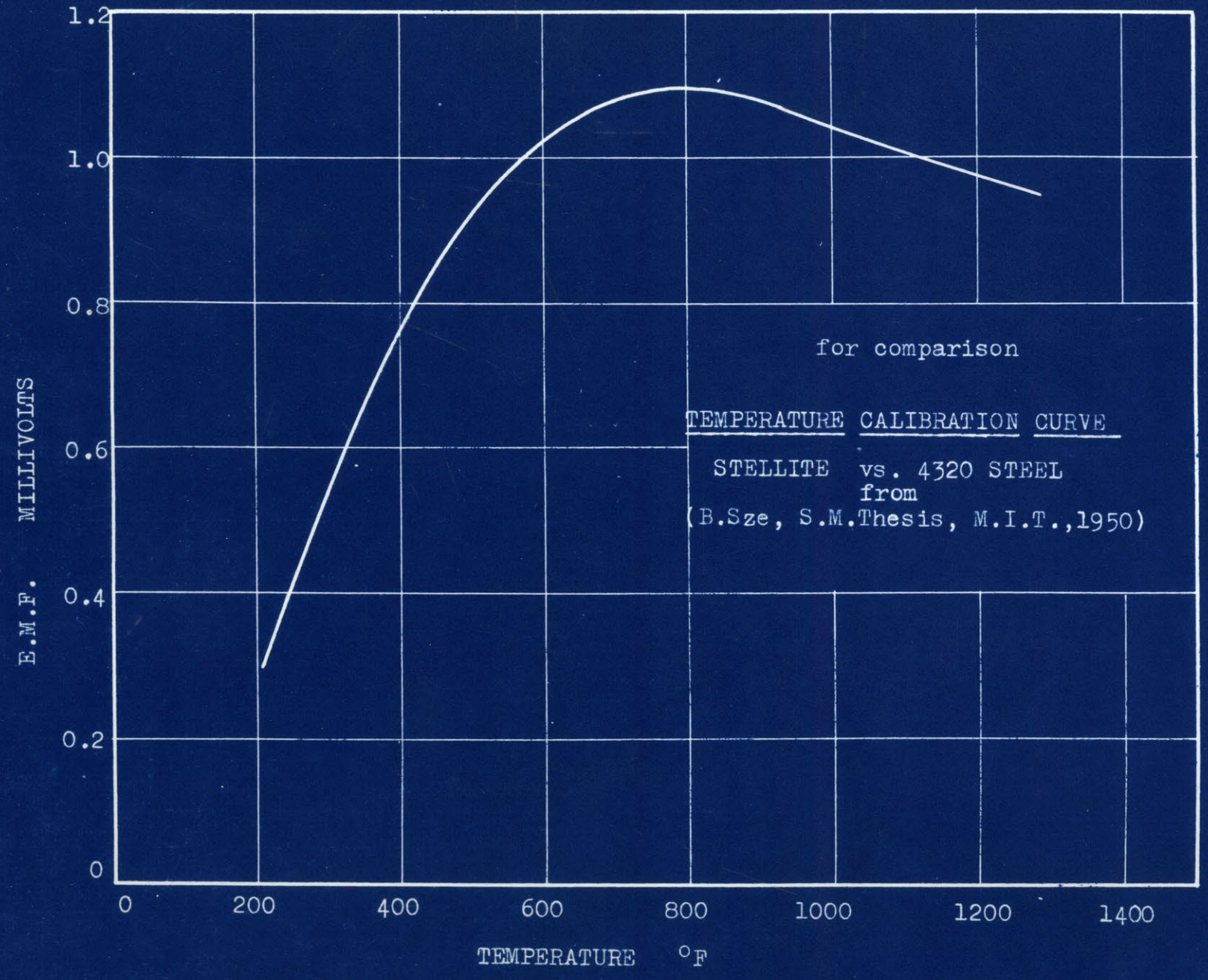
1.2
1.0
0.8
0.6
0.4
0.2
0
E.M.F. MILLIVOLTS
0
200
400
600
800
1000
1200
1400
TEMPERATURE °F
for comparison
TEMPERATURE CALIBRATION CURVE
STELLITE vs. 4320 STEEL
from
(B.Sze, S.M.Thesis, M.I.T.,1950)

Fig. 73a

Fig. 74

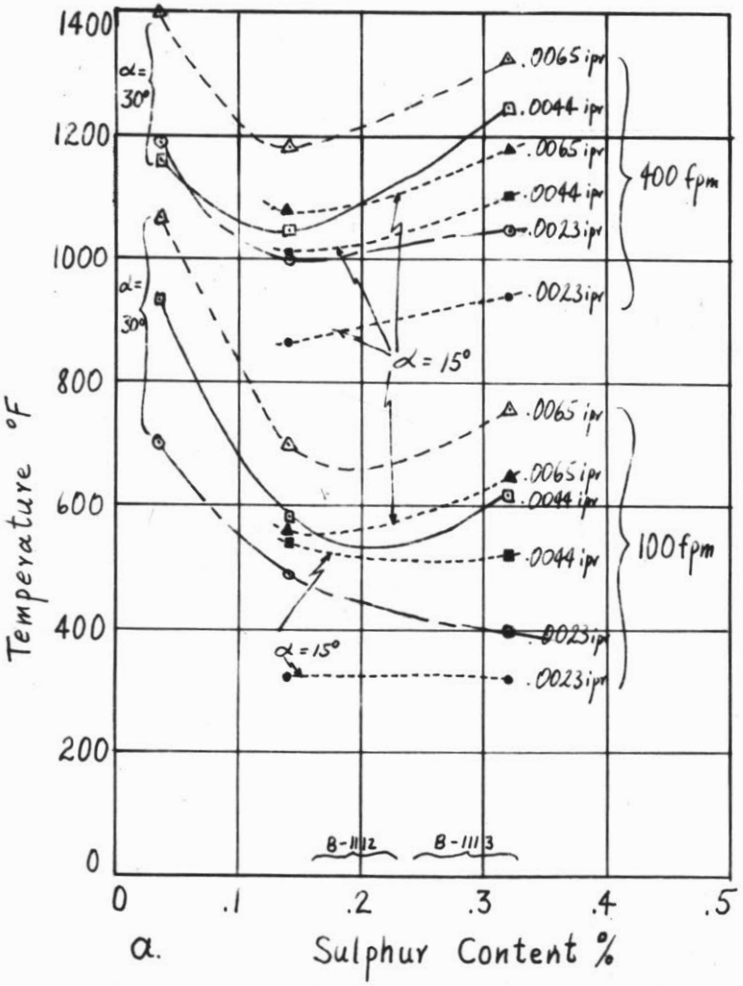


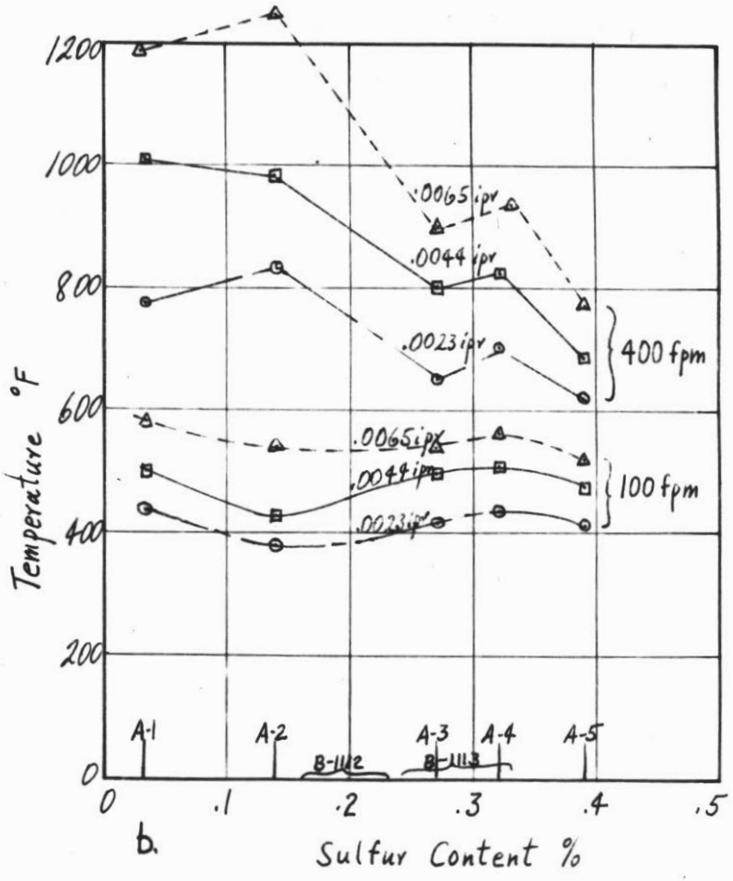


CUTTING TEMPERATURE VS. SULPHUR CONTENT

ORTHOGONAL CUTTING

WORK MATERIAL: 1 7/8" diam. bars of type B-1112 steel containing various amounts of sulphur.

TOOL MATERIAL: Fig. a. 18-4-1 High Speed Steel
Rake angle: 15° and 30° as shown.
Fig. b. K2S Tungsten-Titanium Carbide
Rake angle: 20°
Clearance angle: 5°
Speeds and feeds: as shown.
Width of Cut: 1/8" approx.

FLUID: None

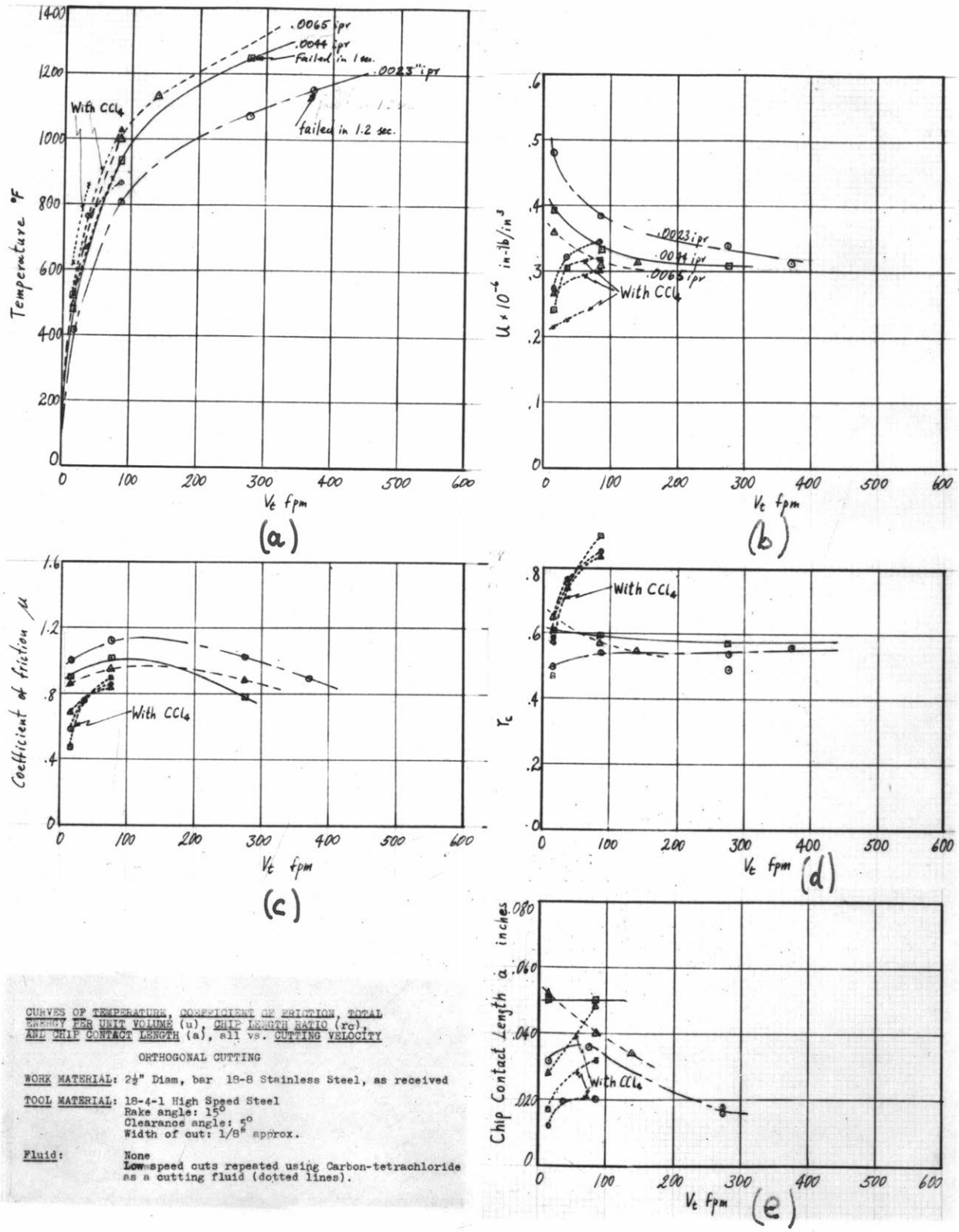


CURVES OF TEMPERATURE, COEFFICIENT OF FRICTION, TOTAL ENERGY PER UNIT VOLUME (u), CHIP LENGTH RATIO (rc), AND CHIP CONTACT LENGTH (a), all vs. CUTTING VELOCITY

ORTHOGONAL CUTTING

WORK MATERIAL: 2½" Diam, bar 18-8 Stainless Steel, as received

TOOL MATERIAL: 18-4-1 High Speed Steel
Rake angle: 15°
Clearance angle: 5°
Width of cut: 1/8" approx.

Fluid: None
Low speed cuts repeated using Carbon-tetrachloride as a cutting fluid (dotted lines).

Fig.75

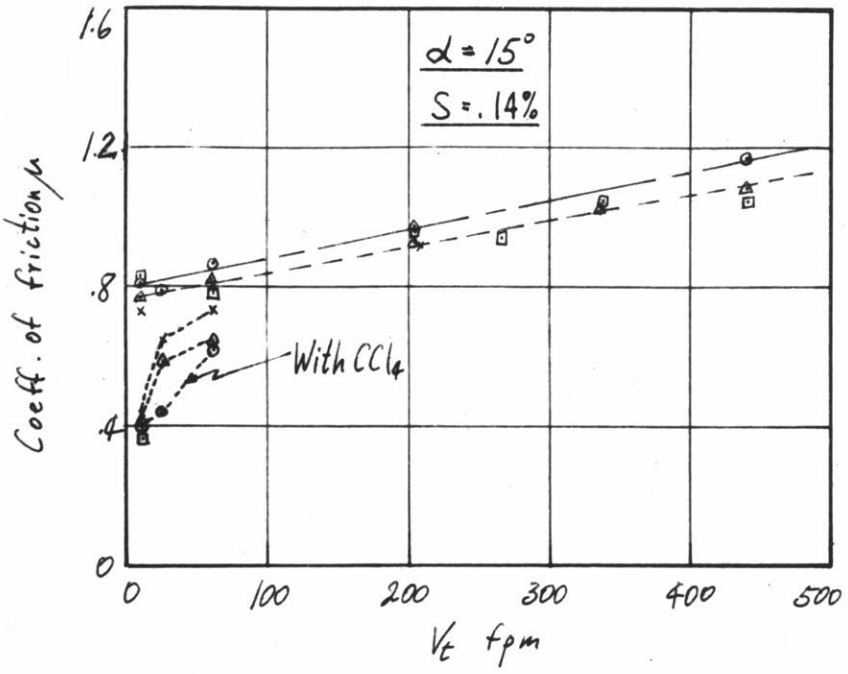


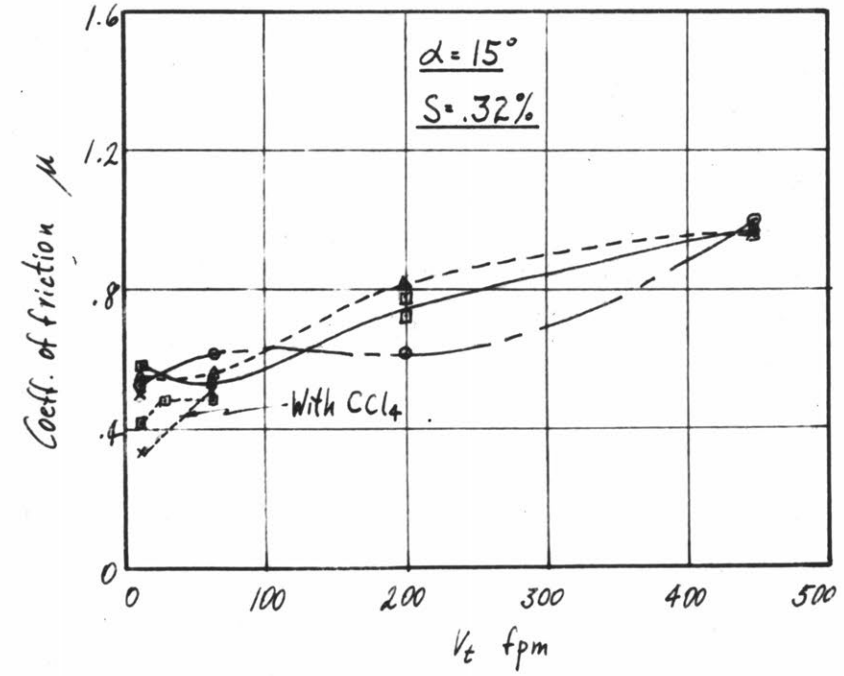


COEFFICIENT OF FRICTION VS. CUTTING VELOCITY

ORTHOGONAL CUTTING

WORK MATERIAL: 1 7/8" diam. bars of type B-1112 steel containing various amounts of sulphur.

TOOL MATERIAL: 18-4-1 High Speed Steel
Rake angle: 15°
Clearance angle: 5°
Width of cut: 1/8" approx.
Feeds as shown by code: ● .0023 ipr
■ .0044 ipr
▲ .0065 ipr
▽ .0087 ipr
× .0116 ipr

FLUID: None
Some low speed tests repeated using Carbon-tetrachloride (dotted lines)

Fig.76

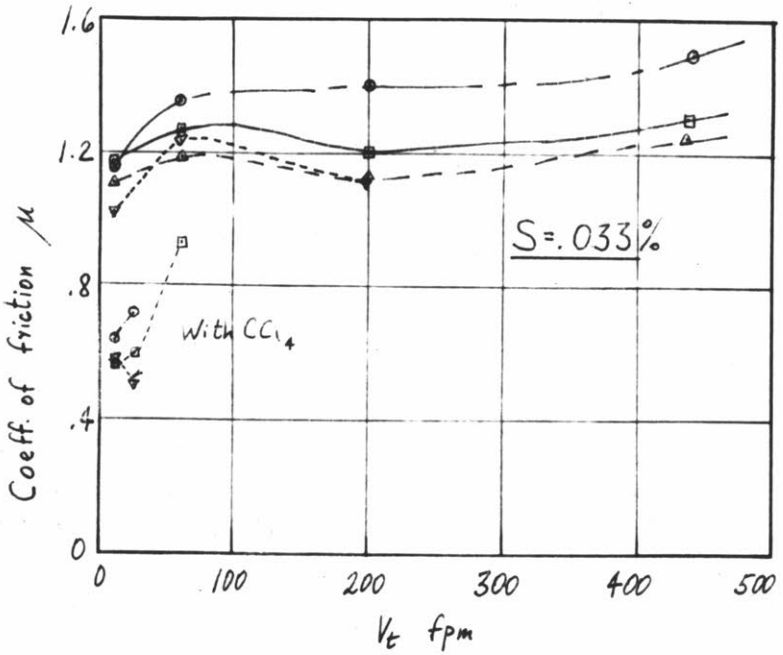


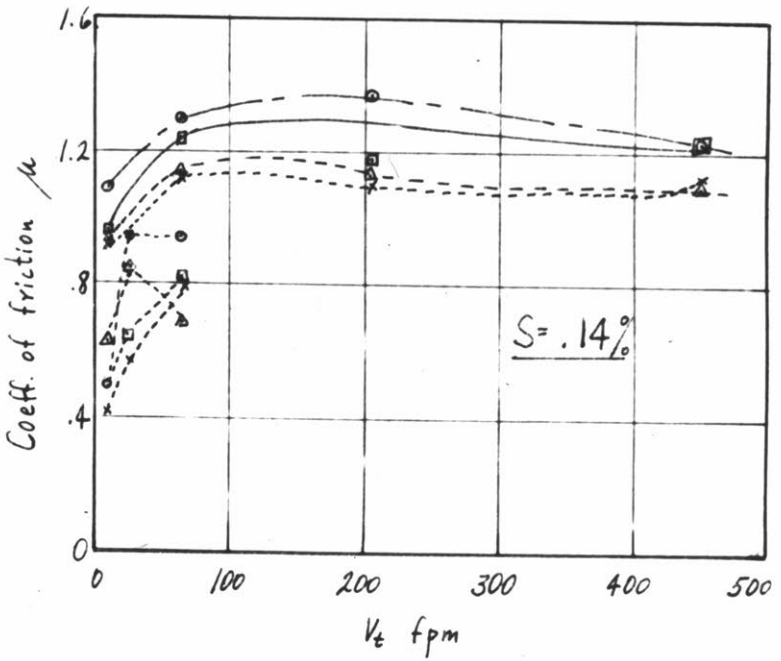


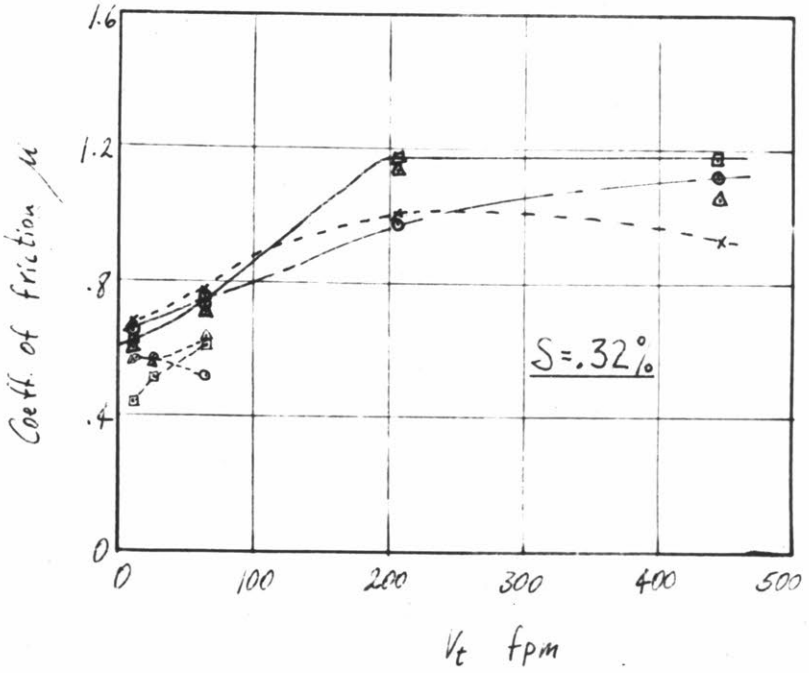


Fig. 77

COEFFICIENT OF FRICTION VS. CUTTING SPEED CURVES

ORTHOGONAL CUTTING

WORK MATERIAL: 1 7/8" Diam. Bars of type B-1112 Steel containing various amounts of Sulphur.

TOOL MATERIAL: 18-4-1 High Speed Steel
Rake angle: 30°
Clearance angle: 5°
Width of cut: 1/8" approx.
Feeds as shown by code:
⊙ .0023 ipr
⊡ .0044 ipr
△ .0085 ipr
× .0116 ipr

FLUID: None.
Some low speed tests repeated using Carbon-tetrachloride (dotted lines).

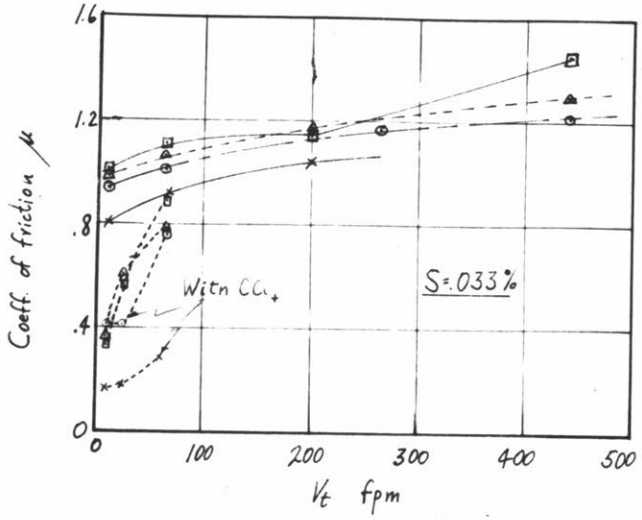


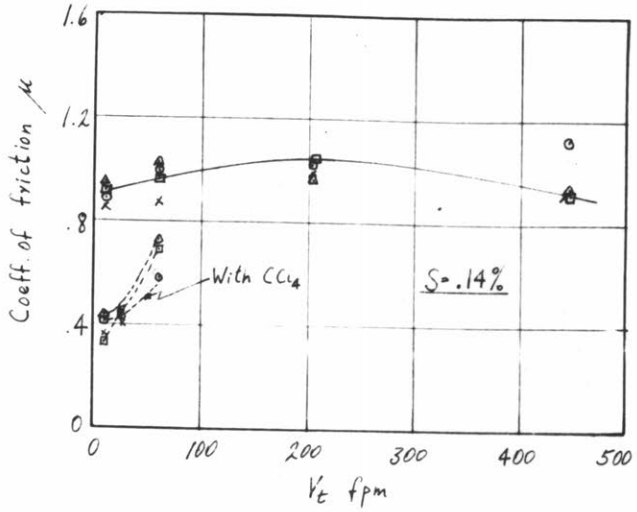


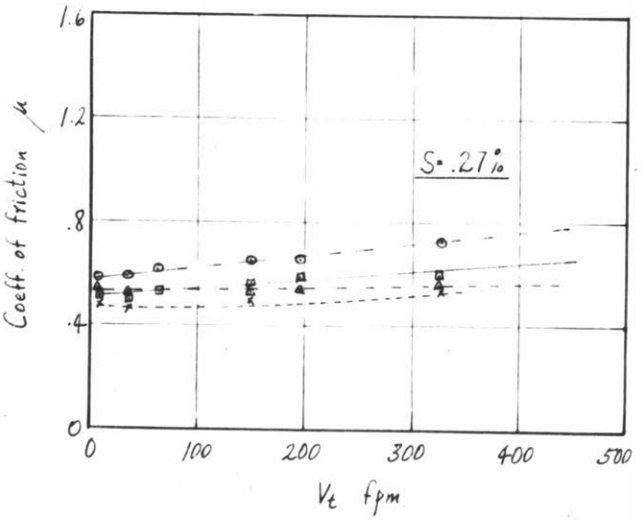


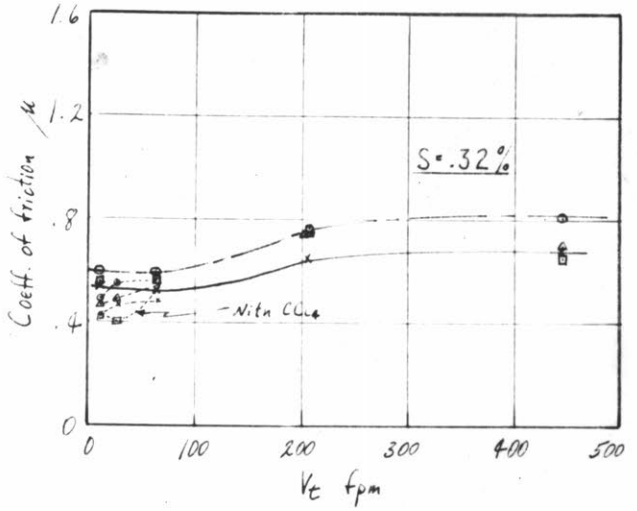


COEFFICIENT OF FRICTION VS. CUTTING SPEED CURVES

ORTHOGONAL CUTTING

WORK MATERIAL: 1 7/8" Diam. Bars of Type B-1112 Steel containing various amounts of Sulphur.

TOOL MATERIAL: K2S Tungsten-Titanium Carbide
Rake angle: 20°
Clearance angle: 5°
Width of cut: 1/8" approx.
Feeds as shown by code: ● .0023 ipr
□ .0044 ipr
△ .0065 ipr
▽ .0087 ipr
x .0116 ipr

FLUID: None
Some low speed tests repeated using Carbon-tetrachloride (dotted lines)

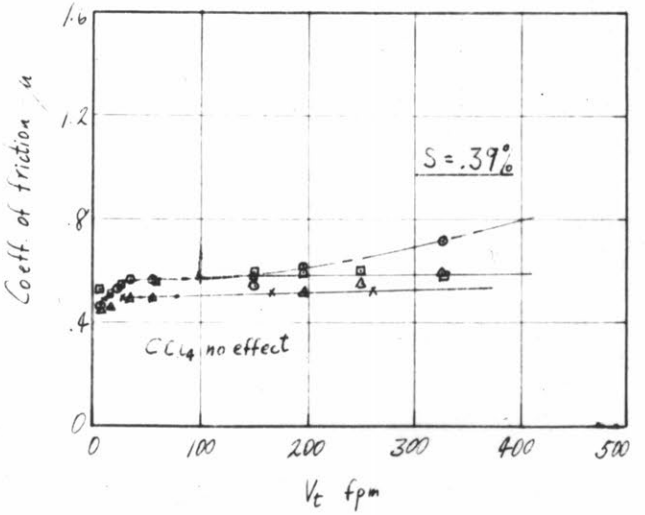


Fig.78

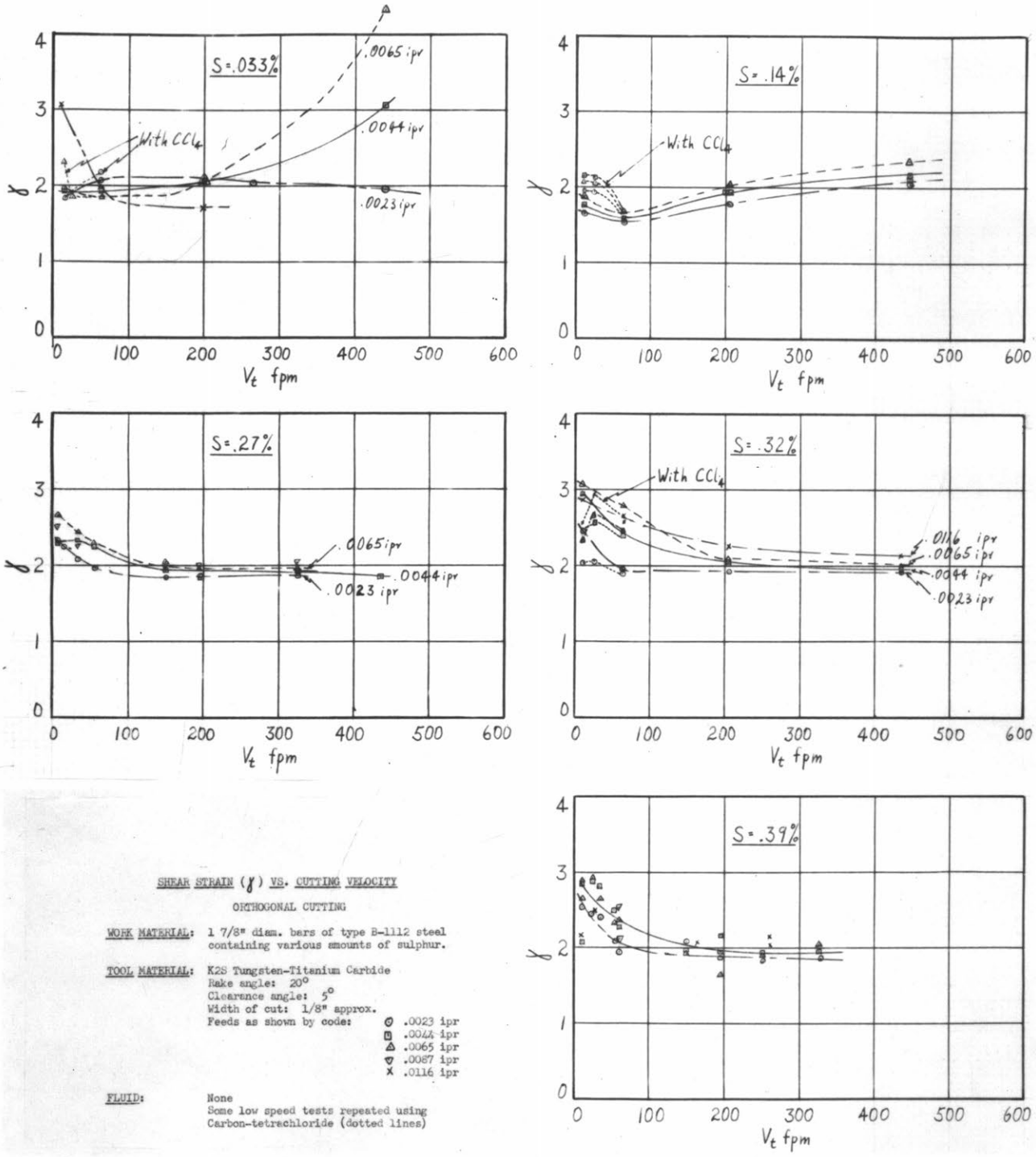


SHEAR STRAIN (γ) VS. CUTTING VELOCITY

ORTHOGONAL CUTTING

WORK MATERIAL: 1 7/8" diam. bars of type B-1112 steel containing various amounts of sulphur.

TOOL MATERIAL: K2S Tungsten-Titanium Carbide
Rake angle: 20°
Clearance angle: 5°
Width of cut: 1/8" approx.
Feeds as shown by code:
- .0023 ipr
- .0044 ipr
- .0065 ipr
- .0087 ipr
- .0116 ipr

FLUID: None
Some low speed tests repeated using Carbon-tetrachloride (dotted lines)

Fig.79

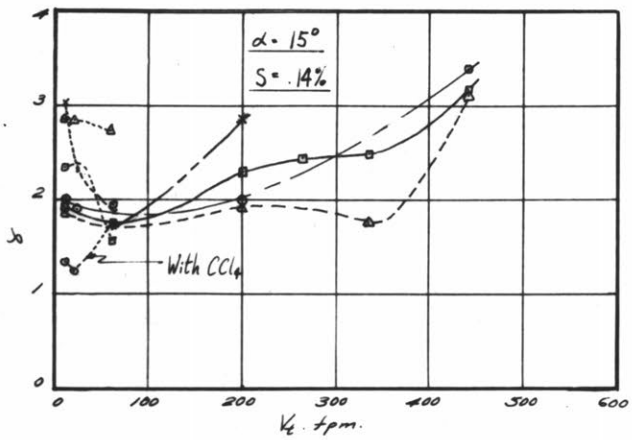


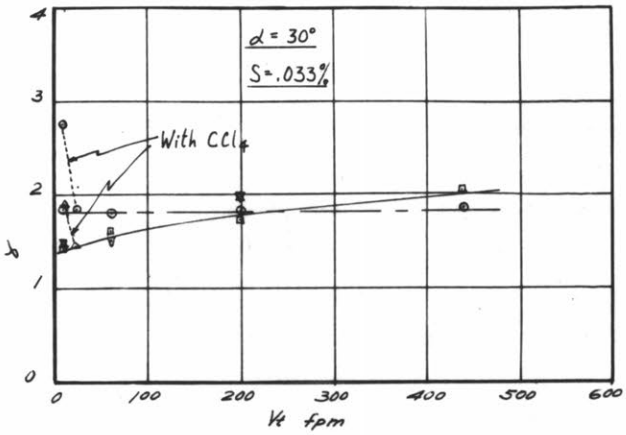


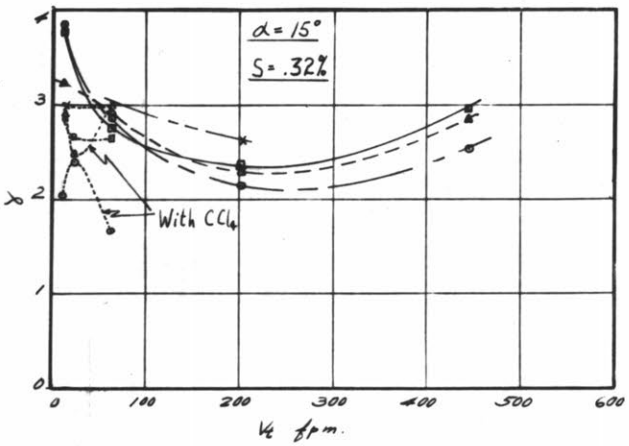


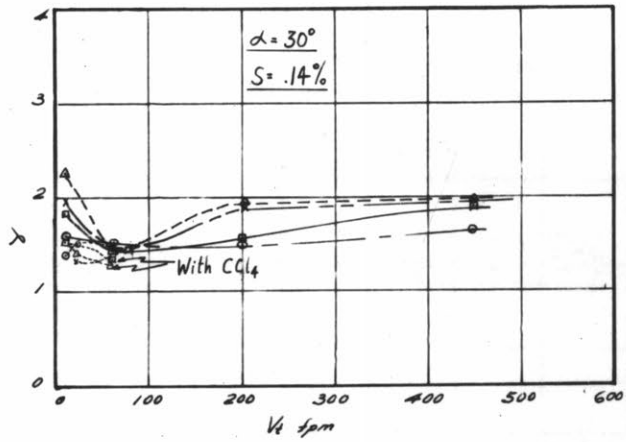


SHEAR STRAIN ($\gamma$) VS. CUTTING VELOCITY
ORTHOGONAL CUTTING

WORK MATERIAL: 1 7/8" diam. bars of type B-1112 steel containing various amounts of sulphur.

TOOL MATERIAL: 18-4-1 High Speed Steel
Rake angle: 15° and 30° as shown
Clearance angle: 5°
Width of cut: 1/8" approx.
Feeds as shown by code:
- ○ .0023 ipr
- □ .0044 ipr
- △ .0065 ipr
- ▽ .0087 ipr
- x .0116 ipr

FLUID: None
Some low speed tests repeated using Carbon-tetrachloride (dotted lines)

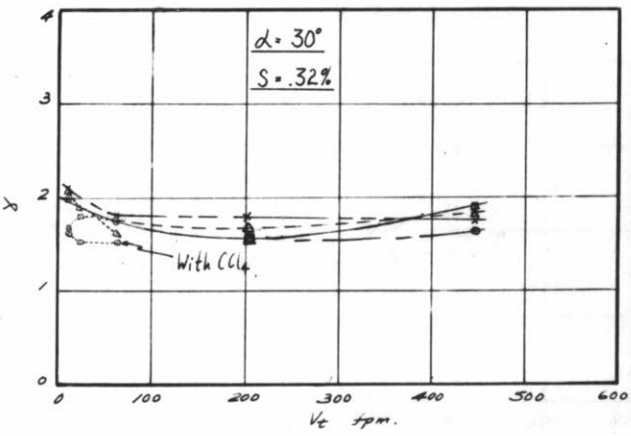


Fig.80

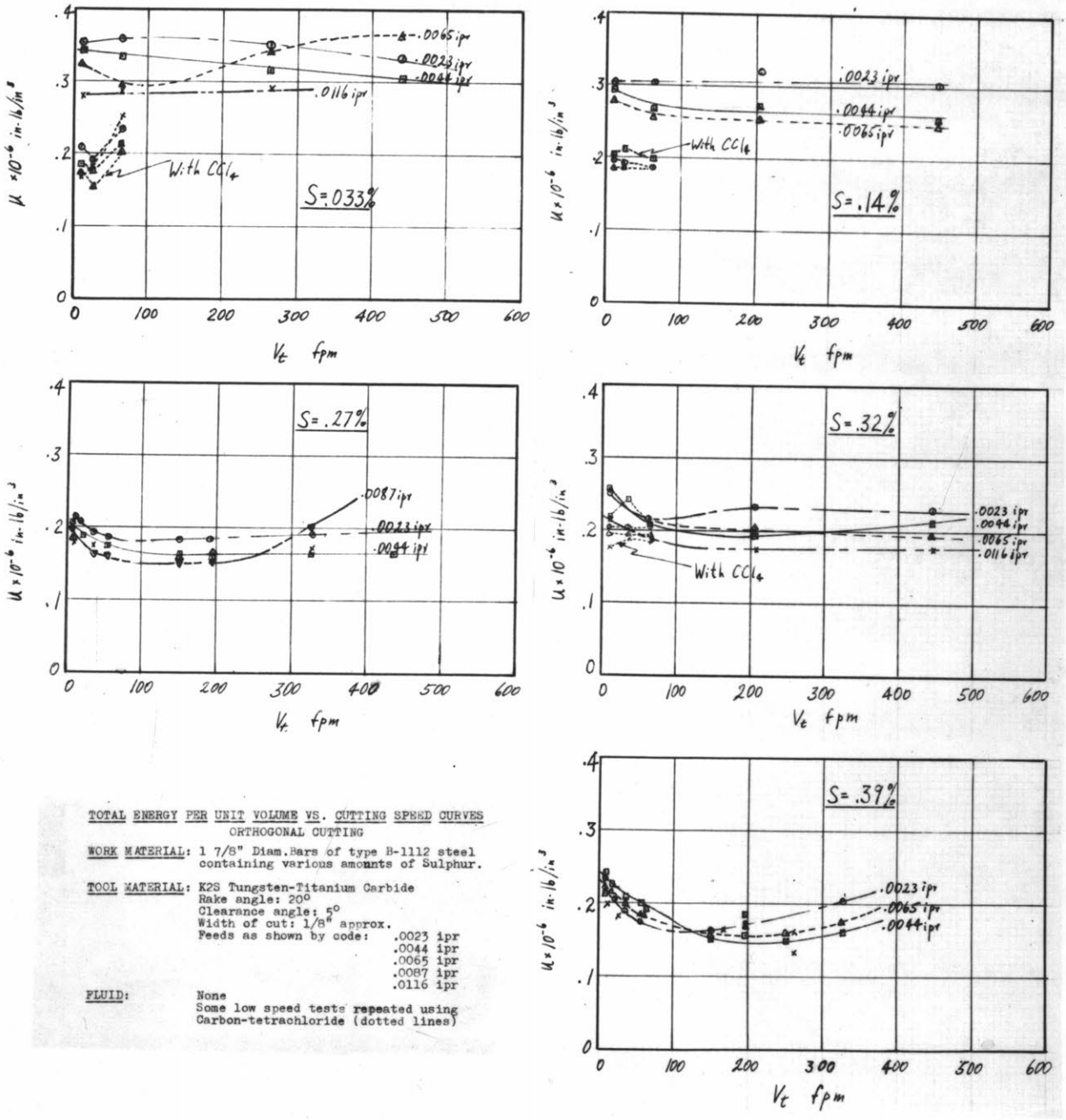


TOTAL ENERGY PER UNIT VOLUME VS. CUTTING SPEED CURVES
ORTHOGONAL CUTTING

WORK MATERIAL: 1 7/8" Diam. Bars of type B-1112 steel containing various amounts of Sulphur.

TOOL MATERIAL: K2S Tungsten-Titanium Carbide
Rake angle: 20°
Clearance angle: 5°
Width of cut: 1/8" approx.
Feeds as shown by code: .0023 ipr
.0044 ipr
.0065 ipr
.0087 ipr
.0116 ipr

FLUID: None
Some low speed tests repeated using Carbon-tetrachloride (dotted lines)

Fig.81

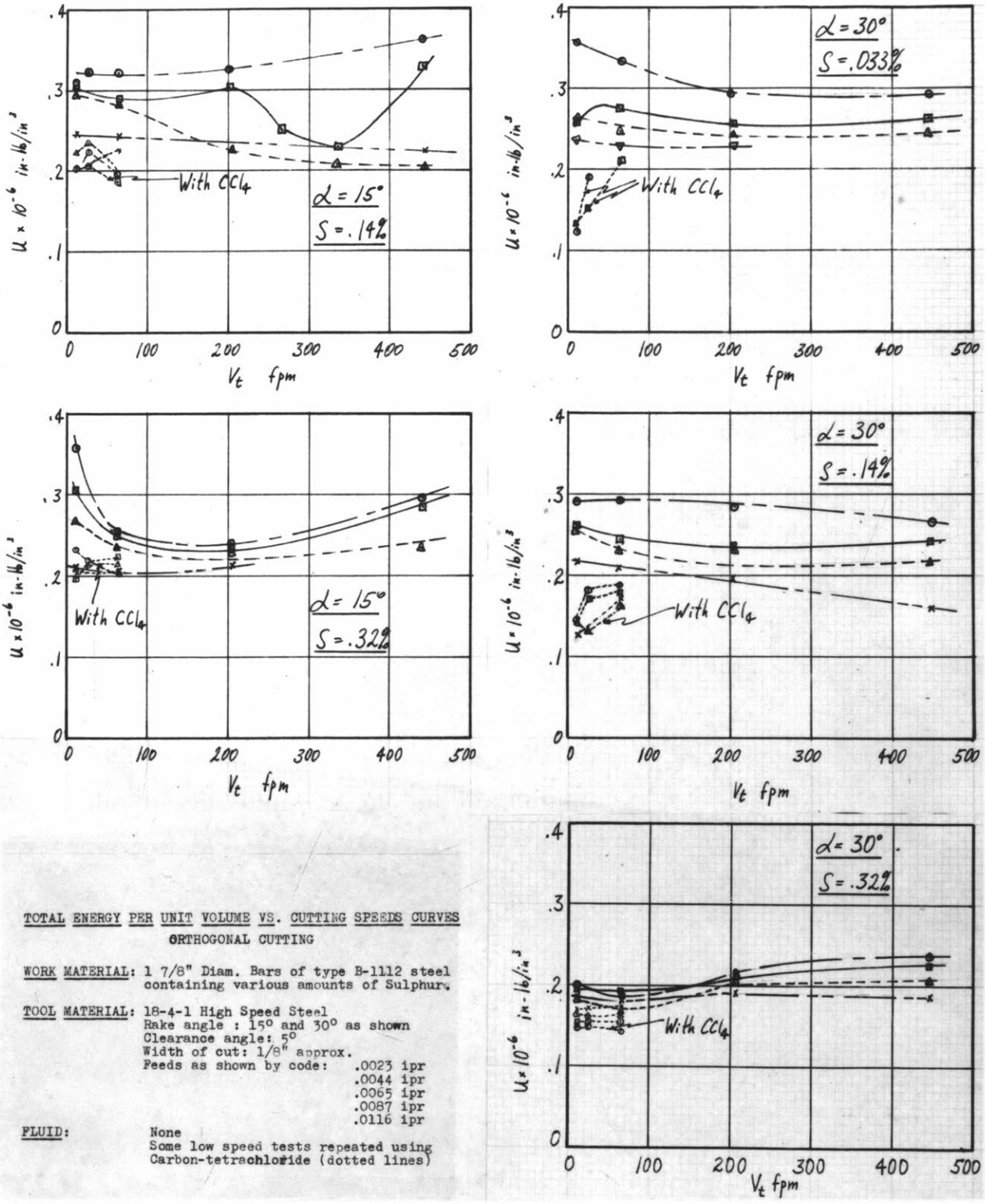


TOTAL ENERGY PER UNIT VOLUME VS. CUTTING SPEEDS CURVES

ORTHOGONAL CUTTING

WORK MATERIAL: 1 7/8" Diam. Bars of type B-1112 steel containing various amounts of Sulphur.

TOOL MATERIAL: 18-4-1 High Speed Steel
Rake angle : 15° and 30° as shown
Clearance angle: 5°
Width of cut: 1/8" approx.
Feeds as shown by code: .0023 ipr
.0044 ipr
.0065 ipr
.0087 ipr
.0116 ipr

FLUID: None
Some low speed tests repeated using Carbon-tetrachloride (dotted lines)

Fig.82

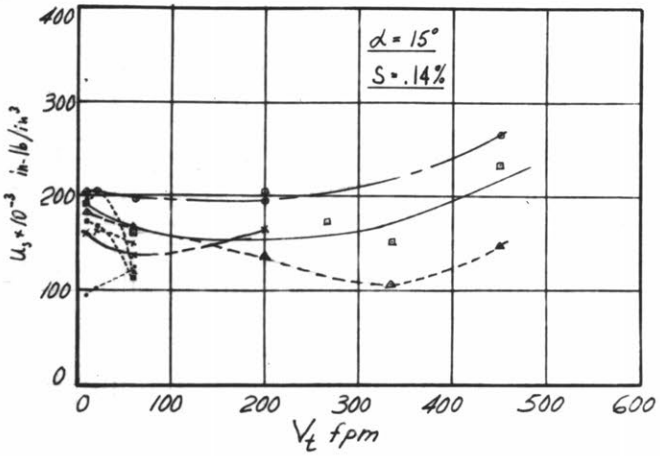


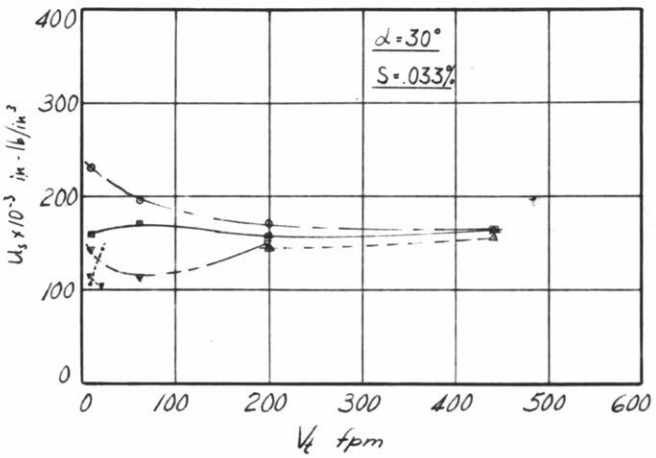


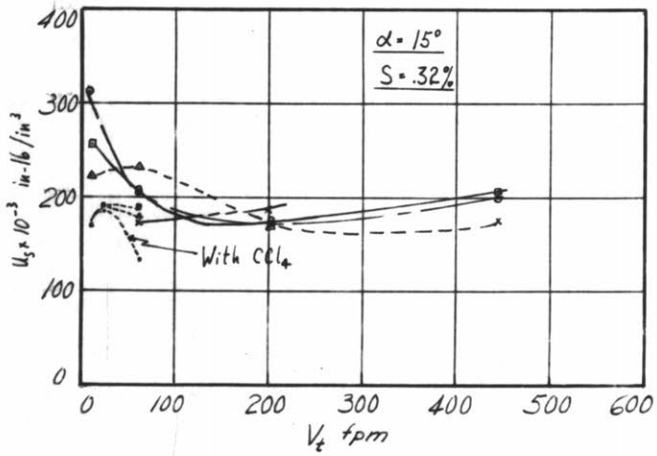


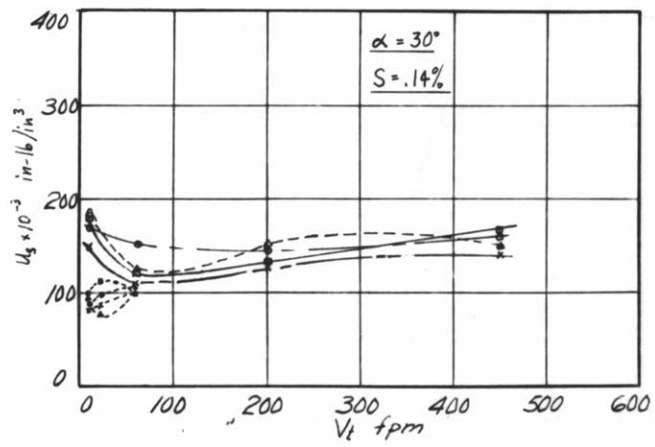


SHEAR ENERGY PER UNIT VOLUME Vs. CUTTING VELOCITY

ORTHOGONAL CUTTING

WORK MATERIAL: 1 7/8" diam. bars of type B-1112 steel containing various amounts of sulphur.

TOOL MATERIAL: 18-4-1 High Speed Steel
Rake angle: 15° and 30° as shown
Clearance angle: 5°
Width of cut: 1/8" approx
Feeds as shown by code:
- ⊙ .0023 ipr
- □ .0044 ipr
- △ .0065 ipr
- ▽ .0087 ipr
- X .0116 ipr

FLUID: None
Some low speed tests repeated using Carbon-tetrachloride (dotted lines)

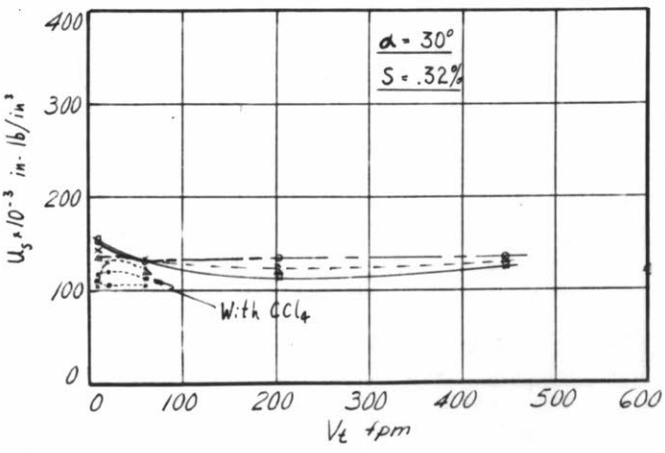


Fig.83

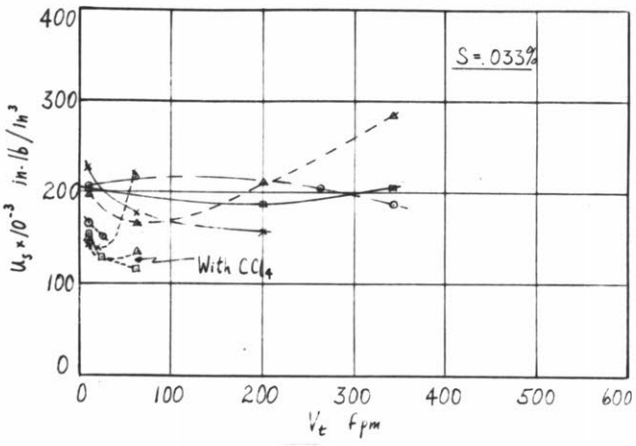


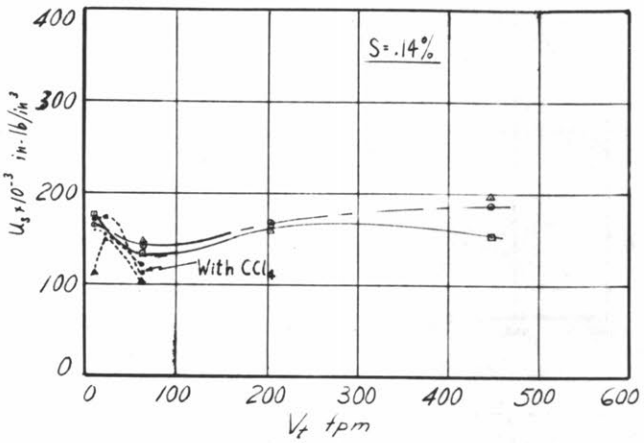


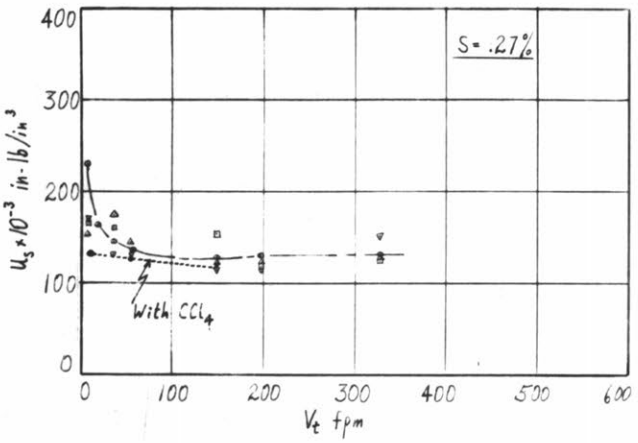


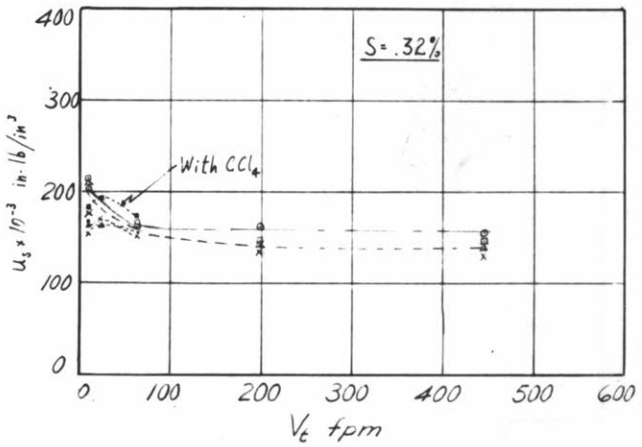


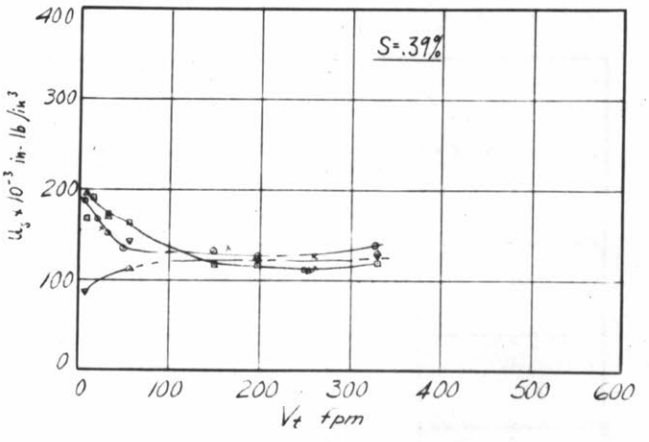


SHEAR ENERGY PER UNIT VOLUME VS. CUTTING VELOCITY

ORTHOGONAL CUTTING

**WORK MATERIAL:** 1 7/8" diam. bars of type B-1112 steel containing various amounts of sulphur.

**TOOL MATERIAL:** K2S Tungsten-Titanium Carbide
Rake angle: 20°
Clearance angle: 5°
Width of cut: 1/8" approx.
Feeds as shown by code:

- ⊙ .0023 ipr
- ⊡ .0042 ipr
- △ .0065 ipr
- ▽ .0087 ipr
- X .0116 ipr

**FLUID:** None
Some low speed tests repeated using Carbon-tetrachloride (dotted lines)

Fig.84

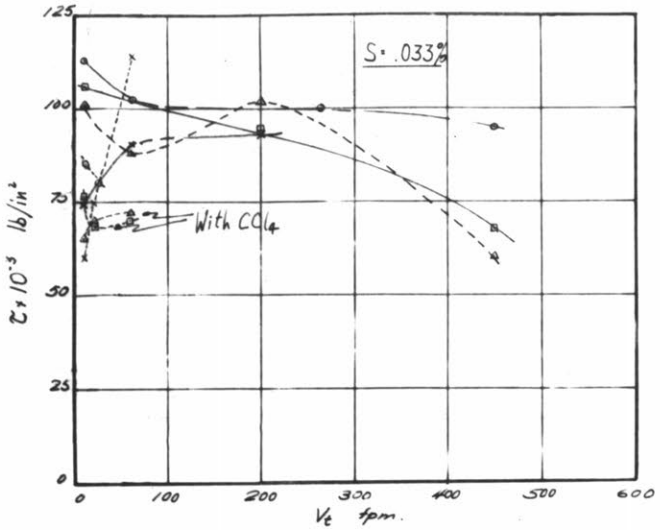


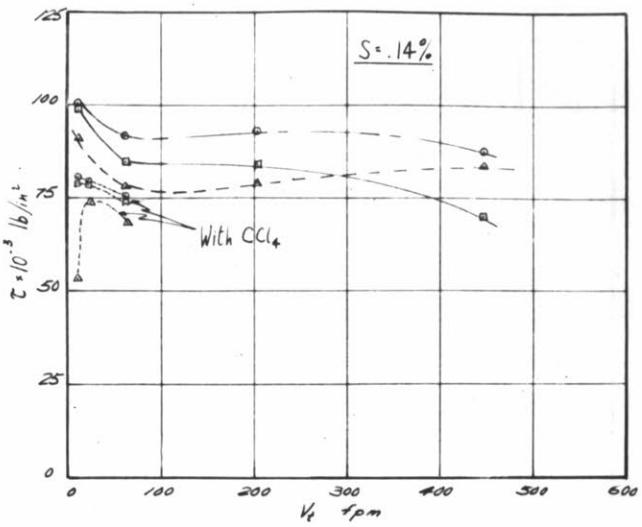


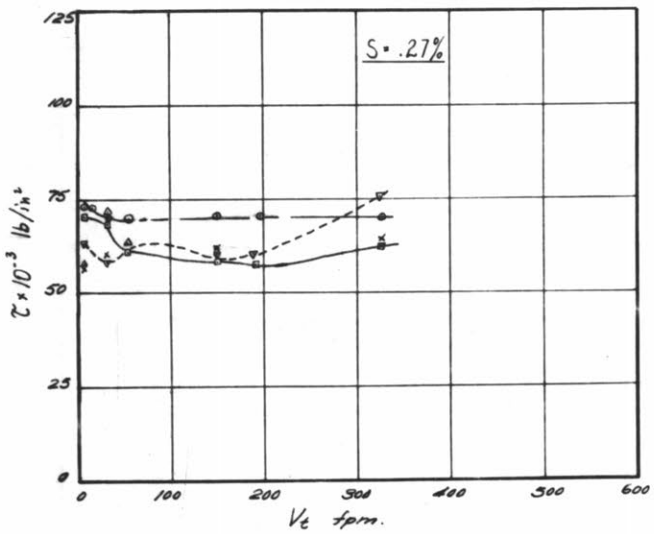


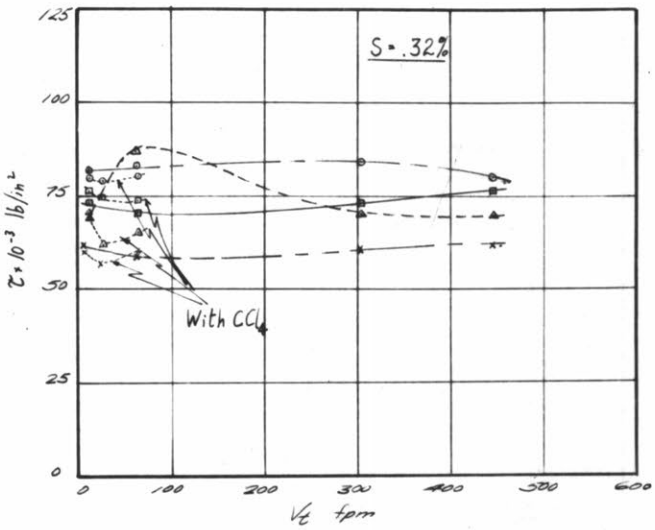


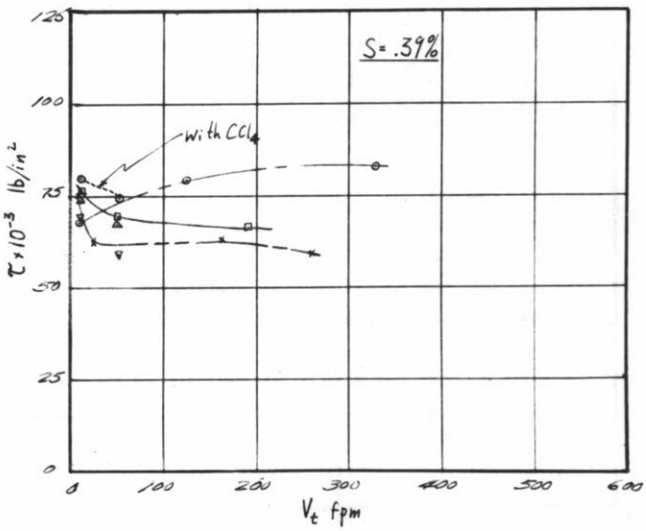


SHEAR STRESS ($\tau$) VS. CUTTING VELOCITY

ORTHOGONAL CUTTING

WORK MATERIAL: 1 7/8" diam. bars of type B-1112 steel containing various amounts of sulphur.

TOOL MATERIAL: K2S Tungsten-Titanium Carbide
Rake angle: 20°
Clearance angle: 5°
Width of cut: 1/8" approx.
Feeds as shown by code:
- ⊙ .0023 ipr
- ▣ .0044 ipr
- △ .0065 ipr
- ▽ .0087 ipr
- x .0116 ipr

FLUID: None
Some low speed tests repeated using Carbon-tetrachloride (dotted lines)

Fig.85

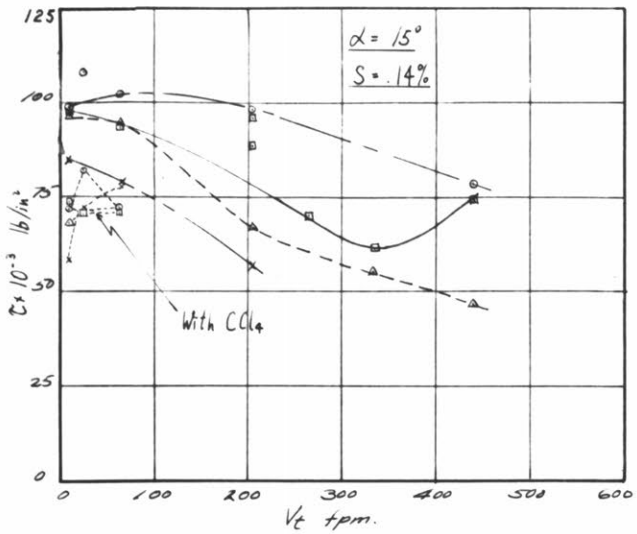


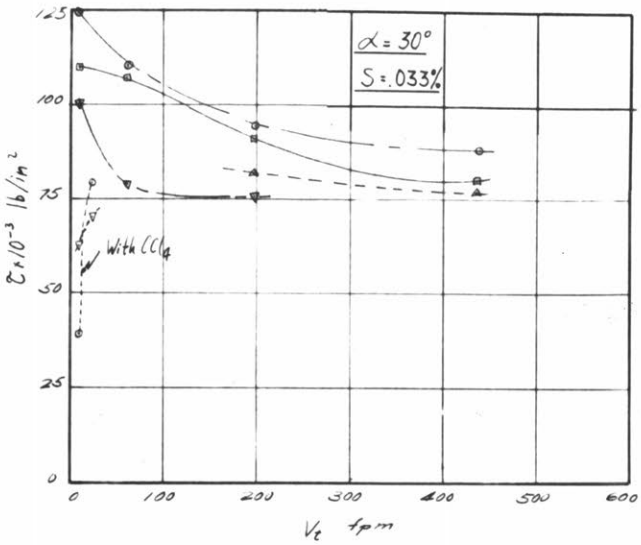


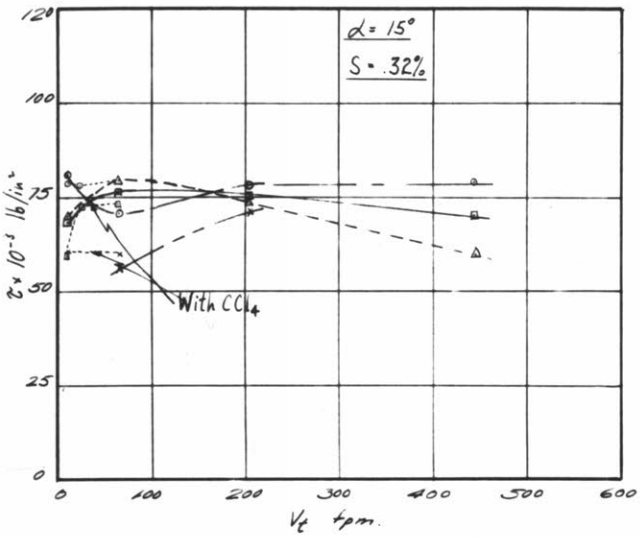


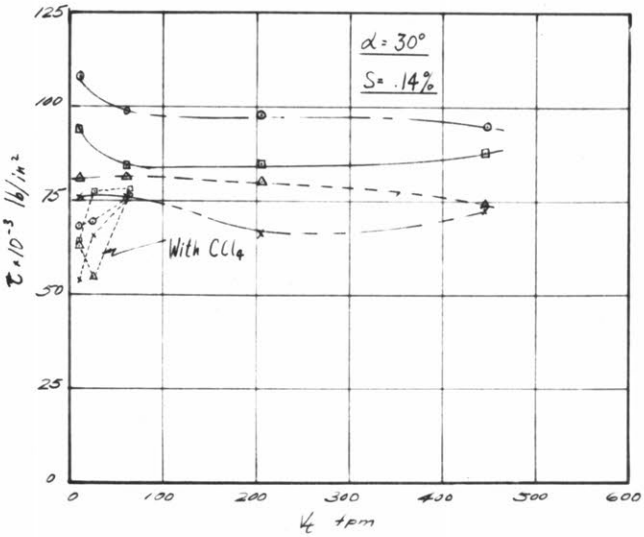


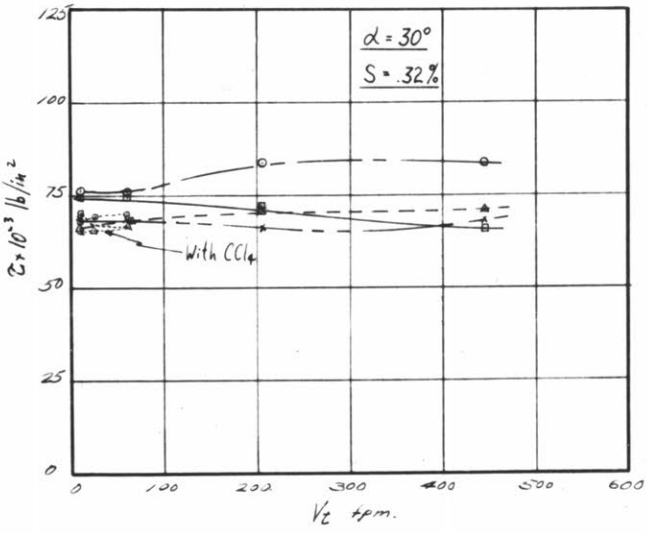


SHEAR STRESS (τ) VS. CUTTING VELOCITY

ORTHOGONAL CUTTING

WORK MATERIAL: 1 7/8" diam. bars of type B-1112 steel containing various amounts of sulphur.

TOOL MATERIAL: 18-4-1 High Speed Steel
Rake angle: 15° and 30° as shown.
Clearance angle: 5°
Width of cut: 1/8" approx.
Feeds as shown by code:
- ○ .0023 ipr
- □ .0044 ipr
- △ .0065 ipr
- ▽ .0087 ipr
- × .0116 ipr

FLUID: None
Some low speed tests repeated using Carbon-tetrachloride (dotted lines)

Fig.86

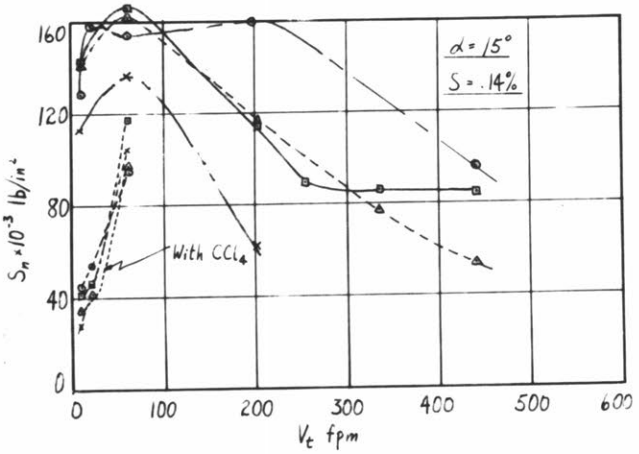


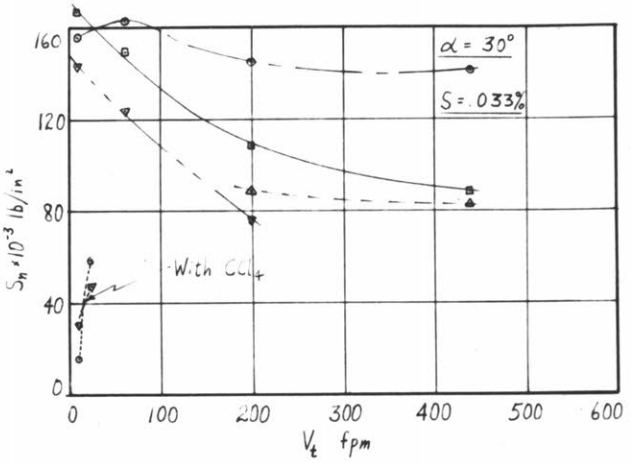


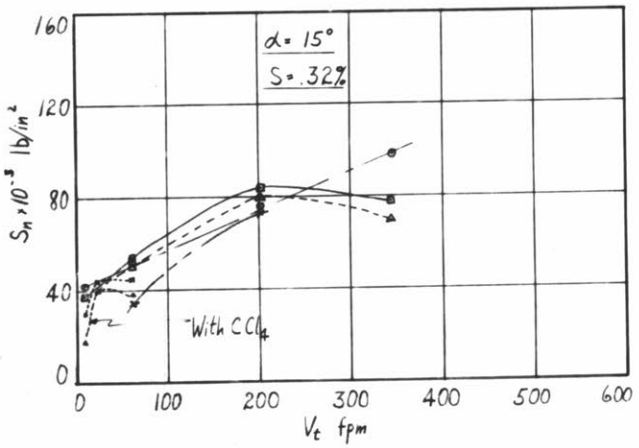


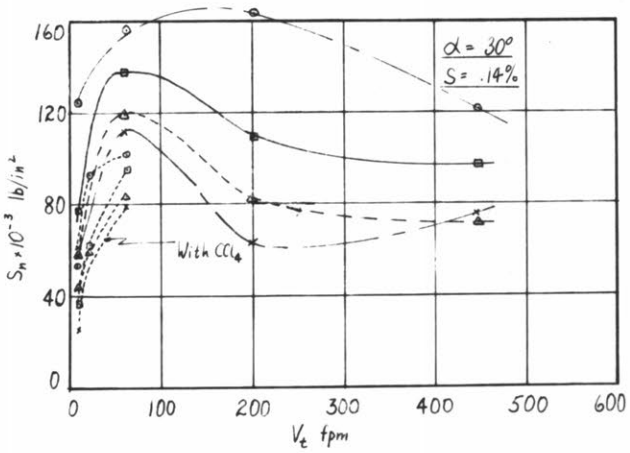


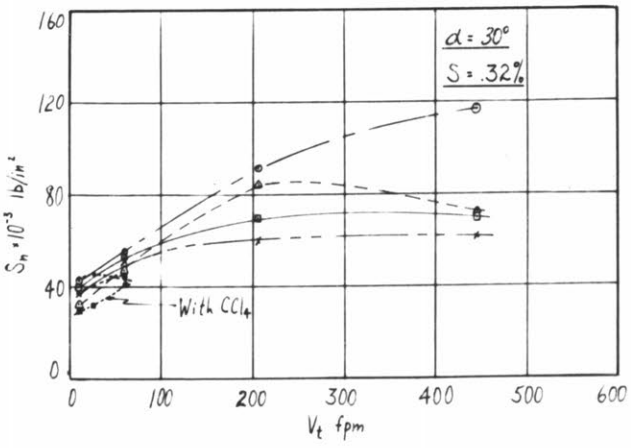


NORMAL STRESS ($S_n$) VS. CUTTING VELOCITY

ORTHOGONAL CUTTING

WORK MATERIAL: 1 7/8" diam. bars of type B-1112 steel containing various amounts of sulphur.

TOOL MATERIAL: 18-4-1 High Speed Steel
Rake angle: 15° and 30° as shown
Clearance angle: 5°
Width of cut: 1/8" approx.
Feeds as shown by code:
- ⊙ .0023 ipr
- □ .0044 ipr
- △ .0065 ipr
- ▽ .0087 ipr
- X .0116 ipr

FLUID: None
Some low speed tests repeated using Carbon-tetrachloride (dotted lines)

Fig.87

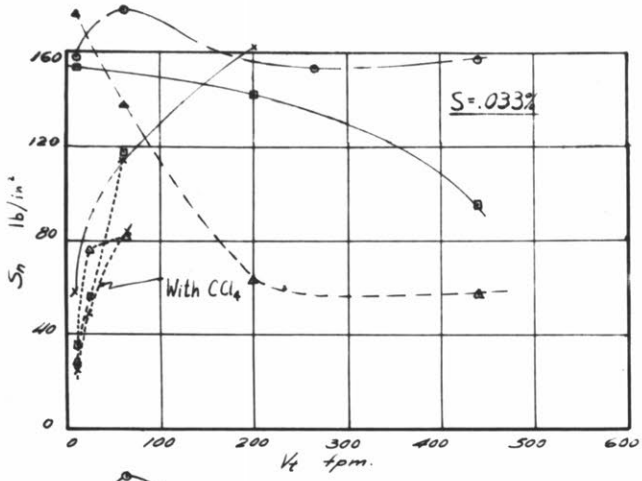


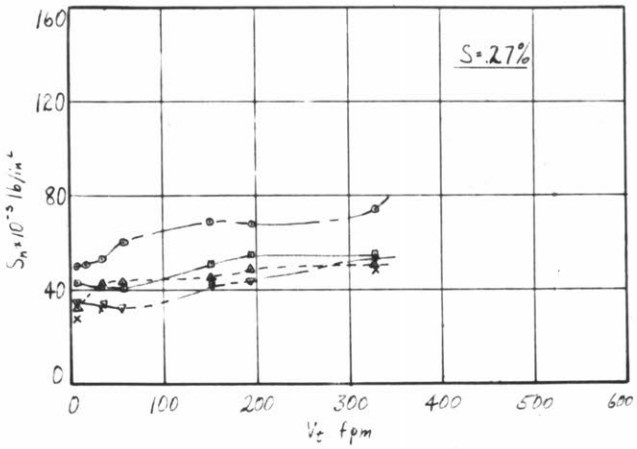


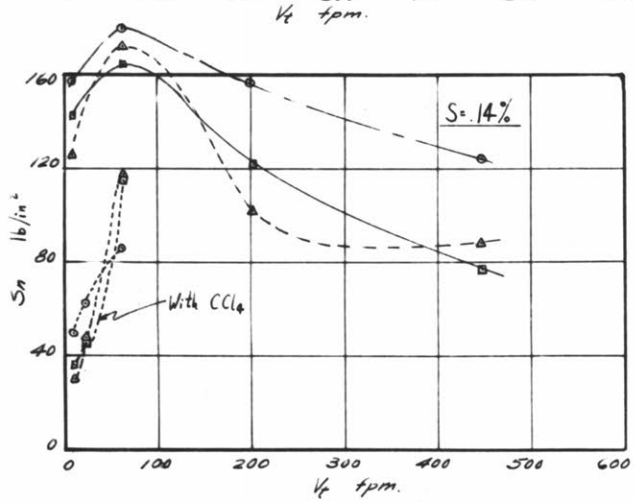


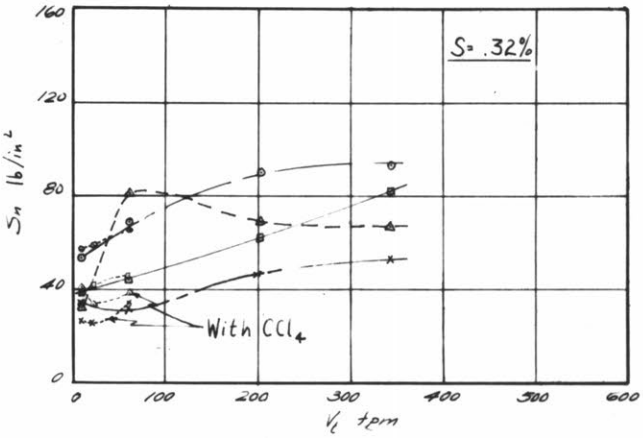


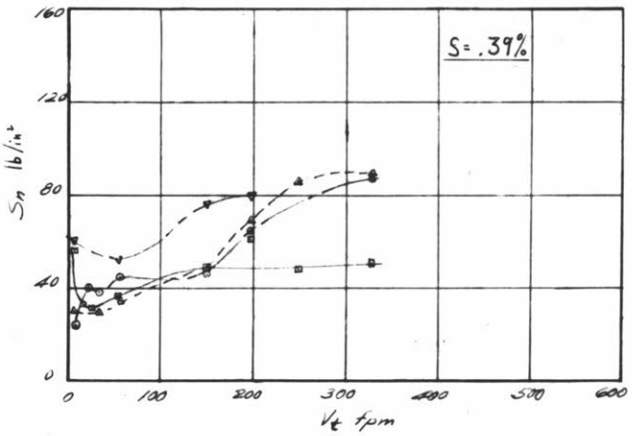


NORMAL STRESS ($S_n$) VS. CUTTING VELOCITY

ORTHOGONAL CUTTING

WORK MATERIAL: 1 7/8" diam. bars of type B-1112 steel containing various amounts of sulphur.

TOOL MATERIAL: K2S Tungsten-Titanium Carbide
Rake angle: 20°
Clearance angle: 5°
Width of cut: 1/8" approx.
Feeds as shown by code:
- ● .0023 ipr
- ■ .0044 ipr
- △ .0065 ipr
- ▼ .0087 ipr
- X .0116 ipr

FLUID: None
Some low speed tests repeated using Carbon-tetrachloride (dotted lines)

Fig.88

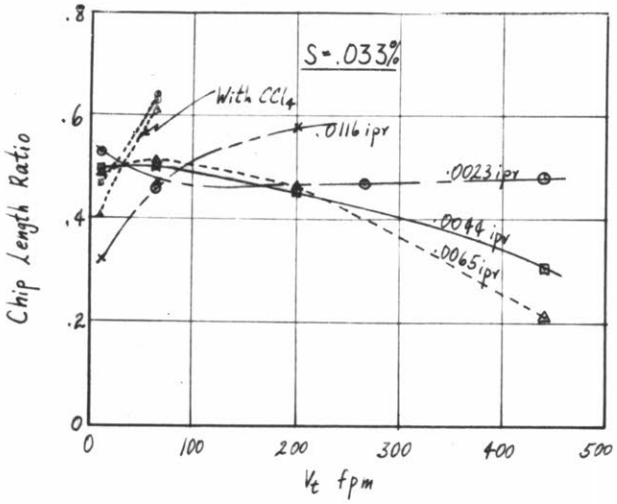


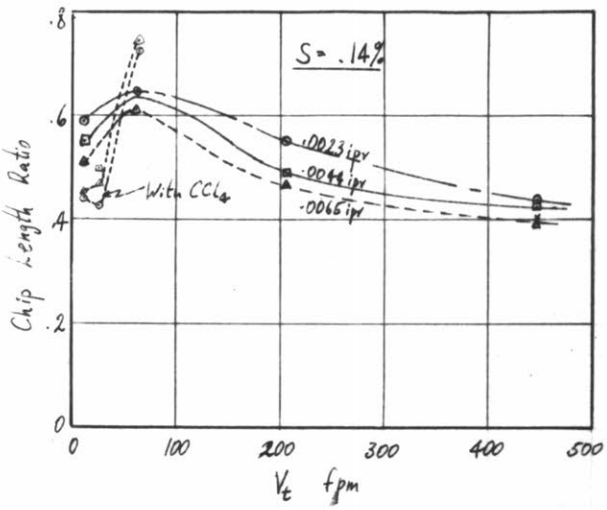


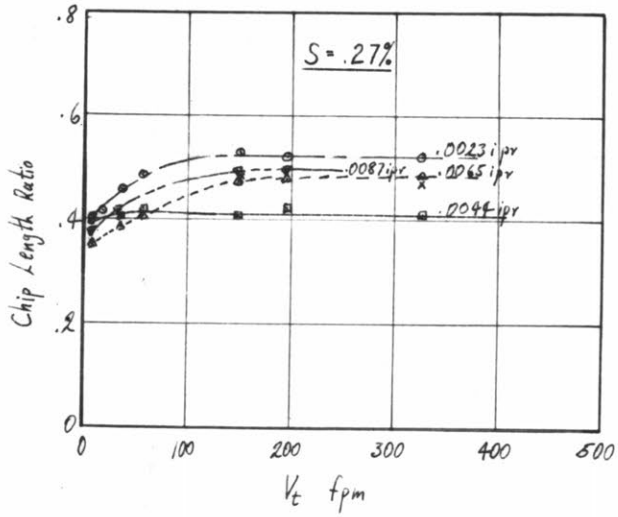


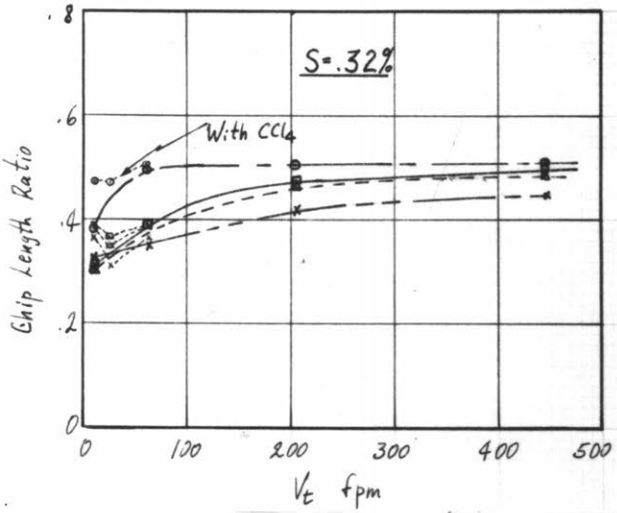


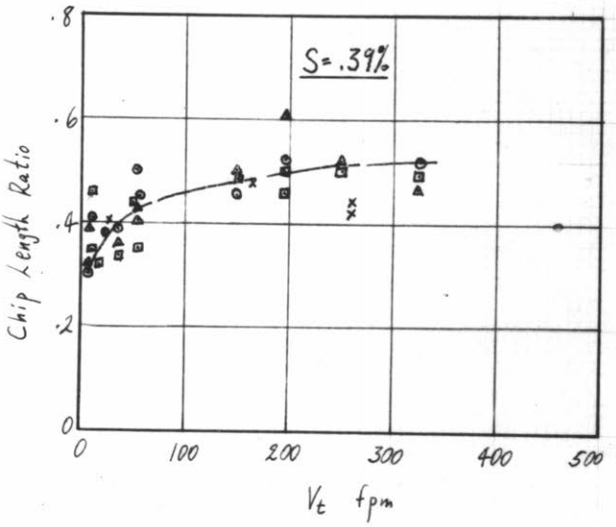


CHIP LENGTH RATIO (rc) vs. CUTTING SPEED
ORTHOGONAL CUTTING

WORK MATERIAL: 1 7/8" diam. bars of type B-1112 steel containing various amounts of sulphur.

TOOL MATERIAL: K2S Tungsten-Titanium Carbide
Rake angle: 20°
Clearance angle: 5°
Width of cut: 1/8" approx.
Feeds as shown, with code:
- .0023 ipr
- .0044 ipr
- .0065 ipr
- .0087 ipr
- .0116 ipr

FLUID: None
Some low speed tests repeated using Carbon-tetrachloride (dotted lines)

Fig.88a

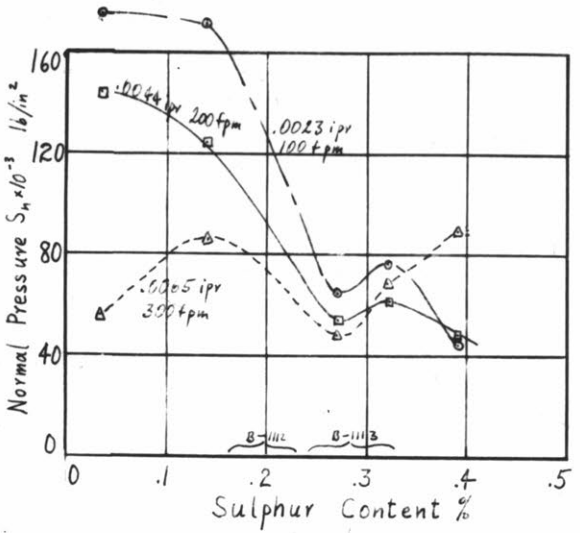


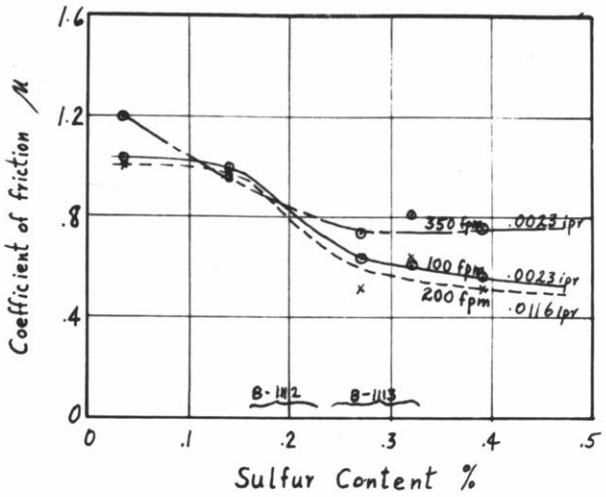


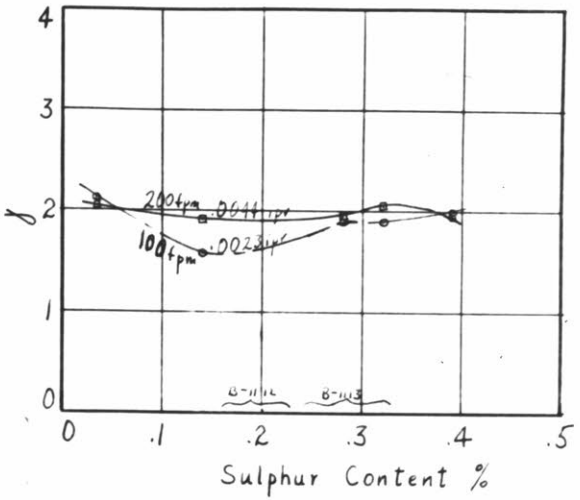


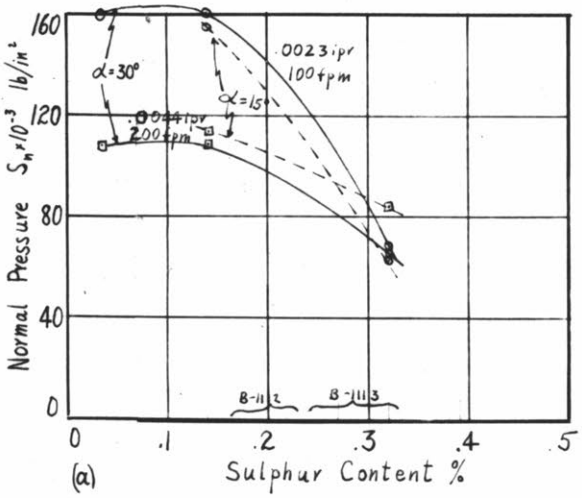


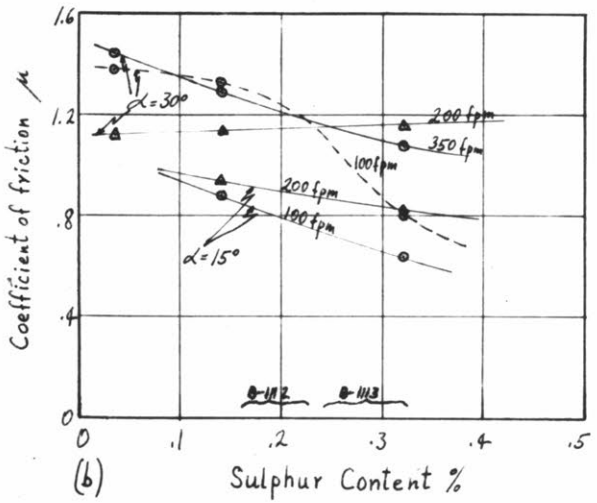


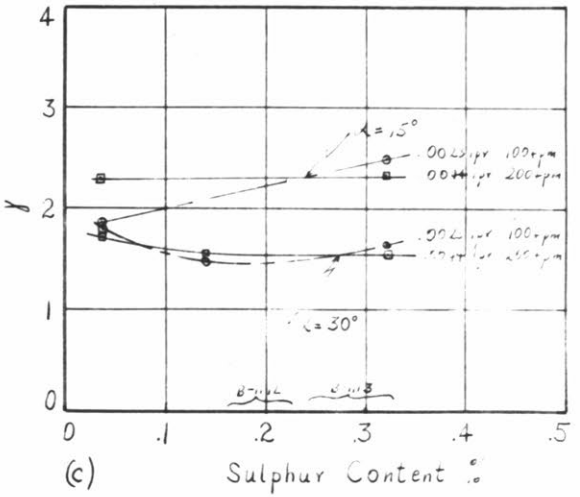


Fig. 89

(a) VARIATION OF NORMAL PRESSURE ($S_n$)
(b) COEFFICIENT OF FRICTION ($\mu$)
(c) SHEAR STRAIN ($\gamma$)
WITH SULPHUR CONTENT

WORK MATERIAL: 1 7/8" diam. bars of type B-1112 steel containing various amounts of sulphur.

TOOL MATERIAL: Top Row: K2S Tungsten-Titanium Carbide
Rake Angle: 20°

Bottom Row: 18-4-1 High Speed Steel
Rake Angle: 15° and 30° as shown.
Clearance Angle: 5°
Width of cut: 1/8" approx.
Feeds as shown by code:
- ⊙ .0023
- ⊡ .0044
- △ .0065
- ▽ .0087
- X .0116

FLUID: None

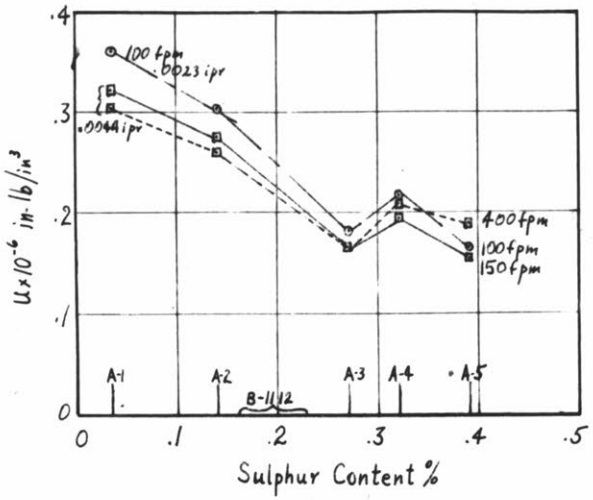


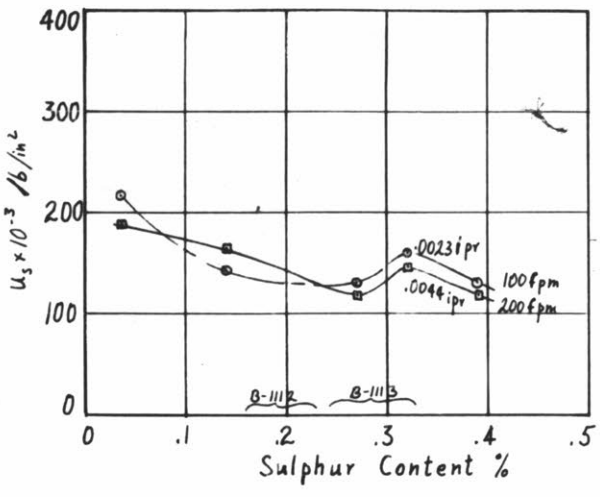


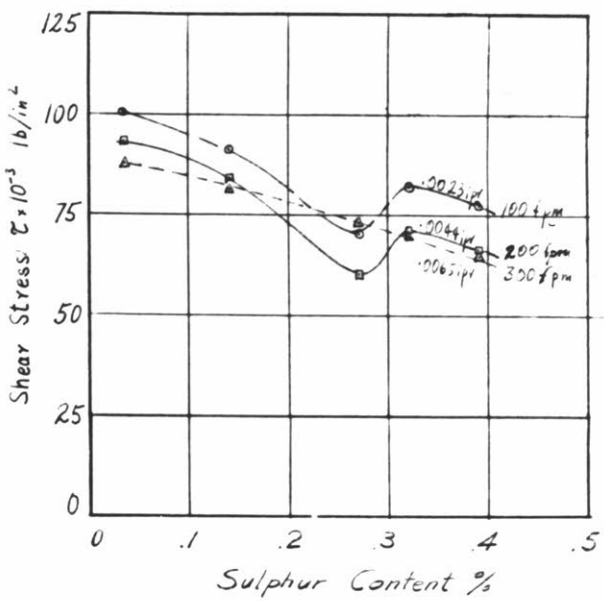


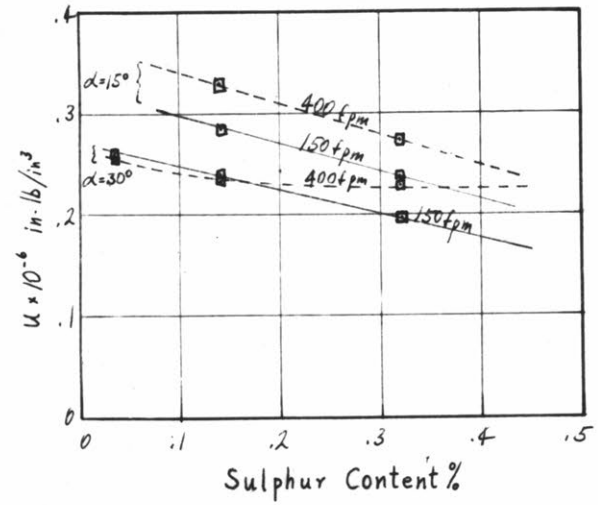


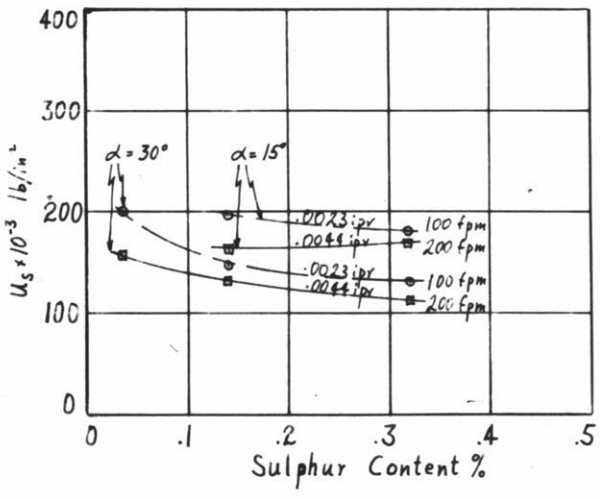


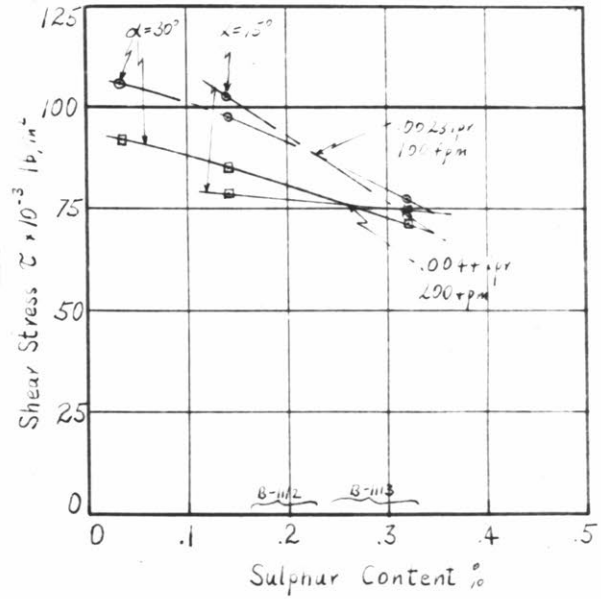


Fig. 90

TOTAL CUTTING ENERGY PER UNIT VOLUME ($u$) VS. SULPHUR CONTENT
SHEAR ENERGY PER UNIT VOLUME ($u_s$) VS. SULPHUR CONTENT
SHEAR STRESS ($\tau$) VS. SULPHUR CONTENT
ORTHOGONAL CUTTING

WORK MATERIAL: 1 7/8" diam. bars of type B-1112 steel containing various amounts of sulphur.

TOOL MATERIAL: Top Row: K2S Tungsten-Titanium Carbide
Rake angle: 20°
Bottom Row: 18-4-1 High Speed Steel
Rake angle: 15° and 30° as shown.
Clearance angle: 5°
Width of cut: 1/8" approx.
Feeds as shown by code:
- ⊙ .0023 ipr
- ⊡ .0044 ipr
- △ .0065 ipr
- ▽ .0087 ipr
- x .0116 ipr

FLUID: None

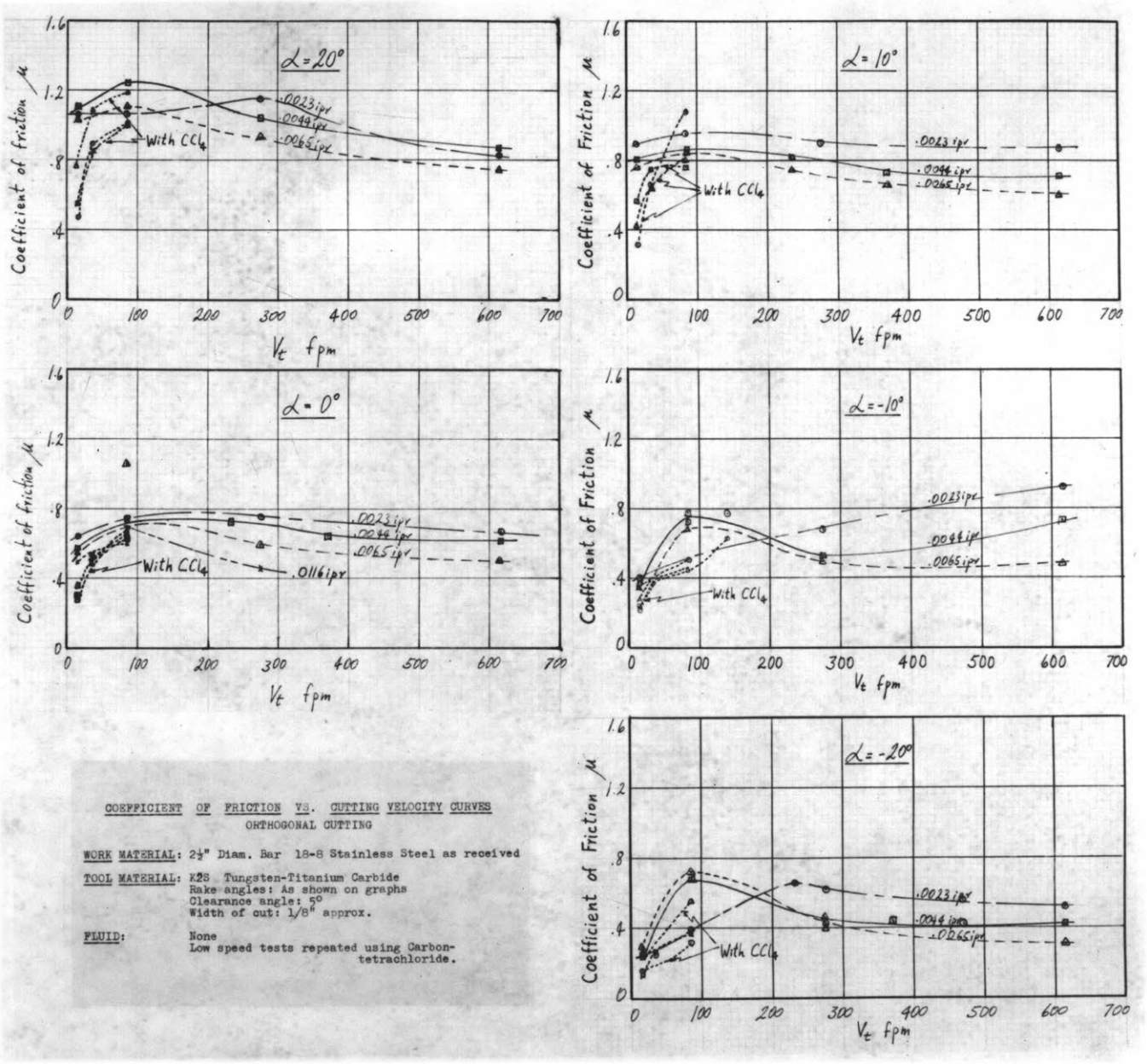


COEFFICIENT OF FRICTION VS. CUTTING VELOCITY CURVES
ORTHOGONAL CUTTING

WORK MATERIAL: 2½" Diam. Bar 18-8 Stainless Steel as received

TOOL MATERIAL: K2S Tungsten-Titanium Carbide
Rake angles: As shown on graphs
Clearance angle: 5°
Width of cut: 1/8" approx.

FLUID: None
Low speed tests repeated using Carbon-tetrachloride.

Fig. 91

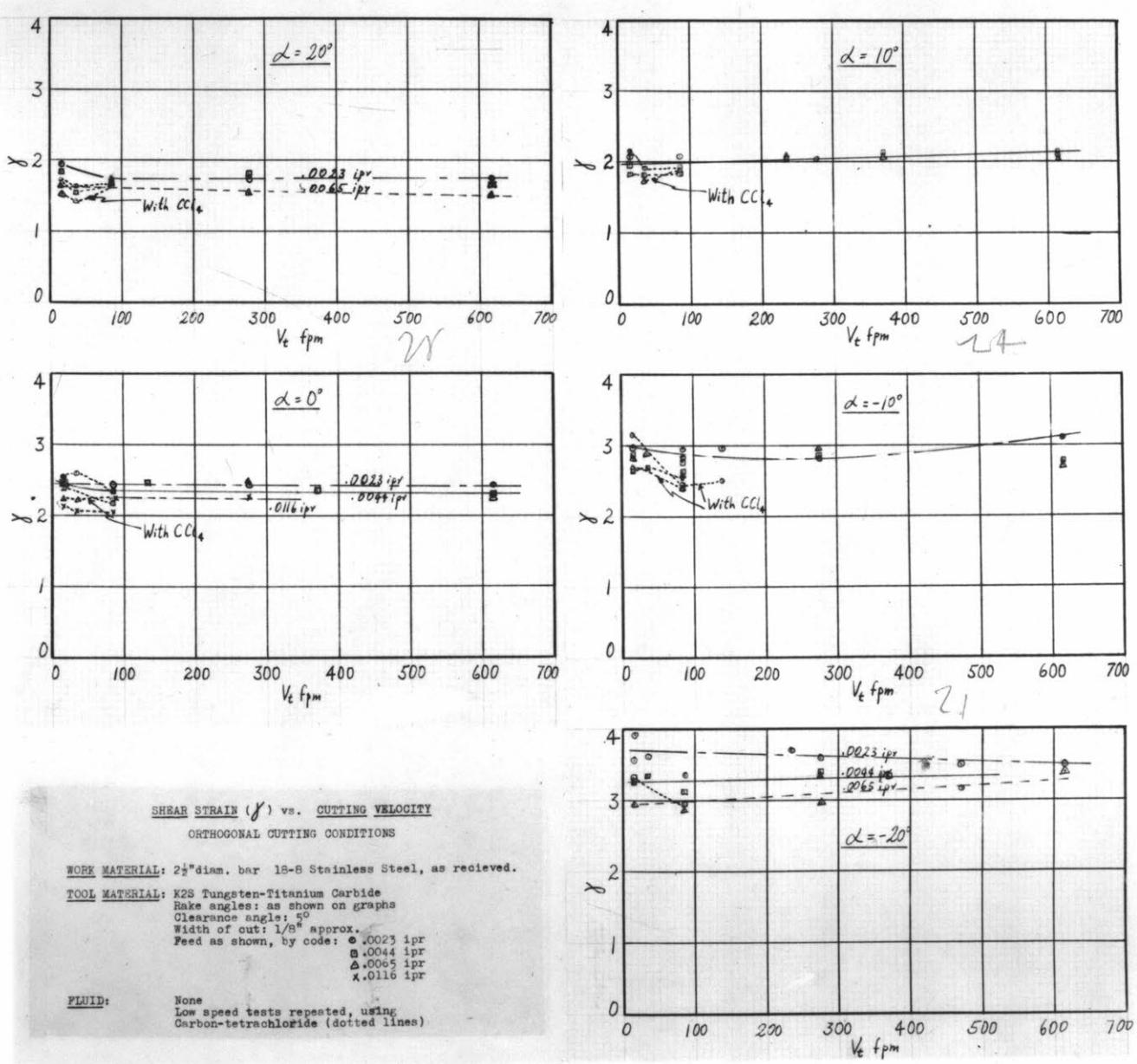


SHEAR STRAIN ($\gamma$) vs. CUTTING VELOCITY

ORTHOGONAL CUTTING CONDITIONS

WORK MATERIAL: 2½"diam. bar 18-8 Stainless Steel, as recieved.

TOOL MATERIAL: K2S Tungsten-Titanium Carbide
Rake angles: as shown on graphs
Clearance angle: 5°
Width of cut: 1/8" approx.
Feed as shown, by code: ● .0023 ipr
■ .0044 ipr
▲ .0065 ipr
x .0116 ipr

FLUID: None
Low speed tests repeated, using Carbon-tetrachloride (dotted lines)

Fig.92

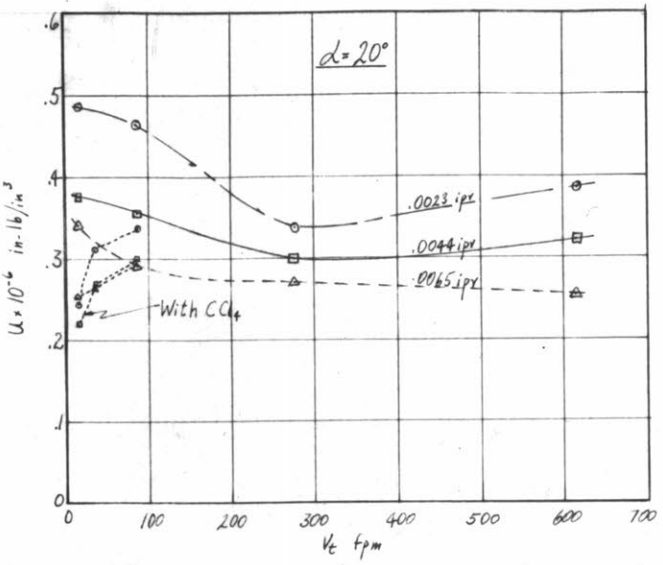


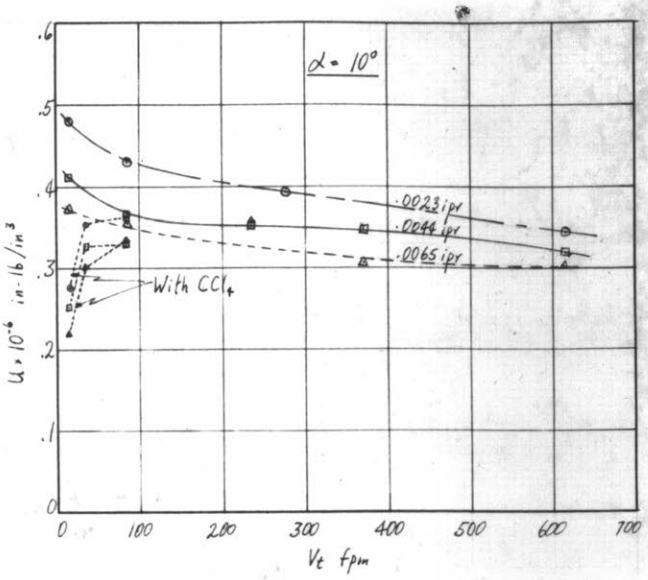


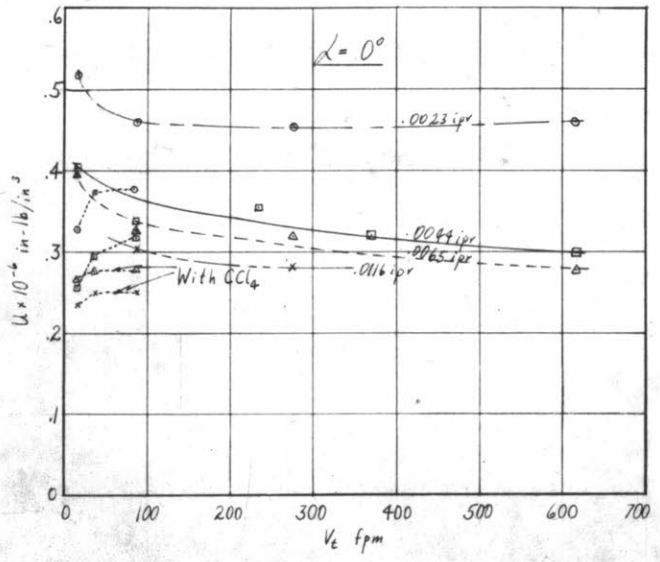


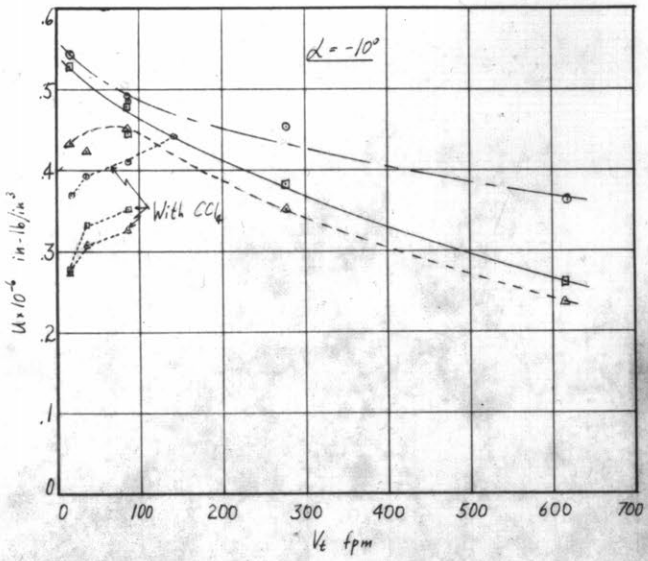


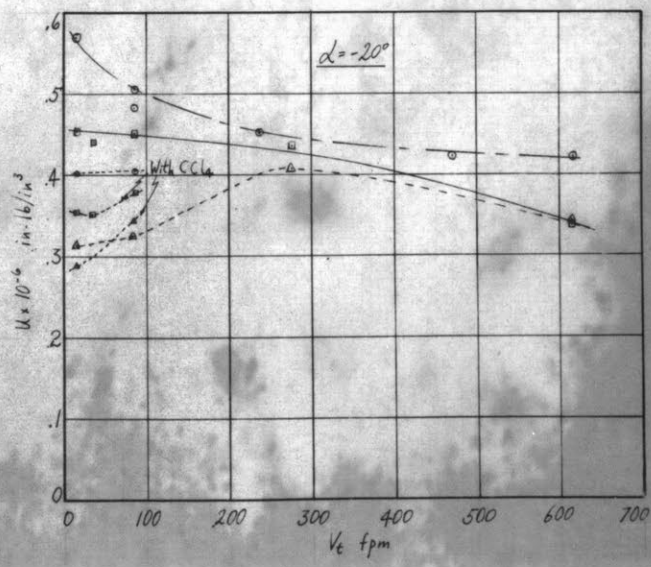


TOTAL ENERGY PER UNIT VOLUME VS. CUTTING VELOCITY CURVES
ORTHOGONAL CUTTING

WORK MATERIAL: 2½" Diam. bar 18-8 Stainless Steel, as received.

TOOL MATERIAL: K23 Tungsten-Titanium Carbide
Rake angles: as shwon on graphs
Clearance angle: 8°
Width of cut: 1/8" approx.

Fluid: None
Low speed tests repeated using Carbon-tetrachloride.

Fig.93

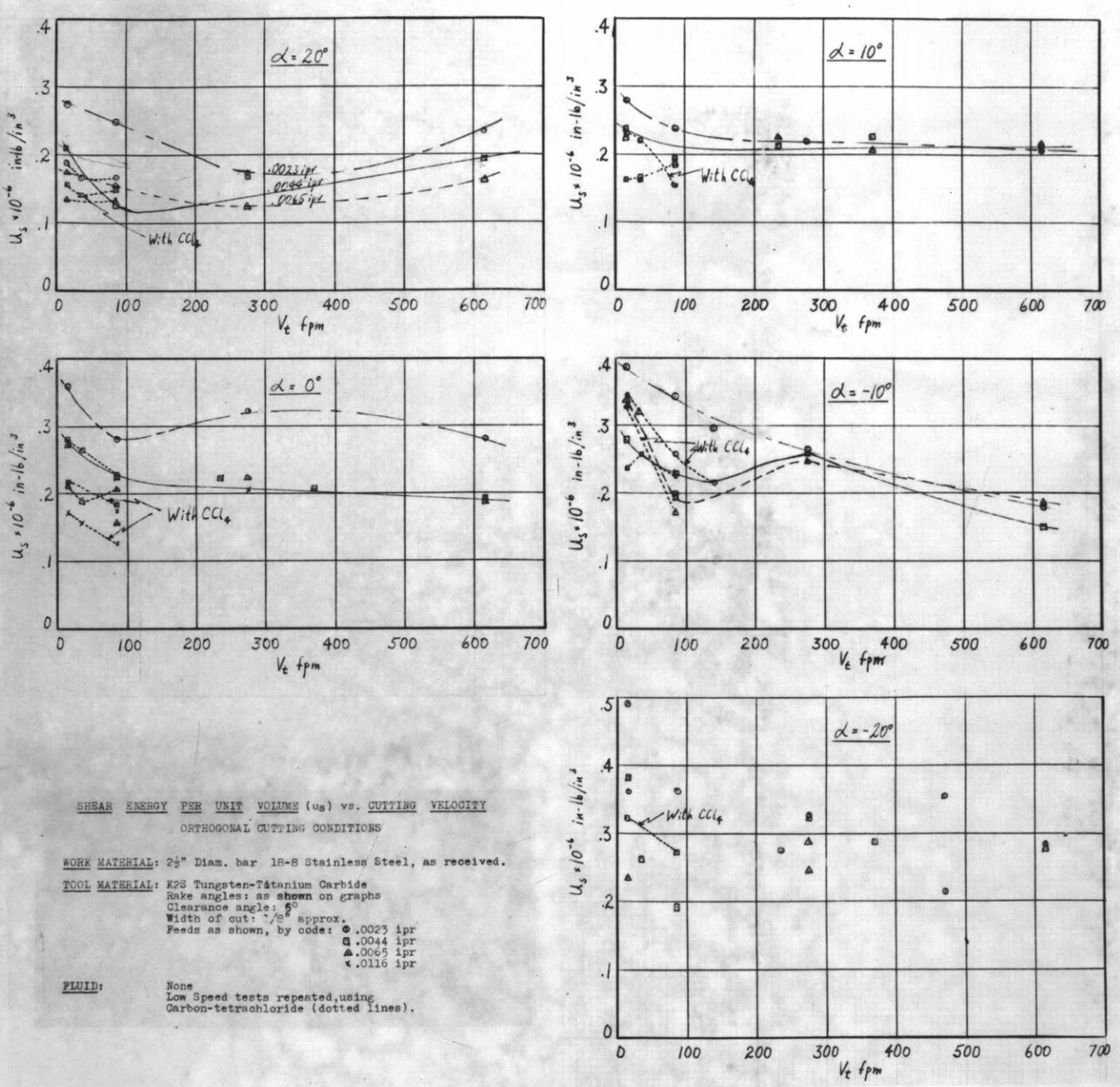


SHEAR ENERGY PER UNIT VOLUME ($u_s$) vs. CUTTING VELOCITY

ORTHOGONAL CUTTING CONDITIONS

WORK MATERIAL: 2½" Diam. bar 18-8 Stainless Steel, as received.

TOOL MATERIAL: K2S Tungsten-Tátanium Carbide
Rake angles: as shown on graphs
Clearance angle: 6°
Width of cut: 1/8" approx.
Feeds as shown, by code: ● .0023 ipr
■ .0044 ipr
▲ .0065 ipr
× .0116 ipr

FLUID: None
Low Speed tests repeated, using Carbon-tetrachloride (dotted lines).

Fig.94

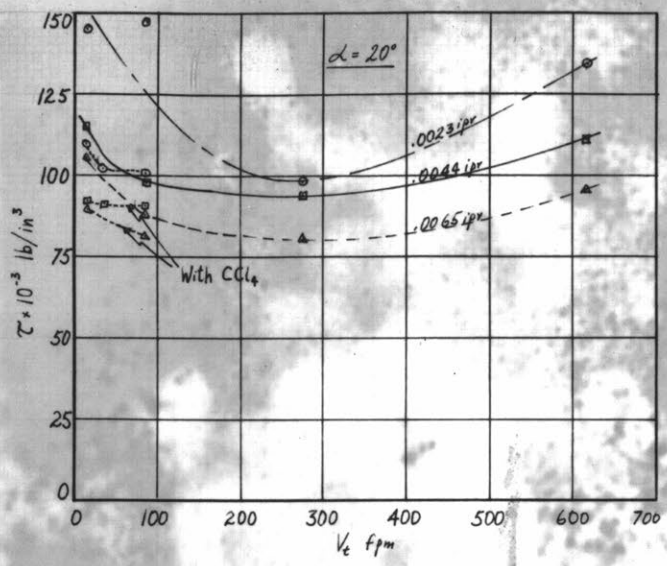


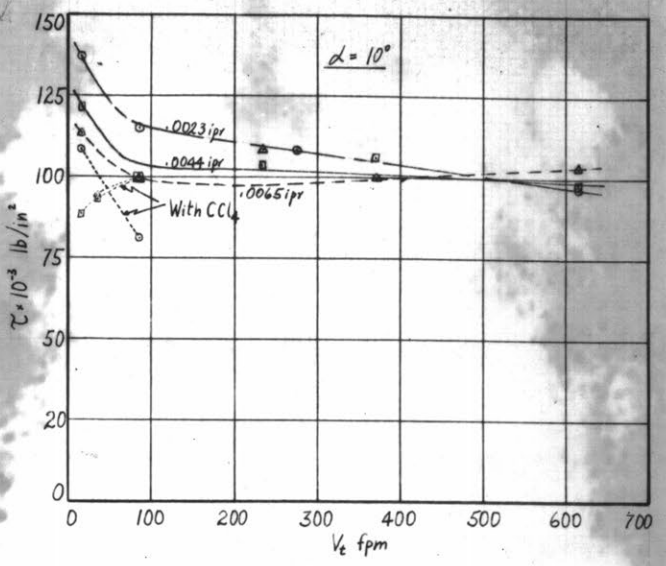


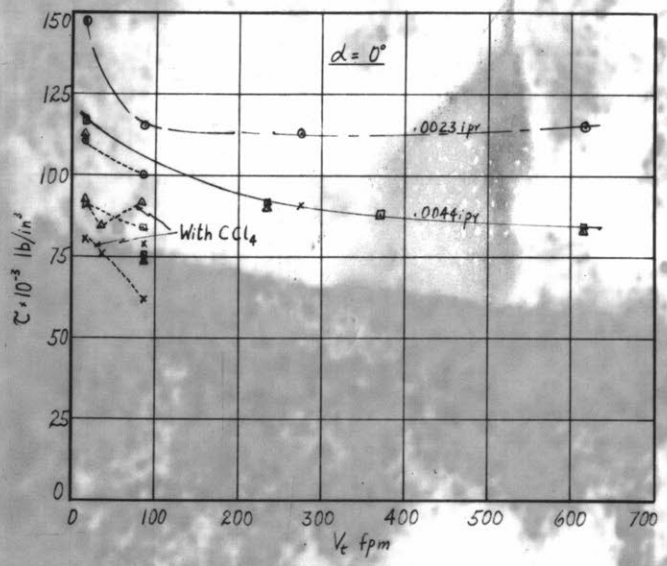


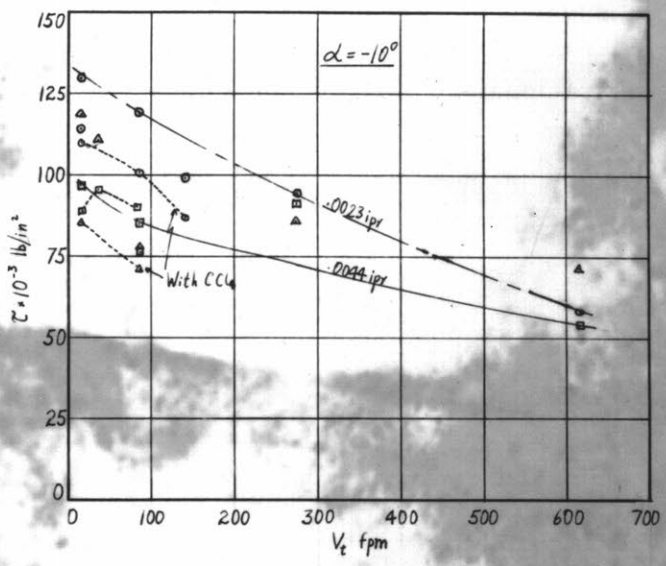


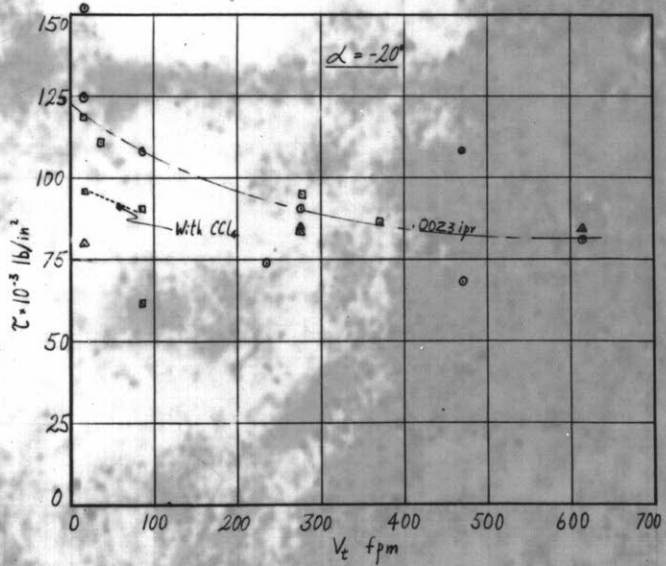


AVERAGE SHEAR STRESS ($\tau$) vs. CUTTING SPEED
ORTHOGONAL CUTTING

WORK MATERIAL: 2½" diam. bar 18-8 Stainless Steel as received.

TOOL MATERIAL: K2S Tungsten-Titenium Carbide
Rake angles: as shown on graphs
Clearance angle: 5°
Width of cut: 1/8" approx.
Feeds as shown, with code: ⊙ .0023 ipr
□ .0044 ipr
△ .0065 ipr
× .0116 ipr

FLUID: None
Low speed tests repeated, using Carbon-tetrachloride (dotted lines).

Fig.95

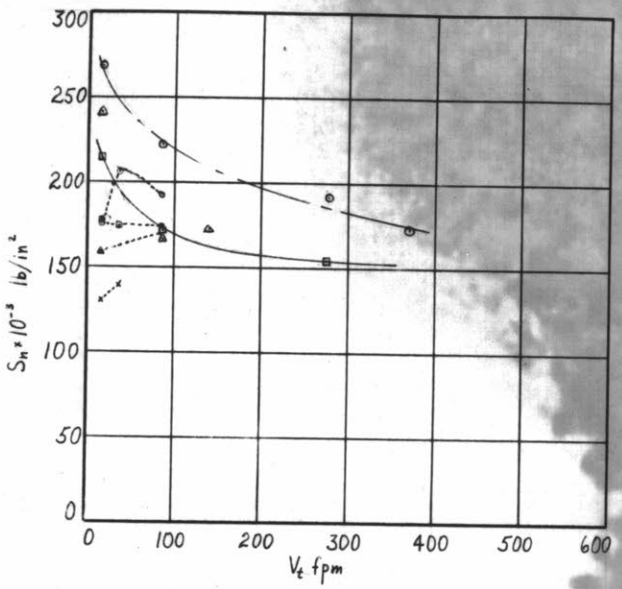


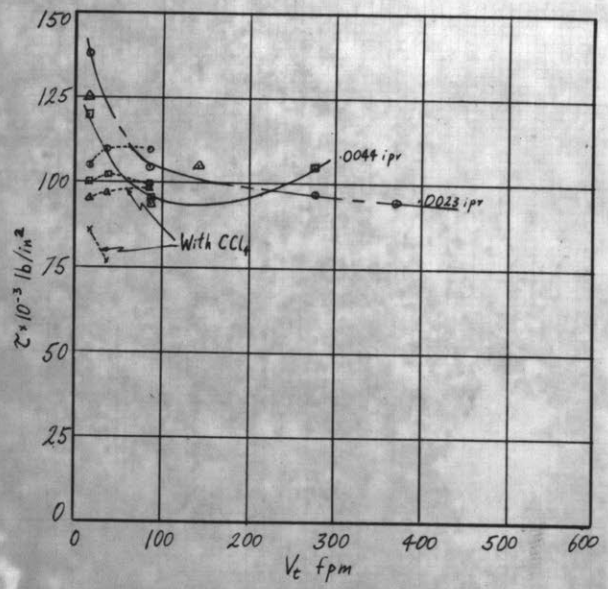


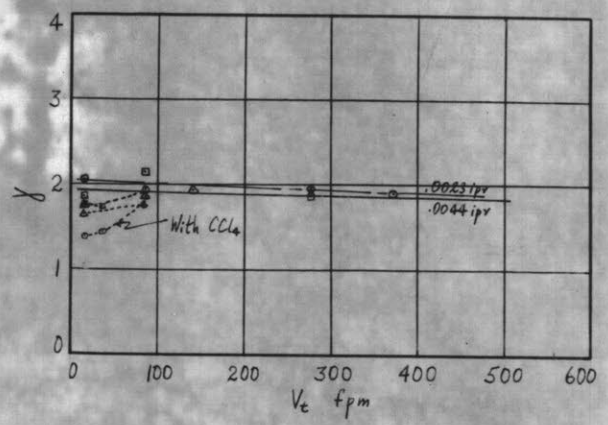


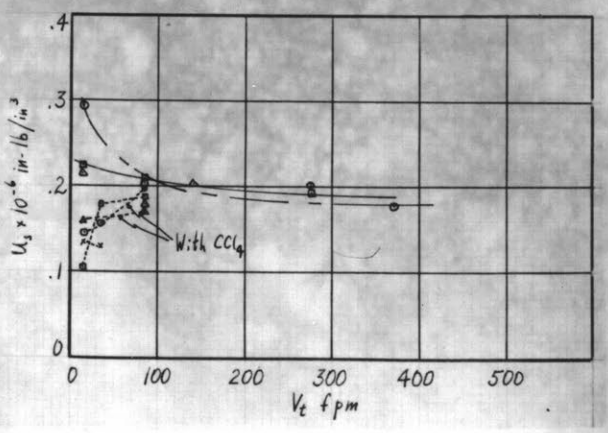


AVERAGE NORMAL STRESS ON SHEAR PLANE ($S_n$)
AVERAGE SHEAR STRESS ($\tau$)
SHEAR STRAIN ($\gamma$)
SHEAR ENERGY PER UNIT VOLUME ($u_s$)
vs. CUTTING VELOCITY

ORTHOGONAL CUTTING CONDITIONS

WORK MATERIAL: 2½" diam. bar 18-8 Stainless Steel, as received.

TOOL MATERIAL: 18-4-1 High Speed steel
Rake angle: 15°
Clearance angle: 6°
Width of cut: 1/8" approx.
Feeds as shown, with code: .0023 ipr
.0044 ipr
.0065 ipr
.0116 ipr

FLUID: None
Low speed tests repeated using
Carbon-tetrachloride (dotted lines)

Fig.96

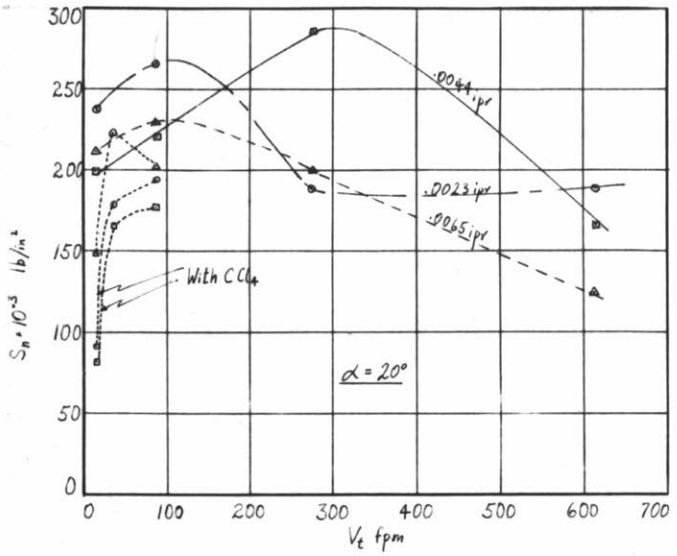


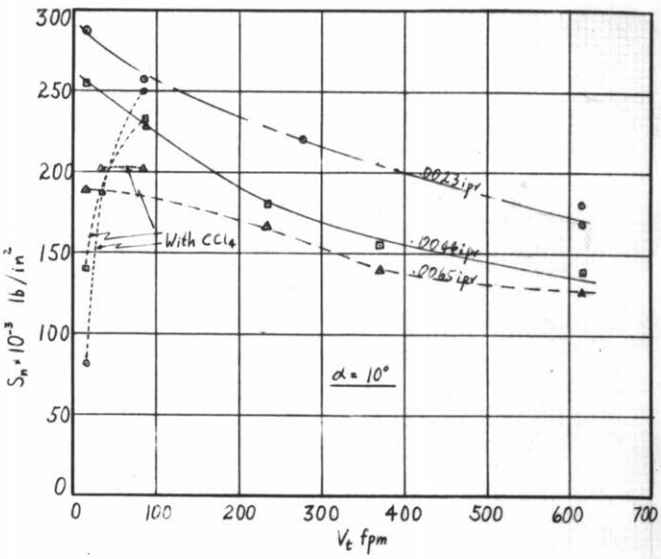


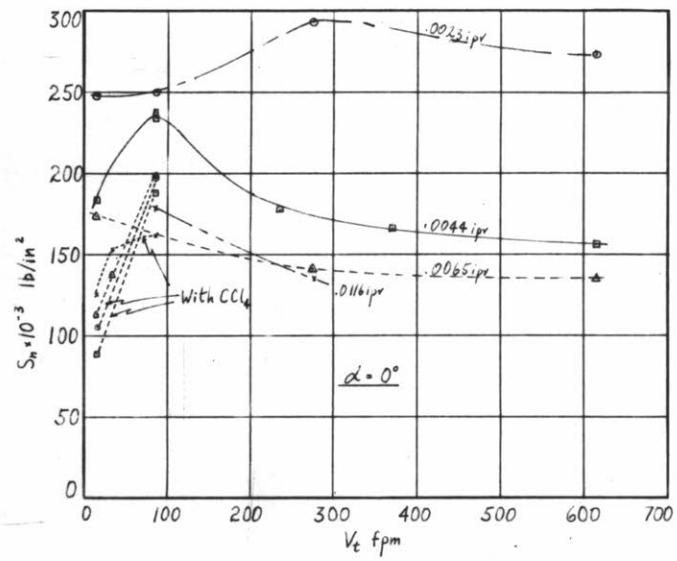


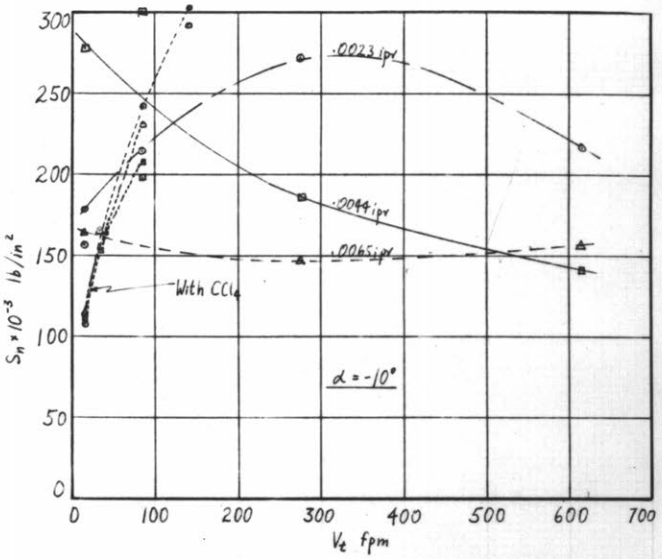


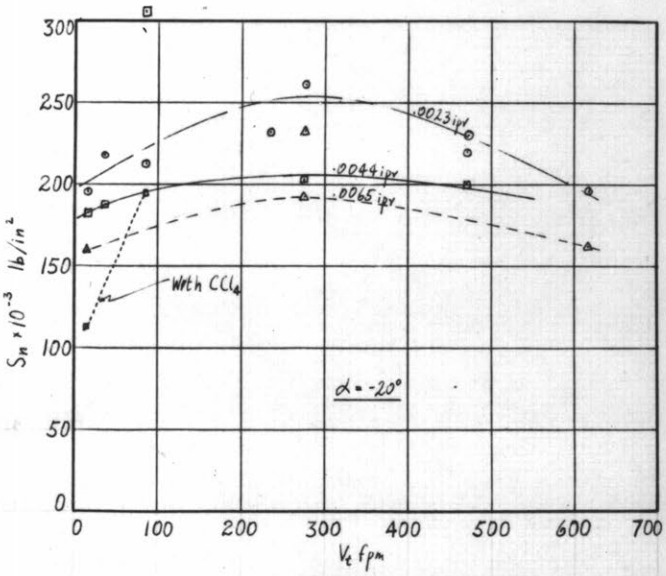


AVERAGE NORMAL STRESS ON SHEAR PLANE ($S_n$) vs. CUTTING VELOCITY

ORTHOGONAL CUTTING CONDITIONS

WORK MATERIAL: 2½" diam. bar 18-8 Stainless Steel, as received.

TOOL MATERIAL: K2S Tungsten-Titanium Carbide.
Rake angles: as shown on graphs.
Clearance angle: 5°
Width of cut: 1/8" approx.
Feeds as shown, with code: ● .0023 ipr
▣ .0044 ipr
△ .0065 ipr
× .0116 ipr

FLUID: None
Low speed tests repeated, using Carbon-tetrachloride (dotted lines).

Fig.97

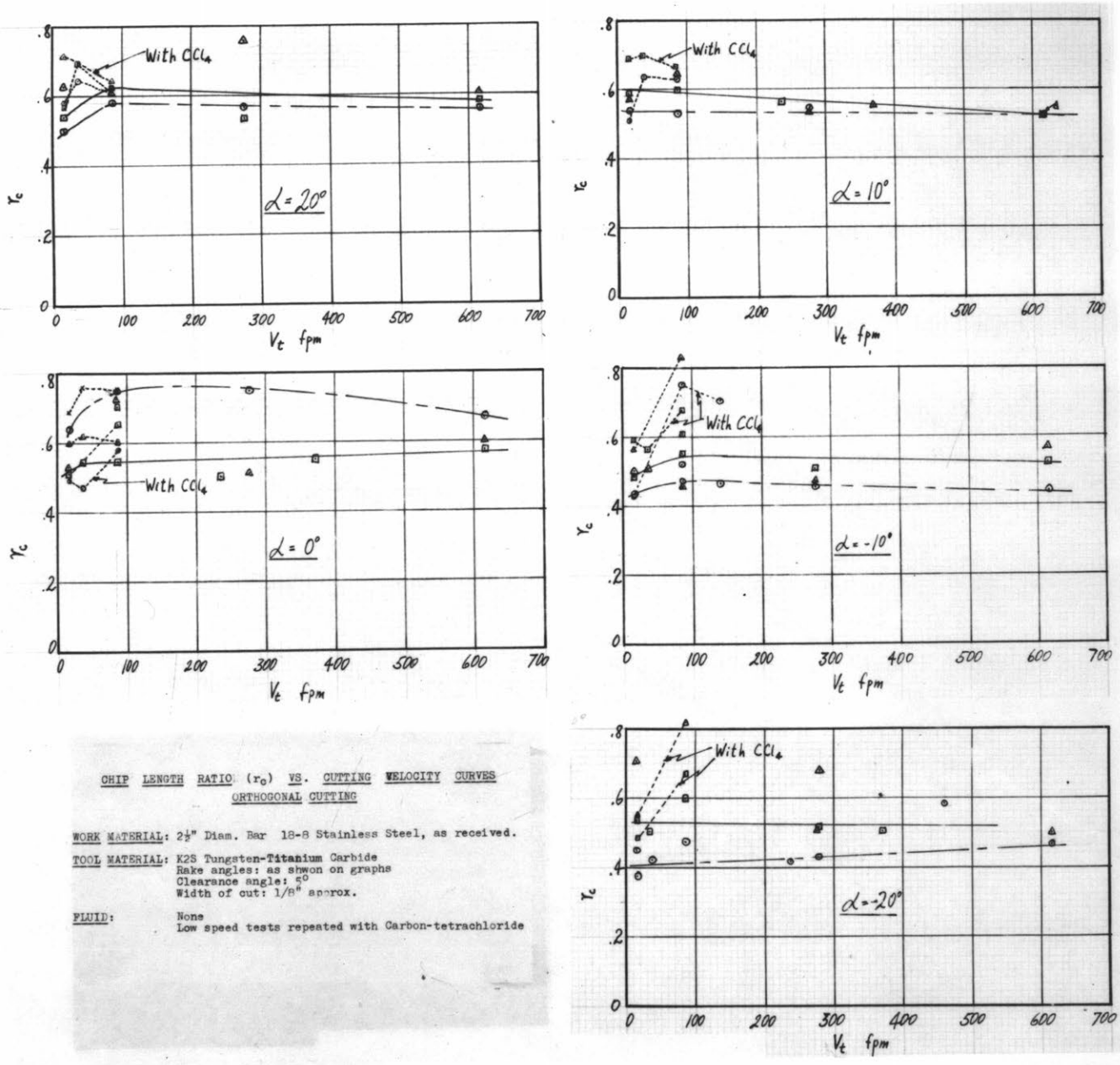


CHIP LENGTH RATIO ($r_o$) VS. CUTTING VELOCITY CURVES
ORTHOGONAL CUTTING

WORK MATERIAL: 2½" Diam. Bar 18-8 Stainless Steel, as received.

TOOL MATERIAL: K2S Tungsten-Titanium Carbide
Rake angles: as shwon on graphs
Clearance angle: 5°
Width of cut: 1/8" approx.

FLUID: None
Low speed tests repeated with Carbon-tetrachloride

Fig.98

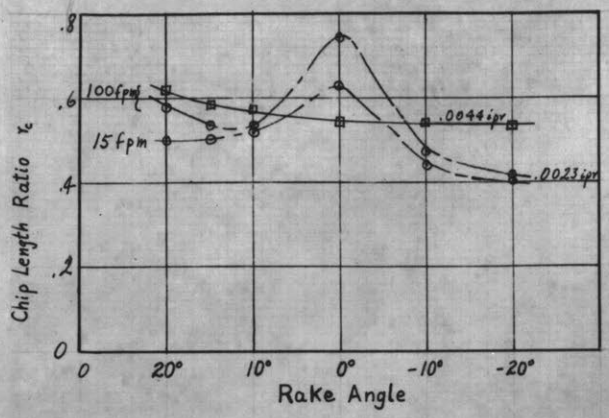


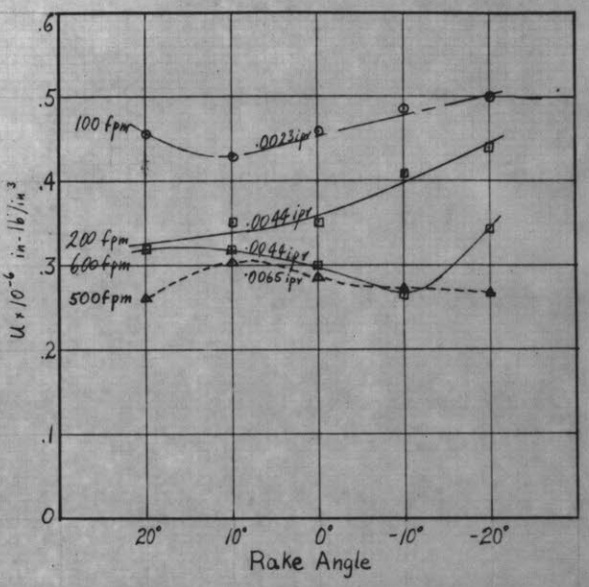


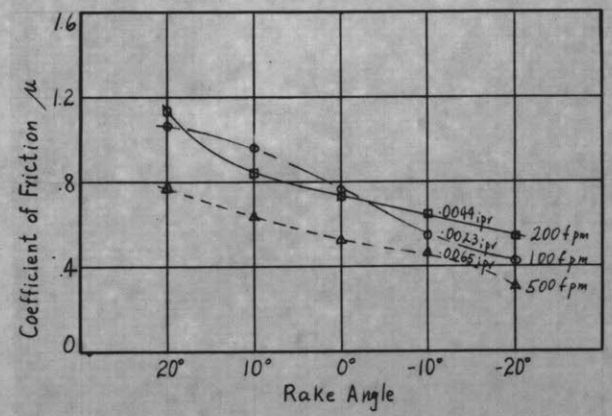


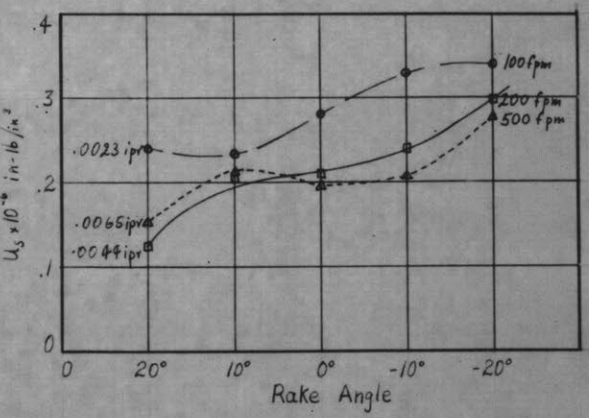


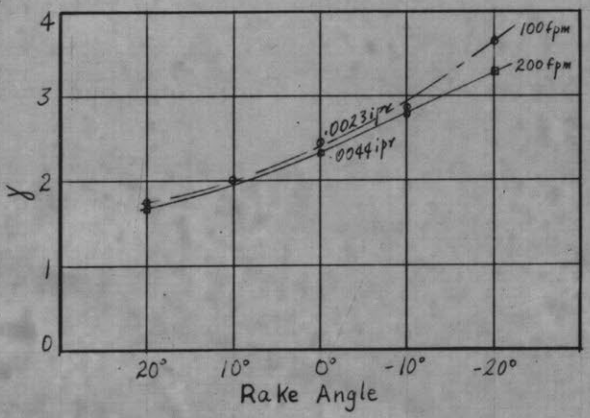


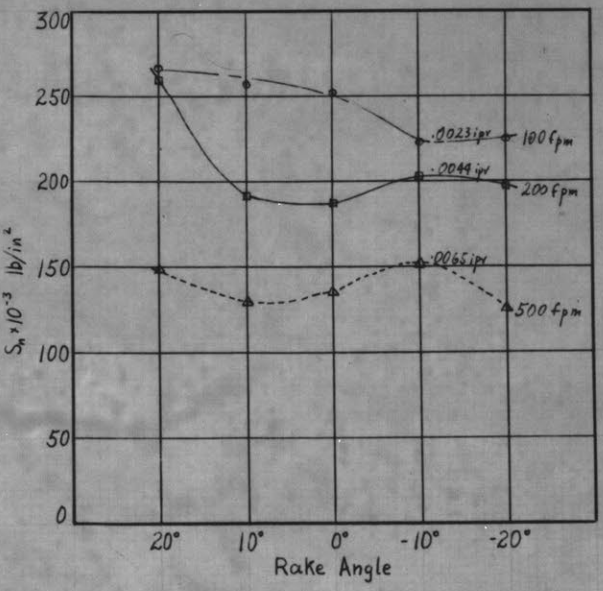


GRAPHS SHOWING THE VARIATION WITH RAKE ANGLE OF THE FOLLOWING:

CHIP LENGTH RATIO ($r_c$) COEFFICIENT OF FRICTION ($\mu$)

SHEAR STRAIN ($\gamma$) TOTAL ENERGY PER UNIT VOLUME ($u$)

SHEAR ENERGY PER UNIT VOLUME ($u_s$) AVERAGE NORMAL STRESS ($S_n$)

ORTHOGONAL CUTTING CONDITIONS

WORK MATERIAL: 2½" diam.bar 18-8 Stainless Steel, as received

TOOL MATERIAL: K2S Tungsten-Titanium Carbide
Clearance angle: 5°
Speeds and feeds as shown on graphs
Width of cut: 1/8" approx.

FLUID: None

Fig. 99